Polymer-bile salts interaction and its impact on the solubilisation and intestinal uptake of poorly water-soluble drugs

Claudia Pigliacelli

School of Pharmacy

University of East Anglia

Thesis Submitted for the Degree of Doctor of Philosophy

2014

For Mum, Dad and Flavia

Acknowledgements

I would like to thank my primary supervisor Dr. Sheng Qi for the invaluable support and encouragement received during my PhD time at UEA. Thanks also to my supervisors Prof. Peter Wilde and Prof. Duncan Craig for their help. I would also like to express my gratitude to Prof. Pete Belton, Dr. Francesca Baldelli Bombelli from the UEA School of Pharmacy for their precious scientific collaboration. Thanks to Dr. Patrick Gunning, Dr. Nicola Woodwards and Mr. Andrew Kirby, Dr. Paul Kroon and Mr. Mark Winterbone from the Institute of Food Research for their help with Nanosight, pendant drop and biological experiments.

I would like to thank all the friends that have been part of my life in Norwich, for the happy times together and for being supportive when I mostly needed. A special thanks goes to Yohan for being a good friend and taking care of me as a brother. Thanks to my housemates Desirè and Hanae, for their friendship and their constant support. Thanks to Francesca and Alberto for all the laughes and their invaluable help and care. Thanks to Lorina, Elisabetta, Marcello, Antonella and Tiziana for being good friends during these years. Thanks to all the other friends from the schools of Pharmacy and Chemistry. I would also like to thank my friends from Italy, in particular Ilaria for being a constant presence and support in my life.

Finally I would like to thank my family, my outstanding parents for their love, their encouragement and support. Thanks to my sister Flavia, for being the special sister she is.

Abstract

The delivery of poorly water-soluble drugs represents one of the main challenges to the pharmaceutical formulation field. In this regard solid dispersion formulations have emerged as an effective approach for improving poorly water-soluble drug dissolution rates and bioavailability. Despite this, the uncertain physical stability and the unclear dissolution mechanism of solid dispersions have strongly limited their application in the pharmaceutical market to date. Significant efforts have been made to improve solid dispersion formulation physical stability, but the mechanism of dissolution is still debated in the literature. This project was designed to better clarify the dissolution mechanism of solid dispersion formulations in media simulating the intestinal environment, with particular consideration of the possible interaction between polymeric carriers and the biosurfactants present in intestinal media. Spray dried solid dispersions were prepared using 4 polymeric matrices and three different model drugs. Solid-state characterisation of the obtained solid dispersion formulations was performed by the use of SEM, ATR-FTIR spectroscopy, PXRD, DSC and TGA techniques, which revealed drug partial amorphisation for all of the formulations. Biorelevant dissolution media FaSSIF and FeSSIF were employed, with and without the presence of lecithin, to assess drugs apparent solubility and spray dried solid dispersions dissolution profiles. In order to investigate the occurrence of interaction between polymeric carriers and bile salts, NMR and surface tension experiments were performed. Polymer/bile salts aggregates were characterized by using light and neutron scattering techniques and cryo-TEM. The possible impact of polymer-surfactant interaction on drug uptake in the intestinal tract was studied by the use of CaCO-2 cell model. Several key achievements were obtained across the project. The occurrence of polymeric carrier/bile salts aggregation was confirmed and aggregate characterization, together with steady state solubility and dissolution results, suggested possible involvement of polymer/bile salts aggregates in drug solubilisation. Finally drug uptake studies revealed a significant increase in the drug absorption in FaSSIF and FeSSIF media in the presence of the polymeric carriers in comparison to simple buffer media. The obtained results highlighted the possible role of polymeric carrier/intestinal fluids components interaction in the drug solubilisation and absorption in the intestinal tract. The achievements of this project are expected to provide insight into the mechanisms of drug solubilisation and stabilisation in the gastrointestinal tract after oral administration of solid dispersion formulations. In particular a better understanding of polymeric carriers behavior in the intestinal fluids during dissolution and of their interaction with intestinal fluids components can have an impact on the development of new solid dispersion formulations and on the design of new pharmaceutical polymers.

List of abbreviations

GIT	Gastrointestinal tract
API	Active pharmaceutical ingredient
FaSSIF	Fasted state simulating intestinal fluid
FeSSIF	Fed state simulating intestinal fluid
NaTC	Sodium taurocholate
PL	Phospholipid
BS	Bile salts
OA	Oleic acid
MO	Monoolein
CMC	Critical micelle concentration
CTAX	Cetyltrimethylammonium salt.
PPO	Poly(propylene oxide)
PVME	Poly(vinyl methyl ether)
OTG	n-octyl ß-D-thioglucopyranoside
HPMC	Hydroxypropyl methylcellulose
PVP	Polyvinylpirrolidone
CAC	Critical aggregation concentration
MW	Molecular weight
SDS	Sodium dodecyl sulphate
PVA	Polyvinyl alcohol
MC	Methylcellulose
PVAc	Polyvinyl acetate
EHEC	Ethyl-(hydroxyethyl)-cellulose
HM-EHEC	Hydrophobically modified Ethyl(hydroxyethyl)-cellulose
DDAO	Dodecyldimethylamine oxide
PVME	Poly(vinylmethylether)
NaPPS	Sodium poly(styrene sulfonate)
ITC	Isothermal titration calorimetry
C_{14} TB	Tetradecyltrimethylammonium bromide
C_nSO_4	Sodium alkyl sulfates
C_nSO_3	Sodium alkyl sulfonates
NMR	Nuclear magnetic resonance
SANS	Small angle neutron scattering

TEM	Transmission electron microscopy
Cryo-TEM	Cryogenic transmission electron microscopy
NaC	Sodium cholate
SEM	Scanning electron microscopy
PXRD	Powder x-ray diffraction
DSC	Differential scanning calorimery
TGA	Thermal gravimetrical analysis
ATR-FTIR	Attenuated reflectance fourier transformed infrared spectroscopy
BCS	Biopharmaceutics classification systems
DOSY	Diffusion-ordered spectroscopy
HPMC-AS	Hydroxypropyl methylcellulose acetate succinate
DLS	Dynamic light scattering
SESANS	Spin echo small angle neutron scattering
DMEM	Dulbecco Modified Eagle's Medium
PBS	Phosphate buffer solution
EDTA	Ethylenediaminetetraacetate

Chapter 1. Introduction

1.1Background of the project

There is a general consensus that lipophilic drug candidates are emerging often from drug discovery. [1,2] Oral delivery of poorly water-soluble drugs still represents a challenge for formulation scientists. [3] The absorption of such compounds in the gastrointestinal tract (GIT) is strongly influenced by their solubility in the gastrointestinal media and by their ability to permeate GIT membranes. The Biopharmaceutics Classification System (BCS), introduced to the pharmaceutical industry in the 90s, divided active pharmaceutical ingredients (APIs) into four groups based on their aqueous solubility and permeability. BCS II and IV (poor permeability) APIs are classified with poor aqueous solubility and their bioavailability can potentially be improved through formulation strategies. [4] Different approaches have been studied to formulate poorly-water soluble drugs in order to enhance their solubility and bioavailability. These include particle size reduction, salt formation, lipid based drug delivery systems, pro-drug formation, complex formation, self-emulsifying drug delivery systems and solid dispersions. [5–11]

Formation of solid dispersions has been proved to be an effective approach to increase the dissolution rate of poorly water-soluble drugs and potentially improve their bioavailability. [12–14] In order to achieve good in vivo-in vitro correlation and accurately predict the in vivo performance of a solid dispersion using in vitro data, increasing attention has been paid to the *in vitro* dissolution media employed to study drug dissolution from solid dispersions formulations and the importance of the dissolution media composition has been highlighted by many recent studies. [15–17] The mimicking of human gastro-intestinal fluids composition is crucial to accurately predict APIs dissolution behavior and assess the effectiveness of solid dispersion on the drug solubility enhancement. The composition of human gastrointestinal fluids is extremely complex and many components may influence the solubilisation of a poorly soluble drug. [18–20] Furthermore dissolution fluids components can also influence the behavior of the drug carrier and impact on the drug release from the formulation. [21] To date there is a lack of knowledge about the possible interaction between the polymeric carriers commonly used in the solid dispersions formulations and gastro-intestinal fluids components and its possible influence on the drug solubilisation and subsequent oral absorption. Such mechanimistic study is extremely challenging due to the complex environment of human GIT. However, it can dramatically improve the

predictability of the in vitro dissolution tests and provide useful guidance for the formulation optimization. The focus of this project was to characterise solid dispersion polymeric carriers/bile salts interactions and identify the possible roles of these interactions in poorly water-soluble drug solubilisation and absorption. Different dissolution media with increasing complexity were employed and the molecular level interactions between the polymer and the media were studied using a wide range of characterisation techniques. The macroscale physico-chemical behaviour of freshly spray dried solid dispersions in these dissolution media was analysed and used to facilitate the interpretation of the potential roles of the identified interactions in the dissolution and drug release process of the drug from a solid dispersion formulation.

1.2 Solid dispersions

1.2.1 General introduction to solid dispersions

The initial definition of solid dispersion given by Chiou was "the dispersion of one or more active ingredients in an inert carrier or matrix in solid state prepared by melting "fusion", solvent or melting solvent method". [22] Solid dispersion can be described as a processed mixture of a drug in a solid inert matrix, where the drug can be dispersed in different states depending on the material matrix used and the preparation method employed. [23] The physical forms of the drug can either exist as crystalline particles, as amorphous drug rich domains or being molecularly dispersed in the carrier polymer. [24]

In comparison to other formulation strategies employed for increasing the bioavailability of lipophilic APIs, such as pro-drug formulation and self-emulsifying drug delivery system for enhanced dissolution and absorption, solid dispersion offers different advantages. The production of solid dispersions is normally low-cost and scalable. Furthermore solid dispersion formulations can widely be applied to various drugs with different physical properties for both solubility enhancement and controlled release purposes. [11] Another advantage offered by solid dispersion technology is the possibility of obtaining and maintaining supersaturation of the drug in the dissolution media, which is gaining increasing interest as a possible tool to improve drug bioavailability. [25] Therefore, the solid dispersion technology represents a promising formulation strategy that is increasingly being remarked by the pharmaceutical industry.

Despite the advantages mentioned above, the use of solid dispersion in clinic is still very limited and only around 10 solid dispersion based products are currently on the pharmaceutical market. Fuller understanding of the relationship between the physical properties and *in vivo* behavior of solid dispersions are needed to more rationalised formulation design of solid dispersions.

1.2.2 Classification of solid dispersions

According to the physical states of the drug in the polymer matrices, solid dispersion can be classified into two main types, phase separated solid dispersion containing crystalline drug, and amorphous solid dispersions (solid solution) in which the drug is ideally molecularly dispersed in the polymer network, but often could be in the form of drug rich domains. In this study, the behaviour of solid dispersions containing crystalline drug and molecular dispersions were studied. The chemical, physical and pharmaceutical features of the two classes are described in the following sections.

1.2.2.1 Solid dispersion containing crystalline drug

The crystalline state of material is characterised by three long-range order symmetry operators including translational, orientational and conformational. [26] The presence of such symmetry confers high physical stability to crystalline materials. Therefore the main advantage of using solid dispersion containing crystalline drug is the stability of the drug in the system. [27] The first reported solid dispersion containing crystalline drug was a simple eutectic mixture. Eutectic mixtures consist of two components that are miscible in the liquid state but only partially miscible in the solid state. Solid eutectic mixtures are commonly obtained by rapid cooling of a co-melt of the two components, in order to obtain physical mixtures of the two compounds fine crystals. [28,29] The release of fine drug crystals once the eutectic mixture is in contact with the dissolution medium can lead to an increase in the drug dissolution rate, which is mainly due to the significantly increased surface area of the systems. Schematic representation of a solid dispersion containing crystalline drug is shown in Figure 1.1.

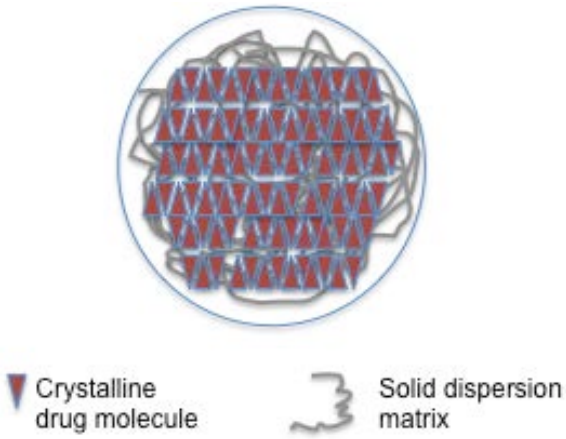

Figure 1.1: Schematic representation of solid dispersion containing crystalline drug

Together with eutectic mixtures other solid dispersion formulations containing crystalline drug have been reported in literature. The proposed solid dispersion systems have been shown to be able to increase drug dissolution rate despite its crystalline form. Such effect has mainly been related to the presence of the hydrophilic carrier which covering the crystalline drug particles promoted their solubilisation. [30,31]

1.2.2.2 Amorphous solid dispersions (solid solutions)

Amorphous solid dispersions are composed of drug molecularly dispersed in the formulation matrix. Amorphous state of a material is characterised by the absence of the long-range order within the structure. [32] The lack of long-range order results in a relative random position of the molecules one to each other and only short-range orientation is present.[33] This results in thermodynamic instability of amorphous materials, due to the higher energy level in comparison to their crystalline counterparts. The properties of amorphous materials made them attractive for solubility enhancement, [34] as they can yield solution concentrations many times higher than their crystalline counterparts. [35–37] The molecular dispersion state of a drug in solid dispersion facilitates the drug solubilisation in the dissolution media, reducing the barrier to solubility presented by solute-solute molecular interactions in the crystalline state. [38] On the other hand the physical instability of amorphous solid dispersion can result in drug recrystallization during the storage. [39–41]

Amorphous solid dispersions are normally obtained by dispersing the drug in an amorphous polymer, which can prevent the drug crystallization in the formulation. [42] They can be characterized by rich drug domains or by a molecular dispersion of the drug in the matrix (Figure 1.2). The latest represents the ideal solid dispersion as higher dissolution rate

is expected when the drug is molecularly dispersed in the inert matrix. [43] Further recrystallisation of drug from drug-rich domains in an amorphous solid dispersion can be characterised by partially crystalline and partially amorphous drug in the dispersions. [44]

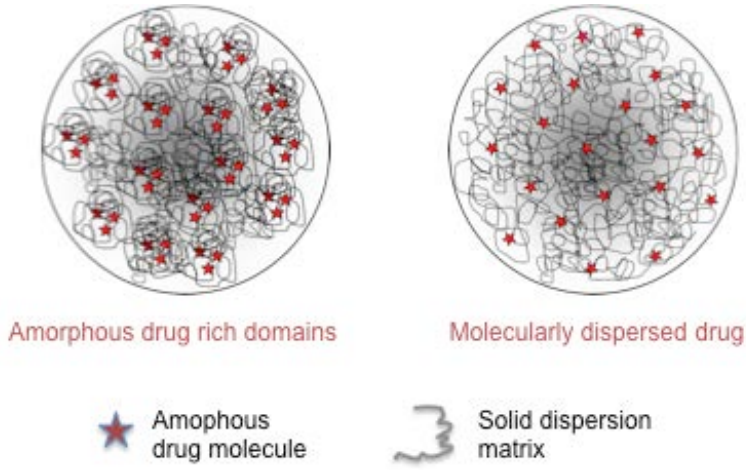

Figure 1.2: Schematic representation of amorphous solid dispersion characterized by amorphous drug rich domains and molecularly dispersed drug.

1.2.3 Preparation of solid dispersions

Processing methods for solid dispersion preparation can be divided into two main classes: solvent evaporation and non-solvent based methods. Classical solvent evaporation methods include spray drying, film casting and co-precipitation. More recently spin coating, electrospinning and electrospraying techniques have also been remarked for their potential applications for pharmaceutical solid dispersions preparation. Non-solvent based methods include melting based methods, such as hot melt extrusion, and milling. The different methodologies are briefly described in following sections 1.2.3.1 and 1.2.3.2.

1.2.3.1 Solvent based methods

The most widely used solvent evaporation method for preparation of solid dispersion is spray drying. Spray drying is a process of the transformation a liquid feed into dried particles by spraying the feed into a heated drying gas (air or nitrogen). [45] Many spray dried solid dispersions have been reported in literature. Most of them demonstrated good ability to increase dissolution rate and solubilise poorly water-soluble drugs *in vitro*. [46] More

recently spray drying technique has found applications in the field of biological therapies, such as spray drying of proteins, viable organisms and plant extracts. [47] Technical and processing aspects of spray drying are described in details in Chapter 2 (Section 2.3.1).

Film casting is based on the pre-dissolution of the drug and polymer in a suitable solvent and casting the obtained solution on a chosen surface under ambient condition or low vacuum. Different works in literature described the possible applications of film casting technique for solid dispersions preparation. [48,49] An essential prerequisite for solid dispersion preparation through film casting methods is the choice of a solvent or a mixture of solvents that allow simultaneous solubilisation of the drug and the polymeric carrier. The choice of appropriate solvent or solvent mixture represents a major limitation for the film casting methodology application.

Spin coating technique is based on the production of films with micron to nanometer thickness on a chosen substrate. Spin coating has widely been used in the semiconductor industry and more recently has been remarked as possible processing method for solid dispersions preparation. [50,51] As for film-casting drug and polymer are pre-dissolved in a solvent or mixture of solvents, but differently from the common film-casting technique, ultra-fast solvent evaporation occurs under fast spinning during spin-coating process. Spin coating technique offers the advantages of high reproducibility and fast preparation. Due to the more intimate mixing through dissolving in a solvent and ultra-fast solvent evaporation which gives the material a quenching effect, spin coated solid dispersions have been shown to more effectively stabilize amorphous drugs in the carrier matrix in comparison to other methods, such as hot melt extrusion. [51]

Co-precipitation method consists in the simultaneous dissolution of the drug and the carrier in a solvent and the subsequent addition of an anti-solvent. The difference in polarity between solvent and anti-solvent causes the precipitation of the polymer and the drug leading to the formation of a solid dispersion. Usually polar solvent and non-polar anti-solvent are employed and high difference in polarity is necessary to promote the formation of solid dispersion. [52] After precipitation completion, filtration or solvent evaporation are performed to obtain the solid dispersion. [53] Solid dispersions obtained by co-precipitation method are normally composed of porous particles, having large surface to volume ratios. The surface to volume ratio and the porosity of the co-precipitated solid dispersion particles may potentially improve dissolution rate of poorly water-soluble drugs. [54] However, due to

the complexity of solvent and anti-solvent selection, the application of co-precipitation for the preparation of solid dispersion has been to date quite limited.

1.2.3.2 Non-solvent based methods

The use of organic solvents in the preparation of solid dispersions may represent a limitation for this strategy formulation, due to both environmental and cost concerns. For this reason non-solvent based methods for solid dispersions preparation have attracted increasing interest in pharmaceutical industry. In this regard hot melt extrusion (HME), a technique widely employed in the plastic industry, [55] represents a possible process for the production of solid dispersion formulation. During a HME process, the raw materials are fed into the extruding system, where a rotating screw extrudes the heated material through different zones (for mixing and transporting purposes). The material exits the extruder through a die and solidifies either under ambient or additional cooling conditions (Fig. 1.3). [56] HME has advantages over other methods such us easy scaling-up, and the efficiency of being a one-step processing. However thermal degradation of heat-sensitive drugs and polymers in preparation restricts the selection of drugs and polymers can be processed by HME. [57]

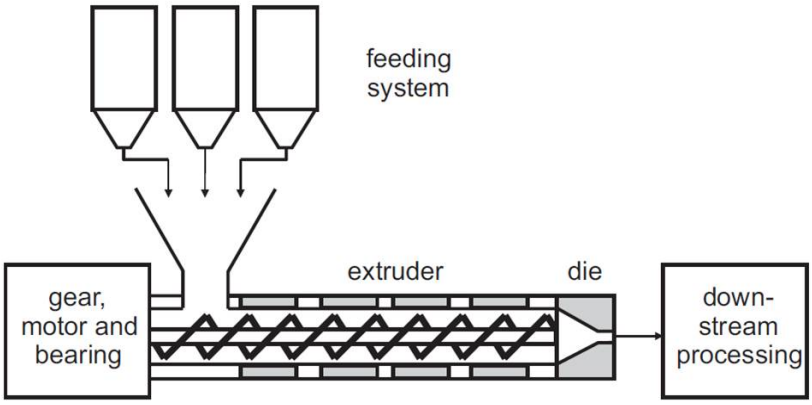

Figure 1.3: Schematic diagram of a hot melt extrusion system [58]

Milling processing allows particle size reduction, conversion of crystalline materials in their amorphous counterparts and formation of co-crystals. Milling technique has been shown to be an effective method to obtaine solid dispersion. [24,59] It can be performed with (wet milling) and without (dry milling) the presence of wetting agents. Wet milling has been employed for the preparation of nano-suspensions, whereby drug and matrix were mixed together in a surfactant solution. Such methodology allowed the reducing of particle size to

the nano-scale, [60] leading to an increase in the drug dissolution rate. For the preparation of solid dispersions through wet milling method the wetting agent removal by lyophilisation is required during downstream processing. [61,62] Dry milling was shown to favor crystalline drug conversion in their amorphous state, facilitating drug dissolution. Despite the reported increase in drug solubilisation obtained by using wet and dry milling, milling techniques presents few disadvantages. Firstly only a certain range of particle size reduction can be achieved depending on the properties of drugs and polymers. Second, milling processing can be time-consuming as hours or days milling periods are required to produce amorphous solid dispersion. [63]

1.2.4 Limitations of solid dispersions

Despite the high number of studies carried out and the significant amount of scientific contributions published in the field of solid dispersions, their commercialization is still limited. A summary of the pharmaceutical products based on solid dispersion technology currently available in the market can be found in Table 1.1. [43,64]

Table 1.1: Summary of marketed pharamecutical products prepared using solid dispersion approach.

Product	Company	API	Polymer	Year of approval	Preparation method
GrisPEG	Pedinal Pharm Inc.	Griseofulvin	PVP	1975	Melt process
Cesamet	Eli Lilly	Nabilone	PVP	1985	Unknown
Sporanox	J&J	Itraconazole	HPMC	1992	Spray drying
Prograf	Astellas Pharma SpA	Tacrolimus	HPMC	1994	Spray drying
Kaletra	Abbott	Lopinavir/Ritonavir	PVP-VA	2005	Melt extrusion
Intelence	Tibotec	Etravine	HPMC	2008	Spray drying
Zotress	Novartis	Everolimus	HPMC	2010	Spray drying
Norvir	AbbVie	Ritonavir	PVP-VA	2010	Melt extrusion
Onmel	Merz Pharma	Itaconazole	HPMC-AS	2010	Melt extrusion
Incivek	Vertex	Telaprevir	HPMC-AS	2011	Spray drying
Zelboraf	Roche	Vemurafenib	HPMC-AS	2011	Co-precipitation
Kalydeco	Vertex	Ivacaftor	HPMC-AS	2012	Spray drying

In formulation science many efforts have been made to address how the drug is dispersed in the inert matrix in the solid state and optimisation of solid dispersion physical stability. [36,50,65,66] However the mechanism of how solid dispersions facilitate the dissolution and absorption of poorly soluble drugs *in vivo* is not clarified. This lack of knowledge

represents a barrier for the solid dispersion *in vivo* performance prediction and consequently for their optimisation. Indeed, a clearer mechanistic understanding of solid dispersion behaviour in the biological fluids would provide guide for the polymeric carriers selection and facilitate the development of new solid dispersions formulation, opening up more possibilities for the commercialisation and use in the clinic.

1.3 *In-vitro* dissolution assessment for solid dispersion

In vitro dissolution test is widely used as a tool to assess the dissolution performance of pharmaceutical formulation. The study of the *in vitro* dissolution of a drug provides useful information in different drug development stages and can potentially predict the drug solubilisation *in vivo* and consequently its bioavailability. [67] The dissolution behaviour of solid dispersion has received significant attention in literature and few possible dissolution mechanisms have been proposed. Proposed dissolution mechanisms and dissolution media are described in Sections 1.3.1 and 1.3.2.

1.3.1 Solid dispersions dissolution

Drug dissolution process has been theoretically described by the Noyes-Whitney equation

$$dW/dt = \frac{DA(C_S - C)}{L} \qquad Eq\ 1.1$$

where *dW / dt* is the dissolution rate, *A* is the surface area, *C* is the concentration of the drug in the bulk media, C_s is the solubility of the drug in the media and *L* is the diffusion layer thickness. [68] Each parameter of the equation can be strongly influenced by the drug formulation in solid dispersion, as besides the possible change in the physical state of the drug obtained by the solid dispersion preparation, the carrier matrix surface, area and thickness are key parameters for the drug dissolution rate. The drug release and dissolution mechanism from solid dispersion formulations is still not clearly understood. Craig proposed two possible models, which are schematically represented in Figure 1.4. A carrier-controlled dissolution model, which proposed the drug dissolution into the concentrated carrier layer prior to release, and drug-controlled dissolution mechanism whereby the un-dissolved drug is released intact into the dissolution medium. [69]

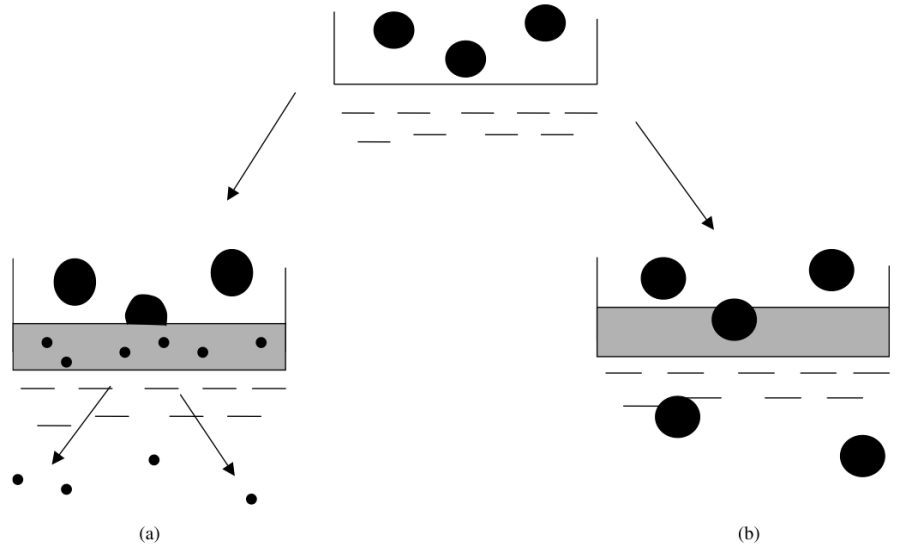

Figure 1.4: Schematic representation of carrier controlled (a) and drug controlled (b) solid dispersion dissolution mechanisms proposed by Craig. [69]

Despite the indications provided in literature on the possible solid dispersion dissolution media, the role of gastro-intestinal fluids components in the dissolution mechanism of dispersions has not been considered. Recently the key role of mimicking the gastro-intestinal fluids for *in vitro* dissolution studies has been highlighted by many works. [15,20,70,71] The following section reviewed the variety of bio-relevant media compositions have been used in the literature.

1.3.2 Biorelevant dissolution media

Mimicking of biological conditions in the study of formulations dissolution profile is essential for more accurate analysis of the *in vitro* and *in vivo* correlation which will be used for predicting *in vivo* therapeutic outcome [18]. As widely described in literature the presence of amphiphilic molecule species in the intestinal fluids plays a major role in the drug solubilisation in the GIT. [70] In the last few decades intestinal fluids have been intensively studied and the key features of intestinal fluids are reviewed in Table 1.1.

Table 1.2: Summary of Intestinal fluids composition. [70]

Region (number of replicates)	Total BS (mM)	Total PL (mM)	Ratio (BS/PL)	Total MG (mM)	Total FFA (mM)	Ratio (FFA/MG)	pH	Surface tension (mN/m)	Osmolality (mOsm/kg)
Fasted state									
D (7)[5]	5.9 ± 1.8	–	–	–	–	–	6.8	–	–
D (4)[6]	3.5 ± 1.8	0.1 ± 0.1	39	–	–	–	6.5 ± 0.5	–	–
D (15)[9]	2.6	–	–	–	–	–	6.2	32.3	178
D (12)[9]	2.82	–	–	–	–	–	6.7	33.6	197
D (6)[12]	2.6 ± 1.6	–	–	–	–	–	7.0 ± 0.4	–	137 ± 54
D (7)[10]	2.5	0.4	6	–	–	–	–	–	–
D (5)[7]	2.7	0.6	4.5	–	–	–	6.6	41.2	224
J (37)[8]	2.9 ± 2.9	–	–	–	–	–	7.1 ± 0.6	–	271 ± 15
J (10)[11]	1.5 ± 1.8	–	–	–	–	–	6.7 ± 0.9	33.7 ± 2.8	278 ± 16
J (6)[12]	3.5 ± 1.6	–	–	–	–	–	6.8 ± 0.4	–	200 ± 68
J (3)[13]	2 ± 0.2	0.2 ± 0.07	10	–	0.09	–	7.5	28 ± 1	–
J (6)[14]	–	–	6	–	–	–	–	–	–
Fed state									
D (7)[5]	13.4 ± 4.3	1.9 ± 0.4	9.6	–	–	–	6.4	–	–
D (5)[8]	14.5 ± 8.8	4.8 ± 1.8	3	–	–	–	–	–	–
D (6)[15]	9.3 ± 0.8	2.4 ± 0.35	3.9	–	–	–	5.7	–	–
D (12)[9]	11.8	4.31	2.7	5.95	39.4	6.6	6.5	27.8	416
D (8)[10]	24	1.5	16	–	–	–	–	–	–
D (5)[7]	3.6	1.8	2	–	–	–	5.9	35	285
D (5)[7]	5.2	1.2	4.3	–	–	–	6.1	35	278
J (3)[13]	8 ± 0.1	3 ± 0.3	2.7	2.2	13.2	6	6.1	27 ± 1	–
J (15)[9]	12	–	–	–	–	–	6.6	28	400
J (6)[14]	0.5–8.6	0.1–3.9	1–3	–	–	–	–	–	–
J (13)[16]	16.19 ± 1.51	–	–	–	–	–	–	–	–
J (16)[17]	15	–	–	–	–	–	–	–	–

D, duodenal fluids; J, jejunal fluids; BS, bile salts; PL, phospholipid; MG, monoglyceride; FFA, free fatty acids. Data represent mean ± SD.

Table 1.2 gives indication of how pH, osmolality, surface tension, bile salts and phospholipid content change in the absence (fasted state) and in the presence of (fed state) food in the GIT, and how all these parameters vary in the different regions of the human intestinal tract. For in vitro studies performance, an effective simulation of the human intestinal fluids is essential for producing good *in vivo-in vitro* correlation data. Dressman et al proposed biorelevant media that could mimick the average fasted and fed upper small intestinal fluid (composition shown in Table 1.2). [67] Although fasted state simulated intestinal fluid (FaSSIF) and fed state simulated intestinal fluid (FeSSIF) only contain a simplified combination of the actual lumenal composition, they have been shown to be capable to closely predict the *in-vivo* dissolution process. [15] For this reason they have been widely used to assess the dissolution of poorly soluble, lipophilic weak acids, weak bases and non-ionisable compounds. [72–74]

As shown by Table 1.2 sodium taurocholate (NaTC) is employed in FaSSIF and FeSSIF to represent bile salts in the intestinal fluids. NaTC is the most often used model bile salt in the biorelevant media. Together with glycocholate, it is the most abundant bile salt in human bile. The pK_a of NaTC is 1.5, thus it is ionized in the pH range of the small intestine. [75] The increased knowledge about intestinal fluid composition has lead to an improvement of the biorelevant media used in pharmaceutical studies for assessing drug dissolution behavior and solubility in simulated intestinal fluids. FaSSIF and FeSSIF have recently been revised,

according to the new knowledge about human intestinal fluids composition. This brought to the preparation of new updated simulated intestinal fluids named FaSSIF-V2 and FeSSIF-V2 (see Table 1.3). [76]

In FaSSIF-V2, the phospholipid concentrations were decreased, causing the bile salts/phospholipid (BS/PL) ratio to increase from 5 to 15. The buffering species were changed from phosphate to maleate and the osmolality decreased from 270 (for FaSSIF) to 180 (for FaSSIF-v2) mOsm/kg. In FeSSIF-V2 the buffering species were also changed to maleate and the BS/PL ratio changed from 4 to 5. Furthermore lipolysis products were added, but in smaller amounts compared with the human intestinal fluids and the obtained oleic acid/monoolein (OA/MO) ratio of 0.16 is still not representative of the intestinal physiological condition. Osmolality was decreased to a level matching the osmolarity of human instestinal media. More recently further modification of fasted and fed states were investigated and Copenhagen fasted and fed states were studied. In this case bile salts/phospholipids or monoolein/oleic acid ratios were increased and adjustment of the ratio is required for each individual drug.[70]

Table 1.3: Summary of Simulating intestinal fluids composition. [70]

	FaSSIF	FaSSIF-V2	FeSSIF	FeSSIF-V2	Copenhagen fasted	Copenhagen fed
BS (mM)	3	3	15	10	2.5[a]	5–20[a]
PL (mM)	0.75	0.2	3.75	2	0.625	1.25–5
BS/PL	4	15	4	5	4	4
MO (mM)	–	–		5	–	0–10
OA (mM)	–	–		0.8	–	0–45
OA/MO				0.16		2–7.5
Buffer species	Phosphate	Maleate	Acetate	Maleate	Trizma maleate	Trizma maleate
pH	6.5	6.5	5	5.8	6.5	6.5
Osmolality (mOsm/kg)	270	180	635	390	270	Varying

BS, bile salts; PL, phospholipid; MG, monoglyceride; FFA, free fatty acids; MO, monoolein; OA, oleic acid; FaSSIF, fasted-state simulated intestinal fluid; FeSSIF, fed-state simulated intestinal fluid. [a]Bile salt as either sodium taurocholate or crude porcine bile extract.

Recently the use of phosphate buffer for in vitro dissolution studies has also been questioned. Indeed phosphate buffer ions do not relate to the gastrointestinal fluids. To overcome this limitation “physiological” bicarbonate buffers mimicking the gastrointestinal fluids in terms of ions content and buffer capacity have been developed. [77] The new buffered system was developed by modification of pH 7.4 Hanks balanced salt solution to obtain a pH 6.8 bicarbonate buffered solution (modified Hanks buffer, mHanks). mHanks system was proved to better assess the in vitro dissolution profile of enteric coatings. [78]

In this study the first version of fasted and fed state prepared by Dressmann et al were chosen for all drug and formulation drug solubility and release studies. NaTC was therefore used as model bile salt. The reason for not choosing the more recently developed but more biorelevant media is that the presence of lipolysis products in the newer media would produce high level of interference with the molecular characterization of the specific polymer-bile salts aggregates, which is the focus of this study. Thus, the original fed and fasted intestinal fluids having the less complex composition were chosen as biorelevant media for all tests performed in this study.

1.4 Bile Salts

Bile salts are bio-surfactants derived from cholesterol metabolism, produced in the liver and stored in the gallbladder. Bile salts are secreted in the small intestine in concentration ranging from 5 to 25 mM. [79] In the intestinal tract bile salts play a primary role in the solubilisation of lipids during the digestion process. Moreover they promote calcium absorption, represent a mean of excretion of waste molecules from the blood and have regulatory properties influencing the bile acid and cholesterol biosynthesis. [79–82] Bile salts are almost quantitatively recoverd in the ileum and transported back to the liver via the portal circulation. In the liver they are extracted by hepatocytes from sinusoidal blood and subsequently resecreted into the bile. This enterohepatic circulation allows bile salts to be recovered up to 90 %, thus only about 10% of bile salts is eliminated in the feces. [83]

1.4.1 Structural features of bile salts

Bile salts structure differs significantly from the classical surfactant structure. Classical detergents present a polar head group and a hydrophobic chain, whereas bile salts are based on a rigid tetracyclic steroid ring structure. The hydrophobic surface is the convex side of the ring and the hydrophilic surface is the concave side of the molecule, where between one and three hydroxyl groups and one acid group are attached (Fig.1.6). Thus, the hydrophilic and the hydrophobic portions of the molecule are not clearly separated as in classical surfactants. [84,85]

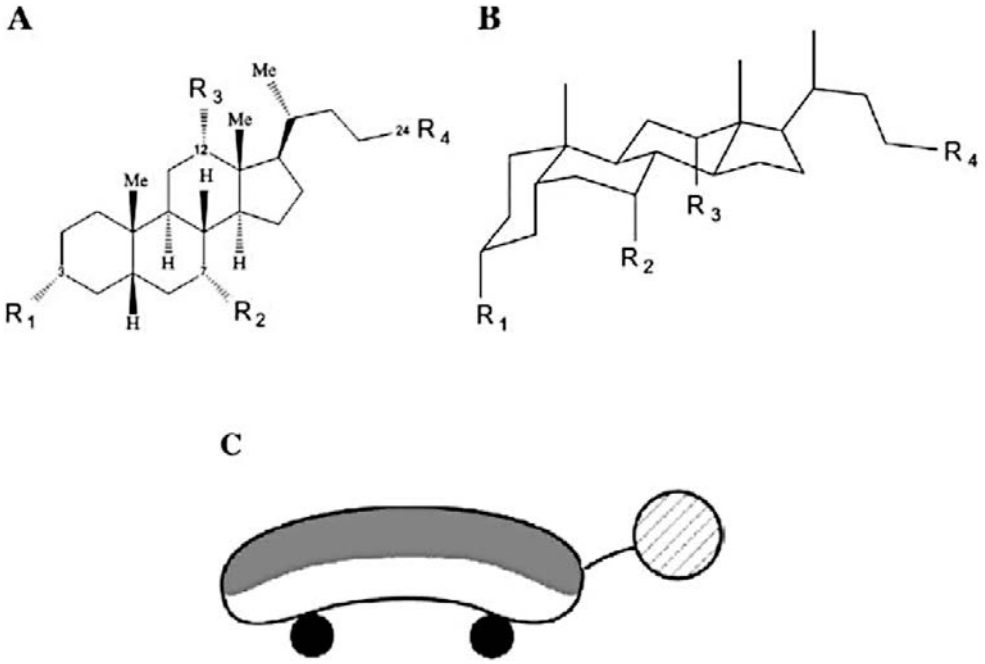

Fig.1.6: Bile salt chemical structure (A) (From R1 to R3 hydroxyl groups, R4 acidic group), three dimensional structure (B) and representation of a dihydro-bile salt (C). [85]

Table 1.4: Position and orientation of –OH groups in bile salts. [85]

Bile salt	Abbreviation	R1	R2	R3
Cholate	C	αOH	αOH	αOH
Deoxycholate	DC	αOH	αOH	H
Chenodeoxycholate	CDC	H	αOH	αOH
Ursocholate	UC	αOH	βOH	αOH
Ursodeoxycholate	UDC	αOH	βOH	H

The unique structure of bile salts can significantly impact on their aggregation behaviour. Compared to classical ionic surfactant, bile salts present smaller aggregation numbers of about one order of magnitude, typically $2<N_{agg}>15$ and the concentration range in which the aggregation process occurs is broader with respect to the classical surfactants. At 37˚C the critical micellar concentration (CMC) of a bile salts mixture, comparable to the one present in the intestinal tract, in a solution containing physiological concentration of electrolytes is 1-2 mM. [86]

1.4.2 Bile salts micellisation

The unique structure of bile salts gives rise to peculiar aggregation behaviour of these biosurfacants. In particular the hydroxyl groups and the acid group play an important

role in the bile salts aggregation. In fact, they create an intermolecular hydrogen-bonding network that contributes to the micelles formation and renders micelle aggregates more rigid. This aggregation driving force is complementary to the hydrophobic effect, which represents the main aggregation driving force. [85,86]

Several association models have been proposed for bile salts. Small proposed the "two step model" with the formation of small primary micelles, resulting from hydrophobic interactions between monomers, and the following aggregation of primary micelles in bigger secondary micelles through hydrogen bonding of hydroxyl groups. [87] Small's model for bile salts aggregation was also confirmed by simulation and NMR studies. [88–90] According to the "disk-like model" bile salts aggregate with their hydrophobic surface oriented towards the inner part of the aggregate and the hydrophilic surface toward the solution. The monomers have an alternating orientation to reduce electrostatic interaction between charged groups. [91] Another model was based on the crystalline structure (in solid state) of bile salts rather than on their solution state. Such model suggested the arrangement of monomers in helical structure, driven by polar interactions. The hydrophobic surfaces of the monomers are pointed to the extern, like in inverted micelles, and the inner part of is filled with cations surrounded by water molecules. A schematic representation of the three models is shown in Figure 1.7

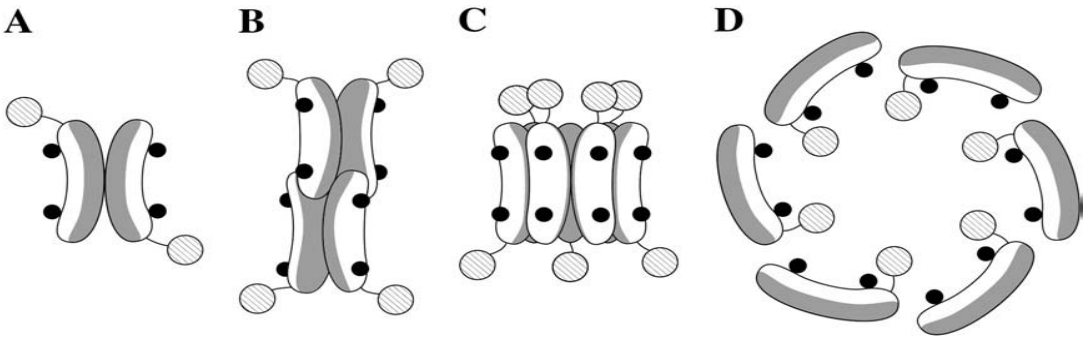

Fig.1.7: Representation of different models for bile salts micelles structure: A and B different primary micelles; B dislike micelle; C helical micelle. [85]

The value of bile salts CMC is strictly dependent on the bile salt structure, the number, location and orientation of hydroxyl groups. Furthermore, similarly to classical surfactants, the CMC value of a bile salt can also be significantly influenced by many external factors, such as solution pH, ionic strength and temperature. Normally higher ionic strength leads to the screening of charged groups favouring bile salts micellisation and therefore resulting in lower CMC values and higher aggregation numbers. [92,93] Bile salts monomers electrostatic repulsion can also be reduced by decreasing charges via pH control.

The temperature influence of the bile salts CMC value is very limited. Normally bile salts CMC shows a minimum value around room temperature and increases above room temperature. [85] Finally pH can also influence bile salts aggregation behaviour and CMC value. The impact of pH on bile salts association occurs when it impacts bile salts molecules ionization state. If the pH value is well above the pKa of the bile salts all the monomers in solution are ionized, but pH shift towards the pKa value yields the presence of undissociated monomers changing the species involved in the aggregation pattern and therefore impacting CMC. [84,94]

1.5 Impact of bile salts on drug absorption in the GIT

Bile salts are important components of gastrointestinal fluids. The presence of bile salts during the drug release from a solid dispersion system can influence the rate of drug release from the formulation and its dissolution. It has been shown that bile salts can improve solubilisation of poorly water-soluble drug in the gastro-intestinal tract. [95] The drug dissolution rate can be increased either via enhancing of the drug molecules wetting, through a decrease of the interfacial energy barrier between the drug molecules and the dissolution medium, or via an increase in the drug solubility due to the micellar solubilisation. [95] Generally the wetting effect predominates for bile salts concentration below the CMC, while the micellar solubilisation occurs at concentrations above the CMC. [96]

The potential role of bile salts in drug solubilisation in the GIT can also be related to their possible interaction with the polymeric carriers employed in pharmaceutical formulations. As already mentioned in this Chapter, the presence of polymer and bile salts in the dissolution medium can potentially lead to the occurrence of their interaction. Such interaction can result in the formation of aggregates that might play a role in the drug solubilisation *in vivo*. Therefore a characterisation of bile salts/polymeric carrier aggregation and its possible impact on the drug solubilisation and uptake in the GIT may provide new insights into the drug dissolution mechanism in the GIT.

1.6 Polymer-surfactant interactions

Polymer-surfactant interactions have been extensively studied in literature and mixture of polymer-surfactants are increasingly being employed in a wide range of applications. [97–103] An overview about polymer-surfactant interactions can be found in the following sections.

1.6.1 "Weakly" and "strongly" interacting systems

The most widely studied polymer-surfactant systems are mixtures of neutral polymers and ionic surfactants, which are referred as "weakly interacting" systems. The name refers to the weak hydrophobic interactions occurring between the polymer chains and the surfactant head groups that represent the predominant interactive forces. Weakly interacting systems containing anionic surfactants have been subject of most interest, while mixtures containing cationic or non-ionic surfactants and neutral polymers have attracted less interest, since they usually do not show the occurrence of significant polymer-surfactant interaction. [97] However, cationic micelles formed by cetyltrimethylammonium salts (CTAX) associate significantly with sufficiently hydrophobic polymers, like poly-propylene oxide (PPO) and poly(vinyl methyl ether) (PVME). [104] Furthermore studies on systems containing PPO and the non-ionic surfactant n-octyl β-D-thioglucopyranoside (OTG) have shown the occurrence of association between neutral micelles and polymer. [105]

Systems containing charged polymers and oppositely charged surfactants are referred as "strongly interacting" systems. In this case the association between mixture components is driven by electrostatic interactions. Nevertheless, hydrophobic interactions between surfactant and polymer chains are also present and can contribute significantly to interactive forces. [106]

The behaviour of polymer-surfactant mixtures is influenced by many factors and is strictly dependent on components structural features, such as polymer hydrophobicity, polymer molecular weight, surfactant charge, surfactant chain length, but can also be influenced by physical and chemical conditions, such pH and ionic strength. [107]

Both bulk solution properties and interfacial aspect of polymer-surfactant system have been largely investigated. [99,108] In this study only weakly interacting systems were investigated. The interactions between a model anionic surfactant, NaTC, and two neutral polymers, hydroxypropyl methylcellulose (HPMC) and polyvinylpyrrolidone (PVP), were studied. In most reported studies, polymers and surfactants with high purity and narrow

molecular weigh distribution were used. However, this is not the case for this project as its goal is to provide better understanding on the interactions of bile salts with pharmaceutical grade polymers which are used in oral pharmaceutical product under simulated physiology conditions.

1.6.2 Polymer-surfactant complexation

It is well known that surfactant molecules in aqueous solution aggregate to form micelles when their concentration is higher than critical micellar concentration (CMC). The dominant force driving for micellization is the gain in entropy attributed to the reduction of the contact area between surfactant hydrocarbon chains (hydrophobic surfaces) and water. This leads to the aggregation of hydrophobic groups in the interior core of micelles. [109]

When a surfactant is added to a polymer aqueous solution an aggregation process starting at a surfactant concentration lower than CMC, usually referred as critical aggregation concentration (CAC), can be observed. Above the CAC the association increases up to polymer saturation. As the polymer is saturated with surfactant micelles/monomers, free surfactant micelles formation occurs (Fig.1.8). [110]

CAC and CMC surfactants values depend on the nature of polymer and surfactant, and are less dependent on molecular weight (MW) of the polymer if the MW is over 4kDa. CAC is insensitive to polymer concentration, while CMC increases as polymer concentration is increased. It is generally agreed that polymer-surfactant aggregation number are smaller than those of pure surfactant micelles. [111–113]

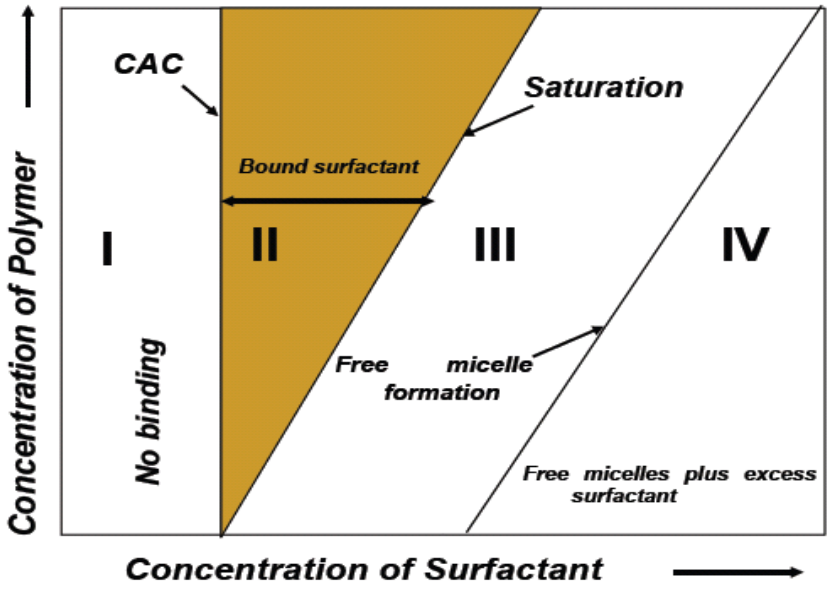

Fig.1.8: Solution phases in a surfactant-polymer system [114]

1.6.2.1 Neutral Polymers

Surfactant-neutral polymer interactions may occur by cooperative binding or association of individual surfactant molecules on polymer chains, or by the formation of surfactant micelles along the polymer chains. Usually the binding model is preferred for polymers with hydrophobic groups, while the later approach is more representative for hydrophilic polymers. [110] For polymer-surfactant solutions containing neutral hydrophilic polymers, the formation of surfactant-polymer aggregates can be described by the widely accepted "pearl-necklace" model (Fig. 1.9). The surfactants form micellar-like clusters (as the pearls) along the polymer structure. It seems likely that the micellization process is polymer-induced, with the polymer acting as a seed for the aggregation process. [115]

Fig. 1.9: Schematic representation of "pearl-necklace" model" of surfactant-polymer association. [116]

For hydrophobic polymers the association with surfactant is driven by strong hydrophobic interaction between individual surfactant molecules and polymer molecules, according to the cooperative binding model. Such interactions are particularly strong for hydrophobically modified polymers, such as hydrophobically modified non-ionic cellulose ester (HM-EHEC), where hydrophobic groups are covalently bonded to the polymer chains. [110]As reported in the review of K.C. Tam and Wyn-Jones, when hydrophobically modified polymers are dissolved in water, there is evidence of both intra- and intermolecular associations of the hydrophobic groups. With the addition of sodium dodecyl sulphate (SDS) the CAC is reached and surfactant micelles are hydrophobically attached to pendant alkyl groups. As more SDS is added, alkyl chains cross-link via the micelles bound. Further addition of SDS results in the formation of dissociated polymer surfactant complexes. At high SDS concentration, in fact, the ratio of bound micelles to pendant chains increases causing the network breakdown (Fig. 1.10). [117]

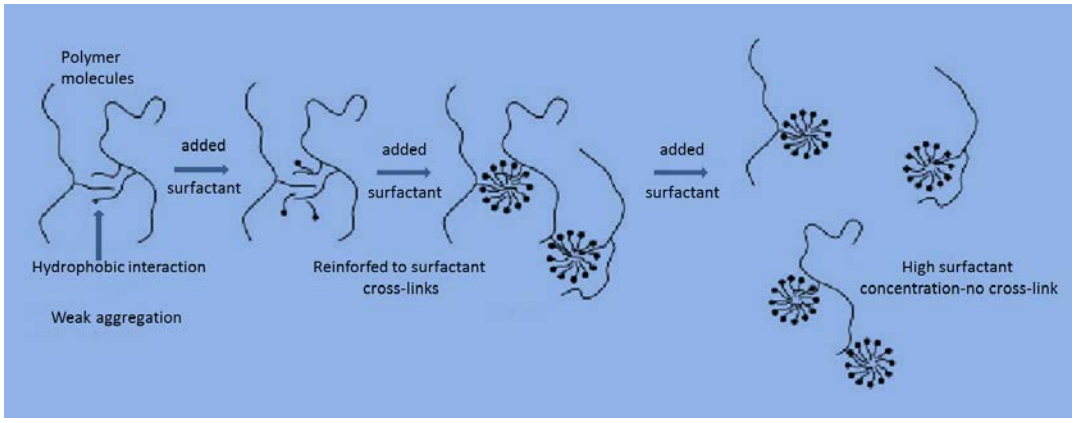

Fig.1.10: Structures occurring at different stages for hydrophobically modified-polymer-surfactant aggregation. Rearranged from reference 108.[110]

1.6.2.2 Charged Polymers

Usually interactions between polymers and surfactants having similar charges are minimal, due to the electrostatic repulsion. [115] In the case of oppositely charged polymer-surfactant systems, cooperative binding occurs above the CAC. [106] At very low surfactant concentration, the solutions are clear, since the polymer-surfactant complex is completely soluble. As further surfactant is added, the solution becomes turbid and cloudiness can be accompanied by phase separation or precipitation. This is due to the reaching of the charge neutralization point, when the concentration of charged surfactant molecules approaches the number of charged groups on the polymer chains. As the surfactant concentration is further increased, more surfactant molecules are bound to the polymer chains and the excess of charge on the complexes promotes solubilisation and the system turns into a single phase. Usually higher polymer concentrations promote phase separation or precipitation. [113,118]

Polymer/surfactant systems interaction models illustrated in this and previous sections are generally accepted. However, the relationship between the structure of surfactant and polymer and their interaction, as well as the interaction driving forces, are still argument of debate in literature. Moreover, multiple factors can impact the occurrence and the pattern of polymer/surfactant aggregation. The main factors impacting the association behaviour of polymer/surfactant systems are reviewed in the following sections.

1.6.3 Factors influencing polymer-surfactant association

As already mentioned in this Chapter, the interaction between polymers and surfactant is affected by different physical and chemical factors. [107] An overview of the

possible factors affecting the occurrence and the features of interactions between polymers and surfactants is given in this section.

1.6.3.1 Polymer Hydrophobicity

Polymer hydrophobicity influences both neutral and charged polymers-surfactant interactions. For example, for non-ionic polymers the interaction with a given anionic surfactant progresses according to the order polyvinyl alcohol (PVA) ≤ polyethylene oxide (PEO)< methylcellulose (MC) < polyvinyl acetate (PVAc) < polyvinyl pirrolidone (PVP), while for cationic surfactant the order is PVP<PEO<PVA<MC<PVAc. [119] In such systems the main driving forces for interactions between polymers and surfactants are the hydrophobic interaction. Consequently, the more hydrophobic is the polymer, the stronger is the association with the surfactant. In the case of ionic polymers, hydrophobic effect may be as important as electrostatic attraction. Therefore polymer hydrophobicity can influence the polymer/surfactant interactions.

A rheological study carried out by Thuresson et al investigated the difference between ethyl-(hydroxyethyl) cellulose (EHEC) and the hydrophobically modified analogue (HM-EHEC) in the interaction with SDS. [120] Rheological results revealed polymer/surfactant interactions occurrence for both polymers. However, while HM-EHEC interacted with SDS at very low surfactant concentrations, the binding between EHEC and SDS occurred at much higher SDS concentrations.

A series of papers by Anthony and Zana focused on the effect of polymer hydrophobicity on polyelectrolyte-oppositely charged surfactant systems. Their study showed that the main interaction between hydrophilic polymers and surfactant is characterised by electrostatic nature. However, if increasing polymer hydrophobicity by changing the number of carbons in the polymer alkyl group, hydrophobic forces contribution to the polymer-surfactant interactions became comparable to the electrostatic force one. [121] The further increase of polymer hydrophobicity resulted in the formation of polyelectrolyte hydrophobic micro-domains. In this case the surfactant binding onto the polymer was not cooperative. The bound surfactant simply lead to the swelling of pre-existing micro-domains, but no formation of new hydrophobic micro-domains was obtained. In the case of weakly hydrophobic polyelectrolytes, the binding with the surfactant was still not cooperative, but new mixed micro-domains were formed. [122]

1.6.3.2 Polymer Molecular Weight

The interaction between polymer and surfactant is significantly influenced by polymer molecular weight. The study carried out by Mészáros et al. showed that the PEO-SDS system behaviour can be divided in three molecular weight (MW) ranges. With MW below 1000 Dalton, no complex formation was observed, and the CAC corresponded to the CMC. For PEO with molecular weight from 1000 to 8000 Dalton, polymer and surfactant interactions occurred and the CAC decreased with increasing the polymer molecular weight. When the molecular weigh was higher than 8000 Dalton the interaction between polymer and surfactant was not dependent anymore on the polymer molecular weight, and the CAC was constant. [123] Thus, it can be argued that a minimum polymer molecular weight is possibly required for the polymer-surfactant complexation to occur. However such molecular weight dependence of the polymer-surfactant interactions may no longer applicable for polymers with extremely high MW values.

1.6.3.3 Surfactant Charge

As already described, neutral polymers usually interact more favourably with anionic surfactants than with cationic and uncharged surfactants. Nevertheless cationic and uncharged surfactants show interactions with hydrophobic polymers, but do not associate with hydrophilic polymers. The surfactant head-group charge can influence the interaction with the polymer. The study by Brackman and Engberts on the interaction between n-dodecyldimethylamine oxide (DDAO) and a series of polymers, (poly(vinylmethylether) (PVME), poly(propylene oxide) (PPO), and poly(ethy1ene oxide) (PEO)) revealed an increase in the micelles stabilization by the polymer when the surfactant average charge was increased. This effect was likely due to the reduction of the electrostatic repulsion by the polymer association. [124]

The surfactant head-group charge distribution has also been shown to influence polymer-surfactant interactions. A study on the interaction between sodium alkyl sulfates (C_nSO_4)/sodium alkyl sulfonates (C_nSO_3) and PEO showed differences in the interaction of the two surfactant with the polymer, as sodium alkyl sulfonates were seen to interact more weakly than their sulfate analogs. Such difference was attributed to the different charge distribution in the surfactant head-groups. [125]

1.6.3.4 Surfactant Chain Length

In homologous series of surfactants the value of CMC decreases with increasing the number of carbons in the surfactant chain length. [113] Taylor et al. studied the effects of surfactant chain length on polymer-surfactant interaction. In their studies, the interactions of sodium poly(styrene sulfonate) (NaPPS) with a series of CnTABs were studied, where n is the number of carbons in the hydrocarbon chain. [126] The study showed that, as for CMC, the CAC values decrease when the number of carbon in the surfactant chain length increases. A similar study was carried out by Wallin and Linse. Their investigation on oppositely charged surfactant-polymer mixtures showed higher surfactant chain length results in a decrease of both CAC and CMC values, with CAC decreasing faster than CMC. [127]

1.6.3.5 Addition of salts

The presence of salts in an ionic-surfactant solution causes the reduction of electrostatic repulsion between surfactant charged head groups. Such effect promotes the micellization and usually leads to decreases on CMC value. [110] Furthermore, the presence of salts in a polyelectrolyte solution can influence the polymer behaviour, since counterions can neutralise polymer charges. Thus, the addition of salt to a polymer-surfactant solution can have strong influence on the aggregation behaviour of the system. [126]

Goddard and Hannan studied the influence of salt addition in the interaction between cationic derivative of hydroxyethyl cellulose and a series of anionic surfactants, showing that the added salt does not influence significantly the formation of polymer-surfactant aggregates and their precipitation. Only when the added salt influences the solubility of one of the components involved in the interaction, an effect of the salt addition on the interaction occurrence can be observed. Nevertheless, many surfactant–polymer systems may be influenced by salt addition to the solution, but opinions about the salt effect on CAC are divided in the literature. [113]

1.6.3.5 pH

Polyelectrolytes are usually sensitive to pH, as their charge, and consequently their solubility and aggregation features, can change according to the solution pH. Thus, in the case of polyelectrolyte-surfactant systems, pH represents a crucial factor for the system behaviour and for the formation of polyelectrolyte-surfactant aggregates. [113]

The study of the system composed by chitosan, a cationic biopolymer, and SDS, showed pH variation effect on the chitosan-SDS interaction. At pH=3, chitosan was highly

soluble in aqueous solution, and isothermal titration calorimetry (ITC) measurements showed the occurrence of strongly SDS-chitosan interaction. At pH=7, chitosan was not soluble and most of its positive charges were neutralised, thus the electrostatic interaction with SDS was weaker and no evidence of strongly binding between SDS and chitosan was found. [128]

1.7 Characterisation of polymer-surfactant interactions

This section reviews the experimental techniques that can be used for the characterisation of polymer-surfactant systems. These include surface tension measurements, nuclear magnetic resonance (NMR), rheology, conductivity measurements, light scattering techniques, fluorescence, isothermal titration calorimetry (ITC). Microscopy techniques can also be employed to characterise polymer/surfactant aggregates morphology.

Surface tension measurement is one of the most commonly used technique for the study of polymer-surfactant systems, as it provides good indication of the intermolecular interactions occurring in the bulk phase. [113] For weakly interacting systems, a typical surface tension profile is shown in Figure 1.11. The point T_1 corresponds to the onset of the interaction between the polymer and the surfactant (CAC). At T_2 the polymer is saturated with surfactant. T_3 corresponds to the CMC and above this concentration the surfactant forms free micelles. [129] In the dilute region ($<T_1$) the surface tension of the polymer/surfactant systems is below that of the surfactant solution, indicating higher surface activity of the polymer/surfactant systems compared to the surfactant alone. [99]

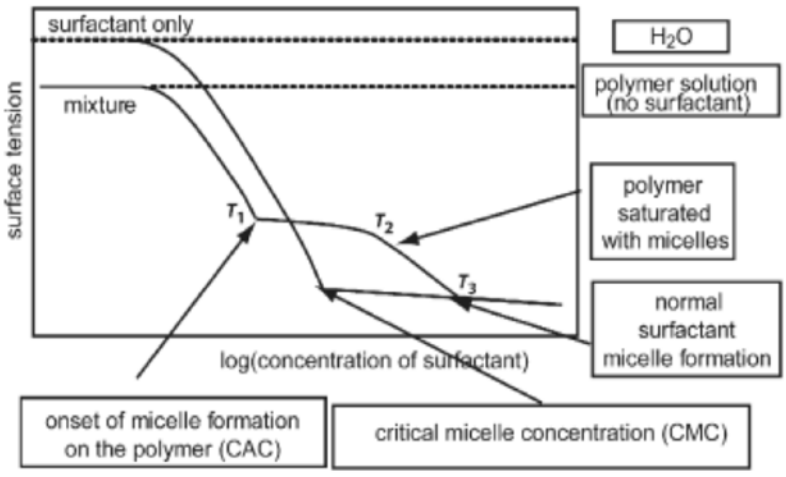

Fig. 1.11: Representation of surface tension profile for polymer-surfactant weakly interacting systems. [113]

In the case of strongly interacting systems, surface tension profiles are more complex and cannot be described by the simple model illustrated in Figure 1.11. The different nature of the interaction between the polymer and the surfactant influences the surface tension profile and can result in the presence of sharp peaks instead of smooth transitions as shown in Figure 1.12.

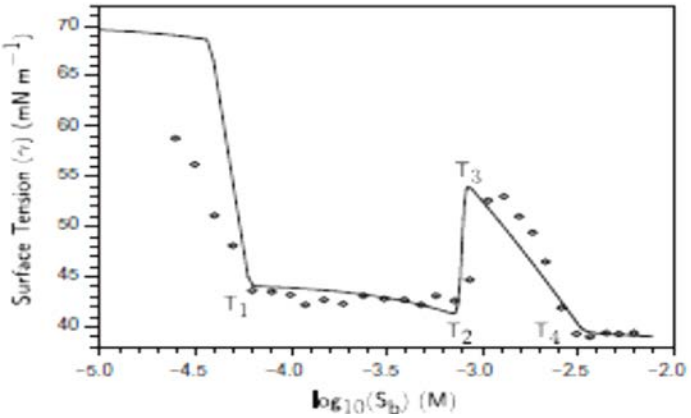

Fig. 1.12: Surface tension profile of the strongly interacting system C_{14} TAB/NaPSS system. [129]

Figure 1.12 represents the surface tension profile of the strongly interacting system tetradecyltrimethylammonium bromide (C_{14} TB) and sodium polystyrene sulfonate (NaPPS). In this case a tension peak (T_3 in Figure 1.12.) is observable. The point T_1 corresponds to the polymer-surfactant monomer saturation at the surface, points T_2 to the formation of the polymer-micelle complex in the bulk, while the peak T_3 represents the saturation of the polymer-micelle complex. Finally T_4 corresponds to the CMC. Each of the critical transition points occurs at surfactant concentrations corresponding to a change in the system, and the surface tension profile depends on the relative stability of the polymer-micelle complex. [129]

NMR has been widely used for the study of physical chemistry of surfactants and polymer-surfactant systems. [130] NMR signal is sensitive to the chemical local environment, thus can be used as a probe for the formation of complexes and aggregates study. [131] Chemical shift measurements provide information about the chemical environment changes and have been used to probe surfactant-polymer aggregations. [132,133] Another NMR technique widely employable for studying polymer surfactant interaction is NMR self-diffusion measurements. The reported studies in literature have shown that self-diffusion NMR technique represents a powerful tool to investigate the influence of polymer addition on surfactant aggregates structure. [134]

Light scattering techniques can provide useful information firstly about the polymer/surfactant interaction occurrence, secondly can be used to characterise the polymer/surfactant aggregates features, in particular aggregates size. As reported in literature, light scattering techniques have previously been used for the characterisation of polymer/surfactant systems, for both weakly and strongly interacting systems. [100,135,136] Light scattering techniques are highly sensitive and non-invasive methods. The occurrence of scattering by the sample is the indication of the formations of "scattering entities". Furthermore light scattering is sensitive to changes in the conformation of scattering entities and can therefore provide information on the occurrence of possible interactions between the species present in solution. [136]

Small angle neutron scattering (SANS) has also been shown to be an effective approach to investigate the occurrence of polymer/surfactant interaction. [137–140] The first neutron studies on polymer/surfactant systems were performed by Cabane et al on polyethyloxide (PEO)/SDS systems. The use of SANS allowed the determination of size, shape and distribution of the surfactant aggregates within the polymer/surfactant system. [141,142].

Imaging techniques such as transmission electron microspcopy (TEM) and cryogenic transmission electron microscopy (cryo-TEM) are also routinely used characterization method for studying colloidal systems including polymer/surfactant aggregates. In cryo-TEM, the samples are vitrified and imaged in the frozen-hydrated state. Cryo-TEM represents an effective tool to determine size and shape of colloidal aggregates. [143] Few studies have been reported in which the used of cryo-TEM technique was aimed to clarify the structure of polymer/surfactant aggregates. [144,145] Moreover cryo-TEM has been employed for the *ex vivo* characterization of intermediate phases of human intestinal fluids (HIFs) produced during lipid digestion. Cryo-TEM allowed the imaging of micellar and vescicles species present in HIF in different stages of lipolysis, highlighting the possible role of such colloidal species in lipid digestion and poorly water soluble drug soluble drug solubilisation in the GIT.[146] Therefore Cryo-TEM technique represents a powerful tool for the investigation of intestinal and simulating intestinal colloidal phases.

In this study surface tension and NMR technique were chosen as the primary methods to investigate the occurrence of polymer/NaTC interactions. Light and neutron scattering techniques were also used as principle methods to characterise the complexes obtained from the aggregations of bile salts and hydroxypropyl methylcellulose (HPMC) and

polyvinylpirroldone (PVP), two model polymers used as the matrix materials of the solid dispersion formulations. Cryogenic transmission electron microscopy (Cryo-TEM) was also used to visualise polymer/NaTC aggregates. The detailed technical information on each technique can be found in Chapter 2.

1.8 Polymer-bile salts interaction during the dissolution of solid dispersions

As described by the previous sections of this Chapter, polymer/bile salts systems have widely been investigated. This project focused on the study of the interactions of bile salts and the polymers used as solid dispersion matrices during the dissolution process of a solid dispersion formulation. In particular for two of the four polymeric carriers employed to prepare solid dispersion in this study, their possible interactions with bile salts was investigated. HPMC and PVP polymers were used as model polymeric carries to study the interaction of polymeric carriers with bio-relevant surfactant in simulated intestinal fluids. Such polymers were chosen because they are commonly employed in pharmaceutical products and in particular in solid dispersions preparation. [147–149] Chemical and physical features of HPMC and PVP can be found in Chapter 2 (sections 2.2.1.1 and 2.2.1.2).

Interactions of HPMC with SDS, cetyltrimethylammonium bromide (C_{16}TAB), sodium cholate (NaC), and NaTC were previously investigated. [150] HPMC can form polymer/surfactant complexes with the studied surfactants. Also for PVP different studies have been performed to determine its ability to interact with surfactants. In particular PVP/SDS system represents one the most studied polymer surfactant systems, with many scientific contribution published about this system. [98,112,113,117,119,151,152] The significant impact of PVP on the SDS self-assembling pattern was shown in many of the cited studies, and can be considered an indication of the occurrence of PVP/SDS interaction.

1.9 Principal aims of the project

The use of solid dispersions for the delivery of poorly water-soluble drugs has been extensively studied, but marketed products using such formulation approach are still very limited. In literature, most research efforts were focused mainly on the improvement of solid dispersion physical stability and dissolution enhancement. Less attention has been paid to

the solid dispersion behaviour in human intestinal fluids and in particular to the possible interactions that may occur between the different components of the intestinal fluids and the components of the solid dispersion formulation. The main aim of this study was ***to investigate the behaviour of solid dispersions in simulated intestinal fluids, to enrich the molecular understanding of the physicochemical interpretation of the behaviour observed and to predict the possible significance of such behaviour in drug absorption in GIT***. In order to mimick the intestinal environment Fed and Fasted state simulated intestinal fluids were used in this study. The project was composed of 4 main stages.

1. Preparation and solid-state characterisation of spray dried solid dispersions by using different carriers and model drugs. Dissolution performance of obtained solid dispersion was assessed in different media and firstly correlated to the drug physical state in the formulation. This part of the project is described in Chapter 3.

2. In order to correlate the dissolution behaviour of the spray dried solid dispersions to the behaviour of the polymeric carriers in the media employed, the possible aggregation of the polymeric carrier with model bile salts, sodium taurocholate (NaTC), was investigated. The interaction between the polymeric carrier and NaTC was studied by NMR and interfacial tension techniques. The obtained data are described in Chapter 4.

3. Polymer-NaTC aggregates obtained in the different media were characterised by the use of light and neutron scattering and transmission electron microscopic techniques. The studies were carried out also in the presence of drug to investigate the possible encapsulation of the drug in polymer-surfactant aggregates and the possible role of such complexes in the drug solubilisation. This part of the project is described in Chapter 5.

4. In the final stage of the project the possible impact of polymer-NaTC aggregates on the drug absorption in the intestinal tract was evaluated by using Caco-2 cells model. Both drug uptake and transport experiments were performed. The biological part of the project is reported in Chapter 6.

Chapter 2. Materials and Methods

2.1 Introduction

The use of hydrophilic polymers has widely been researched as an approach to deliver poorly water-soluble drugs. The choice of the carrier and the preparation method are key factors to achieve a successful formulation. Thorough solid-state characterisation is essential for predicting the physical states of the drug in the formulation and the physical stability of the formulation. [153]

Spray drying technique is one of the commonly applied processing techniques for the production of solid dispersion formulations and is the chosen preparation method in this project. A wide range of characterisation techniques were used to characterize the spray dried solid dispersion formulations, as well as the raw materials used for their production and the corresponding polymer-drug physical mixtures. These include scanning electron microscopy (SEM), powder X-Ray diffraction (PXRD), differential scanning calorimetry (DSC), thermogravimetric analysis (TGA) and Fourier Transform Infrared-Attenuated Total Reflectance (ATR-FTIR). The *in vitro* dissolution behaviour of the obtained spray dried formulations and relative physical mixtures were studied under simulated Fed and Fasted state intestinal conditions. In order to further understand the mechanisms of the *in vitro* drug release behaviour of the spray dried solid dispersions, the molecular interactions of formulation ingredients and the components of the simulated intestinal fluids were investigated. Several techniques were employed to investigate the possible occurrence of interaction between the polymeric carriers used and the components of the simulating intestinal fluids. These include ^{1}H and self-diffusion NMR spectroscopy, surface tension measurements, light and neutron scattering techniques and cryogenic electron transmission microscopy (cryo-TEM).

In the last stage of the project, Caco-2 model cells were used to study the impact of the polymers used in the solid dispersion formulation and the components in the simulated intestinal fluids on the uptake and transport of the model drugs. The key focus of this chapter is to lay the therotical foundations of the methodologies used and the background information of the materials used in the project.

2.2 Materials

2.2.1 Model drugs

Slow drug dissolution is the limiting step for BSC class II drug clinical use. Therefore BSC class II drugs were chosen in this study with the aim to investigate the effect of the formation of solid dispersions on the drug solubilisation. Three different BSC class II drugs (poorly soluble and highly permeable) drugs with different log P values, piroxicam, fenofibrate and griseofulvin, were used in this study. Piroxicam has been selected for its low water solubility (Table 2.1) and its pH sensitivity, in order to investigate the effect on the different pH used in the simulated intestinal fluids on ionisable drugs. Chemical structures, chemical and physical properties of the model drugs are summarised in Table 2.1. Dose/ solubility ratio is referred to an intestinal medium volume of 250 ml (dimensionless).

Table 2.1: Model drugs structure and properties

	Piroxicam	**Fenofibrate**	**Griseofulvin**
Structure	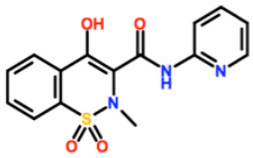	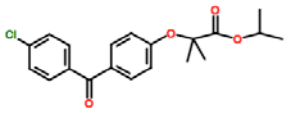	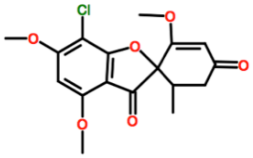
Melting point (°C)	198-200 [154]	80.2 [27]	220.4 [152]
Water Solubility (mg/ml) at 25°C	0.007 [4]	0.0001[155]	0.015 [156]
Log P value	1.8 [157]	5.1[158]	1.77 [159]
Dose (mg)	20 [4]	200 [160]	500 [4]
Dose/solubility ratio (unitless)	1.14[161]	8000	133.33 [161]
pK_a	1,86, 5,46 [6]	-	-

2.2.2 Polymeric carriers

2.2.1.1 Hydroxypropyl methylcellulose (HPMC)

HPMC, also known as hypromellose, is one of the most used amorphous polymer in pharmaceutical formulation. It is a water-soluble cellulose derivative and it can be used as film-coating agent, tablet binder, thickening agent and controlled-release matrix. [162]

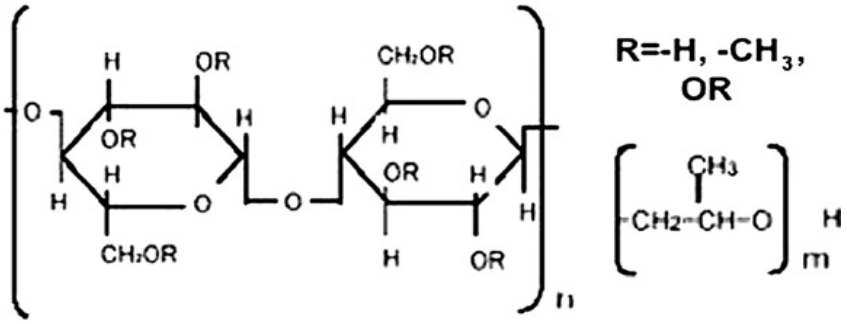

Fig.2.1: Hydroxypropyl methylcellulose chemical structure [162]

The application of HPMC as carrier in drug delivery systems (in most cases modified release formulations) is mainly due to its high swellability and the ability to form a viscous layer around the drug delivery device, when in contact with aqueous media. [163] The drug release mechanism is assumed to be drug diffusion through the hydrated layer for soluble drugs and hydrated layer erosion for poorly water-soluble drugs. [164]

In this project HPMC Methocel® K4M was used to prepare spray dried solid dispersions. According to the producer nomenclature, K is indicating the HPMC chemistry (R group is $–OCH_3$), which is shown in Figure 2.1. The number 4 identifies the viscosity of the polymer in milli-pascal*seconds (mPa*s), measured at 2 % concentration in water at 20 °C. Physical properties of HPMC K4M are summarised in Table 2.2. [165]

2.2.1.2 Polyvinylpirrolidone (PVP)

PVP is an amorphous synthetic polymer consisting of 1-vinyl-2-pyrrolidone groups (Fig. 2.3). PVP is highly water soluble and is widely used in biomedical applications, personal care products as thickening agent and in formulations as binder in granulation and as coating agent. [166] PVP is characterised by high hygroscopicity, which is due to the presence of carbonyl group that can form hydrogen bonding with water. [167]

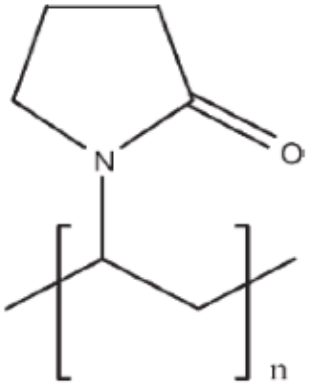

Fig.2.2: Chemical structure of N-vynilpyrrolidone monomer unit.

The amorphous nature and the high water solubility make PVP a possible candidate as polymeric carrier in solid dispersions. In particular it has shown to have the ability to increase the apparent solubility of poorly water soluble APIs and to reduce their recrystallization tendency in the formulation during storage. [168]

There are different grades of PVP homopolymers which are classified according to their viscosity in 1% w/v of PVPs solution by K values via Fikentscher's equation (Kibbe, 2002). A higher K value is related to a higher viscosity of the PVP solution. In this study PVP K 30 was used. Its key physical properties are reported in Table 2.2. [166]

2.2.1.3 Hydroxypropyl methylcellulose Acetate Succinate (HPMCAS)

HPMCAS is the partially esterified derivative of HPMC (Fig. 2.3). It has been developed as enteric coating material, for both regular enteric coating and sustained release formulations. [169] More recently HPMCAS has been studied as possible carrier in solid dispersion formulations prepared via spray drying or hot melt extrusion, leading to a significant enhancement of the dissolution of poorly water-soluble drugs. [170] Furthermore, crystallization inhibition effect on amorphous drugs obtained using HPMCAS has been reported to be higher than the ones obtained by using cellulose derivative, suggesting HPMCAS being a good solid dispersion formulation carrier. [171]

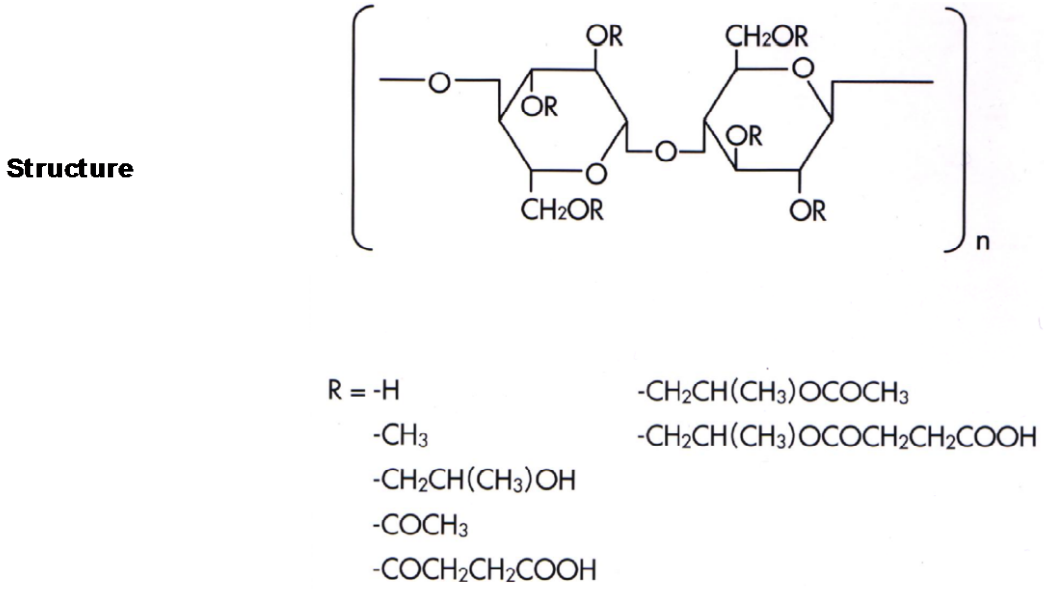

Fig.2.3: Chemical structure of HPMC-AS

According to the substitution ratio of acetyl and succinoyl groups in the polymer, HPMCAS is classified in different grades that dissolve at different pH values. In this study HPMCAS LF grade was used. This HPMCAS grade can be easily solubilised at pH values higher than 5, such as common buffers and simulated intestinal fluid used in this study (for fluids pH and composition refer to Chapter 3, section 3.2.1). Physical properties of HPMCAS LF are shown in Table 2.2. [172]

2.2.1.4 Polyvinylpirrolidone-Vinyl Acetate (PVP-VA 64)

PVP-VA is a copolymer of PVP produced by free-radical polymerization of 6 parts of n-vinylpyrrolidone and 4 parts of vinyl acetate, which yields a water-soluble copolymer having the structure showed on Figure 2.4. [166]

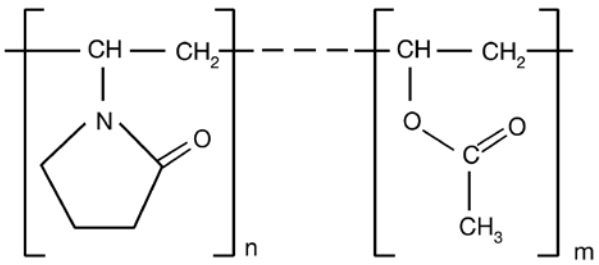

Fig. 2.4: Chemical structure of PVP-VA monomer unit [166]

Similar to the PVP homopolymer, PVP-VA 6:4 is mainly used as a binder in the granules and tablets production, as film forming agent for coating and as matrix material for

solid formulation. Due to the modification with vinyl acetate groups, PVP-VA is characterized by lower hygroscopicity. PVP-VA was chosen for this study to investigate the impact of the derivatization with vinyl acetate groups on the polymer behaviour in simulated intestinal media. The presence of the functional groups increases the hydrophobicity of the polymer, which can impact its interaction with the components of the dissolution media and consequently the drug solubilisation and release from the solid dispersion formulation. The commercial grade of PVP-VA used in this study is Kollidon® VA 64, where 64 indicates the mass ratio of the two monomers, N-vinylpyrrolidone and vinyl acetate. Key physical properties of the polymer are provided in Table 2.2. The sourcing of raw materials employed in this study is summarised in Table 2.3.

Table2.2 Physical features of polymeric carriers

Polymeric Carrier	Molecular Weight	Viscosity , 1%, 20°C, mPa*s	T_g (°C)
HPMC	86000 Mn	3000-5000	186
PVP	44000-54000 Mw	5.5-8.5	168
HPMC-AS	18000 Mw	3	120
PVP-VA	15000-20000 Mn	≈2	106

Table 2.3: Sources of materials employed in this study

Material		Source
Drugs	Piroxicam	Gattefosse'
	Griseofluvin	Sigma Aldrich
	Fenofibrate	Sigma Aldrich
Carriers	HPMC-KM4M	Colorcon
	PVP-Kollidon 30	BASF
	HPMC-AS	Shin-Etsu Chemical Co, Ltd
	PVP-VA	BASF
Chemicals for buffers preparation	Sodium hydroxide	Sigma Aldrich
	Sodium chloride	
	Sodium dihydrogen phosphate dihydrate	
	Glacial acetic acid	
Solvents	Ethanol absolute	Sigma Aldrich
	Methylene Chloride	
	Methanol	
	Acetonitrile HPLC grade	Fisher Scientific
Chemicals for simulating intestinal fluids preparation	Sodium Taurocholate, 99%	Prodotti chimici e alimentari SPA
	Lecithin, from egg yolk	Acros Organics
NMR and neutron experiments	Deuterium oxide, 99%	Apollo Scientific

2.3 Experimental methods

2.3.1 Spray Drying

Spray drying is the process that transforms a liquid feed into dried particles by spraying the feed into a heated drying gas (either being air or nitrogen). Schematic representation of the spray drying process is shown in Figure 2.5. The process involves three main steps. The first step is the atomization of the liquid feed by a nozzle atomizer. In the second step evaporation of solvent from the atomized droplets is achieved by their exposure to a drying gas in the drying chamber, under controlled temperature and airflow conditions. In the final step the resulting dried particles are separated from the drying gas in the cyclone and collected in a receiving vessel. The three phases and the operational parameters in which they are performed have significant impacts on the properties of the final product. [45]

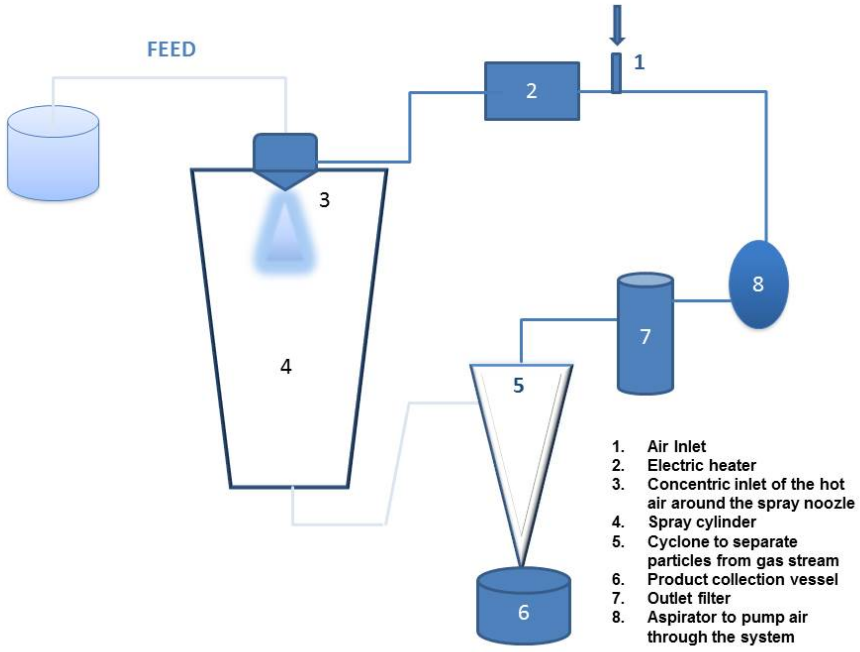

Fig.2.5: Schematic representation of spray dryer

The atomization is the most important step of the spray drying process. In order to break up the liquid bulk in individual droplets, energy is needed. Depending on the type of energy used to achieve atomization, atomizers can be classified in 4 different main categories: centrifugal, pressure, kinetic and sonic. [173] According to the mutual orientation of the drying air system and the atomizer, it is possible to have three different "air-droplet contact systems": cocurrent dryers, counter-current dryers and mixed flow dryers (Fig 2.6).

In the cocurrent systems (most commonly used), the droplets are sprayed in the same direction as the heated air. In this kind of dryers the droplets meet the air at the highest temperature causing rapid surface evaporation and providing safe conditions for heat-sensitive materials for the rapid exposure to the heat flow. In the counter-current dryers, the atomized droplets and the air pass through the dryer in the opposite direction, as the air is supplied from the bottom of the dryer. This system is not suitable for heat-sensitive materials as the droplets meet the air stream when it has already passed part of his path loosing part of its heat. Thus the wet droplets hit the coldest air, while the drying is finished at the highest temperature. In the mixed flow method, the nozzle is positioned at the bottom of the drying chamber, forcing the particles to move upwards when the air flow coming from the opposite direction overcomes the gravity of the particles. [174]

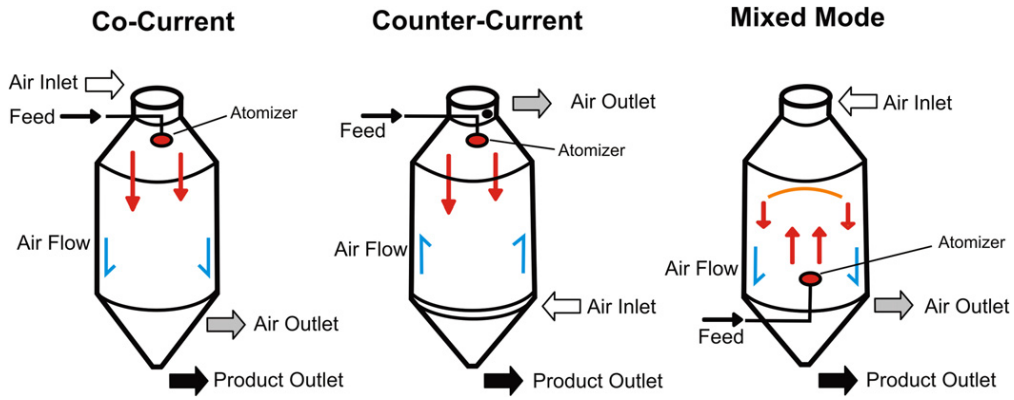

Fig. 2.6 Typical product-air flow patterns in spray dryers [175]

In this study, spray drying technique was applied for the preparation of microparticles using a Buchi Mini-Spray dryer B-290 (BUCHI Corporation, New Castle, USA) equipped with dehumidifier B-296. The atomization of the feed is obtained using a pressure atomizer with nozzle diameter of 0.7mm. A cocurrent product-air flow was applied. Details about the experimental parameters are described in Chapter 3 (section 3.2.2).

2.3.2 Scanning Electron Microscopy (SEM)

SEM is one of the most commonly used electron microscopy technique for studying the morphology of the materials. It based on the use of a high energy electron beam that is scanned over the specimen surface. [176] The signal generation is a result of the interactions between the incident electron beam and the atoms in the sample, which are electronically

detected and amplified. The production of the electron beam can be obtained heating a metallic filament (normally tungsten) or using cold cathode emitters. Different signals from the specimen can be collected such as secondary electrons, backscattered electrons, light emission, specimen current, Auger electrons and X-Ray radiations. Each signal is collected by a proper detector and can provide different information about the specimen when fed to the monitor. The secondary electron signal normally allows the observation of the sample topography, while by the use of some of the other signals produced it is possible to obtain structural information about the specimen. [177]

SEM represents a powerful tool to image solid dispersions formulations and investigate their morphology. [178] In particular for spray dried microparticles it allows the study of the particles shape, size and heterogeneity and can also image the presence of drug crystals in the formulation. [35]

2.3.3 Powder X-Ray Diffraction (PXRD)

PXRD is a powerful technique for the elucidation of crystals and molecular structures. PXRD is commonly applied to characterize pharmaceutical materials in order to study their crystal structure, which can be identified from the material diffraction pattern. [179]

The diffraction of X-Ray by a crystalline material is the result of the atom periodicity in the crystal lattice, thus every deformation of the crystal lattice, that affects the molecular arrangement of the investigated material, causes changes in the XRD pattern. The interaction between the incident X-Ray beam and the crystalline structure is defined by Bragg`s law

$$n\lambda = 2d \sin\theta \qquad \textit{Eq 2.1}$$

where λ is the wavelength of the incident X-Ray beam, n is the order of the diffracted beam, d is the interplanar distance between diffracting planes or atoms, and θ is the incident angle of the X-Ray beam. The positions of the peaks in the diffraction pattern are defined by the interplanar spacing between the set of diffracting planes. The interplanar spacing changes are inversely proportional to the changes in sine θ, thus changing θ different d values are obtained. The interplanar distance changes affect the peaks position and intensity in the XRD pattern (plot of intensities versus the detector angle 2 θ), that is unique for each individual crystals. [180]

Normally, the transition from a crystalline to an amorphous solid form can be related to the loss of distinct P-XRD peaks in the pattern and the appearance of a “halo” pattern. P-

XRD can be a useful tool for characterisation of amorphous and non-crystalline solids and particularly for the study of the formulation process effect on the raw drug crystallinity in the pharmaceutical field. [181] Powder X-Ray Diffraction measurements were performed using a Xtra X-Ray diffractometer (Thermo ARL, Thermo Scientific, Waltman, MA). Details about experimental parameters are described in Chapter 3 (Section 3.2.5)

2.3.4 Differential Scanning Calorimetry (DSC)

Conventional DSC is the most commonly used thermal analysis technique for the characterization of pharmaceutical materials. It provides both qualitative and quantitative information from energy and temperature associated to the thermal events the sample undergoes, when a cooling or heating signal is applied. There are two types of DSC instrument, power compensation and heat flux. In power compensation instruments two separated furnaces for the sample and the reference are used. The two furnaces are heated and the power supplied, to maintain a zero temperature difference between the two furnaces, is measured. For heat flux instruments sample and reference are placed in the same furnace on to different crucibles. In this case both crucibles are heated from the same source and the temperature difference between the sample and the reference is measured. [182] Power difference from the sample and reference furnaces can be obtained from the temperature difference using the following equation

$$dQ/dt = \Delta T/R \qquad Eq.\ 2.2$$

where Q is the heat, t is the time, ΔT is the measured temperature difference between the sample and the furnace and R is the thermal resistance of the heat path between the furnace and the pan. The heat capacity of a material Cp is the quantity of heat required to increase its temperature of 1 K

$$\mathrm{Cp} = \mathrm{dQ/dT} \qquad Eq.2.3$$

Rearranging this equation with time, the heat flow dQ/dt can be expressed as a function of the heating rate as follows

$$dQ/dt = C_p\ (dT/dt) \qquad Eq.\ 2.4$$

where dQ/dt is the heat flow out of the sample, dT/dt is the heating rate and is Cp heat capacity of sample.

DSC allows the study of important thermal behaviour of pharmaceutical formulations, such as extent of drug crystallization, miscibility between the drug and the excipients and glass transition temperatures.

In this study, thermal behaviour of spray dried solid dispersions and physical mixtures was analysed using a Q2000 DSC (TA Instrument, Newcastle, USA). Baseline calibration, cell constant calibration and temperature calibration were performed using a heating rate of 10 ºC/min. Calibrants used include sapphire disk for the baseline calibration, indium for the cell constant calibration, benzoic acid (mp=122.3), tin (mp=231.9) and n-octadecane (mp=28.24), for the temperature calibration. [183]

2.3.5 Thermal Gravimetric Analysis (TGA)

TGA is a thermal analysis method whereby sample mass change is measured as a function of temperature/time. It is often used to investigate chemical or physical processes that the sample undergoes upon heating or isotherm at certain temperature. [184] The most common use of TGA is studying the thermal degradation behaviour of material. TGA instrument includes a suitable analytical microbalance where the pan is attached and a furnace where the sample is heated in a controlled atmosphere, while its weight is constantly measured. [182] For solid dispersions, TGA is commonly used to quantify the residual solvent content of solid dispersions formulation after processing and to study their thermal stability. [66]

In this study, TGA analysis was performed using a TGA 5000 (TA Instruments, Newcastle, USA). To identify water content as measured by weight loss due to sample dehydration, samples were heated from room temperature to 250 ºC at a heating rate of 10 °C/minute.

2.3.6 Attenuated total reflectance-Fourier transformed Infrared spectroscopy (ATR-FTIR)

Fourier Transformed Infrared Spectroscopy (FTIR) is a spectroscopic technique based on the molecular absorption of an electromagnetic wave in the infrared region (wavelength between 750nm and 1mm). The electromagnetic wave can induce molecular bonds vibrations, such as stretching, bending and rocking motions, at specific frequencies for each functional group. Thus, the FTIR spectrum can provide information about functional groups and molecular bonds present in the sample. [185]

It is possible to analyse powder or liquid samples directly using ATR-FTIR, without the preparation of KBr/sample disk, which is necessary in the conventional transmission mode. For ATR-FTIR experiments, the sample is placed on the high reflective index crystal and the incident infrared radiation is partially absorbed by the sample, at the frequencies values corresponding to the molecular vibration of the sample material, while the remaining light is reflected into a detector.

FTIR spectroscopy is a powerful tool to investigate possible drug-polymer interactions in solid dispersions, [186] such as hydrogen bonding, [168] and possible physical state transformation of the drug (from crystalline to amorphous and vice versa). [187]

In this study, ATR-FTIR spectroscopy was performed using a Perkin Elmer Spectrum BX-FTIR (Whaltam, Massachussets, USA) spectrometer, equipped with with an attenuated total reflectance (ATR) accessory (SPECAC, Orpington, UK). 64 scans were collected for each sample, at a resolution value of $2cm^{-2}$. Experiments were performed in triplicate.

2.3.8 Nuclear Magnetic Resonance (NMR)

NMR is a phenomenon occurring when nuclei having a "spin" are immersed in a magnetic field. Spin is a fundamental property of nature, it comes in multiples of 1/2 and can be + or - (nuclear spin number). The interaction between the electromagnetic field and spin active nuclei can result in the absorption of a photon by the nuclei. The frequency, ν, of absorption depends on the nuclei gyromagnetic ratio, γ

$$v = \gamma B \qquad Eq.2.5$$

where B is the magnetic field strength. Also, when placed in an external magnetic field, the spin vector aligns itself with the applied field, and the number of possible orientations is given by 2I+1, were I is the spin number. For a nucleus with I=1/2 the spin can have two possible orientations associated with two different energy levels. The oriented nuclei oscillate around the applied magnetic field B, at a frequency, called Larmor frequency. It is proportional to the two levels energy difference. If the frequency of the absorbed photon matches the Larmor frequency, the nuclei can undergo an energy transition between the two energy states. Irradiation at the Larmor frequency results in the generation of the NMR signal. The effective field applied to each nucleus depends on the types of nuclei and bonds present in the molecule. In each nucleus the electrons immersed in the magnetic field

generate an opposing small magnetic field that affects the effective field for the close nuclei, causing a shift of their resonance frequency, [188] process known as "chemical shift". Thus, NMR technique allows the elucidation of molecules structures, as from the chemical shift it is possible to have information about the local chemical environment, providing the identification of functional groups and chemical bonds with other spectroscopic techniques such as IR.

NMR spectroscopy has found wide applications in pharmaceutical and colloidal sciences, as it can be used as a probe of microstructure and dynamics of self-assembly systems. [131] In this study two different NMR techniques, ^{1}H proton NMR and diffusion-ordered spectroscopy (DOSY), were employed. Both experiments have been performed using a Bruker Ultrashield Plus 400 MHz Spectrometer (Bruker, BioSpin Corporation, The Woodlands, TX). The detailed experimental conditions are described in Chapter 5.

2.3.7.1 ^{1}H proton NMR spectroscopy

^{1}H proton NMR spectroscopy is the most commonly used NMR technique. It is based on the study of ^{1}H nuclei presents in the sample. Chemical shift of ^{1}H can be applied to study molecular structure, phase transition, aggregation and many other chemical and physical processes. In this study ^{1}H proton NMR was applied to study the aggregation of the polymeric carriers with a model intestinal surfactant.

2.3.7.2 DOSY NMR spectroscopy

Diffusion NMR is based on the measurement of molecules Brownian motions, which are driven by the molecules internal energy. When a homogenous gradient B_0 of know magnitude is applied to the sample, the Larmor frequency ω_0 provides a spatial label of the spin, with respect to the direction of the gradient. In normal diffusion experiments the gradient is oriented towards the z-axis. When a $\pi/2$ rf pulse is applied, the macroscopic magnetization rotates from the z-axis to the x-y plane. During the first time period τ, at a time t_1, a gradient pulsed of duration δ and magnitude g is applied, causing a phase shift of each spin. The application of a second rf pulse π at the end of the first period causes the reversing of the phase angle. At a time $t_1+\Delta$ a second pulsed gradient, having same duration and magnitude of the first one is applied. If the spins have undergone a translational motion, the degree of their dephasing is proportional to their displacement in the direction of the gradient (Fig. 2.7). [189]

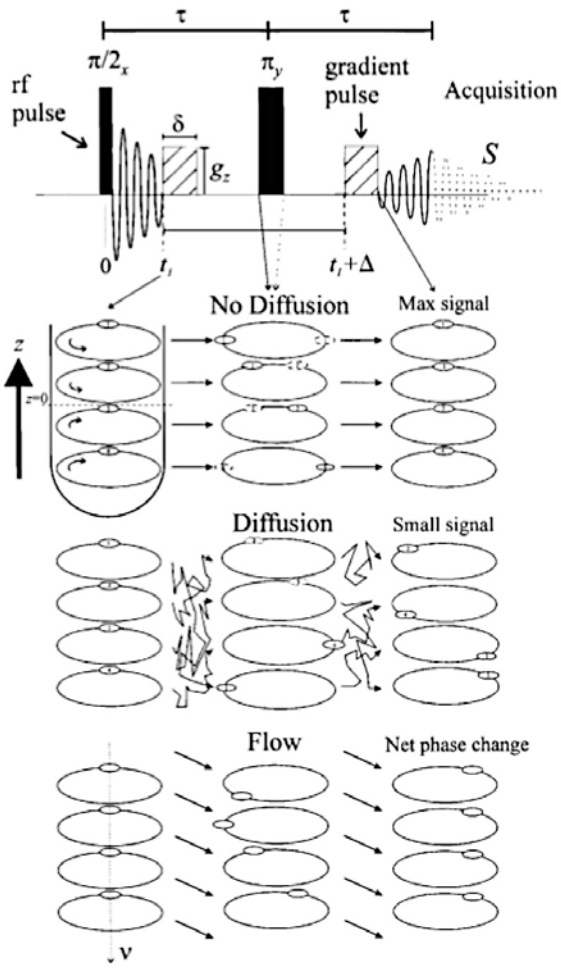

Fig. 2.7: A schematic representation of pulse field gradient sequence and diffusion and flow measurements. [189]

The molecules displacement during the diffusion time Δ leads to the NMR signal attenuation, which is described by:

$$I = I_0 e^{-D\gamma^2 g^2 \delta^2 (\Delta - \delta/3 - \tau/2)} \qquad Eq.2.6$$

where I is the observed intensity, I_0 is the unattenuated signal intensity, D the diffusion coefficient, γ the gyromagnetic ratio, g the gradient strength, δ the length of the gradient, and Δ the diffusion time.

The diffusion coefficient of a molecule D, can be related to the hydrodynamic radius of the molecule, as described by the Stokes-Einstein equation

$$D = K_B T / 6\pi\eta r_s \qquad Eq.2.7$$

where K_B is the Boltzmann constant, T is the temperature, η the viscosity of the medium and rs the hydrodynamic radius of the molecule. Any aggregation phenomena that can affect the molecules size can be tracked and studied using self-diffusion NMR, as any change in the size will affect the self-diffusion coefficient of the studies molecule.

Self-diffusion NMR technique is well-established method for studying surfactant solutions, surfactant self-association equilibria, counterion binding, solubilisation, and hydration phenomena. As widely shown in literature self-diffusion NMR can be a useful tool to study the aggregation of polymers and surfactant, and for this aim it has been used in this study. [103]

2.3.9 Pendant Drop Measurements

Pendant drop technique is used to measure surface/interfacial tension at air/liquid or liquid/liquid interfaces, which can be calculated from the size and shape of a sample drop hanging from the tip of a syringe. The drop shape can provide information about the drop fluid itself or about the surrounding medium.

Due to surface tension, the liquid hanging from the tip of a capillary tube tends to take a spherical shape. In a gravitational field, the sphere is distorted into an elongated "tear drop" shape. The distortion degree increases with drop density and decreases as liquid surface or interfacial tension becomes greater. [190]

The shape of a fluid under equilibrium conditions can be described by the Young-Laplace equation

$$\Delta p = \gamma \left(\frac{1}{S_W} + \frac{1}{S_e}\right) \qquad \textit{Eq. 2.8}$$

where Δp is the pressure difference across the fluid interface, S_w is the smallest diameter of the hanging drop and S_e is the equatorial and bigger diameter of the pendant drop (Fig. 2.8) Once the pendant drop shape is analysed and gravity and liquid densities are known, surface tension can be accurately obtained by applying young-Laplace equation.

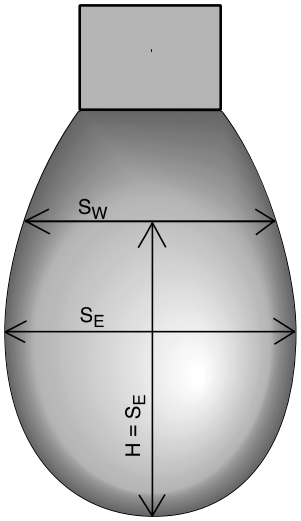

Figure 2.8. Schematic representation of pendant drop experiment. [191]

Pendant drop technique is commonly applied for the study of surfactants behavior, as surface tension can be a probe to investigate surfactants micellization and interaction with other species. [192] Sodium taurocholate interfacial tension was measured with and without the presence of HPMC and PVP, in MilliQ water, phosphate and acetate buffers. The experiments were carried out using FTA200 pulsating drop tensimeter (First Ten Angstroms, Portsmouth, VA, USA). The appropriate solution of protein or surfactant was placed in a glass cuvette. A Hamilton syringe, having a volume of 25 or 50 ml depending on the droplet size required, was fitted with a j-shaped needle. The air bubble was formed using the j-needle and the interfacial tension was measured over 15 minutes. Further details about the sample preparation and experiments setting are discussed in Chapter 4.

2.3.10 Scattering Techniques

Scattering experiments represent a powerful and non-invasive method to determine the structure and organization of particles in a homogeneous medium. Suitable scattering samples include colloids, polymeric macromolecules and micellar aggregates, with sizes ranging from a few angstroms to micrometers. In a dilute system, light and neutron scattering techniques can be used to determine the shape and the arrangement of individual particles, while in a concentrated system, information about positional correlations and spatial arrangement of particles in the sample can be achieved. Furthermore the measure of the absolute scattered intensity yields information on the apparent molecular weight of the objects.

Figure 2.9. Schematic representation of the scattering experiment.

In a typical scattering experiment, an incident beam of wavelength λ is directed on the sample, where the radiation is partially scattered and transmitted (Fig.2.9). The scattered intensity is measured as a function of the scattering angle θ between incident and scattered radii. An important physical parameter is the scattering vector q: defined as the difference between propagation vectors of incident and scattered light

$$q = k_i - k_s \qquad Eq.2.9$$

For elastic scattering, no change of frequency occurs between incident and scattered radiation and the magnitude of incident and scattered wavevector q is equal to |ki |= |ks| = 2π/λ leading to [193]

$$|q| = q = 4\pi/\lambda \sin(\theta/2) \qquad Eq.2.10$$

In this study two different scattering techniques, dynamic light scattering and Nanosight technique, were employed to study the size of polymeric carrier-NaTC aggregates. Neutron scattering experiments were carried out to investigate the local structure of the aggregates.

2.3.10.1 Dynamic Light Scattering (DLS)

In DLS experiments the intensity of the scattered light is studied as a function of time. Scattered light intensity is measured during a time period t_n at defined intervals Δt. [194] Due to the particles "random" motions, scattered light intensity I(q,t) is an averaged value defined by Eq. 2.11.

$$I(q) = \lim_{tn\to\infty} 1/t_n \int_0^{tt_n} I(q,t) * dt \approx \lim_{n\to\infty} 1/n \sum_{j=1}^{n} i(q, j\Delta t) \qquad Eq.2.11$$

Scattered light fluctuations are measured as autocorrelation function C(q,td), that is given by Eq. 2.12,

$$C(q, t_d) = \lim_{n\to\infty} \sum_{k=0}^{n} I(q, k\Delta t) * I(q, (k + j)\Delta t) \qquad Eq\ 2.12$$

where t_d is the aggregates relaxation time, also called τ, that represents the time after which the aggregates are not in the scattering volume anymore, thus do not contribute to the autocorrelation function. For $\tau\to\infty$ I(q,t) and I(q, t+τ) are not correlated and C(q,t) is in this case independent from τ. In this condition the autocorrelation function decreases linearly from $[I(q, o)]^2$ to $[I(q)]^2$. Thus the relationship between C(q,t) and its asintotic value $[I(q)]^2$ can be defined by the Siegert equation

$$\frac{C(q,t)}{[I(q)]^2} = g_2(q, t) = A(1 + b^2|g_1 q, t|^2) \qquad Eq.2.13$$

where $g_2(q,t)$ is the time autocorrelation function and $g_1(t)$ is the field autocorrelation function, A is the baseline obtained from the experiment and b is the coherence factor that depends from the experimental setup and the scattering geometry. [195] According to the spectral profile of the scattered light, $g_1(q,t)$ can be described by different mathematical functions, from which it is possible to estrapolate the distribution of studied structures decay rates. The decay rate is directly related to the aggregates diffusion coefficient D_t

$$D_t = \gamma/_{q^2} \qquad Eq.2.14$$

where q^2 is the scattering vector root square. By applying the Stoke-Einstein equation (Eq. 2.7) the aggregates hydrodynamic radius is obtained.

In this study dynamic light scattering has been used to characterise the size of polymers-bile salts aggregates size distribution in different media. Fixed angle scattering experiments DLS experiments were performed on a Zetasizer Nano ZS, Malvern Instrument, (Malvern, Worcestershire, United Kingdom) fitted with a 633 nm red laser. The autocorrelation functions were measured at a fixed 173° angle (back scattering detection).

2.3.10.2 Nanosight

Nanosight technique, also known as Nanoparticle Tracking Analysis (NTA), is an innovative scattering technique that has been commercialized in 2004. It is based on light scattering properties and as for DLS a light beam is scattered by the sample suspension, by passing through a prism edged glass flat within the sample chamber. The laser emerging from the interface between the glass and the liquid sample, refracts to an intense low profile

resulting in a compressed beam with a reduced profile and a high power density. The compressed beam is visualized via a long working distance, x20 magnification microscope objective is fitted to an otherwise conventional optical microscope onto which is mounted a high-sensitivity CMOS camera, operating at 30 frames per second (fps). The camera subsequently captures a video file of particles moving under Brownian motions (Fig.2.10). [196]

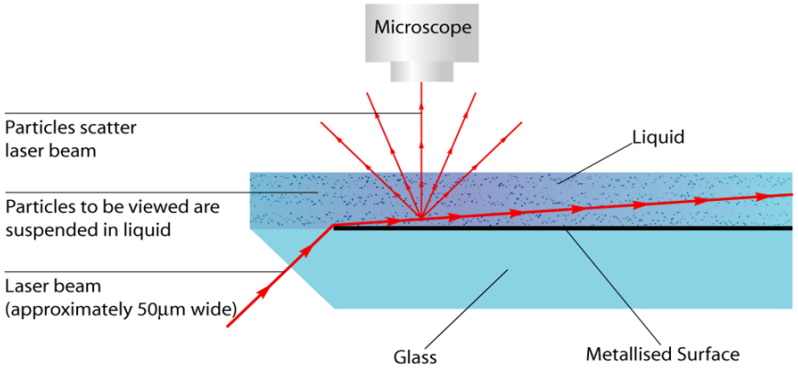

Fig.: 2.10 Schematic representation of NTA experiment [196]

NTA software records a video of the particles undergoing Brownian motions. Each particle is then tracked frame to frame and the distance that each particle move in the x-y space is used to calculate the particle diffusion coefficient according the the Stokes-Einstein equation

$$D_t = \frac{TK_B}{3\pi\eta d} \qquad Eq.2.15$$

where K_B is the Boltzmann constant, T is the temperature, η is the solvent viscosity and d is the distance moved by the particle.

Differently from DLS, NTA sizes each particle individually, making the technique suitable for more diluited sample compared to DLS. Moreover, NTA can be employed for the measurement of particles concentration. The detection threshold is about 10-2000 nm, thus smaller than for DLS. Very small particles (lower than 10 nm) can be studies with NTA technique in case of very high refractive index.

In this study a LM10 Nanosight (Nanosight Ltd- Malvern Instruments Ltd, Malvern Worcestershire, United Kingdom) has been used to visualize and size polymer, bile salts and bile salts-polymer aggregates. The instrument is fitted with a 638 nm laser. Particles tracking analysis was performed using NTA software.

2.3.10.3 Neutron scattering techniques

Neutrons are neutral particles that show the ability to interact with nuclei. Neutron scattering by sample materials is normally weak, as the nuclear force acts only on short distance, but offers the advantage of radiation deep penetration in the sample, enabling the study of materials bulk properties. Samples scattering ability varies in a nonsystematic way with the atomic number, and interactions can be different for different isotopes, as in the case of the hydrogen and the deuterium. [197]

Neutrons can be generated from a nuclear reactor or a particle accelerator. In a nuclear reactor, fast neutrons (1-2MeV) are produced in a fission chain reaction, often from enriched uranium 235U. Emitted neutrons are scattered in the surrounding moderator where they lose energy until they reach an average thermal energy characteristic of the moderator temperature. A H_2O moderator at 50°C corresponds to the most probable neutron wavelength around 1.4 Å. In an electron accelerator source, high-energy electrons interact with heavy elements, producing gamma radiations, which in turn interact with nuclei to generate neutrons. Finally, in a spallation neutron source, heavy particles such as protons are accelerated to very high energies and splinter neutrons from heavy nuclei with a high yield (around 30 neutrons per proton). The high energy of neutrons produced has to be reduced by a moderator in order to be suitable for scattering experiments. [198]

2.3.10.3.1 Small Angle Neutron Scattering (SANS)

SANS is a key technique for the elucidation of large scale structures features. It is used to study the bulk properties of materials and it can be applied for the study of surfactants, colloids, polymers, liquid crystals and other nanomaterials. [199] In a typical SANS experiment, an incident neutron beam of wavelength λ and Intensity I_0 is directed on the sample, where the radiation is partially scattered and transmitted (assuming no absorbance from the sample occurs). Generally the wavelength λ ranges 4÷20Å and the energy and velocity associated to the neutron beam are respectively about 0.025eV and 2200m/s.

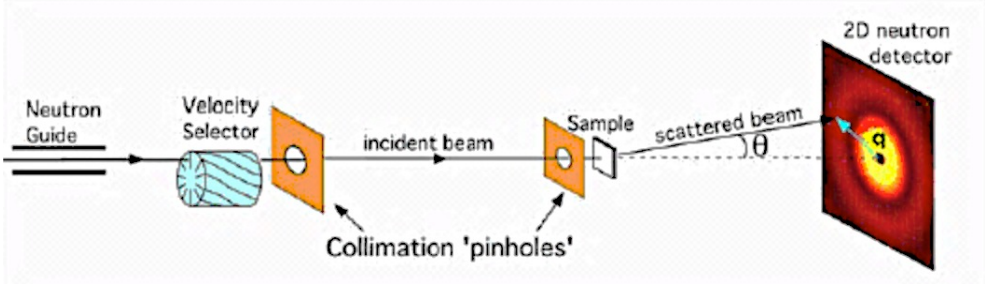

Figure 2.11. Schematic representation of Small Angle Neutron Scattering equipment. [200]

By collimation of the incoming beam, the incoming wave vector is fixed. This provides structural information in reciprocal space, as measuring the scattered intensity in a certain direction the wave vector of the outgoing scattered vector is known. [198]

In SANS experiments different length scales can be investigated in reciprocal space, by detecting the number of scattered nuclei as a function of the wave vector Q. The wave vector is inversely proportional to the distance d

$$Q = {}^{2\pi}/_{d} \qquad \textit{Eq. 2.16}$$

and is also related to the scattering angle θ and the incident beam wavelength λ as shown in equation 2.17

$$Q = \frac{4\pi sin\theta/2}{\lambda} \qquad \textit{Eq.2.17}$$

Typically a SANS beam line has a two-dimensional area detector, between 2 and 20 m after the sample. The size and position of the detector relative to the beam determine the range of Q at a given detector distance. SANS patterns are reported as the neutron beam intensity I(Q) as a function of the scattering wave Q. I(Q) provides information about sample size, shape and interactions between scattering centres. According to the samples features, in particular shape and monodispersity, different mathematical models can be applied to define I(Q) and obtain structural information about the scattering sample. The main parameters are the form factor P(Q) which provides intraparticles information (size and shape), and the structure factor S(Q) from which interparticle information (scattering particles interactions) are obtained (Fig. 2.12).

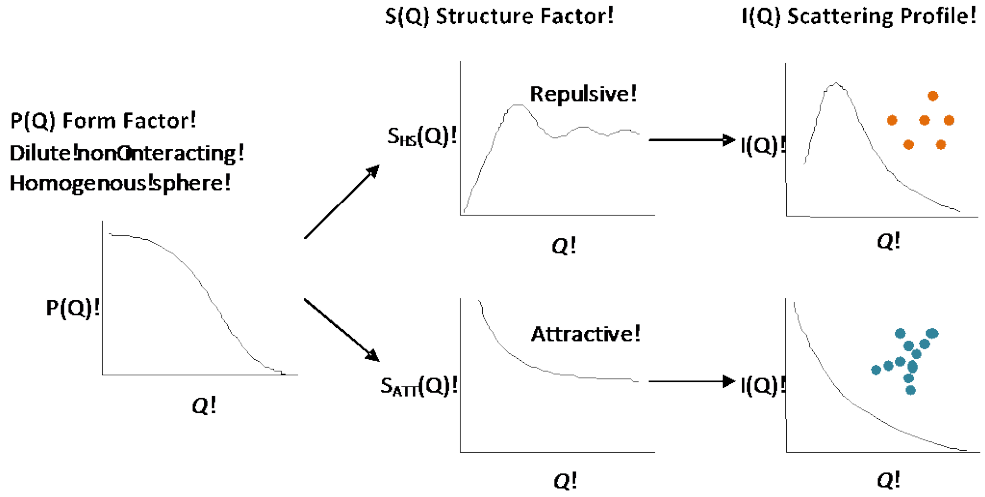

Fig.2.12: Representation of P(Q) and (S(Q) for repulsive and attractive spheres and their contribution to Q. [200]

In this study SANS experiments have been performed to investigate the local structure of polymer-surfactant aggregates. SANS measurements have been carried out at the ISIS SANS2-D spectrometer (ISIS-Rutherford Appleton Facilities-Didcot). Sample have been prepared and measured in D-buffer using 2mm cells. Each experiments has been run in duplicate. Data Mathematical modelling for analysed samples is reported in Chapter 5.

2.3.10.3.2 Spin-Echo small Angle Neutron Scattering (SESANS)

SESANS is a neutron scattering technique based on the use of a polarised neutron beam, to determine directly the wave vector transfer in real-space. One of the advantages of the use of SESANS is that the use of polarisation yields high resolution without much collimation of the beam, resulting in high accumulated beam intensity. [198]

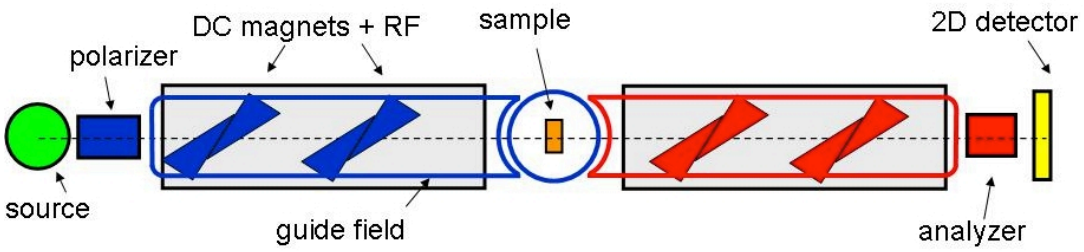

Fig.2.13: Representation of SESANS equipment [200]

As shown in Figure 2.13, a neutron beam is polarised with the polarisation vector perpendicular to the plane. The polarised neutron beam enters in a magnetic region composed of two precession devices with tilted interfaces, having opposite magnetic fields. The precession devices rotate the neutron polarisation vector from parallel to perpendicular to the magnetic field or vice versa, thus starting or stopping, respectively, the Larmor precession in this magnetic field. A sample measured using this SANS set-up will break the symmetry of the Larmor precession, affecting the echo signal and consequently the neutron beam polarization. [201]

In SESANS experiments the neutron beam polarization is measured, yielding the correlation between the scattering length density integrated along the path of the neutron beam. SESANS technique can be used in a very large length scale, as it can be employed to probe structure between 20 nm to 20 μm. In this study, SESANS experiments were performed at the ISIS-SESANS spectrometer (ISIS-Rutherford Appleton Facilities-Didcot). The instrument is brand new and measured samples were the first set of aqueous samples tested with this equipment.

2.3.11 Cryogenic Electron Microscopy (Cryo-TEM)

Cryo-TEM is the electron microscopy performed on thin vitrified aqueous films, kept at liquid nitrogen temperature. The technique allows the direct imagining of micellar structures in aqueous environments. These dynamic structures requires an aqueous environment to form and persist, and do not withstand the drying or the staining and the fixation steps of conventional EM, which might impact the structure size and shape. In Cryo-TEM method the solution is applied to a microscopy grid in such a way that a very thin aqueous film is formed, which then is plunged into a cooling medium, just above its freezing point, where the film very rapidly vitrifies, without crystallization. The grid with vitrified film is then transferred to the microscope, and examined at liquid nitrogen temperature in transmission mode (Fig 2.14). In this way sample images are captured in the vitrified film and are observed without dehydration. Normally vitrification happens extremely fast, thus no significant reorganization of the analyses structures takes place. [202]

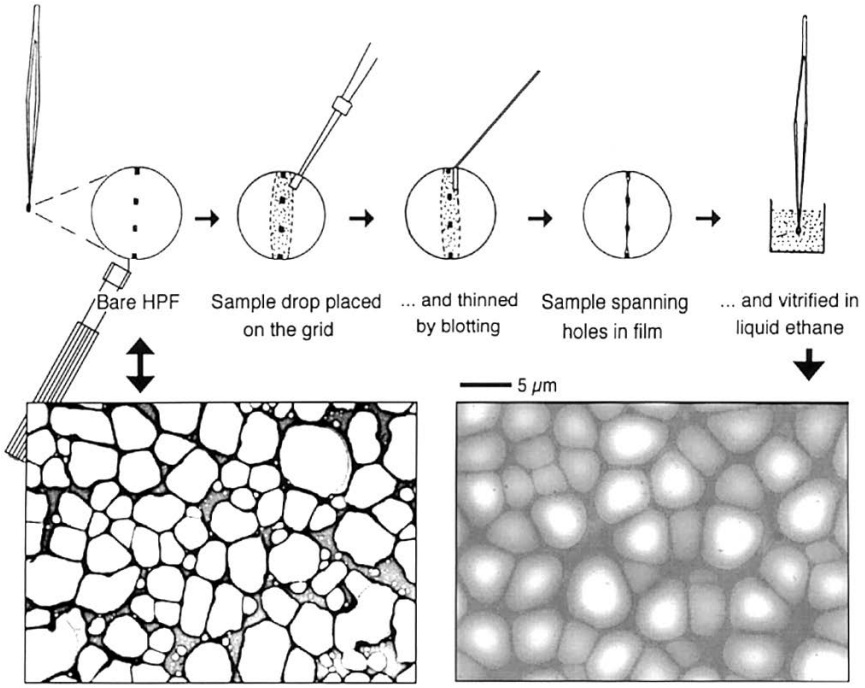

Fig. 2.14: TEM micrographs of a holey polymer film, HPF, empty, and after application of sample, blotting, and vitrification. [202]

The smallest structures that can be resolved using Cryo-TEM are of about 4-5 nm in size. Ordinary surfactant micelles are thus seen only as dots, and it is difficult to claim anything about the size of an object unless it is clearly larger than 5 nm. However, in a few reports the bilayer membrane has been resolved, and its thickness measured. [203] There are also limitations on the upper size of an object, set by the thickness of the film. In practice it

is limited to about 500 nm; otherwise the scattering of electrons by water gets too large, and the cooling rate during vitrification too slow. [202]

Due to the impact of staining and drying steps on samples aggregation TEM was not a suitable technique for bile salts micelles and bile salts-polymer aggregates imaging, thus Cryo-TEM was used for this purpose. Cryo-TEM analysis has been performed in at the Department of Physical Chemistry, Uppsala University, Sweden. The preparation of the samples has been performed according to the routine procedure of the laboratory. [203] For sample preparation, a small droplet of the sample solution was placed under controlled conditions on a pretreated Cu grid of about 20μm thickness, which was covered by a perforated cellulose acetate butyrate film. Excess material was removed by a gentle wiping off with a filter paper. The specimen was vitrified by a rapid transfer into liquid ethane close to its freezing temperature. The sample examination was performed with a Zeiss 902 A electron microscope operating at 80 kV at 100K.

2.3.11 *In vitro* Cellular Drug Absorption and Transport Assessments

In vitro drug absorption and transport using cell models represent a useful tool to preliminarily evaluate cytoxicity and drug permeability across intestinal tissues at the early stage development of the new compound. The use of an efficient *in vitro* cell model can help to determine drug solubility at different intestinal conditions (before and after meals), its pre-absorptive degradation in the gastro-intestinal environment, the rate of absorption and the effective drug amount absorbed. Furthermore, *in vitro* studies based on cells models can give information about the physico-chemical features of the interaction between drug and tissues. [204]

Caco-2 cells derived from human colonic adenocarcinoma have been widely used as model cells for *in vitro* drug absorption prediction. Caco-2 cells are morphologically and functionally similar to enterocites, since they are able to form junctions and express many of the intestinal enzymes. In this project both absorption and transport experiments were performed using Caco-2 cell lines. Information about the cell seeding and growing procedures are discussed in Chapter 6.

In absorption studies a monolayer of cells was seeded in the appropriate plate, and once confluent were treated with the studied samples. After treatment cells were lysed in order to extract and measure the absorbed amount of sample studied. For transport studies a

monolayer of cells was placed in a diffusion apparatus where a lateral and an apical chamber are present (Fig.2.15). The two chambers represent the mucosal and serosal intestinal surfaces. The drug solution was added to one of the two chambers and the presence of drug is measured regularly in the receiving chamber. The small amount of drug required makes Caco2-cells transport experiments suitable to perform screening studies, to point out possible absorption problems of a potential new drug and the characterise drug release from new formulations. [205] The detailed methodologies of drug absorption and transport studies are described in Chapter 6.

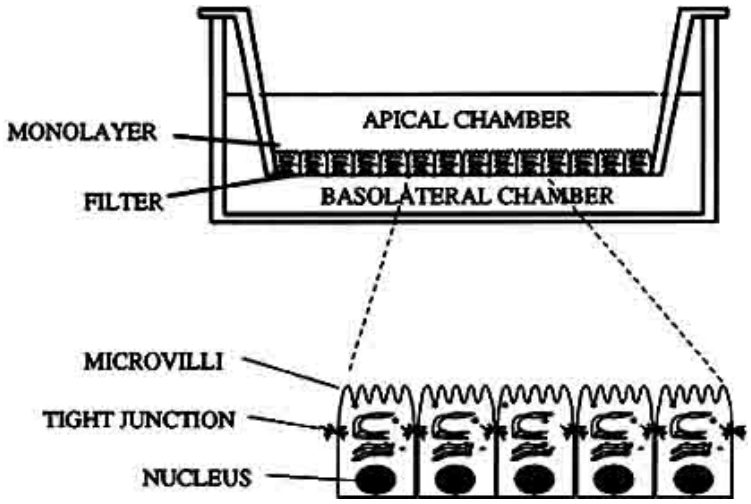

Fig.2.15: Representation of a cells monolayer in vitro experiment [206]

2.3.12 High Performance Liquid Chromatography (HPLC)

HPLC is one of the most widely used technique for complex samples analysis, separation and purification. Physical separation of sample components is obtained by their partitioning between the mobile phase and the stationary phase, according to their relative solubilities or affinities towards the two phases. HPLC is almost universally applicable and offers a remarkable assay precision. Moreover, the use of HPLC allows high-quality separation achievement in the minimum of time, by passing a mobile liquid phase through a finely divided stationary phase under high pressure.

According to the sample properties, the partitioning of its components between the mobile phase and the stationary phase can be based on different criteria. The most commonly used approach is the sample separation according to its components polarity: in

this case it is possible to work in “direct” phase, with the stationary phase having higher polarity than the mobile phase, or in “reverse” phase, with higher polarity in the mobile phase. The mixture separation can be based also on the “ionic exchange” of the sample components with an ionic stationary phase (ionic exchange HPLC) or on their “exclusion” from the stationary phase interaction according to their steric volume (Steric Exclusion HPLC). [207]

HPLC analysis was used for two types of sample: (1) piroxicam steady state solubility samples studied in Fed and Fasted state. The simultaneous presence of different simulating intestinal fluids components, required their separation from the analyte in order to perform a reliable analyte assay. Consequently direct UV-VIS assay was not feasible for such samples; (2) piroxicam Caco-2 absorption and transport studies, which could not be studied using UV-Vis due to the presence of cell media and possible drug metabolites. Samples have been properly processed before being tested by HPLC. Details about sample preparation and HPLC analysis can be found in Chapter 6.

Chapter 3. Preparation and physical characterisation of spray dried solid dispersions

3.1 Introduction

The use of amorphous solid dispersion formulations has been shown to be an effective approach to increase the dissolution rate of poorly water soluble drugs [3,38,208] and potentially improve their oral bioavailability [24,209]. As already described in Chapter 1, spray drying is one of the most commonly used solvent evaporation method to obtain amorphous solid dispersions. [210] In this study spray drying technique was used to prepare solid dispersion formulations. HPMC-K4M and PVP Kollidon 30 were used as main polymeric carriers. The hydrophobically modified derivatives of HPMC and PVP, HPMC-AS LF and PVP-VA, were used to investigate the effect of the polymer hydrophobic modification on the formulation behaviour. Three different poorly water-soluble drugs, piroxicam, griseofulvin and fenofibrate (all classified as BSC class II drugs which are poorly soluble and highly permeable), were applied as model drugs. Detailed description of the physicochemical properties of the carriers and model drugs are presented in Chapter 2, Section 2.2.1.

The main focuses of this chapter are the optimisation of the solid dispersion preparation through spray drying technique and their physical characterisations concerning their solid-state properties and *in vitro* drug release performance. Solid-state characterisations of the spray dried solid dispersions were performed using DSC, TGA, SEM, PXRD and ATR-FTIR. Steady state solubility studies were carried out in order to investigate the impact of the presence of polymeric carriers on the apparent solubility of model drugs in different media. Comparison studies of the dissolution behaviour of spray dried solid dispersions and the corresponding physical mixes of crystalline drug and polymer were performed to evaluate the effect of the polymer and the spray drying processing on the dissolution enhancement of the model drugs.

3.2 Experimental methods

3.2.1 Preparation for solubility and dissolution studies media

Two different simulating intestinal media were used in this study: fasted state simulating intestinal fluid (FaSSIF), mimicking the intestinal condition before meals, and

fed state simulating intestinal fluid (FeSSIF), to reproduce the intestinal environment after meals. The FeSSIF and FaSSIF media were prepared by following the method developed by Dressman et al. [211] The compositions of the fed and fasted state media are listed in Table 3.1.

Table 3.1: FaSSIF and FeSSIF media features and composition

	Fasted state (FaSSIF)	**Fed state (FeSSIF)**
Buffer	Phosphate buffer	Acetate buffer
pH	6.5	5
Buffer ionic strength	2.52	4.06
Sodium Taurocholate concentration (mM)	3	15
Lecithin concentration (mM)	0.75	3.75

For the buffer preparation individual buffer components were accurately weighed and dissolved in MilliQ water. The final pH was checked using a calibrated pH meter, and, when necessary, adjusted by the addition of small quantities of HCl or NaOH 1M. Sodium taurocholate solutions were prepared by dissolving weighed amount of the surfactant in previously prepared buffers. Solutions obtained are referred as blank FaSSIF and blank FeSSIF in this study. FaSSIF was prepared by adding 11.8 mL of a solution containing 100 mg /mL lecithin in methylene chloride, obtaining an emulsion. The methylene chloride was eliminated under vacuum at about 40°C for fifteen minutes at 250 mbar, followed by 15 minutes at 100 mbar. This resulted in a clear, micellar solution, having no perceptible odour of methylene chloride. After cooling to room temperature, the volume was adjusted to 2 L with blank FaSSIF. The same procedure was used for FaSSIF preparation, but in this case 59.08 mL of a solution containing 100mg/mL lecithin in methylene chloride were added to the blank FeSSIF.

3.2.2 Steady state solubility studies of model drug in dissolution media

The impact of polymeric carriers on the apparent solubilities of model drugs was studied in different media. The media used in this part of study include buffer pH 5, buffer pH 6.5, blank FaSSIF, blank FeSSIF, FaSSIF and FeSSIF. Supersaturated solution of the

model drugs were prepared by dissolving excess amount of drug in the tested medium. The same sample was tested in the presence of HPMC, with concentrations from 2 to 9 mg/ml, and of PVP with concentrations from 1 to 19 mg/ml. Samples were left under constant magnetic agitation at 37 ºC for 72 hours to allow the dissolution with maximum drug concentration to reach equilibrium.

After 72 hours, samples studied in the two buffers and in the two blank media, were filtered using a syringe filter with 0.45μm pore size and the drug concentration was assayed using a UV-VIS spectrometer (Perkin Elmer, Whaltam, Massachussets, USA). The wavelength of maximum absorbance (λmax) used was 334 nm for Piroxicam, 296 nm for Griseofulvin and 290 nm for Fenofibrate.

For piroxicam samples steady state solubility studies were performed also in FaSSIF and FeSSIF, to investigate the impact of lecithin on the drug solubilisation. For the complex intestinal media containing lecithin, UV-VIS spectroscopy is not a suitable assay method, as the presence of lecithin caused UV-VIS absorbance in a wide range of wavelengths. Therefore the piroxicam samples in FaSSIF and FeSSIF were assayed using HPLC Perkin Elmer (Whaltam, Massachussets, USA). After 72 hours of mixing, the samples were centrifuged at 5000 rpm for 5 minutes. Approximately 1 ml of supernatant was transferred into HPCL chromacol ambered vials. HPLC analysis was performed using a reverse phase C18 column, 5 μm (pore size), with 250 x 4.6 mm dimensions (Phenomenex, Macclesfield, Cheshire, UK). For the analysis, the mobile phase consisted of acetonitrile (MeCN)-phosphate buffer (40:60 v/v). Phosphate buffer was prepared by dissolving properly weighed buffer components in fresh MilliQ water and the pH was adjusted to pH 2.5 with phosphoric acid. An injection volume of 10 μL and a flow rate of 1.0 mL min^{-1} were used. UV-VIS scan of the drug in the mobile phase showed piroxicam maximum absorbance shifted to 316 nm in the MeCN/phosphate buffer system. For this reason λ value for UV detection during HPLC analysis was set at 316 nm. The retention time of piroxicam was measured as approximately 6.5 minutes in this study. Details of piroxicam HPLC calibration curve are shown in Appendix. All the samples have been prepared and analysed in triplicate (n=3).

3.2.3 Preparation of physical mixtures

Polymeric carriers (HPMC and PVP) and APIs physical mixtures (Piroxicam, Griseofulvin and Fenofibrate) physical mixtures were prepared by gently mixing raw (unprocessed) material powder using mortar and pestel for about 2 minutes.

3.2.4 Preparation of drug loaded solid dispersion by spray drying

HPMC PVP, HPMC-AS and PVP-VA were used as polymeric carriers. Three different model drugs, piroxicam, griseofulvin and fenofibrate were loaded into the polymeric dispersions via spray drying. The spray drying parameters were set as follows: inlet temperature 85 °C, aspirator setting 100%, pump setting 5% (4 ml/min $^{-1}$). For the preparation of piroxicam solid dispersions with three different w/w polymer:drug ratios (2:1, 4:1, 9:1) were prepared. Piroxicam was dissolved in ethanol (1.5 mg/ml), while HPMC and PVP were dissolved in MilliQ water. The resulting polymer concentrations for the 3 different drug:polymer ratios employed were: 3 mg/ml for the drug:polymer ratio 1:2, 6 mg/ml for the drug:polymer ratio 1:4, 13.5 mg/ml for the drug polymer ratio 1:9. Drug and polymer solutions were mixed in the proportion 1:1(v/v) before the spray drying process. Griseofulvin and fenofibrate solid dispersion were prepared at the polymer:drug ratio 2:1. Solution preparation and concentration were the same used for piroxicam solid dispersions preparation.

3.2.5 Assay of actual drug content in spray dried formulations

The actual drug content of spray dried solid dispersions was determined using UV-Vis spectrophotometer (Perkin Elmer Lambda 35, Whaltam, Massachussets, USA). About 1 mg of sample was dissolved in 5 ml of ethanol and left under magnetic stirring for 1 hour in closed vials. Samples were then diluted up to 1/5 of initial concentration and filtered using a Ministar single use filter (0.40 μm; Sartorius AG, Goettingen, Germany). Drug content was calculated from the absorbance measured at the λ_{max} of piroxicam, griseofulvin and fenofibrate at 334 nm, 296 nm and 290 nm, respectively. Experiments were repeated in triplicate (n=3).

3.2.6 Scanning electron microscopy (SEM)

In order to investigate the morphology of the spray dried microparticles, powder samples were attached to double-sided adhesive carbon pads mounted on aluminium stubs. Subsequently samples were coated with a thin layer of gold using a Polaron SC7640 Au sputter coater (Quorum Technologies, East Grinstead, United Kingdom) fitted with a rotary stage. Coating conditions were 2.1kV, 20mA, 30sec, average distance sample-target 50mm, coating thickness few nm. Coated samples were examined with a JSM 4900LV SEM (JEOL

Ltd, Tokyo, Japan), fitted with a tungsten filament. A 20 kV acceleration voltage and 10mm working distance were used.

3.2.7 Powder X-Ray diffraction (PXRD)

PXRD measurements were performed using a Xtra X-Ray diffractometer (Thermo ARL, Thermo Scientific, Waltman, MA). The X-Ray tube composed of Copper was operated under a voltage of 45kV and current of 40mA. The PXRD patterns were recorded from 3° to 60° 2θ at a step of 0.01°/min.

3.2.8 Differential scanning calorimetry (DSC)

Thermal behaviour of raw materials, spray dried solid dispersions and physical mixtures was analysed using a Q2000 DSC (TA Instrument, Newcastle, USA). Samples (n = 3) were accurately weighed (2 to 3 mg) into standard aluminium crimped pans (TA), and scanned between -20 ˚C and 250 ºC with a heating rate of 10 ºC/min.

3.2.9 Attenuated total reflectance-Fourier transformed infrared spectroscopy (ATR-FTIR)

Raw materials, physical mixtures and solid dispersions formulations were analysed using ATR-FTIR spectroscopy, in order to investigate the occurrence of possible carrier-drug interactions. ATR-FTIR spectroscopic studies were performed using a Perkin Elmer Spectrum BXTR-IR (Whaltam, Massachussets, USA) equipped with attenuated reflectance (ATR) accessory (SPECAC, Orpington, UK). Spectra were collected in absorbance mode and 64 scans were collected for each sample, at a resolution value of 2 cm^{-2}. All experiments were performed in triplicate (n=3).

3.2.10 Thermal gravimetrical analysis (TGA)

Spray dried samples were analysed using TGA to quantify the residual solvent (including organic solvent and moisture) content in the formulations after the spray drying process. All TGA measurements were performed using a TGA 5000 (TA Instruments, Newcastle, USA) heating from room temperature to 250 ºC at a heating rate of 10^{o}C/minute. All experiments were performed in triplicate (n=3).

3.2.11 *In vitro* dissolution studies

In vitro dissolution studies of the crystalline drugs alone, physical mixtures of crystalline drug and polymers, and spray dried solid dispersion formulations were performed using a BP paddle method (D8000, Copley Scientific Ltd., Nottingham, UK). Before performing the dissolution study, all the samples were sieved using a 63μm sieve, to control the particle size. All tests were performed in 500 ml of medium at 37.0 ± 0.5 ˚C, with a rotation speed of 50 ± 1 rpm. Four different media were used for dissolution studies, buffer pH5, buffer pH 6.5, blank FaSSIF and blank FeSSIF. At predetermined sampling points, 5 ml sample was collected from each vessel using a syringe, filtered through a 0.45 μm membrane filter and replaced with an equivalent volume of fresh medium. Measurements of drug release were made using a UV-VIS spectrophotometer (Perkin-Elmer Lambda 35, USA). The wavelength of maximum absorbance (λmax) used was 314 nm for piroxicam, 296 nm for griseofulvin and 290 nm for fenofibrate. The dissolution studies were conducted in triplicate and the average drug release was calculated.

3.3 Results and discussion

3.3.1 The effect of polymer on the apparent solubilities of the model drugs

The aqueous solubility of a drug is one of the determinants of its dissolution rate and the intestinal absorption of compounds with aqueous solubility values lower than 0.1 mg/ml, is limited by their poor solubility in aqueous environments [212]. In order to investigate the impact of the polymeric carriers employed on the model drugs apparent water solubility, the equilibrium solubility of crystalline model drugs was studied in the different intestinal simulating fluids employed.

3.3.1.1 Piroxicam

Table 3.2 shows the apparent solubility values of piroxicam (PXM) in different media obtained from the steady state solubility studies performed with and without the presence of HPMC.

Table 3.2: Piroxicam apparent solubility values in different media, with and without the presence of HPMC (2, 4 and 9 mg/ml) (n=3)

Medium	Piroxicam apparent solubility values (μg/ml)			
	PXM	**HPMC:PXM 2:1 (HPMC 2mg/ml)**	**HPMC:PXM 4:1 (HPMC 4mg/ml)**	**HPMC:PXM 9:1 (HPMC 9mg/ml)**
Buffer pH 6.5	34.1±0.2	186.2±6.2	284.4±62.1	188.2±3.1
Buffer pH 5	14.5±0.1	55.3±2.8	54.9±8.1	55.4±4.2
Blank FaSSIF	41.6±3.6	208.8±1.2	203.5±49.2	196.1±8.2
Blank FeSSIF	58.3±8.1	70.8±7.3	77.5±2.3	76.9±2.1
FaSSIF	206.6±19.1	211.9±31.2	226.6±10.2	258.2±1.9
FeSSIF	34.9±3.5	45.2±1.8	45.1±16.2	129.3±2.2

As shown by apparent solubility values reported in Table 3.2, piroxicam was more soluble at pH 6.5 than at pH 5. This is in agreement with the drug Pka_1 and Pka_2 values, which are 1.86 and respectively 5.46. Bile salts, lecithin and HPMC all show effect on increasing the apparent solubility of the model drug. The graph in Figure 3.1 shows how the presence of NaTC in the Blank FaSSIF and Blank FeSSIF media causes only a slight in increase of the drug solubility in blank FaSSIF, and a more significant increase in blank FeSSIF in which piroxicam solubility was 4 times higher than in buffer pH 5. As shown by Table 3.1 NaTC concentration in blank FeSSIF is five times higher than in blank FaSSIF. It is likely that the presence of bile salt reduces the fluid surface tension, impacting the drug powder aggregates wetting and consequently increasing the surface area available for drug solubilisation. Furthermore, as reported in literature, bile salts can increase drug solubility through direct solubilisation effect by the bile salts micelles. [96] Lecithin also showed to have an impact on piroxicam solubilisation, particularly in FaSSIF where drug solubility value increased from 41.6±3.6μg/ml (in blank FaSSIF) to 206.6±19.1μg/ml (FaSSIF). Lecithin-bile salts complexes have been extensively studied and the formation of bile-salts/lecithin mixed micelles is widely discussed in literature. [213–215] Bile salts/lecithin aggregates physical features are discussed in Chapter 5. Their effect on enhancing the apparent solubility of poorly water-soluble drugs has been extensively described. [216–218] The data obtained in this study showed an increase of the FaSSIF and FeSSIF media piroxicam solubilisation ability,

compared to blank FaSSIF and blank FeSSIF, as a possible consequence of the lecithin-bile salts aggregates solubilisation capacity.

HPMC effect on drug solubilisation can clearly be observed from data reported in Table 3.2 and their plot in Graph 3.1. Compared to the solubility of the drug alone, the apparent solubility of piroxicam increased in the presence of HPMC, indicating the solubilisation effect of the carrier on the drug. HPMC is known to have self-assembling properties and to decrease surface tension as a consequence of its aggregation. [219] Therefore, increased piroxicam solubility in the presence of HPMC may be related to HPMC microenvironment surfactant properties, as already described by Mitchell. [220] The solubilisation effect of HPMC on piroxicam did not increase significantly with increasing HPMC concentration, suggesting that a "saturation" of the HPMC solubilisation effect on the drug may have reached at the low HPMC concentration used in this study.

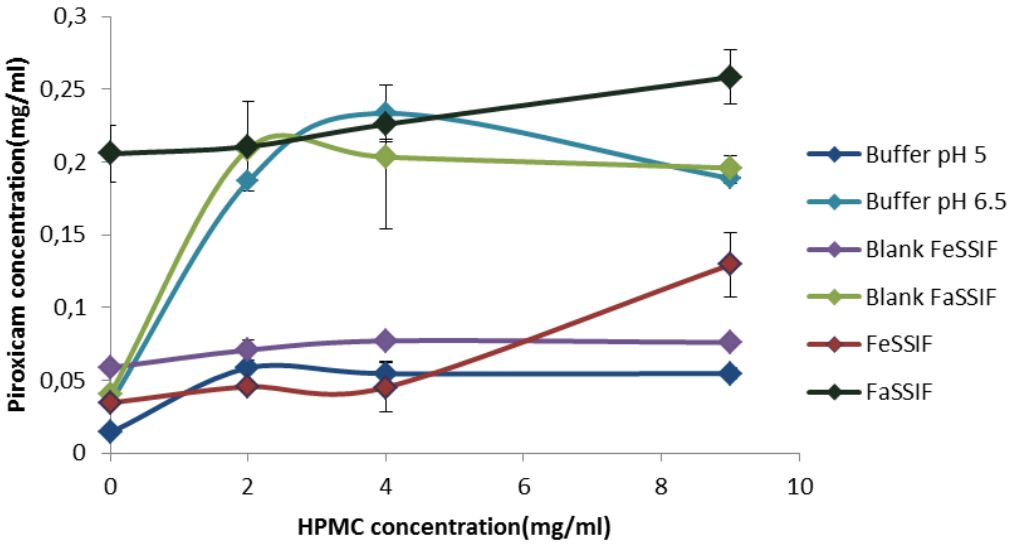

Fig. 3.1: Phase solubility diagrams of piroxicam at different HPMC concentrations in buffer pH5, buffer pH 6.5, blank FaSSIS, blanf FeSSIf, FeSSIF and FaSSIF at 37 ˚C (n=3)

The same drug solubilisation determinations were performed in the presence of PVP. Obtained results, summarised in Table 3.3 and shown in Figure 3.2, confirmed that the solubilisation effect of piroxicam increases with increasing PVP concentration. Similar to the HPMC:piroxicam systems, this solubilisation effect is most significant when FaSSIF was used as the media. Obtained results indicate a significant influence of the presence of both polymeric carrier and bile salts on the drug solubilisation. This effect and its possible impact on drug uptake will be discussed in details in the following Chapters of the Thesis.

Table 3.3: Piroxicam apparent solubility values in different media, with and without the presence of PVP (1, 2, 4, 9 and 19 mg/ml) (n=3)

Medium	Piroxicam apparent solubility values (μg/ml)					
	PXM	PVP:PXM 1:1 (PVP 1 mg/ml)	PVP:PXM 2:1 (PVP 2mg/ml)	PVP:PXM 4:1 (PVP 4 mg/ml)	PVP:PXM 9:1 (PVP 9 mg/ml)	PVP:PXM 19:1 (PVP 19 mg/ml)
Buffer pH 6.5	34.1±0.2	205.9±4.9	0.203±8.3	282.6±83.2	263.1±62.5	319.2±36.7
Buffer pH 5	14.9±1.2	22.5±1.3	19.8±3.2	46.9±3.7	54.8±11.5	68.9±40.1
Blank FaSSIF	41.9±3.5	205.7±20.4	201.1±5.2	344.5±3.2	332.5±4.2	324.7±24.1
Blank FeSSIF	58.4±8.8	52.6±1.2	60.5±1.5	77.3±2.5	76.9±2.1	130.8±12.5
FaSSIF	206.8±19.2	232.4±29.6	233.5±26.1	312.4±20.8	393.3±32.5	597.1±3.6
FeSSIF	34.9±3.5	39.8±1.5	38.4±1.8	40.3±1.9	55.6±1.7	56.8±4.3

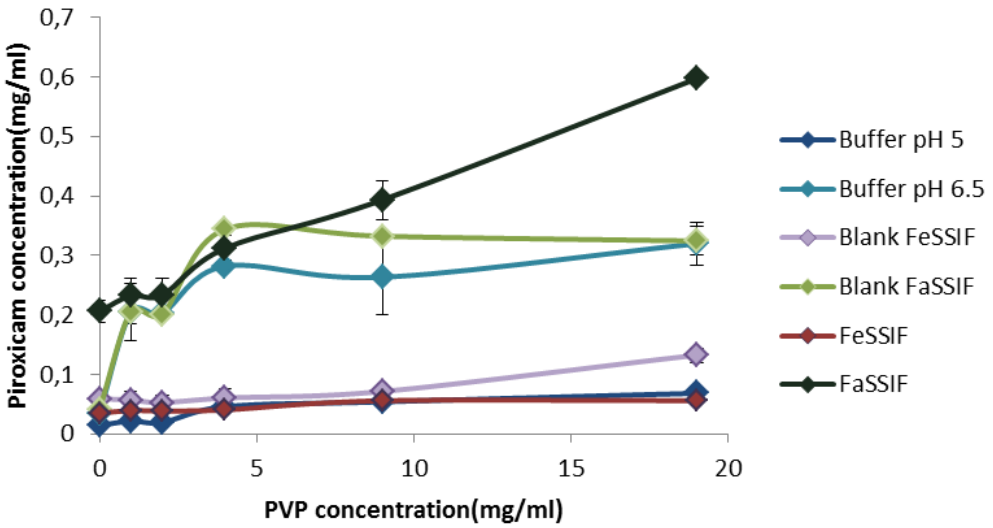

Fig. 3.2: Phase solubility diagrams of piroxicam at different PVP concentrations in buffer pH5, buffer pH 6.5, blank FaSSIS, blank FeSSIf, FeSSIF and FaSSIF at 37 ˚C (n=3)

PVP showed stronger impact on piroxicam solubilisation than HPMC. This effect can be related to the different physicochemical behaviour of the polymers in aqueous media, and possibly different interactions with the components of dissolution media used. Further investigation was performed to clarify the different HPMC and PVP solubilisation capability and the results are discussed in Chapters 4 and 5.

3.3.2.2 Fenofibrate

Fenofibrate is practically insoluble in water and, having no ionizable function groups in the molecular structure, its solubility is not affected by the medium pH. As shown in Table 3.4 the solubility values of fenofibrate in the two buffers are extremely low, and the data obtained are in good agreement with literature data reporting fenofibrate solubility in pure water. [221] This confirms that the pH has no impact on the drug solubilisation, and the difference in osmolality between acetate (pH 5) and phosphate (pH 6.5) buffers seemed to have a negligible effect on fenofibrate solubilisation. The presence of NaTC caused the drug solubility to increase of 10 folds in blank FaSSIF and of 8 folds in FeSSIF. This significant solubility enhancement may be attributed to the micellar solubilisation in the media, particularly for FeSSIF where, due to the higher NaTC concentration, a higher number of micelles is expected. As a consequence of this, the drug solubilisation is more significant in blank FeSSIF compared to blank FaSSIF.

Table 3.4:Fenofibrate apparent solubility values in different media, with and without the presence of HPMC (2, 4 and 9 mg/ml) (n=3)

Medium	**Fenofibrate apparent solubility values (μg/ml)**			
	Fenofibrate	**HPMC:Fenofibrate 2:1 (HPMC 2 mg/ml)**	**HPMC:Fenofibrate 4:1 (HPMC 4 mg/ml)**	**HPMC:Fenofibrate 9:1 (HPMC 9 mg/ml)**
Buffer pH 6.5	0.4±0.3	7.8±4	6.6±1.4	11.5±2.3
Buffer pH 5	0.9±0.5	6.7±1.3	13.5±1.6	12.2±1.2
Blank FaSSIF	4.7.±0.5	14.8±1.6	8.5±1.6	20.3±4.5
Blank FeSSIF	7.2±0.9	13.2±5.4	16.9±2.3	38.4±6.7

In Figure 3.3 fenofibrate solubility values in the different media are shown as a function of HPMC concentration. As for piroxicam, the impact of HPMC on the drug solubilisation is extremely significant in all the media used, leading to a solubility increase of almost 30 folds in the two buffers and of about 5 times in the blank FaSSIF and blank FeSSIF media (compared to the crystalline drug). As in the absence of HPMC, the highest solubility value was obtained in the Blank FeSSIF medium, confirming the primary role of the NaTC micelles in the drug solubilisation. The solubility value of fenofibrate increased from 7.2 μg/ml to up to 38.4 μg/ml increasing the polymer weight ratio. This result suggests

a possible formation of new solubilising aggregates in solution, which are likely to be a result of NaTC-polymer aggregation. As already mentioned, NaTC-polymers aggregation has been studied and characterised and are discussed in Chapters 4 and 5.

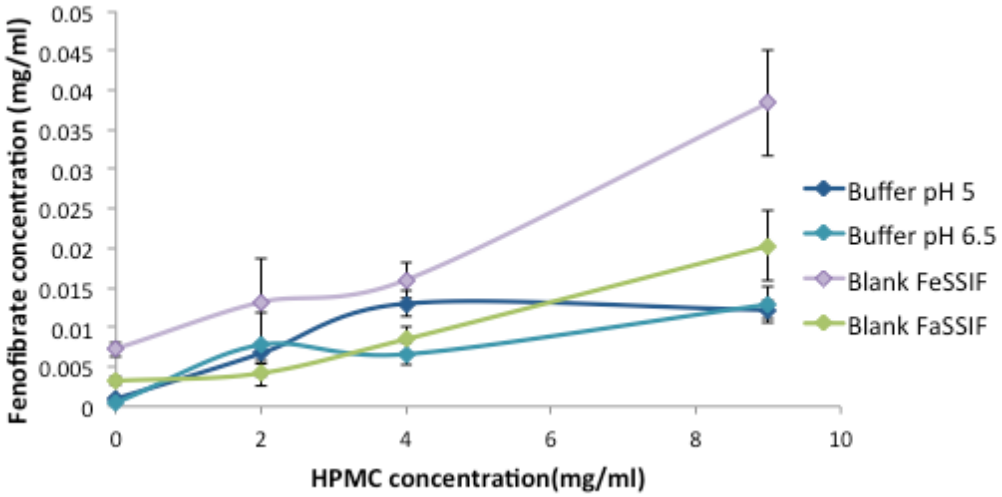

Fig. 3.3: Phase solubility diagrams of fenofibrate at different HPMC concentrations in buffer pH5, buffer pH 6.5, blank FaSSIS and blank FeSSIF at 37 ˚C (n=3)

Fenofibrate apparent solubility has been studied also in the presence of PVP and obtained results are summarised in Table 3.5 and Figure 3.4. As showed in Table 3.5 also for PVP-fenofibrate systems the presence of polymer caused an increase of the drug solubility. Compared to HPMC the impact of polymer on the drug solubilisation seems to be lower, differently from what obtained for piroxicam. The different results obtained with piroxicam and fenofibrate might firstly be a consequence of the different intrinsic solubility of the two drugs, but they also suggest a possible difference in the polymer solubility enhancement mechanism for the two drugs. This might be due to different intermolecular interaction of piroxicam and fenofibrate with the two carriers, which will be discussed in section 3.3.7 of this Chapter.

Table 3.5: Fenofibrate apparent solubility values in different media, with and without the presence of PVP (2, 4 and 9 mg/ml) (n=3)

Medium	Fenofibrate apparent solubility values (µg/ml)			
	Fenofibrate	PVP:Fenofibrate 2:1 (PVP 2mg/ml)	PVP:Fenofibrate 4:1 (PVP 4 mg/ml)	PVP:Fenofibrate 9:1 (PVP 9 mg/ml)
Buffer pH 6.5	0.4±0.3	5.9±2.8	6.6±1.4	5.8±1.7
Buffer pH 5	0. 9±0. 5	6.2±0. 5	13.9±1.6	9.0±0.2
Blank FaSSIF	4.7±0.5	6.0±1.2	7.0±2.1	7.1±1.3
Blank FeSSIF	7.2±0. 9	17.0±5.4	14.4±1.4	14.9±2.4

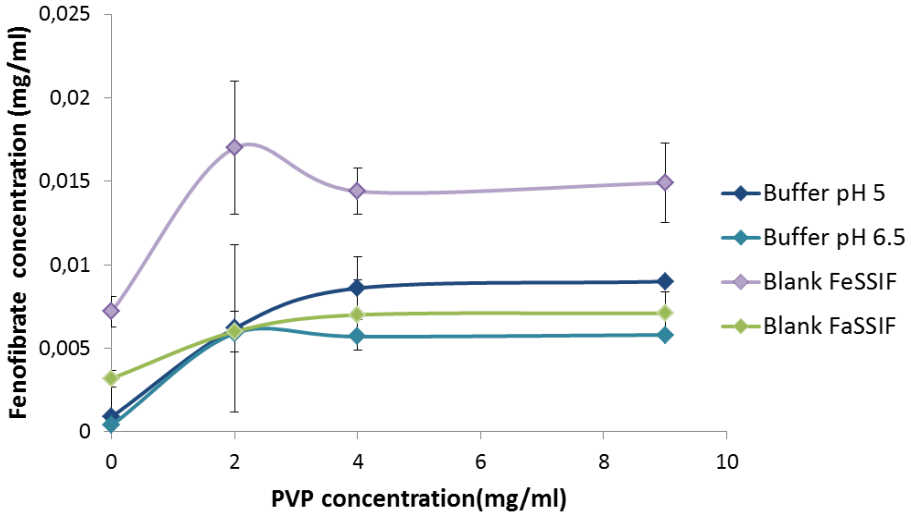

Fig. 3.4: Phase solubility diagrams of fenofibrate at different PVP concentrations in buffer pH 5, buffer pH 6.5, blank FaSSIS and blank FeSSIF at 37 ˚C (n=3)

3.3.2.3 Griseofulvin

Apparent solubility values obtained for Griseofulvin in the different media, with and without the presence of HPMC, are summarized in Table 3.6. As for fenofibrate, griseofulvin does not have ionizable groups, thus pH was not expected to impact its solubility. Indeed solubility values obtained at pH 5 and pH 6.5 were very close and slightly higher than literature data obtained in pure water. [222] Differently from piroxicam and fenofibrate, comparing the results obtained in buffer at pH 6.5 and in blank FaSSIF,

griseofulvin solubility values did not change significantly with the presence of NaTC in blank FaSSIF. In blank FeSSIF griseofulvin solubility was two folds higher than in buffer at pH 5. This confirmed the primary role of NaTC micelles in the drug solubilisation in blank FeSSIF where, as already discussed, high number of micelles is present compared to blank FaSSIF.

Table 3.6: Griseofulvin apparent solubility values in different media, with and without the presence of HPMC (2, 4 and 9 mg/ml) (n=3)

Medium	Griseofulvin apparent solubility values (μg/ml)			
	Griseofulvin	HPMC:Griseofulvin 2:1 (HPMC 2mg/ml)	HPMC:Griseofulvin 4:1 (HPMC 4 mg/ml)	HPMC:Griseofulvin 9:1 (HPMC 9 mg/ml)
Buffer pH 6.5	115.6±18.9	105.0±1.0	105.8±1.2	95.0±8.1
Buffer pH 5	106.8±9.7	83.9±1.8	130.2±22.5	128.3±12.6
Blank FaSSIF	0116.4±16.2	129.9 ±16.4	184.9±3.4	202.3±1.5
Blank FeSSIF	205.2±28.2	316.5±3.0	305.2±60.	311.7±9.7

Figure 3.5 shows the impact of HPMC on griseofulvin solubilisation. No significant effect was obtained in the two buffers and in blank FaSSIF at the lowest HPMC concentration (2mg/ml). HPMC concentration increase yielded a slight increase of the drug solubility, particularly for blank FaSSIF media, where a drug solubility of 202.3±1.5 μg/ml is obtained at the highest HPMC concentration (9 mg/ml) employed. Results obtained in blank FeSSIF show a different trend compared to the other media used. Indeed griseofulvin solubility increased to 316.5±3.0 μg/ml in the presence of the carrier (HPMC concentration=2mg/ml), but did not further increase when more polymer was present. Similar to the piroxicam data, this result suggests a possible “saturation” of HPMC solubilisation effect.

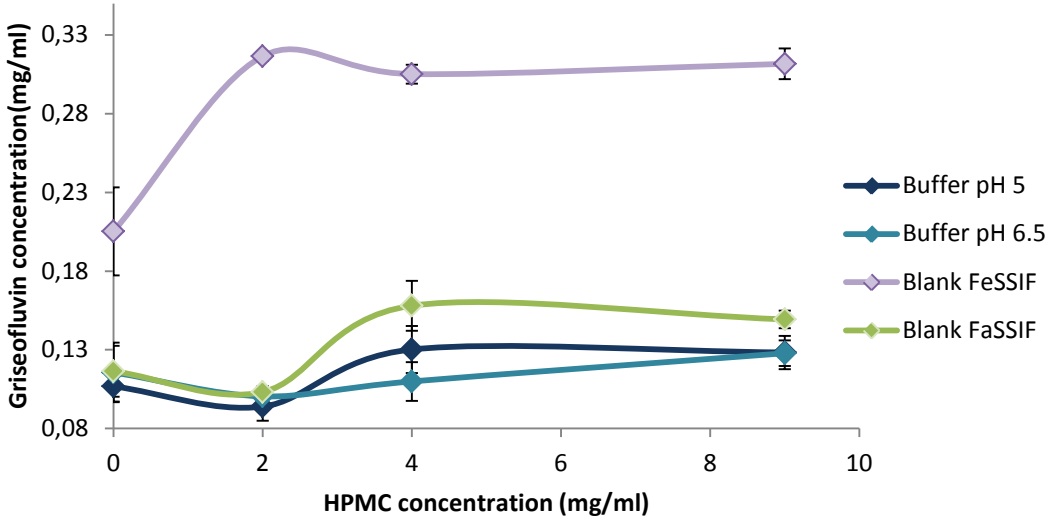

Fig. 3.5: Phase solubility diagrams of griseofulvin at different HPMC concentrations in buffer pH 5, buffer pH 6.5, blank FaSSIS and blank FeSSIF at 37 ˚C (n=3)

As for piroxicam and fenofibrate, griseofulvin solubility studies have been performed also in the presence of PVP. Table 3.7 shows griseofulvin solubility values obtained in the presence of PVP, in the 4 different media used for the study.

Table 3.7: Griseofulvin apparent solubility values in different media, with and without the presence of PVP (2, 4 and 9 mg/ml) (n=3)

Medium	Griseofulvin apparent solubility values (µg /ml)			
	Griseofulvin	PVP:Griseofulvin 2:1 (PVP 2mg/ml)	PVP:Griseofulvin 4:1 (PVP 4 mg/ml)	PVP:Griseofulvin 9:1 (PVP 9 mg/ml)
Buffer pH 6.5	111.6±012.3	105.0±01.0	105.8±1.2	95.0±8.1
Buffer pH 5	105.0±1.1	102.8±8.9	103.2±3.7	197.0±4.9
Blank FaSSIF	105.8±12.3	105.6±1.5	158.9±15.9	197.7±17.3
Blank FeSSIF	95.0±8.1	97.5±10.6	149.3±5.6	201.2±1.6

As shown in Figure 3.6 PVP effect on griseofulvin solubilisation resulted to be different from HPMC one. No drug solubilisation increase was obtained in the presence of PVP (2mg/ml) in the two buffers and in Blank FeSSIF. Griseofulvin solubilisation

significantly increased increasing PVP concentration in blank FaSSIF, showing a maximum drug solubility value of 201.2±1.6 µg/ml in blank FeSSIF.

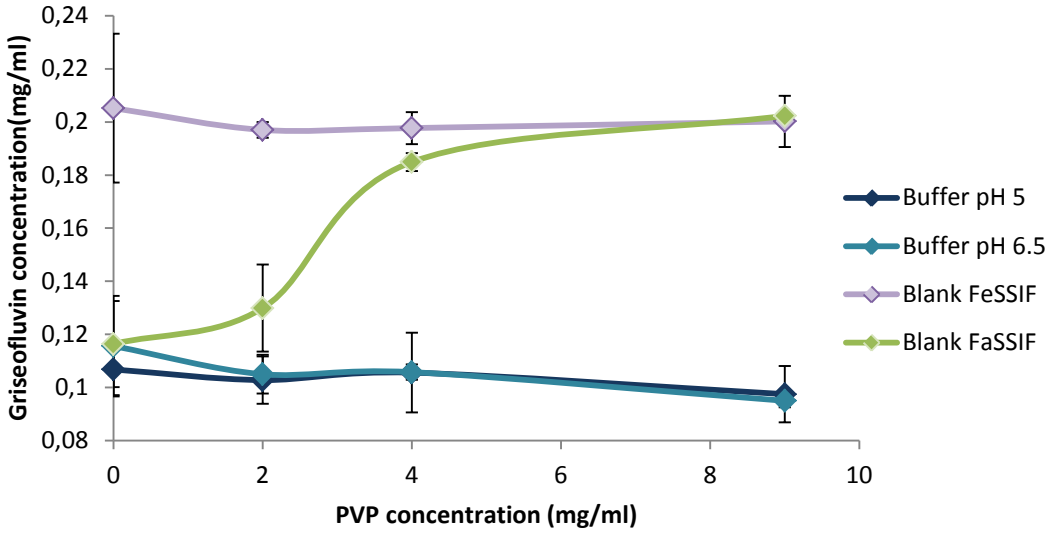

Fig. 3.6: Phase solubility diagrams of griseofulvin at different HPMC concentrations in buffer pH5, buffer pH 6.5, blank FaSSIS, blanf FeSSIF, FeSSIF and FaSSIF at 37 ˚C (n=3)

3.3.3 Spray dried solid dispersion preparation

The yields of the spray drying processes performed to obtain solid dispersion formulation are summarised in Table 3.8. Yields values have been calculated as a percentage of the raw materials weight used. Spray drying pf unprocessed piroxicam without the presence of polymeric carriers was also attempted, but was not successful.§

Table 3.8: Summary of yield and outlet temperature values obtained during spray drying process for the different samples

Spray dried sample	Outlet T(°C)	Yield(%)	Number of replicates
HPMC	50±1	26.1±1.2	3
HPMC:Piroxicam 2:1	53.7±4	23.4±5.9	3
HPMC:Piroxicam 4:1	52±3	11.8±4.9	3
HPMC:Piroxicam 9:1	51.7±2.1	19.34±4.27	3
PVP	52±2	13.50±7.02	3
PVP:Piroxicam 2:1	53.7±4	13.47±6.01	3
PVP:Piroxicam 4:1	53.67±1.52	15.66±5.05	3
PVP:Piroxicam 9:1	51.67±2.51	20.26±6.52	3
PVP-VA	50	7.7	1
PVP-VA:Piroxicam 2:1	48	10	1
HPMC-AS	53	<1	1
HPMC-AS:Piroxicam 2:1	46	2	1
HPMC:Fenofibrate 2:1	48±1	6.8±0.7	2
HPMC:Griseofulvin 2:1	48.5±1.5	12.7±1.83	2
PVP:Fenofibrate 2:1	49.5±2.12	13.83±8.71	2
PVP:Griseofulvin 2:1	51.15±2.12	20.85±1.2	2

As clearly shown by the table, yield values have been low for all the samples. This is a consequence of the low solid concentration used. The practically feasible solid concentration was limited by the poor solubility of the model drugs in the EtOH:H_2O mixture, thus, it was not possible to increase the solid concentration without causing the occurrence of drug precipitation. In particular for HPMC-AS and PVP-VA samples only 1 replicate has been studied, thus the results obtained are preliminary and spray-drying parameters for this samples need further optimisation in future work.

Table 3.9 summarises theoretical and actual drug loadings of the formulation prepared. Actual drug loading values were determined assaying the drug concentration by UV-VIS analysis, as described in Section 3.2.3.

Table 3.9: Summary of theorical and actual drug loading of spray dried formulations

Spray dried sample	Theoretical drug loading (%w/w)	Actual drug loading (%w/w)	Number of replicates
HPMC:Piroxicam 2:1	33.3	35.4±2.7	3
HPMC:Piroxicam 4:1	25	19.34±4.27	3
HPMC:Piroxicam 9:1	10	11.8±4.9	3
PVP:Piroxicam 2:1	33.3	20.26±6.52	3
PVP:Piroxicam 4:1	25	15.66±5.05	3
PVP:Piroxicam 9:1	10	13.47±6.01	3
PVP-VA:Piroxicam 2:1	33.3	10	1
HPMC-AS:Piroxicam 2:1	33.3	2	1
HPMC:Fenofibrate 2:1	33.3	6.8±0.7	2
HPMC:Griseofulvin 2:1	33.3	12.7±1.83	2
PVP:Fenofibrate 2:1	33.3	13.83±8.71	2
PVP:Griseofulvin 2:1	33.3	20.85±1.2	2

From values shown in Table 3.9 it is possible to conclude that the drug encapsulation efficiency in the spray dried polymeric microparticles was not very reproducible for few of the formulation prepared. Furthermore the actual drug loading is lower than the theoretical one, a part from PVP formulations with the highest drug loading and for the formulation HPMC:Piroxicam 2:1.

3.3.4 TGA Analysis

TGA experiments were performed for all the spray dried solid dispersions, in order to estimate residual solvent and moisture content of the fresh samples. The presence of water and solvents in amorphous system can impact their physical state, as due to its low glass transition temperature (T_g) value (136-165K), [223] water can lower the T_g of the amorphous systems, increasing the molecular mobility within them. Furthermore residual solvent might be toxic and prevent the formulation use in the clinic. This plasticizing effect can lead to physical transition of amorphous systems, facilitated by the gained molecular mobility of the system, [224] and can consequently promote crystallization. Obtained TGA results are shown in Figure 3.7 a, b and c and summarised in Table 3.10.

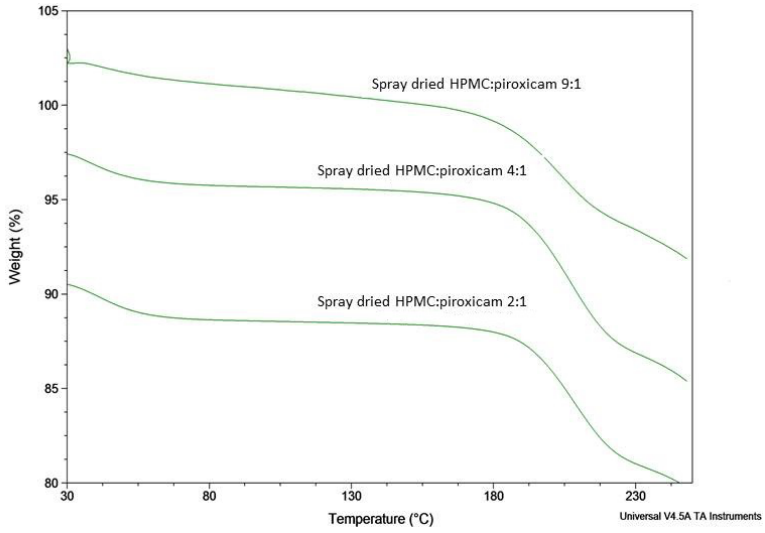

a

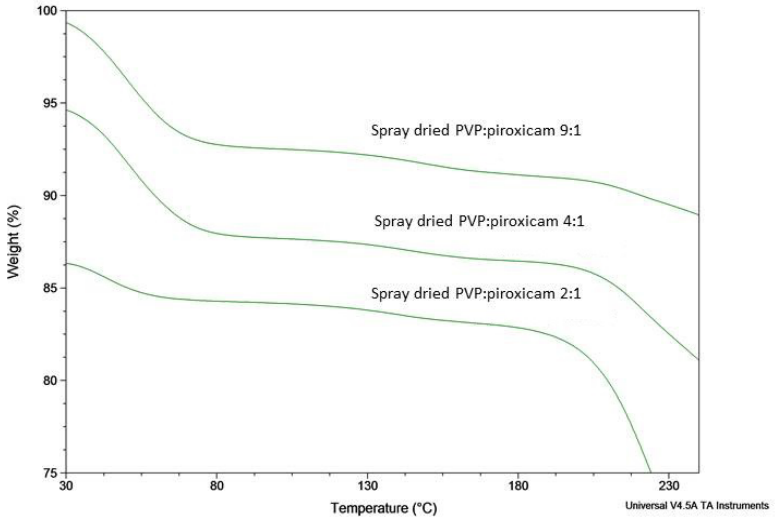

b

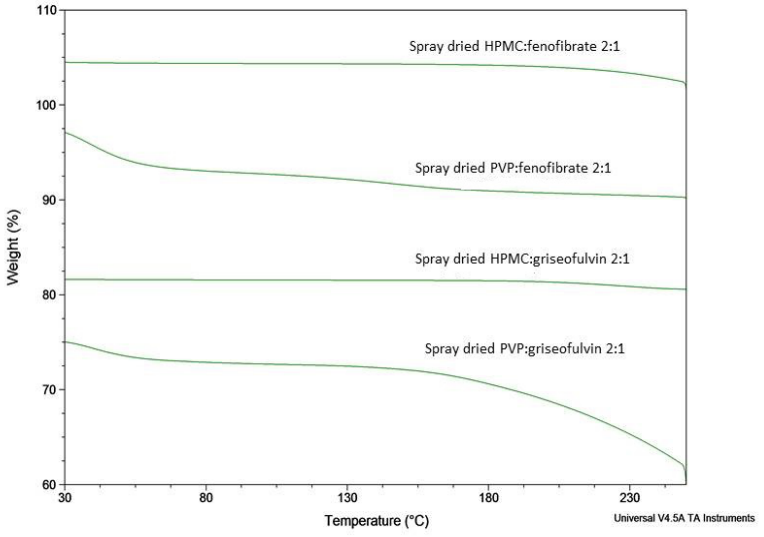

c

Figure 3.9:TGA thermograms for HPMC:piroxicam (a), PVP:piroxicam (b) and HPMC:fenofibrate, PVP:fenofibrate, HPMC:griseofulvin and PVP:griseofulvin spray dried samples (c).

As described in Section 3.3.3, samples have been spray dried from a mixture of ethanol/distilled water 1:1. The boiling point of the mixture is 79.6 °C. Analysis of the TGA curves was performed between 30 and 110 °C. In Figure 3.36a it can be seen that a weight loss is present for HPMC:piroxicam samples starting at about 30 °C, which corresponds to the moisture/solvent content loss. Piroxicam thermal decomposition occurs after melting (200-230 °C in a single step). The occurrence of piroxicam decomposition can be seen in Figure 3.9 a and 3.9 b with an onset at about 200-205 °C. Moisture/solvent content loss themal can also be seen for PVP: griseofulvin 2:1and PVP:fenofibrate 2:1 spray dried samples in Figure 3.9 c.

Table 3.10: summary of residual moisture content of spray dried samples (n=3)

Spray dried sample	Moisture-Solvent content %
HPMC:piroxicam 2:1	0.81±0.14
HPMC:piroxicam 4:1	1.582±0.41
HPMC:piroxicam 9:1	1.438±0.11
PVP:piroxicam 2:1	2.91±0.83
PVP:piroxicam 4:1	7.4±0.31
PVP:piroxicam 9:1	6.97±0.45
HPMC:fenofibrate 2:1	3.03±0.61
PVP:fenofibrate 2:1	0.19±0.04
HPMC:griseofulvin 2:1	0.50±0.04
PVP:griseofulvin 2:1	0.09±0.01

As summarised in Table 3.10 freshly spray dried samples showed significant moisture/solvent content. For both PVP and HPMC based spray dried solid dispersion the moisture content% increased increasing the polymer weight ratio. Considering the hydrophilic nature of the two polymers, a higher polymer load is expected to increase the amount of moisture residual from the processing and moisture absorbed by the final product. [225] In particular PVP samples show high residual moisture, due to the high polymer hygroscopicity. [167] Obtained data clearly show that residual moisture is not only dependent on the polymer but also on the hygroscopicity of the whole drug-polymer system. Indeed, PVP:griseofulvin solid dispersion showed a low moisture content (0.09 %), compared to PVP:fenofibrate and PVP:piroxicam samples. Such difference might be due PVP-griseofulvin interaction. It has been reported that the strength of polymer-drug interactions,

as well as drug–water interaction can influence the system moisture uptake. [226] Therefore, it is possible that griseofulvin-water interaction is weaker and less likely to occur compared to the other model drugs, while PVP interacts more strongly with griseofulvin than with other drugs. TGA analysis has not been performed on PVP-VA and HPMC-AS spray dried samples. As previously discussed, such samples have been prepared only in one replicate and due to the low spray drying yield, solid state characterisation could not be completed.

3.3.5 Spray dried solid dispersions morphology

SEM was used to study the morphologies of the spray dried microparticles. Figure 3.8 shows spray dried HPMC and HPMC:Piroxicam microparticles.

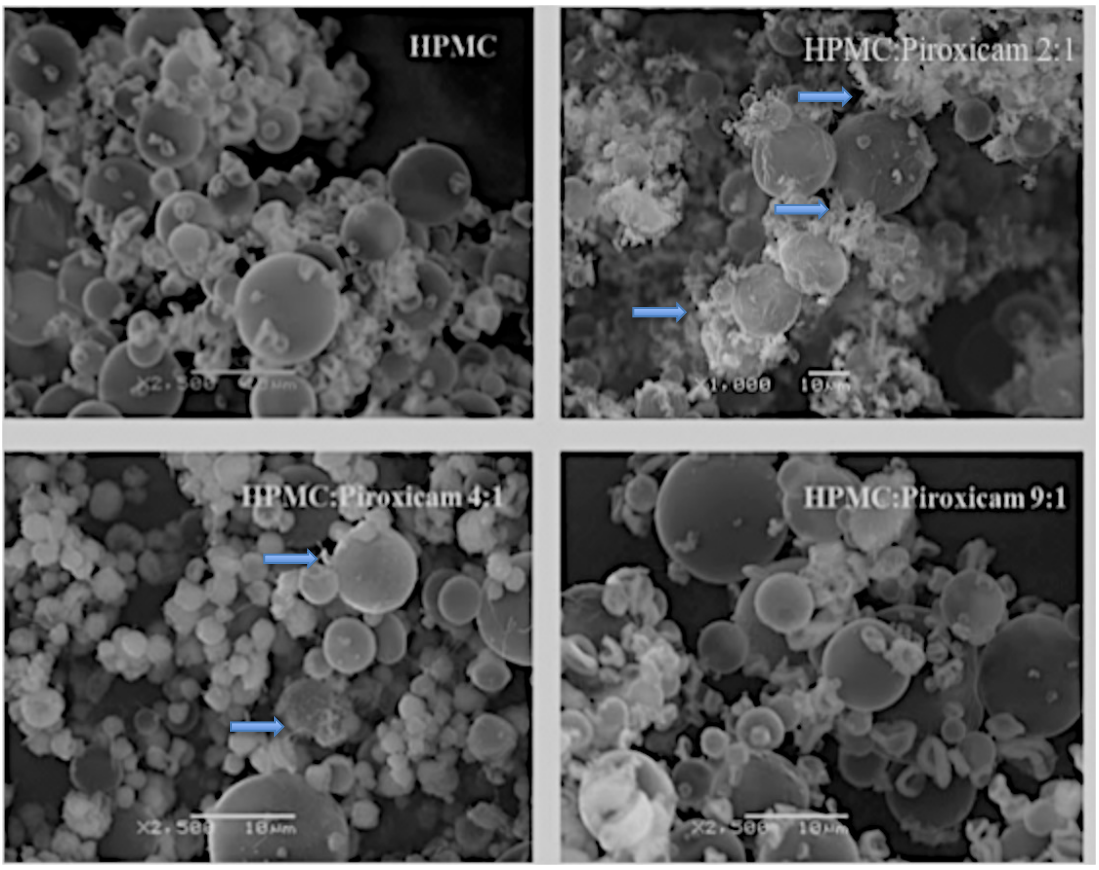

Fig.3.8 : SEM images of spray dried HPMC, HPMC:Piroxicam 2:1, HPMC:Piroxicam 4:1, HPMC:Piroxicam 9:1 microparticles. Blu arrows indicate drug crystals.

HPMC:piroxicam solid dispersions are spherical microparticles with sizes in the range of 2-10 µm for all the formulations. No significant different in size is observable changing the drug:polymer ratios. For the formulation with higher drug loading, HPMC:piroxicam 2:1 and 4:1, few drug crystals can be observed in the image, suggesting

that increasing the polymer amount the drug is more likely to be dispersed in its amorphous form in the formulation. For all samples few microparticle appear to be collapsed, effect which has been suggested by other researchers to be due to the slow evaporation of the solvent. [48]

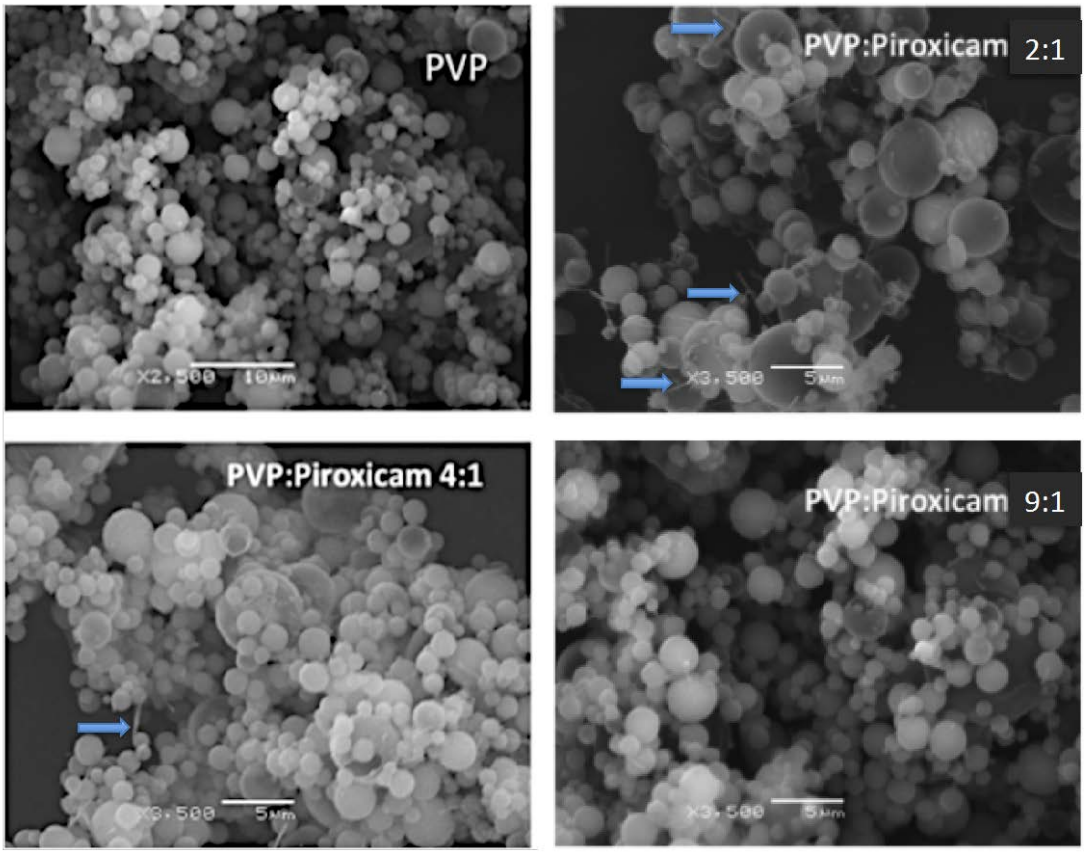

Fig.3.9: SEM images of spray dried PVP, PVP:piroxicam 2:1, PVP:piroxicam 4:1, PVP:piroxicam 9:1 microparticles

As shown in Figure 3.9 spray drying of PVP:piroxicam mixtures yielded smaller microparticles compared to HPMC:piroxicam systems. Indeed sizes between 0.5 and 5 μm were obtained for PVP:piroxicam 2:1 formulation. Sizes obtained are similar to PVP:piroxicam spray dried solid dispersions described in literature. [227] Differently from HPMC based systems microparticles sizes increased increasing the amount of polymer in the solid dispersion. Few piroxicam crystals are visible for samples with higher drug loading.

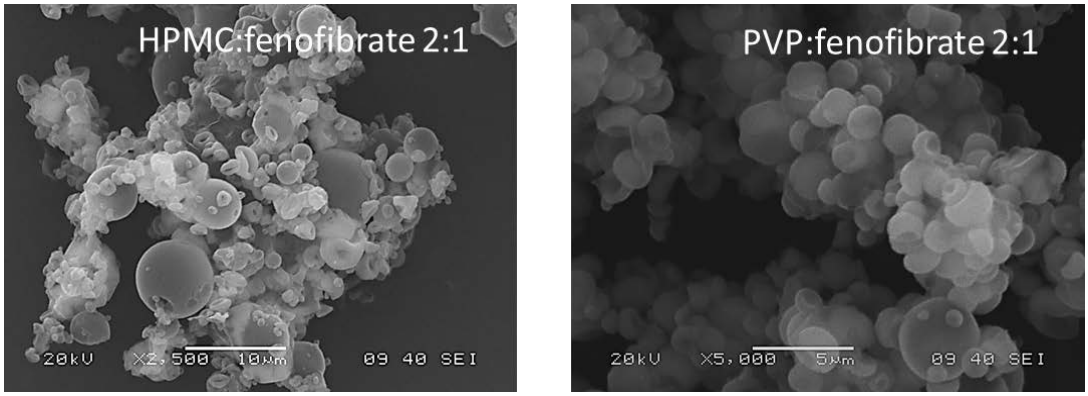

Fig 3.10: SEM images of microparticles of spray dried HPMC:fenofibrate 2:1 and PVP:fenofibrate 2:1

Figure 3.10 shows SEM images of HPMC:fenofibrate 2:1 and PVP fenofibrate 2:1 spray dried solid dispersions. As for piroxicam samples, HPMC based microparticles resulted to be bigger that PVP microparticles, confirming HPMC tendency to yield bigger particles. Indeed HPMC:fenofibrate microparticle sizes appear to be in the range of 1-10 µm, having a spherical shape with the presence of few collapsed particles. PVP:fenofibrate microparticles are in the range of 1-5 µm and are more regularly spherical shaped. Few particles appear to be broken, confirming that spray drying of fenofibrate formulation needs to be optimised, as already highlighted by the very low yield values obtained from the spray drying process (see Table 3.9). No drug crystals are visible in any of the two formulations despite they contain highest drug loading tested.

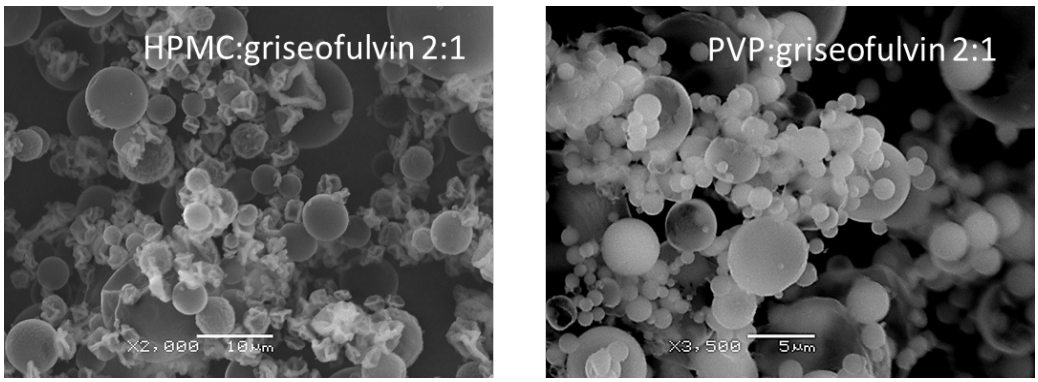

Fig 3.11: SEM images of spray dried HPMC:griseofulvin 2:1 and PVP:griseofulvin 2:1 microparticles

As shown in Figure 3.12 both HPMC:griseofulvin 2:1 microparticles resulted to be in the same range of sizes obtained for HPMC:fenofibrate 2:1 and HPMC:piroxicam formulations, 2-10 µm. Also in this case particles appear spherical shape and few of them are collapsed. PVP:griseofulvin 2:1 spray dried microparticles are between 1 and 5 µm in size and spherical as for PVP:piroxicam 2:1 and PVP:fenofibrate 2:1 formulation. Thus, the

drug does not have a significant effect on the microparticles shape and size, which seems to be dependent mainly on the polymeric carrier used. No drug crystals are visible in the SEM images.

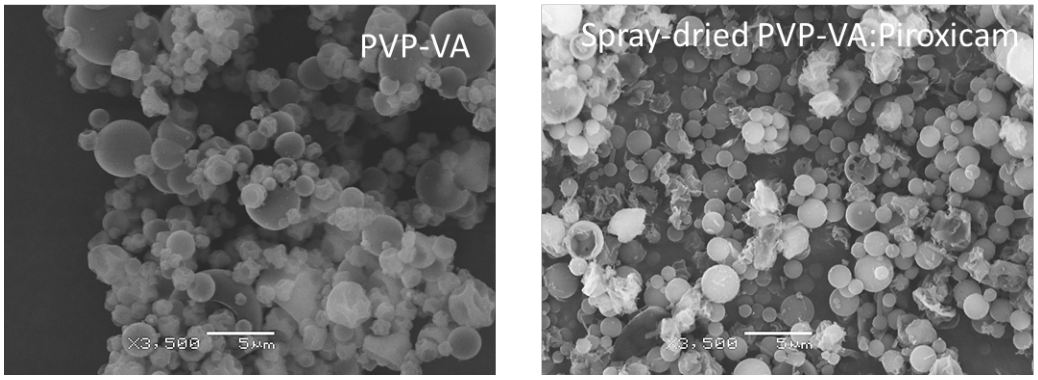

Fig 3.12: SEM images of spray dried PVP-VA and PVP-VA:piroxicam 2:1 microparticles

Figure 3.12 shows SEM images of spray dried PVP-VA and PVP-VA:piroxicam 2:1 spray dried microparticles. As previously specified, only one replicate was performed for these particular systems. For this reason obtained results need to be considered preliminary data. PVP-VA micropartcles are slightly bigger in size than the ones obtained spray drying the correspondent homopolymer PVP, indeed few of the particles in the image are above 5 μm in size. Piroxicam crystals were not visible in the SEM image, suggesting that the drug in the solid dispersions is in its amorphous form.

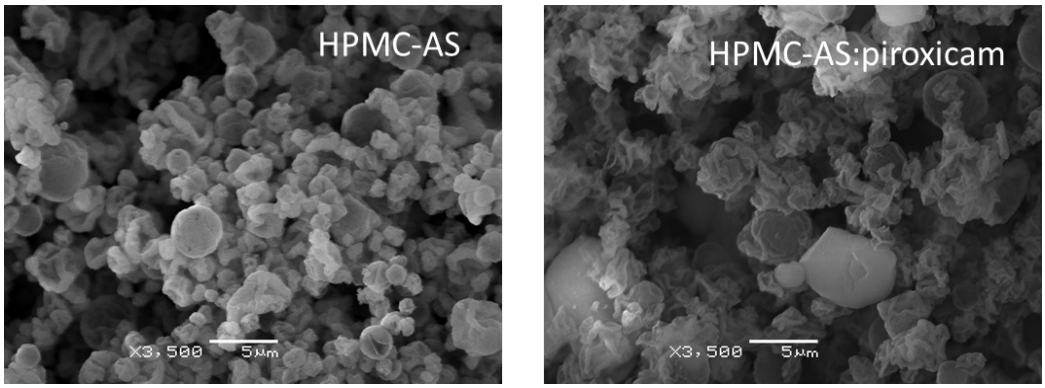

Fig 3.13:SEM images of spray dried HPMC-AS and HPM-AS:piroxicam 2:1 microparticles

As shown in Figure 3.13 spray dried HPMC-AS microparticles show an irregular shape, with few spherical particles and many collapsed ones. The particles surface does not appear smooth as for HPMC, PVP and PVP-VA spray dried microparticles. HPMC-AS microparticles are smaller than the correspondent spray dried HPMC particles, having sizes

in the range of 1-5 µm. In the presence of piroxicam bigger microparticles with irregular shapes were obtained. No drug crystals are visible in the image, suggesting that piroxicam is mainly in its amorphous form in the spray dried formulation. As only one replicate was studied, an optimisation of the spray drying process for HPMC-AS sample would be needed, in order to improve the process yield and the features of the obtained microparticles.

3.3.6 PXRD analysis of spray dried formulations

In order to confirm the physical states (either molecularly dispersed in the polymer, being phase separated crystalline drug, or phase separated amorphous domains) of drug in the spray-dried formulations, PXRD analysis was performed on all the spray dried samples. As already discussed in Chapter 2 (section 2.3.3), X–Ray Diffraction method determines crystallinity and polymorphic purity by measuring the diffraction of X-Rays by a powder, which is directly dependent on the three dimensional periodicity of the atoms and molecules in the crystal lattice. [228] Figure 3.14 shows PXRD results obtained for HPMC:Piroxicam formulations.

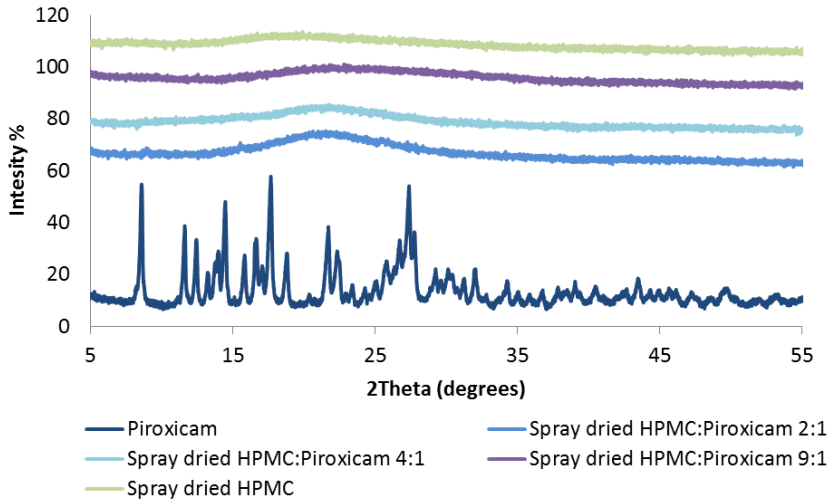

Fig 3.14: PXRD results of freshly prepared spray dried HPMC:piroxicam formulations compared to raw piroxicam and spray dried HPMC.

The PXRD result of the piroxicam as received matches the diffraction pattern of piroxicam crystalline form I (cubic form) reported in literature. [229] PXRD patterns of the spray dried formulation show the loss of sharp crystalline piroxicam diffraction peaks. It can be seen that spray dried HPMC:piroxicam samples with all drug loadings show amorphous halos rather than crystalline peak features, indicating that no significant amount of crystalline piroxicam is present after spray drying. From Figure 3.14 it is possible to observe

few weak crystalline diffraction peaks at 8.6, 16.66 and 27,74 2θ with low intensities in the spray dried HPMC:piroxicam 2:1 sample indicating trace of crystalline drug which is absent in the other two formulations with lower drug loadings. This result is in agreement with SEM images, in which the presence of piroxicam residual crystals in spray dried formulations with 2:1 polymer:drug ratio were present. No crystalline peak were observed for the spray dried formulation HPMC:piroxicam 4:1, despite the few drug crystals present in SEM image (Fig 3.8). Such disagreement is likely to be due to the difference in the limit of detection of different instruments. The few crystal quantity is possibly below the limit of detection of PXRD, thus no crystalline peak was observed. PXRD results suggest that the presence of higher proportions of polymer can reduce drug crystallization in the spray dried solid dispersions and stabilise the amorphous drug.

P-XRD analysis has been performed also on spray dried PVP:piroxicam formulations, as shown in Figure 3.15.

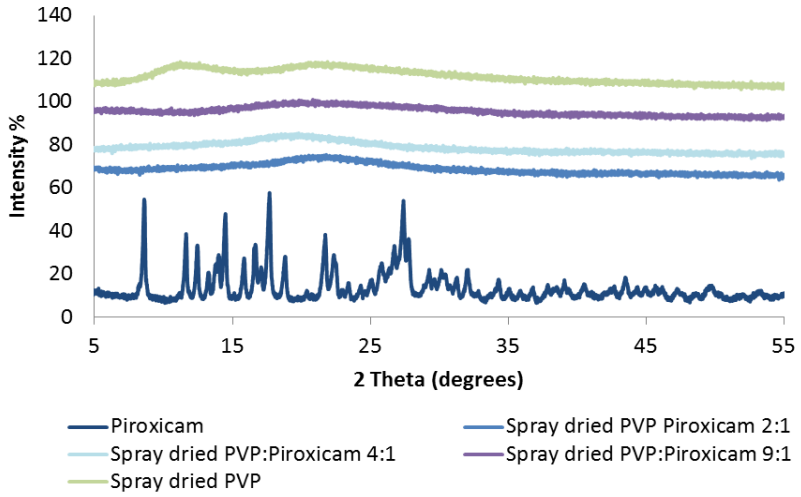

Fig 3.15: PXRD results of freshly prepared spray dried PVP:piroxicam formulations compared to raw piroxicam and spray dried PVP.

As for HPMC:piroxicam samples, spray dried PVP:piroxicam formulations XRD patterns show the presence of amorphous halos, indicating no significant amount of crystalline drug in the sample after spray drying process. However, in contrast to the HPMC formulations, the formulation with lowest PVP content (PVP:piroxicam 2:1) shows fully amorphous pattern. This indicates that PVP may have stronger inhibitive effect on the growth of piroxicam crystals in the spray dried solid dispersions. It may be attributed to the stronger interaction between PVP and the model drug than HPMC.

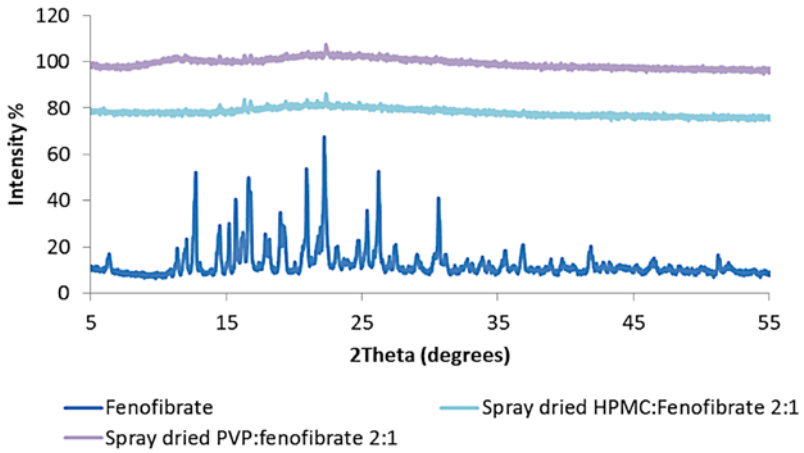

Fig 3.16: PXRD results of freshly prepared spray dried PVP:fenofibrate 2:1 and HPMC:fenofibrate 2:1 formulations compared to raw fenofibrate.

Figure 3.16 shows P-XRD results obtained for spray dried HPMC:fenofibrate 2:1 and PVP:fenofibrate 2:1. Despite the absence of drug crystals in the SEM images (see Figure 3.10), diffraction peaks of crystalline fenofibrate (14.52, 15.22, 15.81, 21.94, 22.22, 26.23 2θ for spray dried HPMC:fenofibrate 2:1, and 14.2, 15.22, 15.81, 22.22, 26.26, 30.66 2θ for spray dried PVP:fenofibrate 2:1) can be clearly seen in the diffraction patterns of the spray dried formulations indicating the presence of residual crystalline drug in both formulations. No significant difference in the degree of crystallinity of fenofibrate in the spray dried formulations can be identified from P-XRD results of PVP and HPMC based spray dried samples.

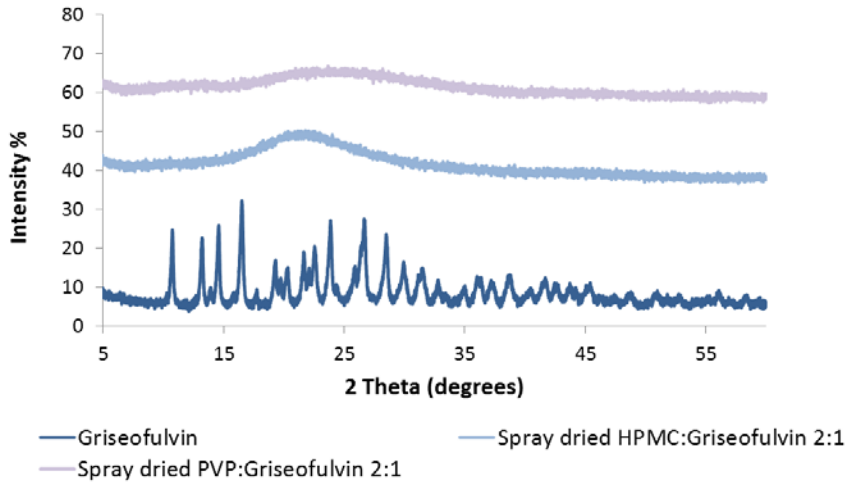

Fig 3.17: PXRD results of freshly prepared spray dried PVP:griseofulvin 2:1 and HPMC:griseofulvin 2:1 formulations compared to raw griseofulvin.

Spray dried formulations containing griseofulvin were also analysed using P-XRD. The results are shown in Figure 3.17. Differently from spray dried fenofibrate and piroxicam samples with high drug loading, for which few weakly intense crystalline diffraction peaks were present, in this case only the amorphous halo is present for both PVP and HPMC based griseofulvin formulations. No diffraction peaks can be observed indicating the amorphous nature of the model drug (either as phase separated amorphous drug-rich domains or molecular dispersions with the polymers) in the spray dried formulations. This result is in agreement with SEM images, where no drug crystals were visible in the spray dried formulations (Figure 3.11).

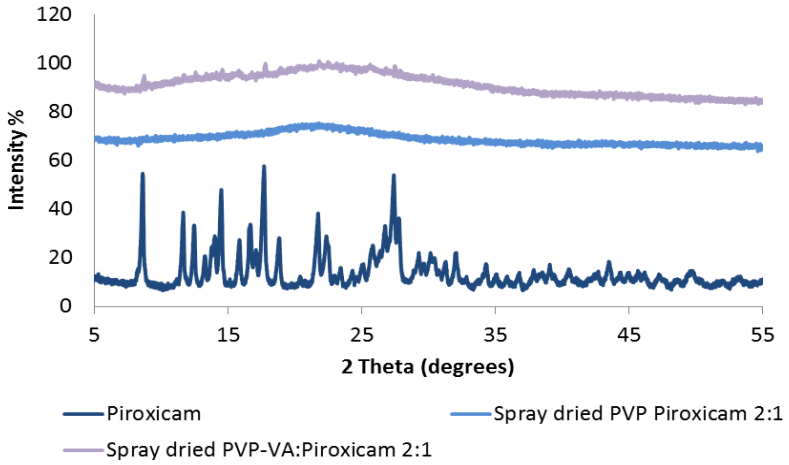

Fig 3.18: PXRD results of freshly prepared spray dried PVP:piroxicam 2:1 and PVP-VA:piroxicam 2:1 formulations compared to raw piroxicam.

Figure 3.18 shows a comparison between P-XRD patterns of raw piroxicam, spray dried PVP:piroxicam 2:1 and spray dried PVP-VA:prioxicam 2:1. It can be observed that a higher level of crystalline drug is obtained in the spray dried formulations of PVP-VA piroxicam 2:1. This result indicates that the hydrophobic modification of the polymer with vinyl-acetate groups contributes to the reduced stabilisation capability of the polymer on the amorphous drug. The lower hydrophilicity of PVP-VA in comparison to PVP was expected to reduce the risk of drug crystallisation in the solid disperions, as less water content, which can have a plasticizing effect and induce drug crystallization, was expected. [230] However, this advantage may be outweight by the fact that the structutral modification also reduced the potential hydrogen bonding sites with the model drug which can contribute to lower miscibility and solubulity with the model drug.

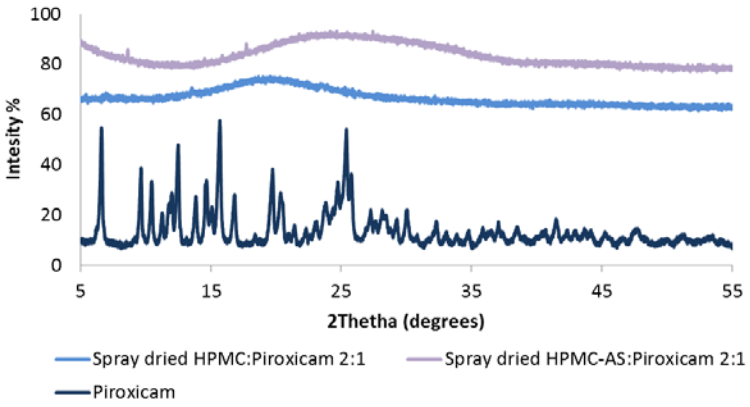

Fig 3.19: PXRD results of freshly prepared spray dried HPMC:piroxicam 2:1 and HPMC-AS:piroxicam 2:1 formulations compared to raw piroxicam.

P-XRD analysis has been performed also on HPMC-AS:piroxicam 2:1 sample and the obtained diffraction pattern is shown in Figure 3.19. Diffraction peaks of crystalline drug can be clearly observed in both spray dried HPMC:piroxicam 2:1 and HPMC-AS:piroxicam 2:1 solid dispersion samples, suggesting that, as for PVP-VA, the hydrophobic modification of the polymeric carrier did not lead to improved stabilisation and solubilisation of amorphous drug by the polymer. It is interesting that the peak position of the diffractions in the two spray dried formulations are different indicating different polymorphic forms of piroxicam were obtained in the HPMC and HPMC-AS based solid dispersions.

3.3.7 ATR-FTIR spectroscopic analysis

Physical properties of raw drugs, physical mixtures and spray dried samples were also investigated using ATR-FTIR spectroscopy. In particular the technique was employed to study the possible polymeric carrier-APIs interaction, which has been reported to have an important impact on the stabilisation effect of the amorphous drug at solid state and dissolution performance of solid dispersions, due to the reduction of agglomeration of the hydrophobic drug particles. [231]

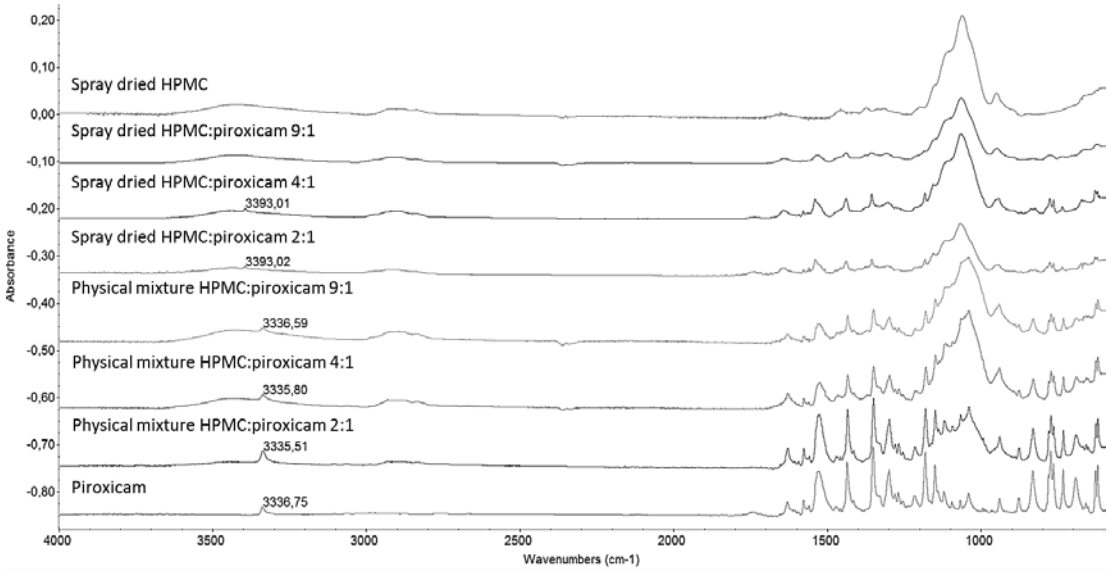

Fig 3.20: ATR-FTIR spectra of raw Piroxicam, HPMC:piroxicam 2:1, 4:1 and 9:1 physical mixtures and spray dried HPMC:piroxicam 2:1, 4:1 and 9:1 samples.

Figure 3.20 shows ATR-FTIR results obtained for piroxicam, HPMC:piroxicam physical mixtures and spray dried solid dispersion formulations. As described in the literature, different piroxicam polymorphic forms have been reported to have different FTIR spectra. Three main polymorphic forms, known as cubic form β, needle form α and a monohydrate, have been studied. Recently, a new polymorphic structure was proposed by Reck et al. and was designated as α_2, but only minor crystallographic differences were proposed between the needle form, renamed as α_1, and form α_2. [168] According to Mihalić, piroxicam cubic and needle forms FTIR spectra differ only slightly in the fingerprint region, while the overlapped –NH and –OH stretching bands at 3385 cm^{-1} in the spectrum of the needle form and at 3330 cm^{-1} in the spectrum of the cubic form. [232] Further work from Janik et al indicated that absorption bands at 3393 and 3341cm^{-1} correspond to the vibration of free –NH and H-bonded –NH groups (intermolecular H-bonding between piroxicam molecules). [233]

In Figures 3.20 it can be observed that a well-defined peak is present in the piroxicam ATR-FTIR spectrum at 3337 cm^{-1}, confirming that the raw crystalline drug is cubic form β, as already proved by PXRD pattern (section 3.3.5). In the spectra of the physical mixtures, an intense peak at 1060 cm^{-1} is assigned to HPMC. It can also be seen that the ATR-FTIR spectra of the physical mixtures are summations of piroxicam and HPMC spectra. No shift on the NH 3337 cm^{-1} peak of the crystalline drug can be observed, suggesting that no interaction between the drug and the polymeric carrier occurred in the physical mixtures.

The spectra of the spray dried solid dispersions show clear shifts of the piroxicam N-H streching towards higher wavenumbers (3393 cm^{-1}), ß cubic form of piroxicam is known to be composed of dimers where two piroxicam molecules are connected via the formation of intermolecular H-bond between amide –NH group and oxygen in the sulfoxide group.[233,234] The lack of hydrogen bonding revealed by ATR-FTIR for the spray dried formulation is likely to be due to the drug amorphisation and consequent reduction of intermolecular interaction between piroxicam molecules. In the spray dried HPMC:piroxicam 9:1 spectrum no -NH or -OH strecthing peak is observed. This is likely to be due to the drug concentration is below the limit of detection of ATR-FTIR.

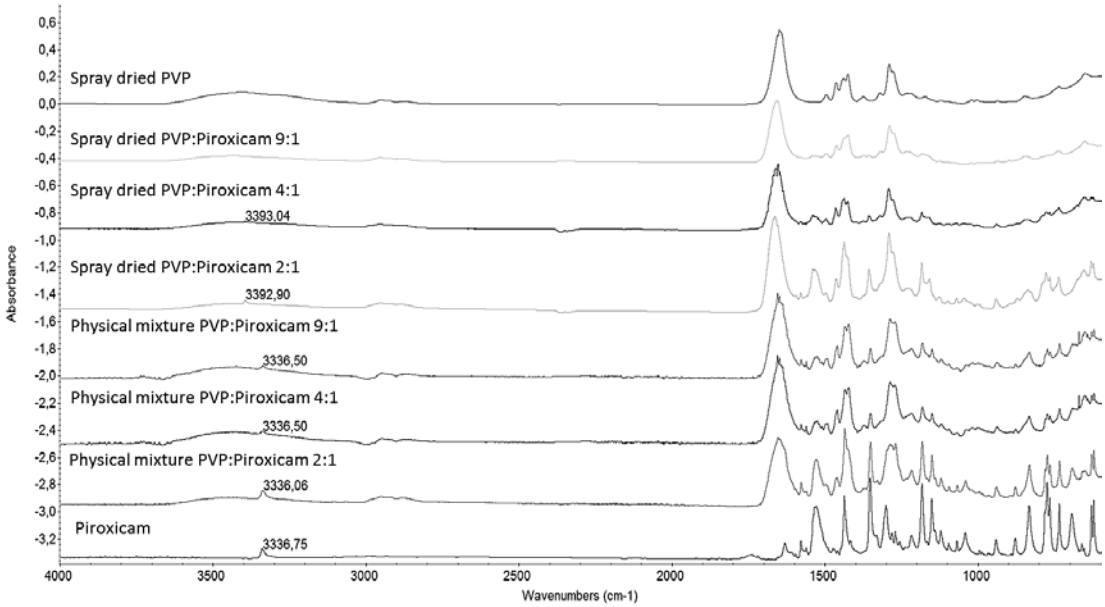

Fig 3.21: ATR- FTIR spectra of raw piroxicam, pvp:piroxicam 2:1, 4:1 and 9:1 physical mixtures and spray dried PVP:piroxicam 2:1, 4:1 and 9:1 samples.

ATR-FTIR spectra of raw piroxicam, PVP:piroxicam 2:1, 4:1 and 9:1 physical mixtures and spray dried solid dispersions are shown in Figure 3.21. In the presence of PVP a broad well defined peak can be observed at 1650 cm^{-1} which is assigned to the polymer carbonyl stretching vibration. [227] As reported in literature, each pirrolidone moiety of PVP has two functional groups , =N- and C=O that can potentianlly interact with the drug via hydrogen bonding. Due to steric hindrance of the tertiary amine, the carbonyl group of PVP is more favorable for hydrogen bonding. [235] The ATR-FTIR spectra of PVP:piroxicam physical mixtures are simply the summation of the PVP and crystalline piroxicam spectra, revealing that no interaction between the drug and the carrier occurred in the physical mixtures. In contrast, the ATR-FTIR spectra of spray dried solid dispersions show a shift in the piroxicam -NH stretching vibration peak from 3337 to 3392 cm^{-1}, suggesting that, piroxicam -NH groups are not involved in intermolecular H-bonding network (between

piroxicam molecules), as a result of the drug amorphisation. The weakening in intensity of the N-H or O-H strecthing piroxicam peak can be related to the conversion of piroxicam from crystalline to amorphous form. It can be seen that the piroxicam –NH strecthing vibration peak intensity is not visible in the sample PVP:piroxicam 9:1. As already mentioned, the lack of –NH drug peak in spray dried with low drug loading is likely to be due to the drug concentration is below the instrument detection limit.

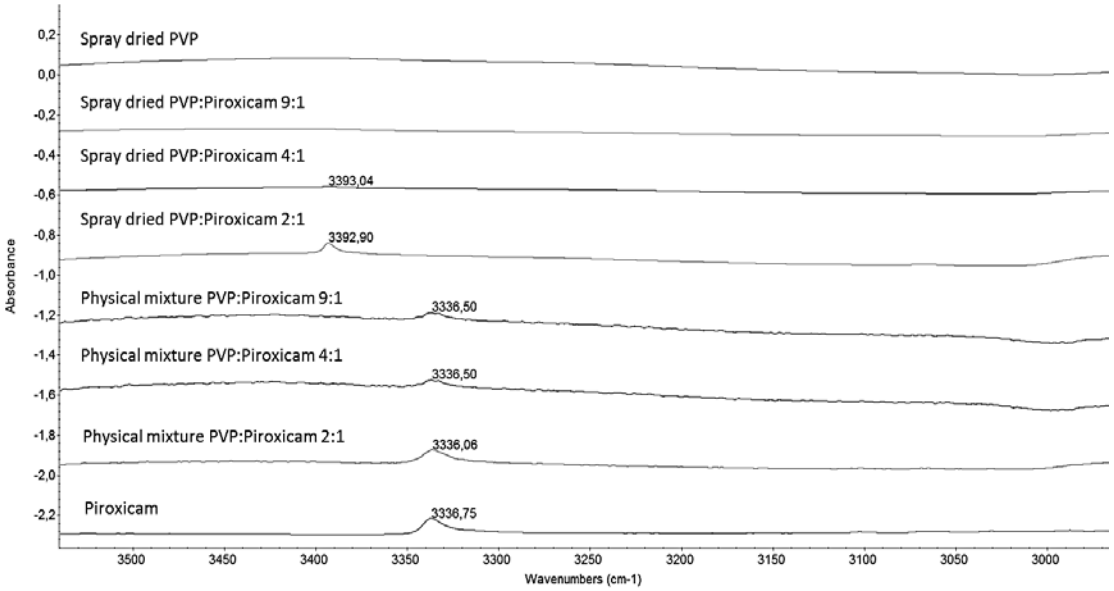

Fig 3.22: ATR-FTIR spectra of raw piroxicam, PVP:piroxicam 2:1, 4:1 and 9:1 physical mixtures and spray dried PVP:piroxicam 2:1, 4:1 and 9:1 samples.

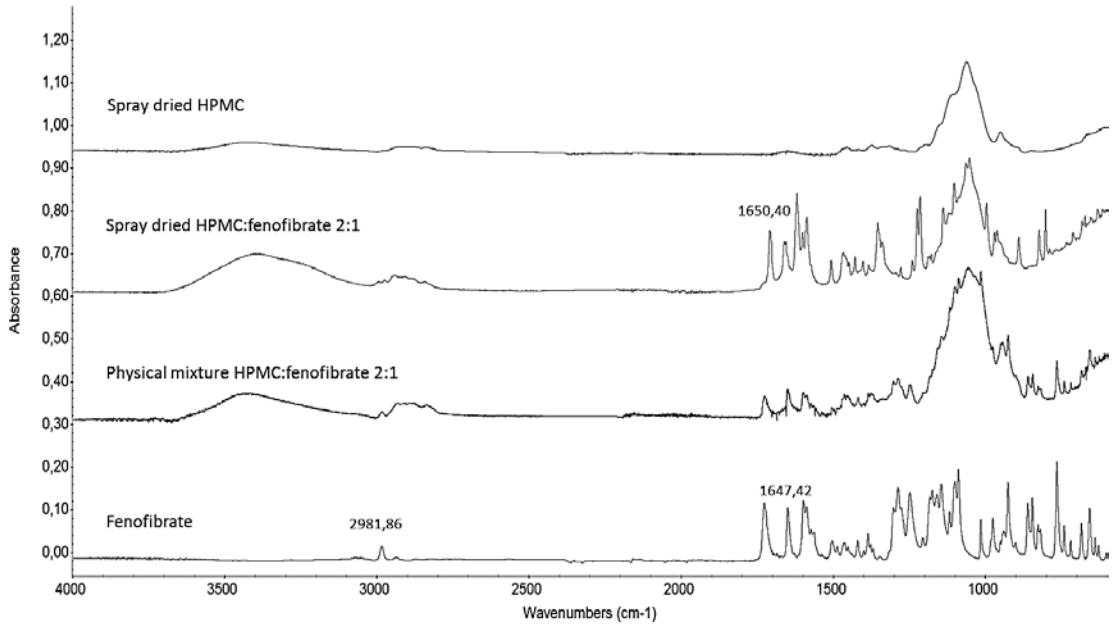

Fig 3.23: ATR-FTIR spectra of raw fenofibrate, HPMC:fenofibrate 2:1 physical mixture and spray dried solid dispersion.

ATR-FTIR analysis has been perfomed also on the physical mixtures and spray dried solid dispersions of HPMC:fenofibrate 2:1 and PVP:fenofibrate 2:1. Obtained spectra are shown in Figure 3.23 and 3.24. Fenofibrate lacks proton donors but the two –C=O groups can act as proton acceptors, [236] leading to the occurrence polymeric carrier-fenofibrate interaction, which has already been reported in literature. [237] Figure 3.23 shows that fenofibrate peaks are broader and less resolved in the spectra of spray dried solid dispersion, particularly for the stretching vibration peak of alkylic groups at 2982 cm^{-1}. This suggests that the drug might be mainly amorphous in the solid dispersion. A slight shift on the fenofibrate carbonyl group from 1647 cm^{-1} to 1650 cm^{-1} can be observed, which may be due to the interaction of the fenofibrate carbonyl group with HPMC proton donor groups.

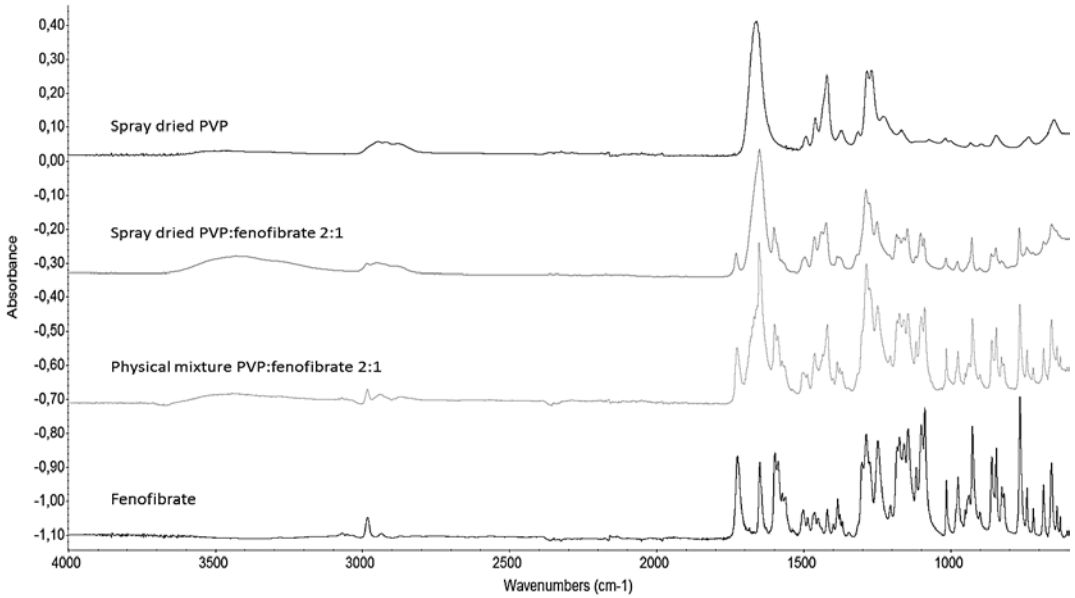

Fig 3.24: ATR-FTIR spectra of raw fenofibrate, PVP:fenofibrate 2:1 physical mixture and spray dried solid dispersion.

Figure 3.24 shows ATR-FTIR analysis of PVP:fenofibrate 2:1 physical mixtures and spray dried samples, compared to the raw drug and the spray dried polymeric carrier. In this case fenofibrate carbonyl group peak (1647 cm^{-1}) cannot be used as a reference of hydrogen bonding formation, due to the overlapping with the PVP carbonyl peak. As for HPMC:fenofibrate samples, fenofibrate peaks appear less defined, particularly for the the alkylic group peak at 2982 cm^{-1}, suggesting that the physical state of fenofibrate in the formulation may be mainly amorphous, as already obeserved by P-XRD studies.

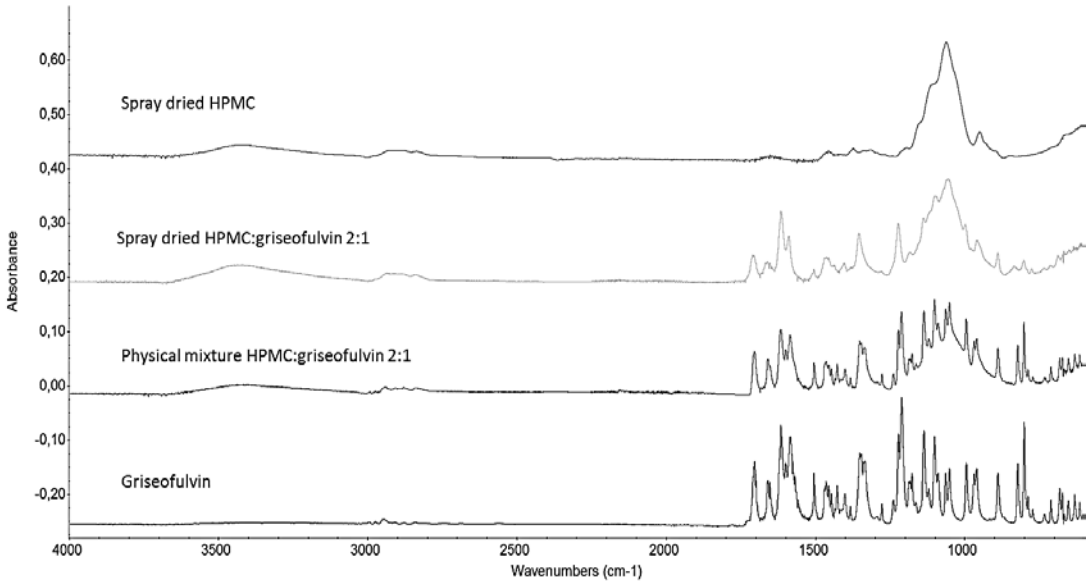

Fig 3.25: ATR-FTIR spectra of raw griseofulvin, HPMC:griseofulvin 2:1 physical mixtures and spray dried samples.

The ATR-FTIR spectrum of crystalline griseofulvin (Figure 3.25) shows sereval peaks in the region 1750-1550 cm^{-1}, which are related to the carbonyl stretching of the benzofuranone ring, the carbonyl stretching of the cycloexanone ring and the C=C stretch of the cyclic ring. [238] The wavenumbers of these groups bands are 1703 cm^{-1}, 1614 cm^{-1} and 1583 cm^{-1}, respectively. No significant shift of the peaks is observed in the spectrum of the spray dried HPMC:griseofulvin solid dispersion, indicating that minimal interaction between the drug and the polymeric carrier occurred. Nevertheless significant peak broadening can be observed, as a possible consequence of the drug conversion from crystalline to amorphous state.

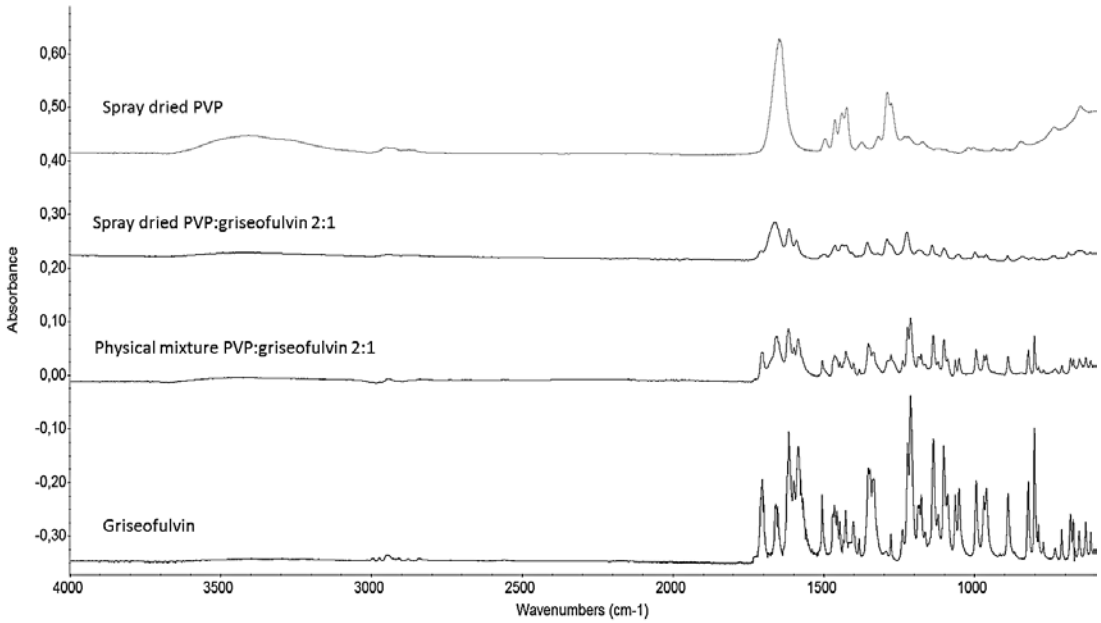

Fig 3.26: ATR- FTIR spectra of raw griseofulvin, PVP:griseofulvin 2:1 physical mixtures and spray dried samples.

Similar result can be observed for PVP:griseofulvin 2:1 spray dried solid dispersion (Figure 3.26). Only minimal shift (1-2 wavenumbers) of the peaks were observed (1701cm^{-1}, 1616 cm^{-1} and 1584 cm^{-1}), suggesting that no significant interaction occurred between griseofulvin and PVP. Obtained results are in agreement with literature data, which reported a lack of interaction between PVP and griseofulvin. [239] As for HPMC:griseofulvin samples, peak shape changes can be seen, suggesting drug amorphisation in the spray dried formulation.

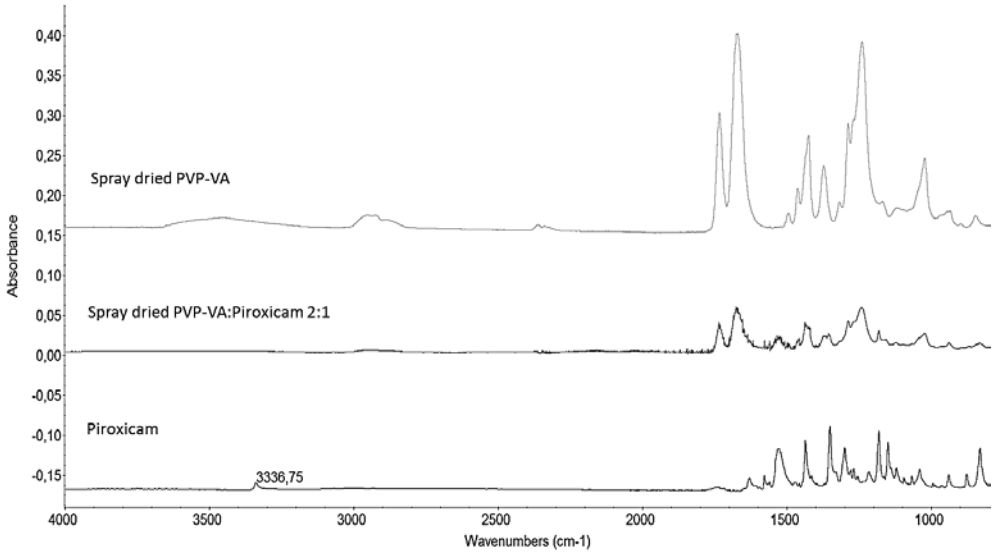

Fig 3.27: ATR-FTIR spectra of raw Piroxicam, spray dried PVP-VA:piroxicam 2:1 and spray dried PVP-VA samples.

ATR-FTIR spectrum of spray dried PVP-VA:piroxicam formulation is shown in Figure 3.27. It can be seen that the –NH piroxicam band at 3337 cm^{-1}, is not present in the spray dried sample spectrum. Piroxicam peaks in the fingerprint region are overlapped with the PVP-VA ones, thus they cannot be used as a reference for the drug characterization. Due to the absence of NH drug peak in the spectrum, it was not possible to predict drug/polymeric carrier interaction occurrence or possible drug amorphisation. As already mentioned in section 3.3.3 for spray dried PVP-VA samples, only one replicate was prepared and analysed. Therefore further studies on PVP-VA possible use to prepare piroxicam solid dispersions would be necessary.

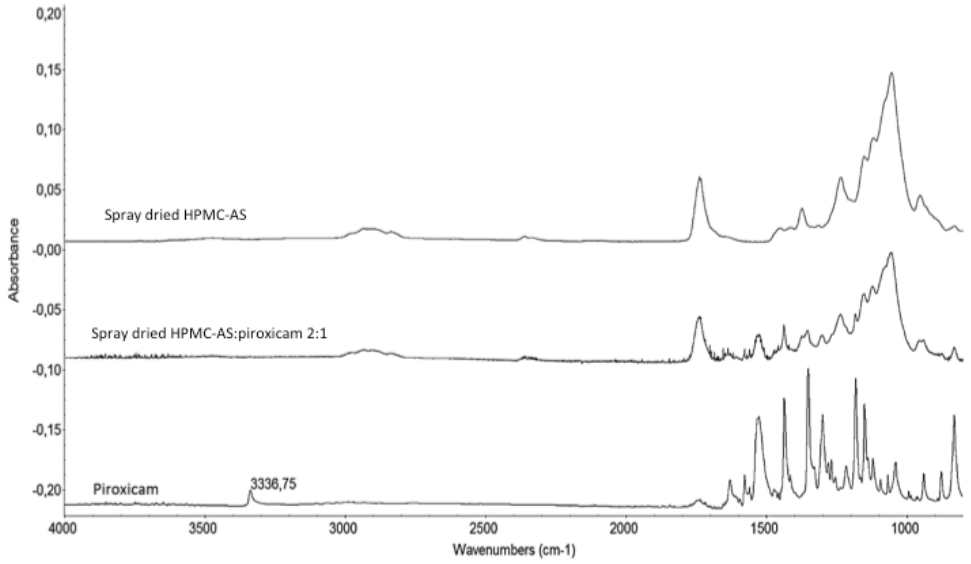

Fig 3.28: ATR-FTIR spectra of raw Piroxicam, spray dried HPMC-AS:piroxicam 2:1 and spray dried HPMC-AS samples.

Similar observations can be obtained for HPMC-AS spray dried formulation spectrum, shown in Figure 3.28. The piroxicam–NH band is not visible in the spray dried HPMC-AS:piroxicam 2:1. Also in this case drug peaks in the fingerprint region are overlapped with the HPMC-AS peaks, thus they cannot provide indication of drug physical state and drug/polymer interaction occurrence. Further studies would be useful to better clarify these points.

3.3.8 DSC Analysis

DSC analyses were performed on raw APIs, polymeric carrirers:APIs physical mixtures and spray dried solid dispersions, in order to evaluate qualitatively and quantitatively the possible occurrence of physical state modifications of the spray dried solid components.

Figure 3.29 shows DSC results obtained for raw piroxicam, HPMC:piroxicam 2:1, 4:1 and 9:1 physical mixtures and spray dried HPMC:piroxicam 2:1, 4:1 and 9:1 solid dispersions. The thermogram of crystalline piroxicam shows a melting endothermic peak at 201.0 °C, which is in good agreement with literature data. [154]

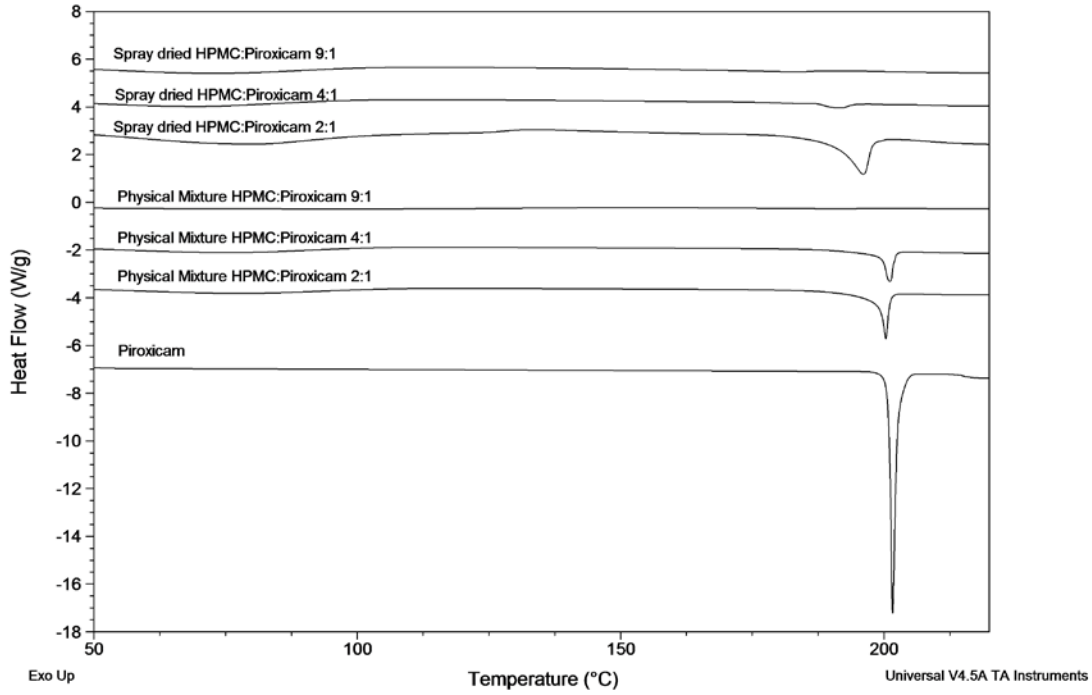

Figure 3.29: DSC thermograms, raw Piroxicam, HPMC:piroxicam 2:1, 4:1 and 9:1 physical mixtures and spray dried HPMC:piroxicam 2:1, 4:1 and 9:1 samples.

The melting endotherm peak temperatures of piroxicam for the physical mixtures (between 200.8 to 201.1 °C) were very close to the raw drug melting point value (201.66 °C; Table 3.11). Therefore minimal melting point depression was obtained. Melting point depression provides indication about the drug-polymer miscibility. [240] Obtained data indicates piroxicam and HPMC have low miscibility.

From Figure 3.31 it can be seen that no melting endotherm peak was noted in the thermogram of spray dried HPMC:piroxicam 9:1, suggesting the formation of a completely amorphous system. Samples with higher drug loading, HPMC:piroxicam 2:1 and 4:1, showed the presence of drug melting endothermic peaks, revealing the presence of drug crystals in the spray dried sample. In order to quantitatively estimate the crystallinity of the model drug in the spray dried formulations, the melting enthalpy obtained for the spray dried samples were divided by the melting enthalpy of the pure crystalline drug and the obtained results are summarised in Table 3.10. The crystallinity of the model drug were 13.38% and 4.38% for HPMC:piroxicam 2:1 and 4:1, respectively. Data clearly show that at lower

HPMC weight fractions both amorphous and crystalline drug are present. This is in agreement with literature data, [48] which showed that the barrier to drug crystallization increases increasing HPMC weight fraction. DSC data are in agreement with SEM and P-XRD data which revealed the presence of crystalline drug in the two HPMC:piroxicam spray dried solid dispersion having drug loadings of 33.3% and 20% (w/w). This indicates the solubility between piroxicam and HPMC is below 20% (w/w).

Table 3.10: Melting points, melting point onsets and melting entalphy values obtained by DSC analysis for the raw drug, HPMC:piroxicam physical mixtures and spray dried solid dispersions, and residual drug crystallinity in spray dried samples (n=3).

Sample	Melting Point (°C)	Melting point onset (°C)	Melting enthalpy (J/g)	Drug crystallinity %
Piroxicam	201.7±0.01	201.0±0.01	115.50±3.88	-
Physical Mixture HPMC:piroxicam 2:1	201.1±0.43	199.2±0.01	28.65±1.77	-
Physical Mixture HPMC:piroxicam 4:1	201.0±0.33	199.5±0.11	17.97±2.41	-
Physical Mixture HPMC:piroxicam 9:1	200.8±0.01	199.6±0.14	5.41±1.93	-
Spray dried HPMC:piroxicam 2:1	196.7±0.01	190.7±0.14	15.46±0.27	13.38
Spray dried HPMC:piroxicam 4:1	191.7±0.09	187.5±0.20	5.05±0.68	4.38
Spray dried HPMC:piroxicam 9:1	-	-	-	-

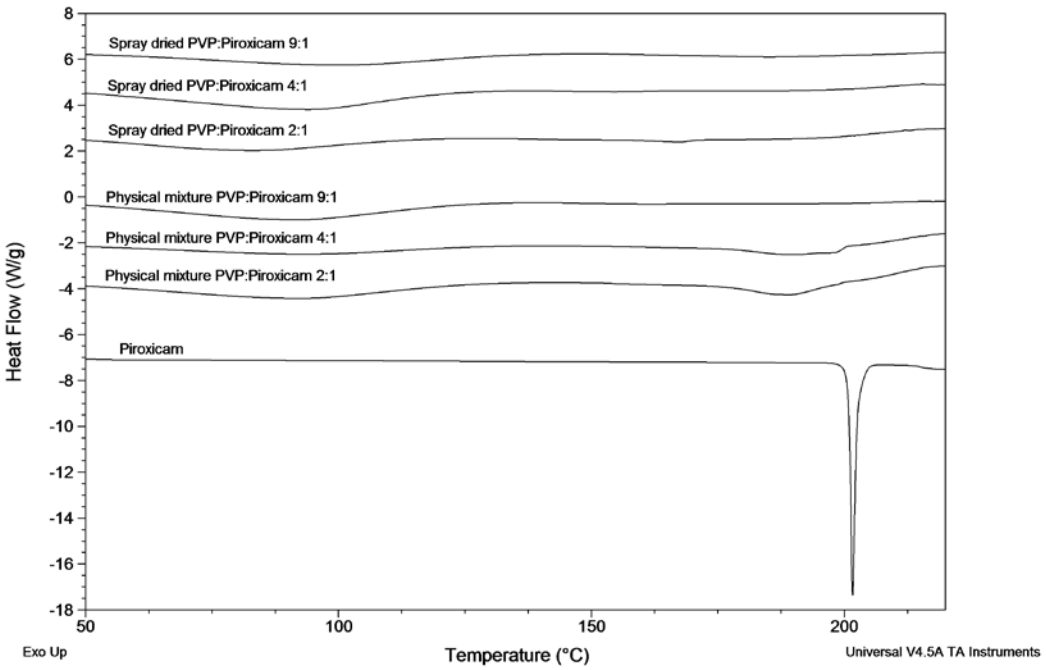

Figure 3.30: DSC thermograms, raw Piroxicam, PVP:piroxicam 2:1, 4:1 and 9:1 physical mixtures and spray dried PVP:piroxicam 2:1, 4:1 and 9:1 samples.

Figure 3.30 shows DSC results obtained for PVP:Piroxicam physical mixtures and spray dried samples. Differently from HPMC:piroxicam systems, significant melting point depression was obtained for the PVP:piroxicam physical mixtures (Table 3.11). The drug melting peak also shows significant reduction of melting enthalpy in comparison to the raw crystalline drug. Both results indicates high miscibility between PVP and piroxicam, suggesting that, despite the high heating rate used (10 °C/min) during the DSC analysis, PVP:piroxicam interaction occurred during the melting which leads to the melting point depression of the crystalline drug in the physical mixtures. Compared to HPMC:piroxicam system low amount of crystalline drug were detected in the solid dispersion with polymer:drug ratio 2:1 and 4:1, as summarised in Table 3.10. As for HPMC:piroxicam sample system, the sample with highest polymer weight fraction did not shown any endothermic peaks, revealing that piroxicam is completely amorphous in this sample.

Table 3.11: Melting points, melting point onsets and melting entalphy values obtained by DSC analysis for the raw drug, HPMC:piroxicam physical mixtures and spray dried solid dispersions, and residual drug crystallinity in spray dried samples (n=3).

Sample	Melting Point (°C)	Melting point onset (°C)	Melting enthalpy (J/g)	Drug crystallinity %
Piroxicam	201.7±0.01	201.0±0.01	115.50±3.88	-
Physical mixture PVP:piroxicam 2:1	189.0±0.11	174.1±0.37	47.24±4.49	-
Physical mixture PVP:piroxicam 4:1	190.1±0.01	172.9±0.19	47.39±1.60	-
Physical mixture PVP:piroxicam 9:1	184.8±0.28	152.5±1.15	28.03±6.14	-
Spray dried PVP:piroxicam 2:1	167.4±0.04	156.3±1.28	8.35±3.02	7.22
Spray dried PVP:piroxicam 4:1	153.8±0.30	137.9±0.08	1.06±0.09	0.92
Spray dried PVP:piroxicam 9:1	-	-	-	-

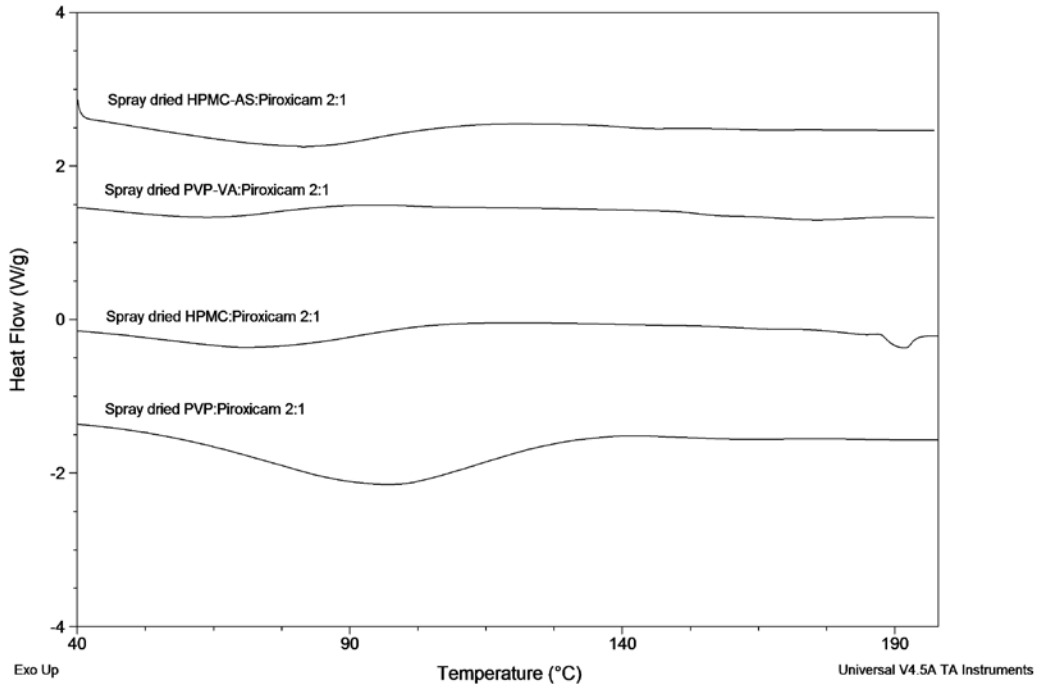

Figure 3.31: DSC thermograms of raw piroxicam, spray dried HPMC:piroxicam, PVP:piroxicam, HPMC-AS:piroxicam and spray dried PVP-VA:piroxicam samples.

Figure 3.31 reports DSC thermograms obtained for spray dried HPMC-AS:piroxicam and PVP-VA:piroxicam 2:1, compared to the correspondent spray dried homopolymer:piroxicam system. No melting endothermic peaks could be seen in the thermograms of the spray dried formulations except for the piroxicam-HPMC formualation. This result is in disagreement with P-XRD results, which showed the presence of trace amount of crystalline drug in PVP-VA:piroxicam and HPMC-AS:piroxicam solid dispersions. This disagreement is likely to be associated with the characterization method used. During the DSC heating, the trace amount of crystalline drug could easily dissolved into the heated and viscous glassy polymer and lead to the absence of clear melting of crystalline drug.

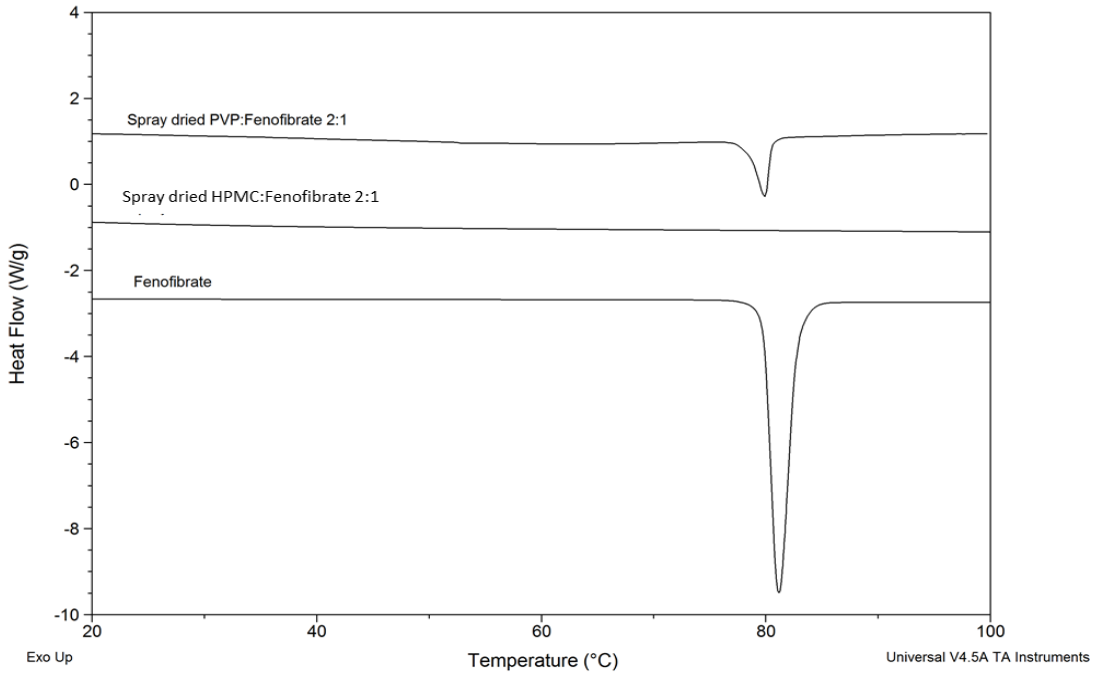

Figure 3.32: DSC thermograms of raw fenofibrate, spray dried HPMC:fenofibrate 2:1 and PVP:fenofibrate samples.

Figure 3.32 shows DSC results of spray dried HPMC:fenofibrate and PVP:fenofibrate 2:1 solid dispersions compared to the thermogram of the raw crystalline drug. Crystalline fenofibrate shows a melting endothermic peak at 81°C, in agreement with literature data. [27] The DSC result of the spray dried HPMC:fenofibrate solid dispersion shows no fenofibrate melting peak, indicating that the drug was mainly amorphous in the spray dried formulation. Differently HPMC:fenofibrate thermogram showed an intense endothermic peak having a melting enthalpy of 12.74 J/g. This is associated with the presence of 13.05% (w/w) crystalline drug in the PVP:fenofibrate 2:1 spray dried

formulation. PXRD results (section 3.3.6) showed the presence of residual crystallinity in both formulations. The absence of the crystalline drug melting is likely to be associated with the dissolution of the low quantity of the crystalline into the formulation during DSC heating.

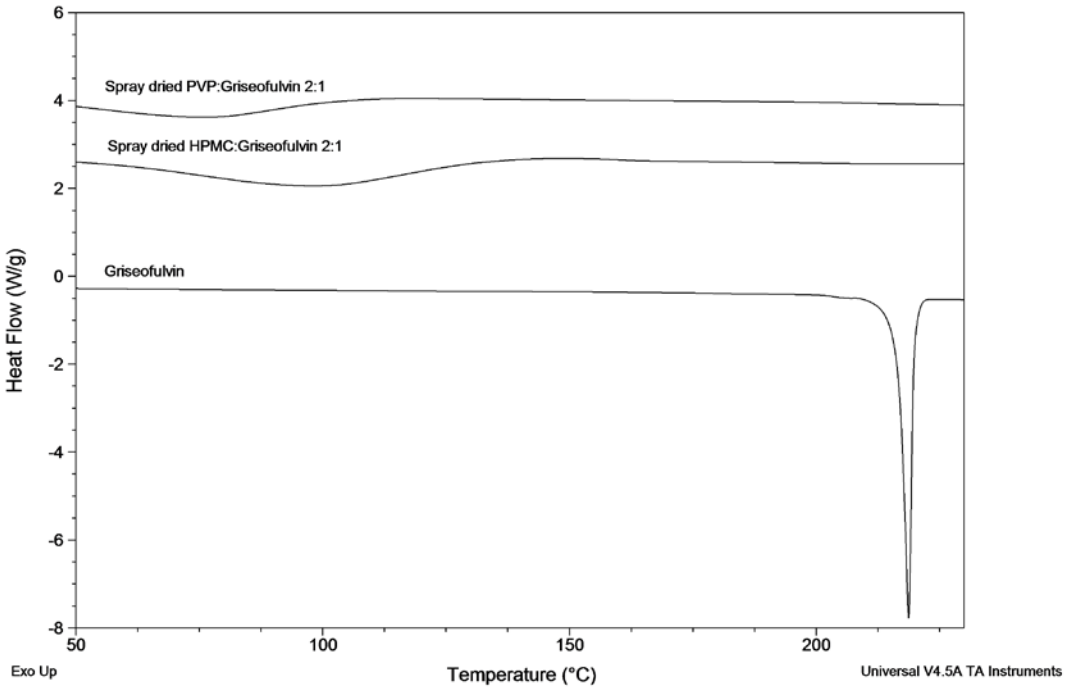

Figure 3.33: DSC thermograms of raw griseofulvin, spray dried HPMC:griseofulvin 2:1 and PVP:griseofulvin 2:1 samples.

DSC results obtained for PVP:griseofulvin and HPMC:griseofulvin 2:1 are shown in Figure 3.33. Raw griseofulvin melting point was in complete agreement with reported data. [27] No melting peak was observed for the two spray dried samples, proving that no residual drug crystallinity was present in the two samples. The DSC results are in good agreement with the PXRD data, which showed the presence of amorphous halos in the PXRD patterns (Section 3.3. 6). Figure 3.33 also shows the presence of broad endothermic peaks for both spray dried HPMC:griseofulvin and PVP:griseofulvin samples between 50 and 120°C. These broad endothermic peaks correspond to the release of residual solvent/moisture from the formulation. The absence of exothermic melting peak of crystalline griseofulvin in the DSC result of the spray dried formulation indicates higher miscibility and solubility of griseofulvin in the polymeric carriers employed in comparison to the other model drugs.

3.3.9 Dissolution Studies

Dissolution studies of raw model drugs, physical mixtures and freshly spray dried samples were carried out in buffer pH 5, buffer pH 6.5, Blank FaSSIF and blank FeSSIF in non-sink conditions. As for solubility studies, the use of different media allowed the study and comparison of the drug dissolution performance in conditions simulating the ionic strength, the pH and the GIT surfactant concentrations of the intestinal media. As reported in literature, [67,241] each of this factor can significantly impact the drug dissolution profile, together with the carrier used. Due to its influence on the dissolution rate, [242] particle size was controlled by sieving of the samples as previously described in section 3.2.8.

Figure 3.34 shows results obtained for HPMC:piroxicam physical mixtures and spray dried formulations in buffer pH 5 and Blank FeSSIF, compared to the raw drug. It can be seen that the for all the drug:polymer ratios employed, the physical mixtures showed faster drug dissolution compared to the raw drug in the buffer (pH=5). This indicates that HPMC has a dissolution enhancing effect, as already shown by steady state solubility results (Section 3.3.2). The rates of dissolution of piroxicam from spray dried samples are faster than the correspondent physical mixture in buffer, indicating that dissolution enhancement effect of formulating the drug in solid dispersion. Such result can be related to the physical state of the drug, that, as shown by the solid-state characterisation of the spray dried sample, is mainly in its amorphous form. For all the samples fastest dissolution profile was obtained in blank FeSSIF, confirming the important effect of NaTC on the drug solubilisation. NaTC effect can be observed also from the behaviour of the raw drug, for which the dissolution is much faster in the blank FeSSIF than in the buffers.

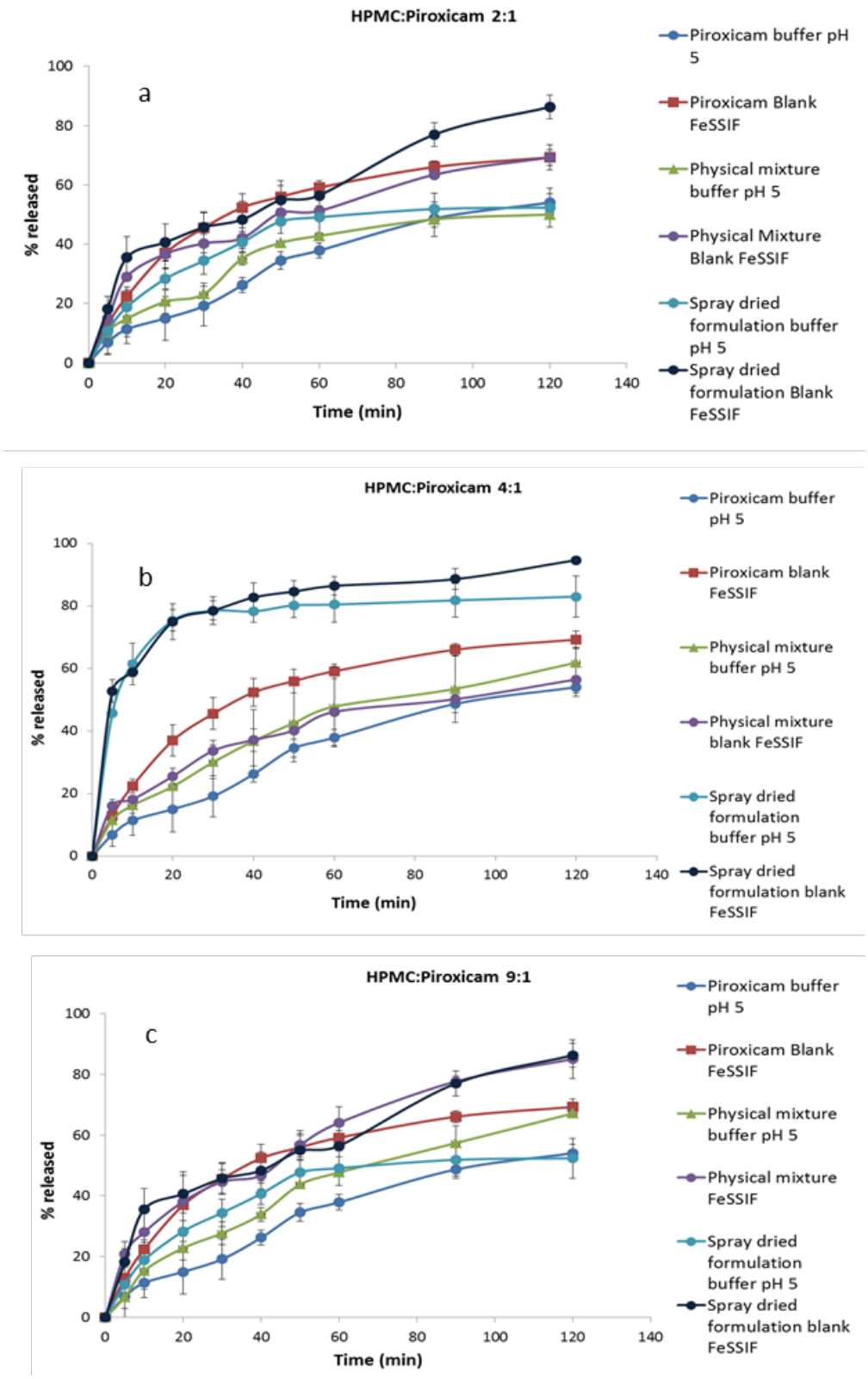

Figure 3.34: Dissolution profile of raw piroxicam, physical mixtures HPMC:piroxicam and freshly spray dried HPMC:piroxicam sample in buffer at pH 5 and Blank FeSSIF (polymer drug ratio: a=2:1, b=4:1, c=9:1) (n=3).

Comparing Figure 3.34 a, b and c, it is possible to observe that the fastest dissolution profile was obtained for the spray dried solid dispersion having polymer:drug ratio 4:1. Indeed, the dissolution rate resulted to be lower for the sample HPMC:piroxicam 9:1 in the same condition. This suggests that high HPMC weight load can result in "slowing effect" of the drug dissolution. HPMC is well known to swell after imbibition of water, forming a gel network. [164] Therefore when the HPMC:piroxicam system is in contact with water, a gel diffusive layer is formed. The presence of higher proportion of HPMC is likely to render the diffusion layer more viscous, resulting a slower drug diffusion and release.

Figure 3.35 shows dissolution results obtained for the same samples in buffer pH 6.5 and Blank FaSSIF. Dissolution rate is faster than at pH 5 and Blank FeSSIF, confirming the higher piroxicam solubility at pH 6.5 than at pH 5, as already revealed by steady state solubility studies (Section 3.3.2). Differently from the previous dissolution result, the dissolution profiles obtained of raw piroxicam in buffer pH 6.5 and in blank FaSSIF were similar, revealing a limited NaTC effect on piroxicam solubilisation. The same result can be observed also for the physical mixtures and the spray dried solid dispersions. The different effect of the blank FaSSIF and blank FeSSIF is due not only to the pH values, but also to the NaTC concentrations used and to the micellar species present in solution. A full characterisation of the NaTC aggregates present in blank FaSSIF and blank FeSSIF will be discussed in Chapter 5. For all the drug:polymer ratios used the fastest dissolution profiles were obtained for the spray dried formulations, confirming that the spray drying processing impacted positively the drug solubilisation due to the amorphous state of the drug in the solid dispersions. The comparison of Figure 3.35 a, b and c indicates that the fastest dissolution profile was obtained from the spray dried formulation having polymer:drug ratio 2:1, for which 100% of drug release was reached in 30 minutes, yielding a drug concentration of 0.022 mg/ml.

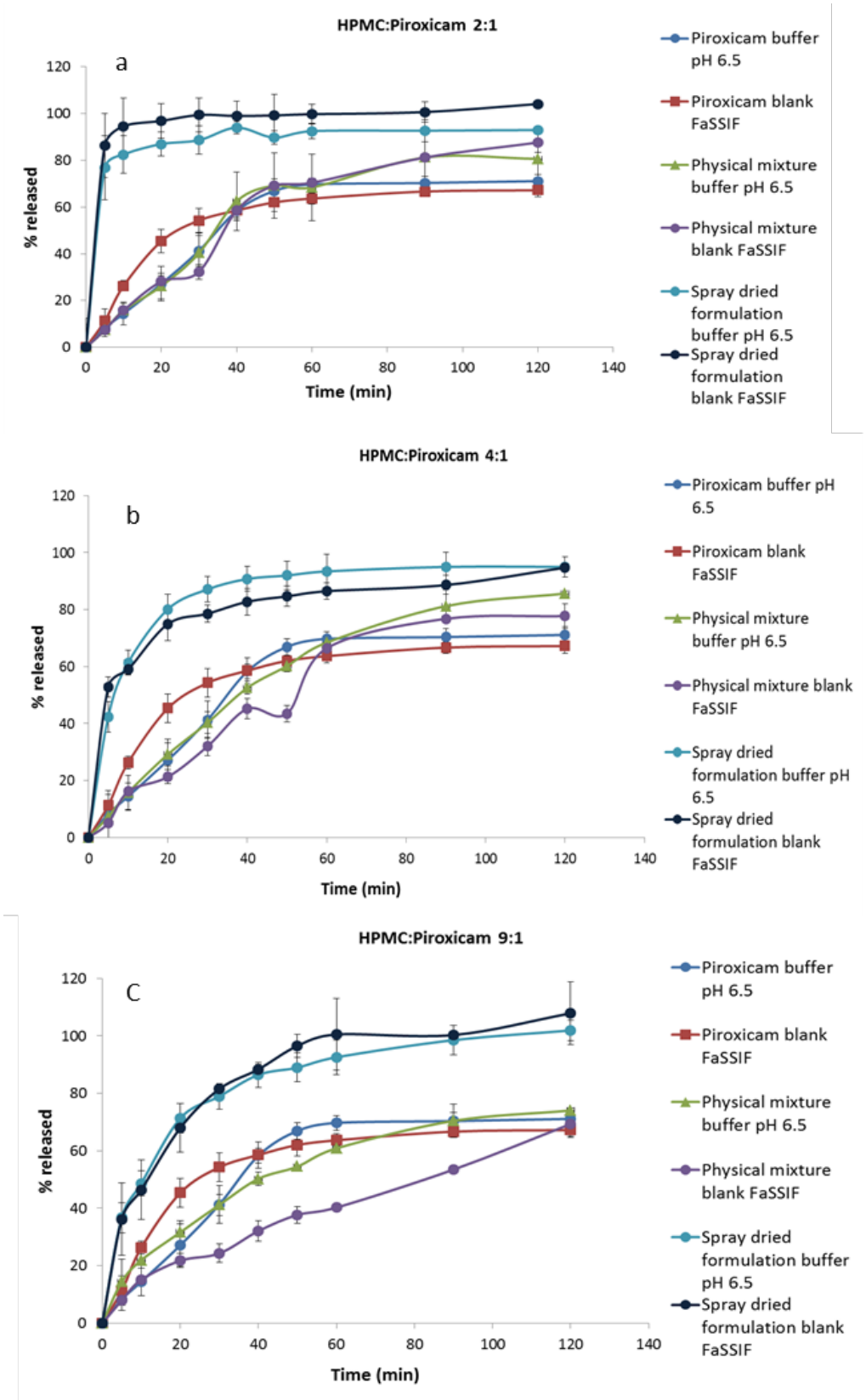

Figure 3.35:Dissolution profile of raw piroxicam, physical mixtures HPMC:piroxicam and freshly spray dried HPMC:piroxicam sample in buffer at pH 6.5 and Blank FaSSIF(polymer drug ratio: a=2:1, b=4:1, c=9:1) (n=3).

The dissolution profiles of physical mixture and spray dried PVP:piroxicam 2:1(a), 4:1(b) and 9:1(c) samples in buffer pH5 and FeSSIF are reported in Figure 3.36. As for HPMC:piroxicam systems, the primary effect of NaTC on the drug solubilisation can be observed for the physical mixtures and the spray dried samples. Figure 3.36 a shows that for the sample PVP:piroxicam 2:1 the fastest piroxicam dissolution profile was obtained from the spray dried formulation. Figures 3.36 b and c clearly show that this result is not confirmed by PVP:piroxicam 4:1 and 9:1 dissolution results. Indeed, for these two samples the drug dissolution resulted to be faster for the physical mixtures than for the spray dried formulations.

PVP is widely used as solubility and dissolution enhancer, due to its ability to increase the wettability of poorly soluble components. Obtained results clearly show that PVP is able to significantly increase the drug dissolution profile, even when it is in its crystalline form. The higher rate obtained with physical mixtures is still not well understood. A possible explanation may be the formation of PVP:piroxicam interaction (such as hydrogen bonding) in the spray dried solid dispersions. The occurrence of PVP:piroxicam interaction has already been demonstrated by ATR-FTIR and DSC results. The drug:polymer interaction might retard the drug solubilisation, as the drug is bound to the carrier and this might retard the occurrence of the drug interaction with water, slowing it solubilisation and and its diffusion through the diffusive layer. Indeed for physical mixtures both drug and polymer are not involved in intermolecular interactions and the drug diffusion is only dependent on the PVP hydration and on the diffusive layer formation.

The same results can be observed also for PVP:piroxicam dissolution studies performed in buffer pH 6.5 and blank FaSSIF (Figure 3.37). Also in this case physical mixtures yielded faster dissolution profile compared to the correspondent spray dried samples, confirming the possible effect of polymeric carrier:drug interaction on the drug dissolution performance.

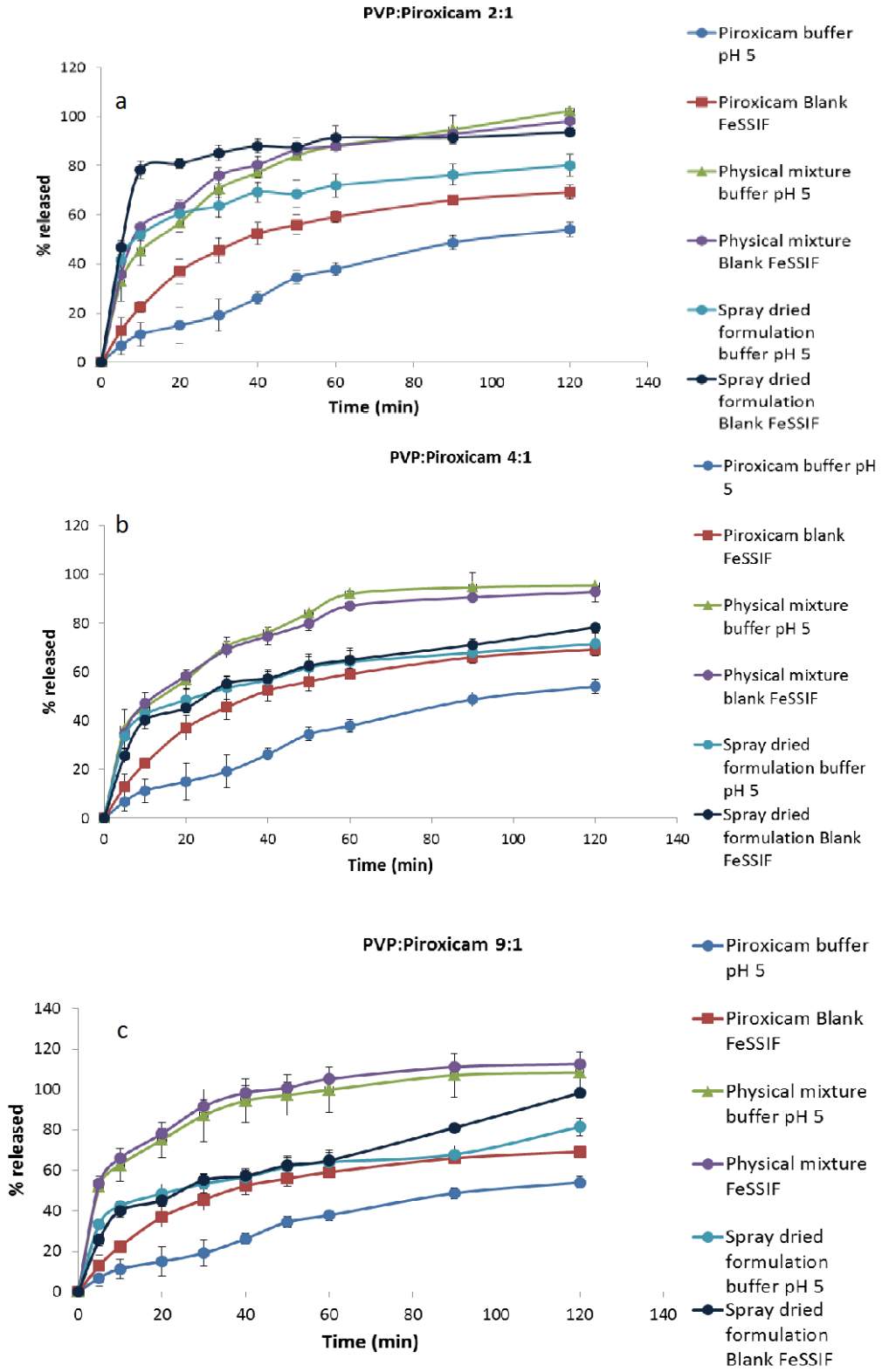

Figure 3.36: Dissolution profile of raw piroxicam, physical mixtures PVP:piroxicam and freshly spray dried PVP:piroxicam sample in buffer at pH 5 and Blank FeSSIF (polymer drug ratio: a=2:1, b=4:1, c=9:1) (n=3).

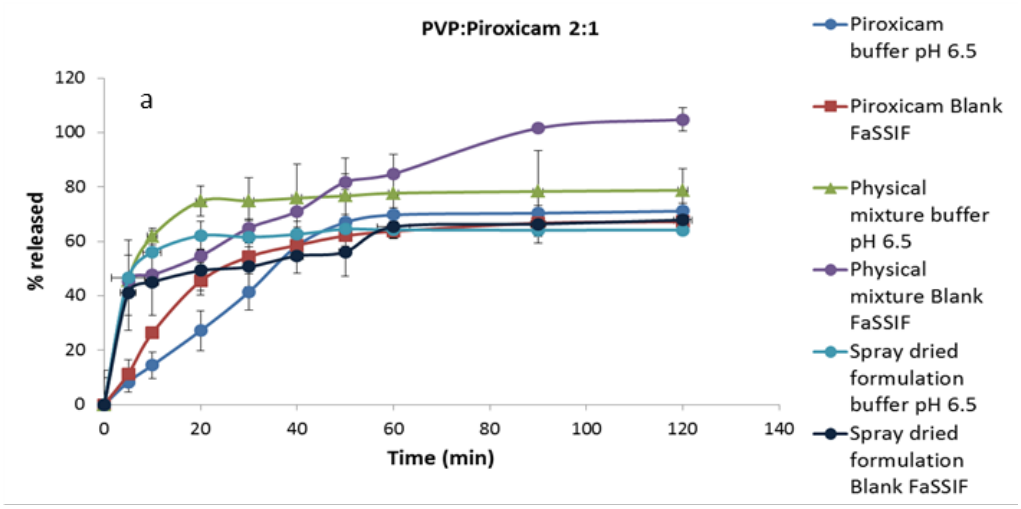

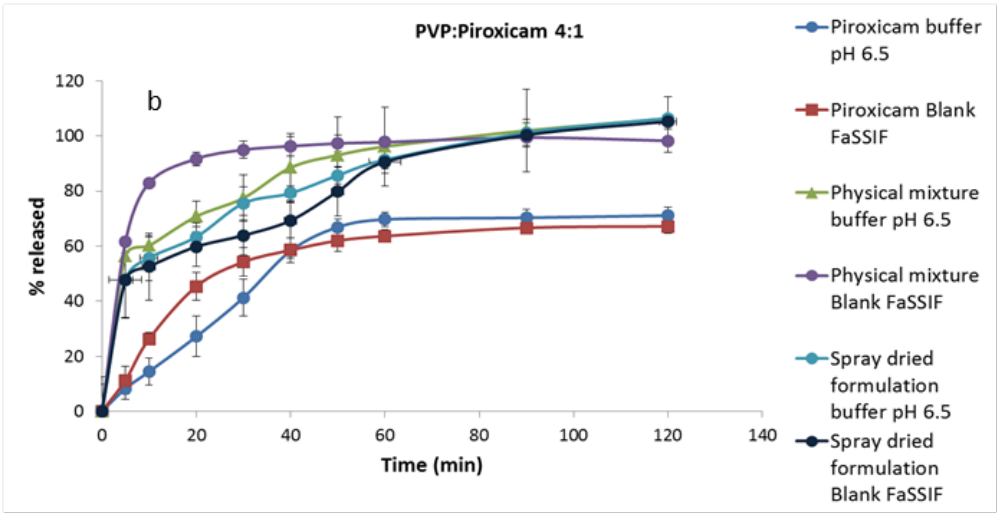

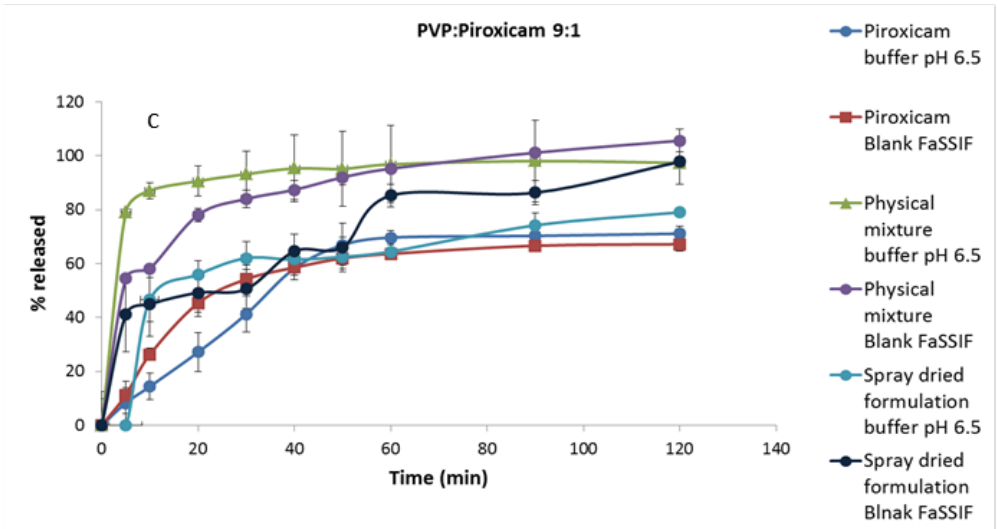

Figure 3.37: Dissolution profile of raw piroxicam, physical mixtures PVP:piroxicam and freshly spray dried PVP:piroxicam sample in buffer at pH 6.5 and Blank FaSSIF (polymer drug ratio: a=2:1, b=4:1, c=9:1) (n=3).

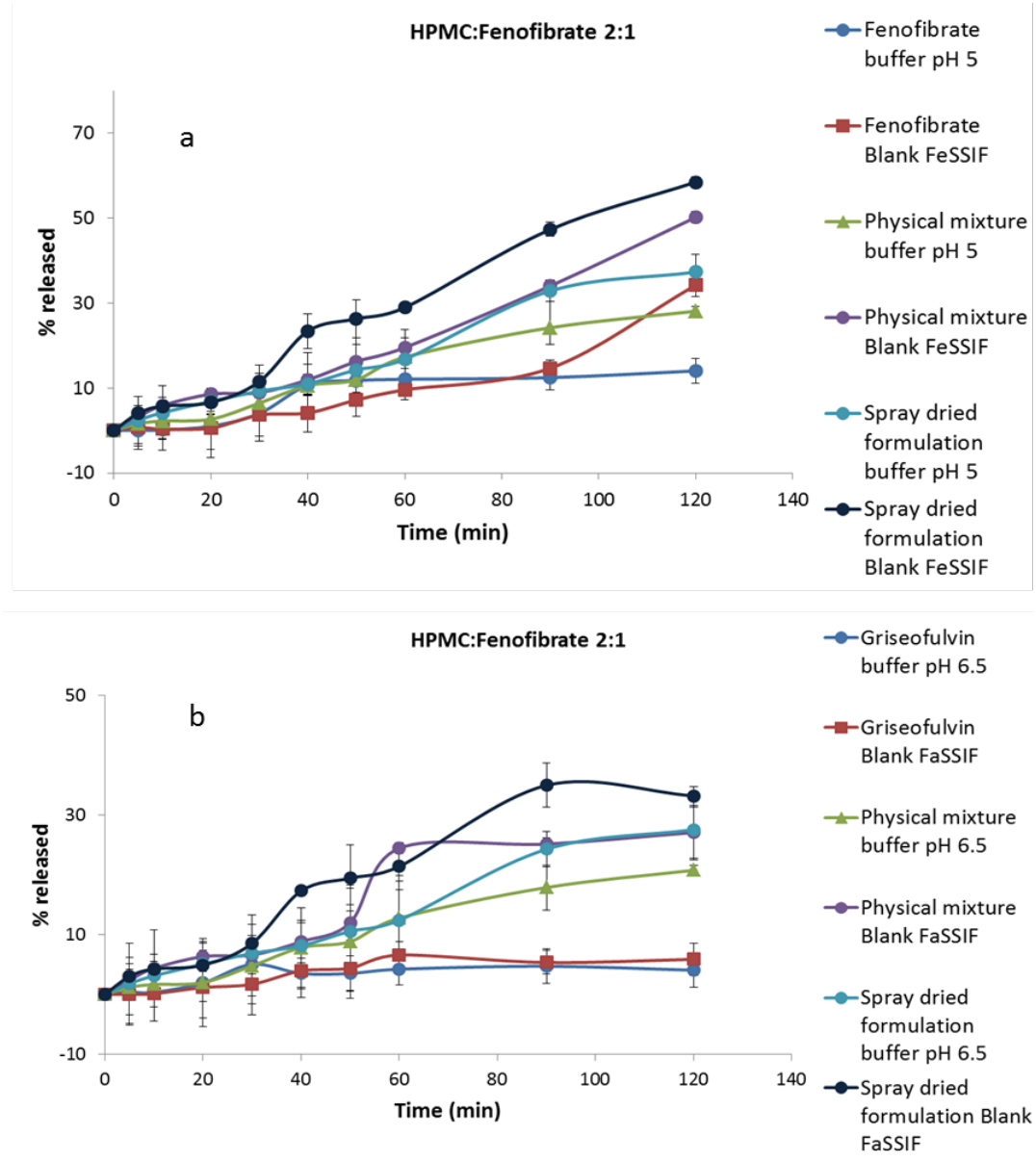

Figure 3.38: Dissolution profile of raw piroxicam, physical mixtures HPMC:fenofibrate 2:1 and freshly spray dried HPMC:fenofibrate 2:1 sample in buffer at pH 5 and Blank FeSSIF (a) and in buffer pH 6.5 and FaSSIF (b) (n=3).

Dissolution data of raw fenofibrate, HPMC:fenofibrate 2:1 physical mixture and spray dried solid sample are reported in Figure 3.38. Fenofibrate dissolution was extremely slow and less than 10% of the drug was released after 2 hours in the two buffers employed, in agreement with reported data. [243] No significant difference can be seen between buffer pH 5 and blank FaSSIF (b), while a higher fenofibrate solubilisation was reached in blank FeSSIF (a), with 30% of drug released after 2 hours. Dissolution rate did not increase dramatically for physical mixtures and spray dried samples, but a solubilisation enhancement effect is observable for both systems. Fenofibrate dissolution extent resulted

to be higher in blank FeSSIF, confirming the effect of NaTC micelles on the drug solubilisation.

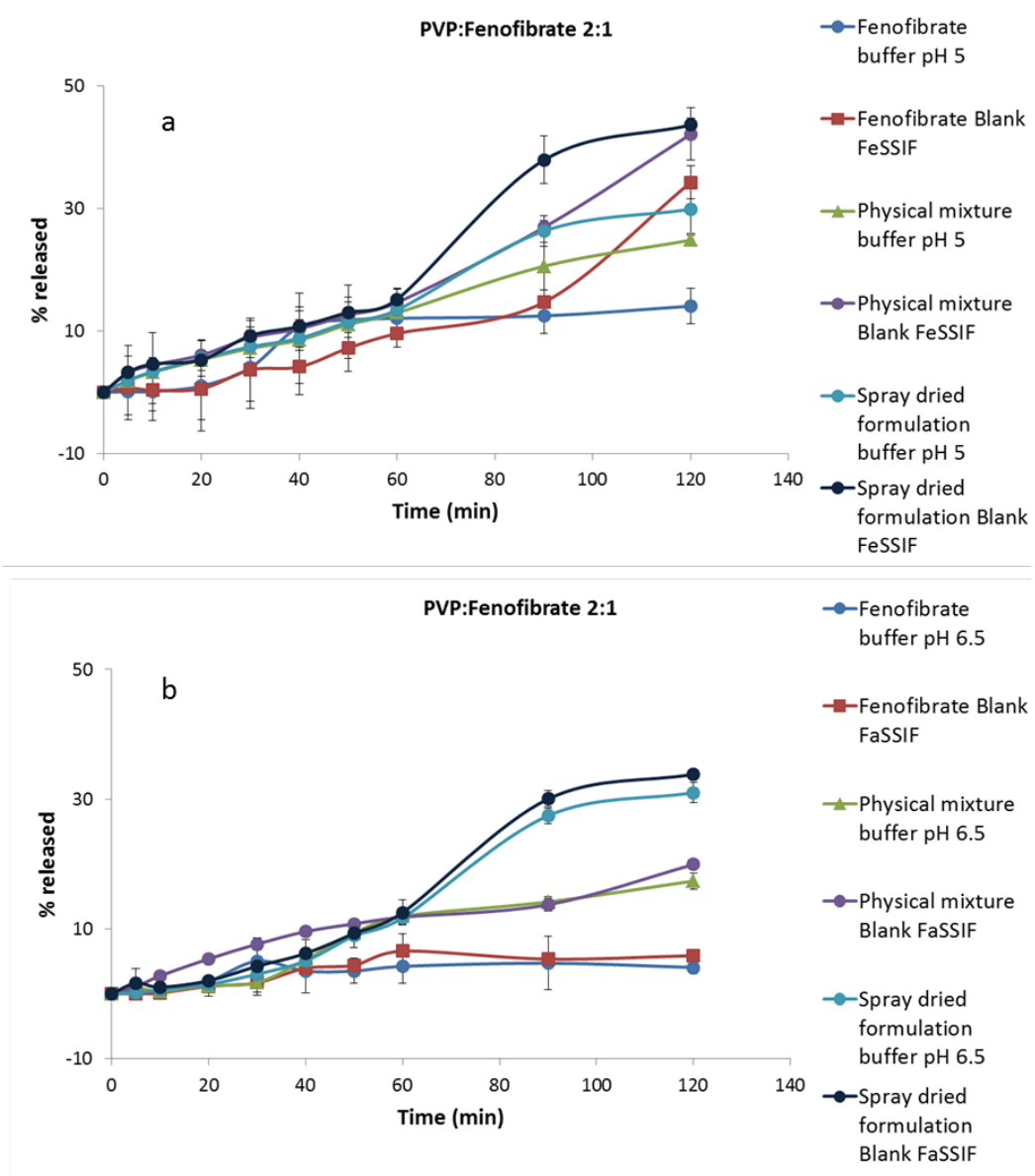

Figure 3.39: Dissolution profile of raw fenofibrate, physical mixtures PVP:fenofibrate 2:1 and freshly spray dried PVP:fenofibrate 2:1 sample in buffer at pH 5 and Blank FeSSIF (a) and in buffer pH 6.5 and FaSSIF (b) (n=3).

Figure 3.39 shows dissolution results obtained for HPMC:fenofibrate 2:1 physical mixtures and spray dried solid samples, compared to raw fenofibrate data. Fenofibrate dissolution resulted very slow also for PVP:fenofibrate systems and the dissolution extent was slightly lower than for HPMC:fenofibrate samples. As for HPMC:fenofibrate systems physical mixtures and spray dried solid dispersions yielded higher fenofibrate dissolution

extent, but the release remains slow in both cases. As already observed in steady state solubility results, fenofibrate solubilisation was not affected by media pH and ionic strength.

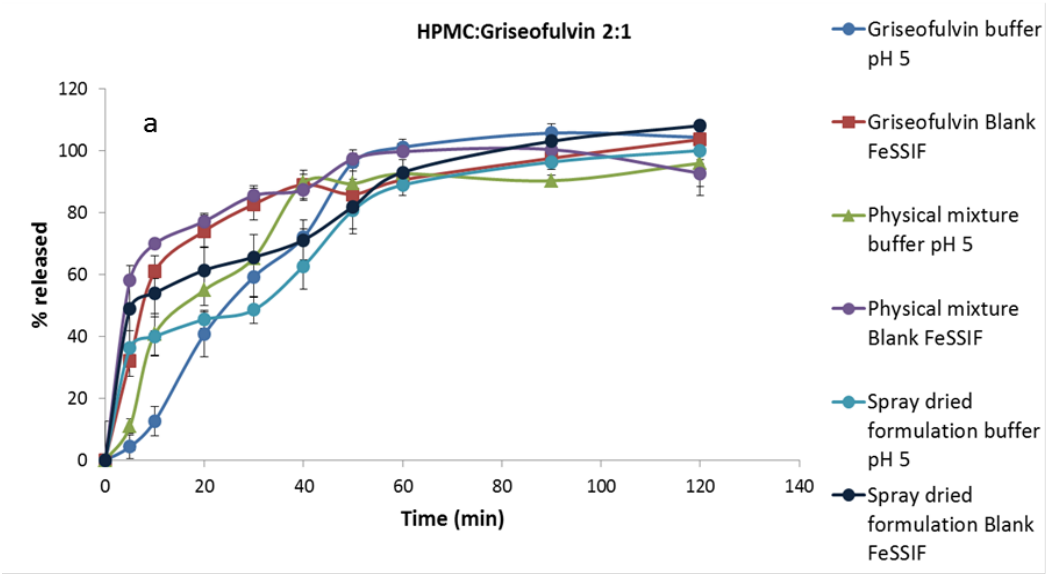

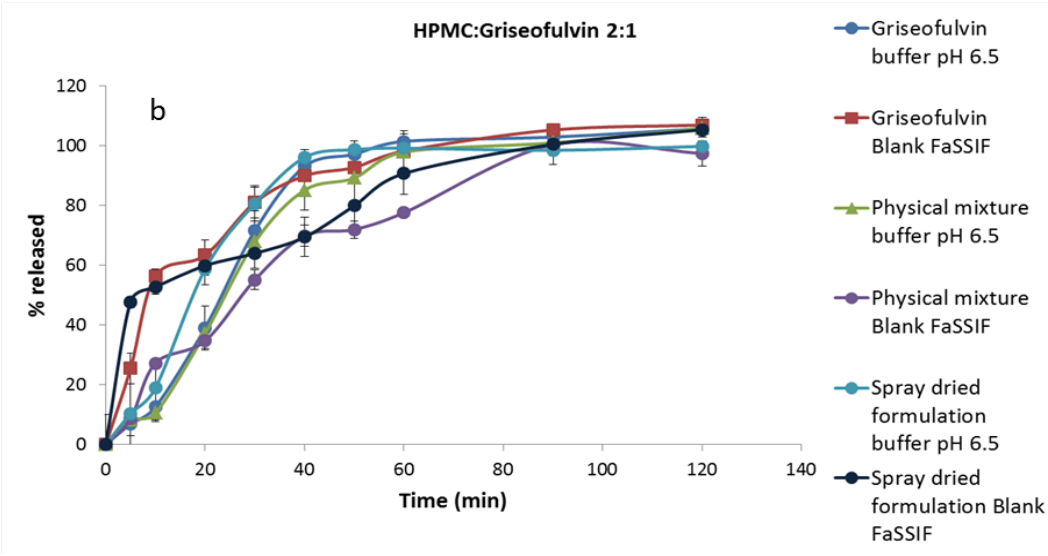

Figure 3.40: Dissolution profile of raw griseofulvin, physical mixtures HPMC:griseofulvin 2:1 and freshly spray dried HPMC:griseofulvin 2:1 sample in buffer at pH 5 and Blank FeSSIF (a) and in buffer pH 6.5 and FaSSIF (b) (n=3).

Dissolution profiles of raw griseofulvin, HPMC:griseofulvin 2:1 physical mixtures and spray dried samples are shown in Figure 3.40. The dissolution behaviour of griseofulvin is pH independent, as the results obtained for the raw drug at pH 5 and 6.5 are very similar. NaTC slightly affected the dissolution profile of the drug, as well as the presence of polymer. The graph clearly shows that the dissolution profiles obtained are very similar for physical mixtures and spray dried formulations, and no significant difference can be observed between them. Griseofulvin intrinsic water solubility is higher than for piroxicam and

fenofibrate, therefore higher griseofulvin weight ratio should probably be tested to observe a significant difference between the samples studies.

Similar results can be observed for PVP:griseofulvin sample (Figure 3.41). Indeed also for this system no significant difference between physical mixture and spray dried sample was observed. Dissolution profile of PVP:griseofulvin system were slightly slower than HPMC:griseofulvin ones.

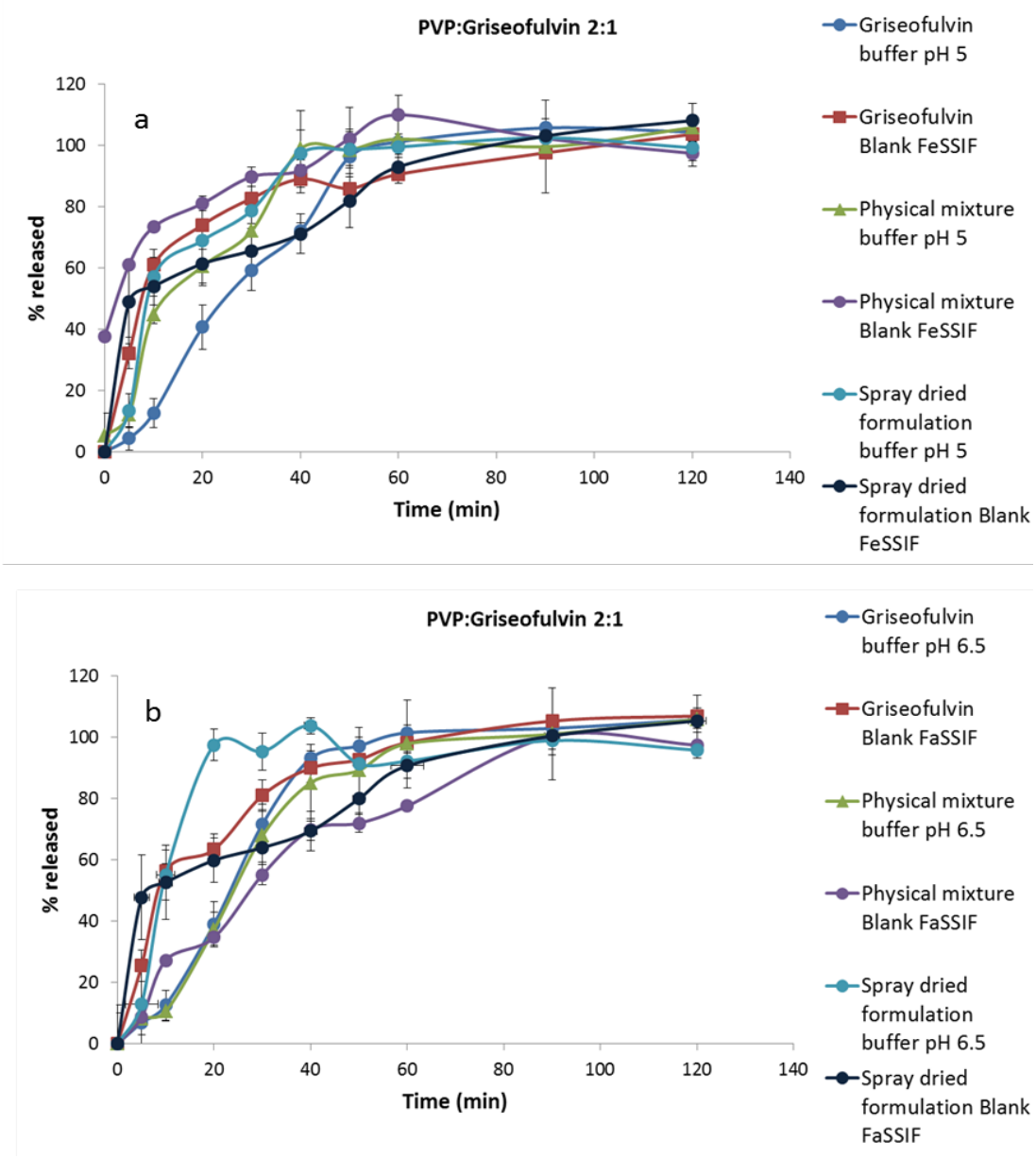

Figure 3.41: Dissolution profile of raw griseofulvin, physical mixtures PVP:griseofulvin 2:1 and freshly spray dried PVP:griseofulvin 2:1 sample in buffer at pH 5 and Blank FeSSIF (a) and in buffer pH 6.5 and FaSSIF (b) (n=3).

The dissolution results obtained for the different sample tested clearly indicate that more factors are involved in the drug solubilisation mechanism. The concomitant presence of polymeric carrier and surfactant in the dissolution media yielded the fastest dissolution profiles. The role of the carrier, of the surfactant and of their possible interaction in the drug dissolution process is not well understood and will be investigated in Chapters 4 and 5.

3.4 Conclusions

In this Chapter the preparation and characterisation of spray dried solid dispersion was discussed. Three different model drugs, piroxicam, fenofibrate and griseofulvin, and two model polymers, HPMC and PVP, were used to prepare the spray dried solid dispersion. Round shaped microparticles were obtained as revealed by SEM analysis. The solid-state characterisation of the systems was performed using PXRD, ATR-FTIR, DSC and TGA experiments. Obtained results confirmed the transition of the model drug from their crystalline to their amorphous state (and molecular dispersions in the cases of solid dispersions with low drug loadings) after spray drying process, although residual crystallinity was revealed by DSC and PXRD analysis in the samples with high drug loadings. The interaction (hydrogen bonding) between the polymer and the drug were confirmed by ATR-FTIR analysis.

Solubility studies of the model drugs were performed in different media. In order to mimick the intestinal pH and ionic strength two different buffers were employed. The additions of NaTC and lecithin to the media were performed to further simulate the biorelevant intestinal fluids before and after meal. The medium composition resulted to be critical for the drug solubilisation, together with the type of polymer and polymer concentration used in the formulations. Higher solubility values were obtained in the presence of polymeric carrier and of NaTC.

To investigate the impact of the spray drying process on the drug dissolution performance, dissolution studies were carried out for the raw drugs, polymeric carrier:drug physical mixtures and spray dried samples in four different media. The use of different media allowed the study of the effects of pH and ionic strength on the drug dissolution behaviour of the spray dried solid dispersions. Both factors have significant effects on the *in vitro* dissolution behaviour of piroxicam loaded formulations due to pH-sensitivity of the drug. The presence of NaTC showed significant impact on the drugs dissolution rate and extent (which can be interpreted as solubilisation), particularly for piroxicam and fenofibrate. The solid-state characterisation revealed the physical state of the drug and gave essential

indication about the possible choice of a carrier. The mechanism of drug solubilisation was further investigated in the following chapters via studying the behaviour of polymer and bile salts in simulated intestinal fluids.

Chapter 4. Probing the molecular interactions between polymeric carriers and Bile Salts

4.1 Introduction

The use of hydrophilic polymeric carriers for the delivery of poorly water-soluble drugs has been extensively studied.[244] Polymer based solid dispersions have shown to be a successful approach to improve the dissolution rate of poorly soluble drugs. [11,24] Furthermore, in the last decades, increasing attention has been paid to the composition of the dissolution media employed in dissolution in-vitro screening tests. [70] Different studies have shown that the composition of the dissolution media used can significantly impact on in vitro drug dissolution performance. The use of simulating fluids mimicking the gastro-intestinal condition resulted to be useful to achieve good in-vitro/in vivo correlations, as correlation between in vitro dissolution test and in vivo absorption may be more similar when physiological conditions are mimicked. [71,245]

Therefore both the choice of carrier polymer and the dissolution media can have significant effects on the dissolution study of a solid dispersion containing poorly soluble drugs. However the possible intermolecular interaction occurring between the polymeric carrier and the components of the biorelevant medium, such as bile salts, cholestral and other digestic enzymes, are still poorly understood due to the complex nature of the simulated GI fluids. Even less is known about the impacts of these possible interactions between polymeric carriers and media components on poorly water-soluble drug dissolution behavior. This project only focused on investigating the intermolecular interactions between polymers and bile salts. Qi and her co-workers' study on HPMC/surfactant interactions showed some indicative results on the possible role of such interactions in the drug solubilisation solid dispersions during dissolution process. [246] Therefore a fuller understanding of polymeric carriers-bile salts interaction and of its possible role on drug solubilisation during dissolution from solid dispersions will benefit the further exploit of solid dispersions.

The focus of this Chapter was to characterise the potential molecular interactions between polymeric carriers employed in Chapter 3 (PVP and HPMC) and the model bile salt (NaTC) used to prepare the biorelevant media for steady state solubility and dissolution studies. ^{1}H and DOSY NMR techniques were used to study the NaTC aggregation behaviour, with and without the presence of polymer, in conditions reproducing the intestinal pH and

osmolarity. The same characterisation was performed by interfacial tension measurements, carried out using pendant drop technique.

4.2 Experimental methods

4.2.1 NMR Spectroscopy

Two different NMR techniques, ^{1}H NMR and diffusion-ordered spectroscopy (DOSY) were employed in this part of the study. Both experiments were performed using a Bruker Ultrashield Plus 400 MHz Spectrometer (Bruker, BioSpin Corporation, The Woodlands, TX).

4.2.1.1 ^{1}H proton NMR

^{1}H proton NMR measurements were carried out using 5mm NMR tubes. All experiments were performed at 37 °C, in order to simulate the physiological temperature. 124 scans were acquired, relaxation delay was set at 1s and the pulse length was 90 °. All the samples were prepared in D_2O. In order to investigate the NaTC aggregation, ^{1}H proton NMR was performed on NaTC/D_2O samples with NaTC concentrations from 1 to 90 mM. This concentration range was employed to allow the study of the system from below to well above the bile salt CMC (3-12mM). The same experiments were performed in phosphate and acetate buffers with pH 5 and 6.5, respectively. These are the conditions employed in steady state solubility and dissolution studies described in Chapter 3. In order to make the NMR experiments feasible, buffers were prepared in D_2O. The actual pH values of the deuterated buffers were 4.89±0.06 for the buffer at pH 5 and 6.48±0.34 for the buffer at pH 6.5 (n=3). The chemical shift of NaTC was measured in D_2O, in the two deuterated buffers and also in the presence of PVP and HPMC (0.5 mg/ml), in order to evaluate the impact of the polymer on the surfactant chemical shift. Samples were prepared by weight and were allowed to equilibrate for 1 hour before taking the measurement. All the samples were analysed in triplicate (n=3). The proton chemical shift of NaTC was determined as a function of concentration. Internal referencing was performed as described in section 4.3.1. Data were analysed using TopSpin 3.2 Software.

4.2.1.2 DOSY NMR

DOSY NMR experiments were performed using 5mm NMR tubes. Experiments were carried out at 37 °C. 16 scans were acquired for each sample. Relaxation delay and the pulse length were set at 1s and 90 °, respectively. Diffusion was measured using stimulated echo and Eddy current compensation, applying bipolar gradient pulses for diffusion and 2 spoil gradient pulse. The gradient pulse duration and the diffusion delay length were set at

2.5 s and 0.2 s, respectively. The list of samples analysed and their preparation methods can be found inSection 4.2.1.1. Data were analysed using TopSpin 3.2 Software. No restricted diffusion was observable. Experiments were performed in triplicate (n=3).

4.2.2 Interfacial tension measurements

Interfacial tension measurements were carried out using FTA200 pulsating drop tensiometer (First Ten Angstroms, Portsmouth, VA, USA). NaTC interfacial tension was measured with and without the presence of HPMC and PVP (0.5 mg/ml). All experiments were performed in MilliQ water, phosphate and acetate buffers with pH 5 and 6.5, respectively. The appropriate solution was placed in a glass cuvette. A Hamilton syringe, having a volume of 50 µl, was fitted with a j-shaped needle. An air bubble was formed using the j-needle and the interfacial tension was measured over 15 minutes. Samples were prepared by dissolving the polymer at the required concentration in the medium. Obtained polymeric solutions were left at 37 °C for 1 hour, to allow system equilibration. Increasing amounts of NaTC were added to the sample and interfacial tension measurement for 15 minutes. NaTC concentration between 1 and 20mM were analysed. All experiments were performed in duplicate (n=2).

4.3 Results and discussion

4.3.1. ^{1}H proton NMR of raw materials

Figure 4.1 shows the ^{1}H NMR spectrum of NaTC. ^{1}H peaks were assigned according to literature data. [247,248] The detailed peaks assignment is summarised in Table 4.1.

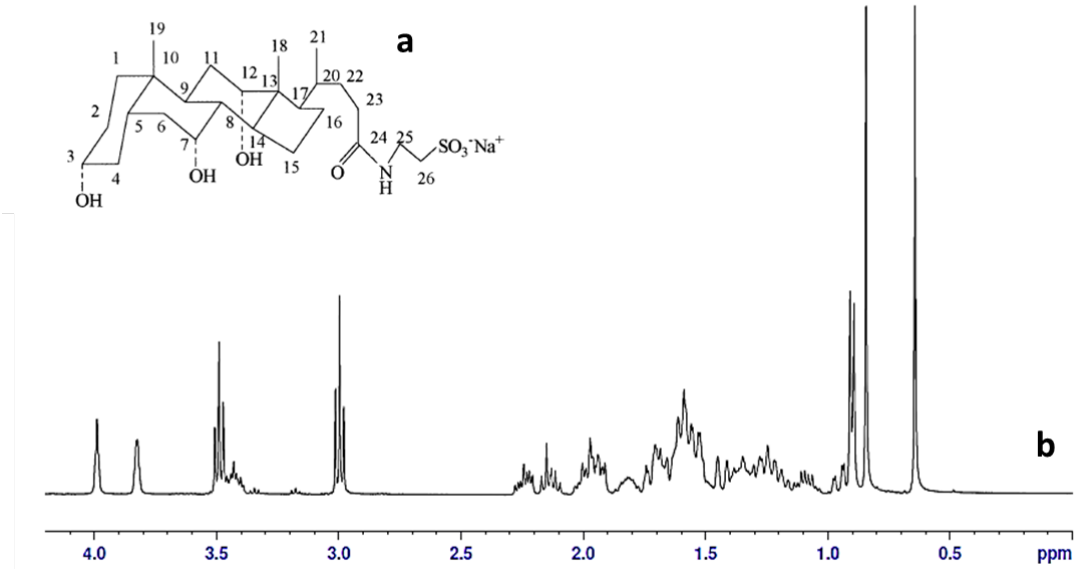

Figure 4.1: Chemical structure (a) and ^{1}H NMR spectrum of NaTC (b)

Table 4.1: NaTC 1H NMR peak assignment according to literature data [247,248]

Proton	Resonance (ppm)	Proton	Resonance (ppm)
1 CH_2-	1.06(β), 1.82(α)	**15 –CH_2-**	1.24(α), 1.70(β)
2 –CH_2	1.35(α), 1.61(β)	**16 –CH_2-**	1.35, 1.94 (remains unassigned)
3 HO-CH	3.48	**17 –CH**	1.70
4 -CH_2	1.52(β), 1.97(α)	**18 -CH_3**	0.64
5 –CH	1.49	**19 -CH_3**	0.83
6 -CH_2	1.52(α), 2.01(β)	**20 –CH**	1.45
7 HO-CH	3.82	**21 –CH_3**	0.93
8 –CH	1.67	**22 –CH_2**	1.32, 1.74
9 –CH	2.11	**23 –CH_2-**	2.24
11 –CH_2-	1.59(β), 1.65(α)	**25 –CH_2-**	3.16
12 –CH-OH	3.99	**26 –CH_2-**	3.00
14 –CH	1.82		

H12 signal exhibited a larger change when NaTC concentration was varied compared to the other protons, showing chemical shift variation and peak brodening. For this reason its chemical shift was used as a reference to study the impact of NaTC concentration of micelles formation, with and without the presence of polymers (HPMC and PVP), in MilliQ water and buffered solutions. In order to have reliable measurements, internal referencing of the H12 signal was performed. The chemical shift of H12 was compared to the one of proton H18.

It is well known that liquid state NMR is normally a limited approach to characterise polymeric system. Indeed a fast decay of the NMR signal, due to relaxation, can occur. The line widths in the NMR spectra are proportional to the relaxation rates. Therefore the signal-to-noise ratios of the NMR spectra of large molecules, such as polymers, are often poor. [249]

In order to exclude possible interference of the PVP and HPMC signals with the NaTC spectrum, ^{1}H NMR was performed on different concentrations of the two polymers. As shown by Figure 4.2 a and b, the signal of the two polymers is poor and very weakly intense in comparison with the signal of D_2O. Therefore no significant interference with the NaTC signal was observed.

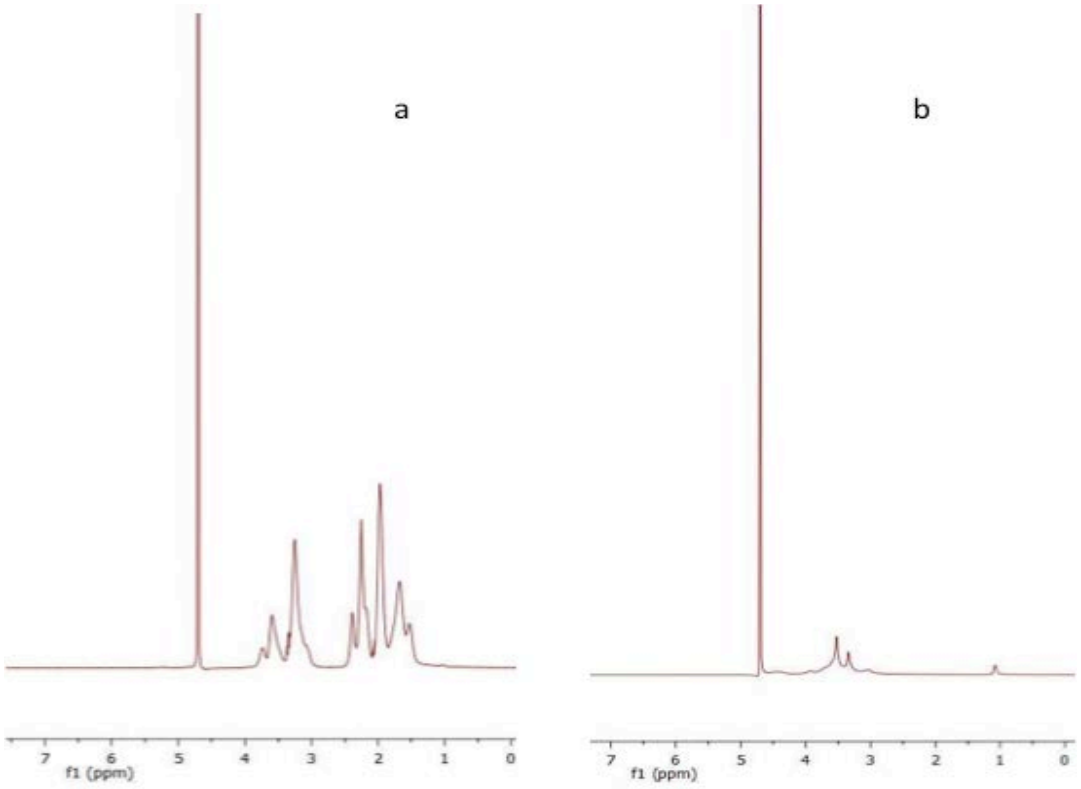

Figure 4.2: ^{1}H NMR spectra of PVP and HPMC in D_2O

4.3.2. ^{1}DOSY NMR of raw materials

Figure 4.3 shows DOSY NMR spectrum of NaTC 30mM. Self-diffusion coefficient (*D*) values are plotted against log *D* as a function of chemical shift δ values (ppm). It can be seen that two self-diffusion coefficients are present on the y-axis, one related to NaTC and the other to D_2O. D_2O self-diffusion coefficient was 1.58 D/10^{-9} m^2/s which is in agreement with literature data. [250]

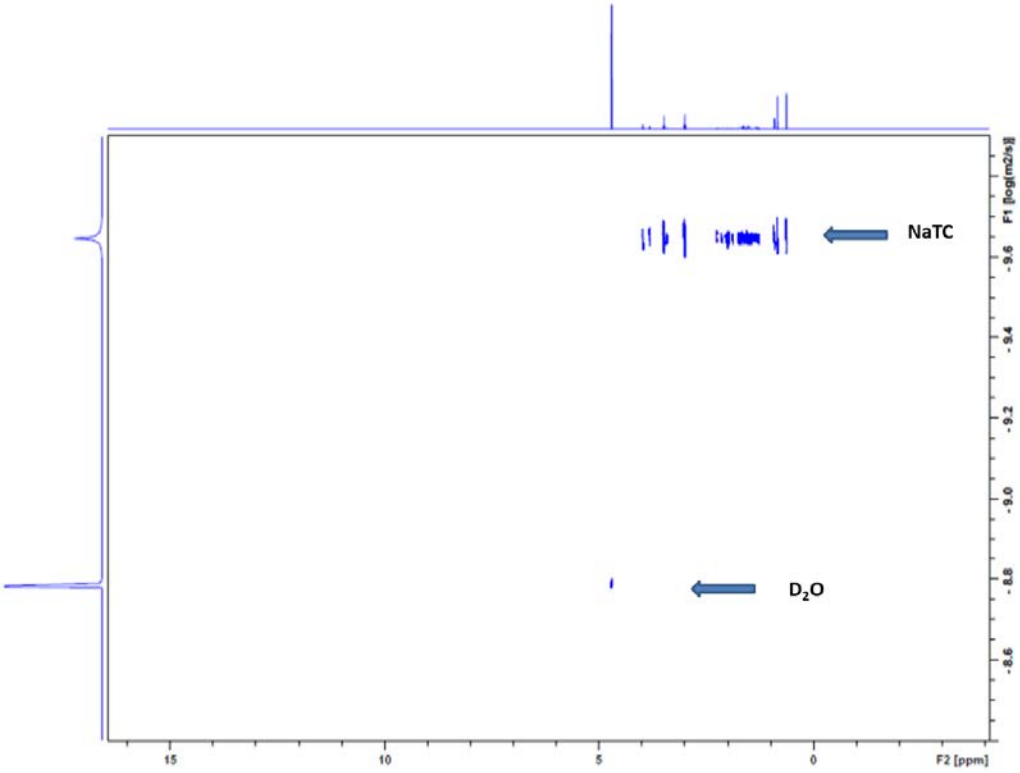

Figure 4.3: DOSY NMR spectra of NaTC 30mM in D_2O

Self-diffusion coefficient measurements were performed also for HPMC and PVP (data not shown). However due to slow diffusion of the polymers in solution, it was not possible to obtain the self-diffusion coefficient values of the polymers alone.

4.3.3 ^{1}H NMR and DOSY studies on the aggregation behaviour of NaTC

As already discussed in Chapter 1, the aggregation behaviour of bile salts is still not completely clarified in literature. [82,251] NaTC has widely been studied as one type of model bile salts, but its aggregation pattern is still not well understood and different CMC values have been proposed in literature. Table 4.2 summarises CMC values of NaTC reported in

literature. The experimental conditions and characterisation techniques employed are also indicated.

Table 4.2: Summary of NaTC CMC values reported in literature

Reference	Technique	Experimental conditions	CMC (mM)
[252]	Light Scattering	37 °C, pH 7.4, [Na^+] 0.15	8.5
[253]	Fluorescence	20±1°C, water	8-12
[91]	Electric paramagnetic resonance (ESR)	25°C, pH>10, [Na^+] 0.15 M	5-7
[254]	Electrode measurements	25°C, [NaCl] 0.01 M	12
[255]	Chromatography	PBS pH 7.4, [Na^+] 154mM	Not defined
[256]	Fluorescence	25°C, water	8-12
[257]	Light scattering	25°C, water	12
[258]	Spectral shift	25°C, water	3-5
[259]	NMR	25±1°C, D_20	6.5-8.3
[260]	Fluorescence, Light scattering	15±1°C, [NaCl] 15-300mM	1-15

As shown by the data in Table 4.2, the CMC value of NaTC appears to be dependent on the characterisation technique and the testing conditions employed. Few research groups have described the aggregation behaviour of NaTC being a not well-defined and a "progressive process" even at very low concentrations rather than a sharp transition of aggregation behaviour at a critical concentration point. [255,260]

In this work ^{1}H proton NMR was employed to assess NaTC aggregation in D_2O and in phosphate and acetate buffers used in dissolution and solubility studies. NaTC H12 chemical shift was plotted as a function of NaTC concentration. Figure 4.4 shows the results obtained using three different media.

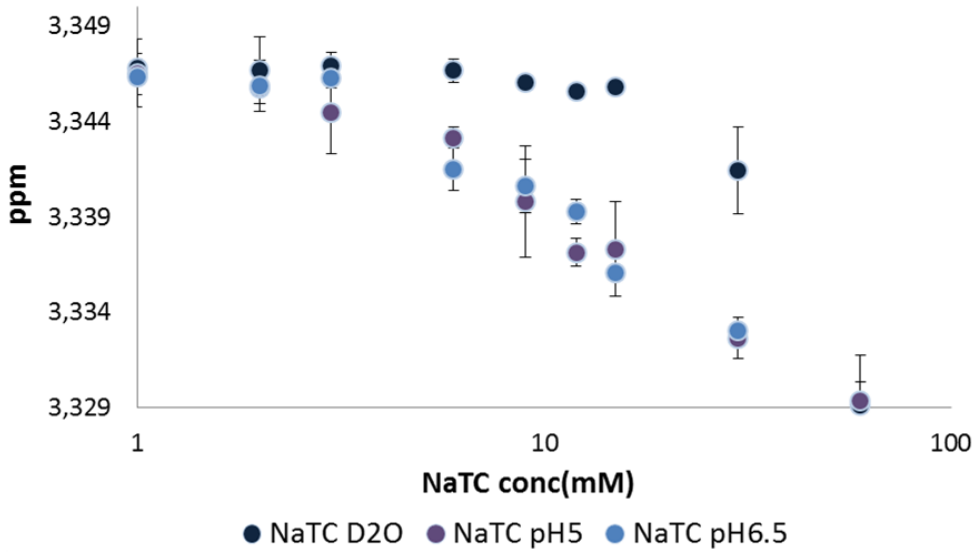

Figure 4.4: NaTC H12 chemical shift as a function of NaTC concentration in D_2O, buffer pH 5 and buffer pH 6.5

From Figure 4.4 it can clearly be seen that NaTC H12 ∂ did not change significantly within the NaTC concentration range of 1-12mM. When NaTC concentration was further increased to 15mM, a significant ∂ change was observed, as shown in Figure 4.4. Therefore 12mM can be assigned as the CMC of NaTC. This value is in very good agreement with NaTC CMC values obtained in water by previous works as shown in Table 4.2. Experiments performed in deuterated buffer (*d*-buffer) yielded a completely different trend. The ∂ values were observed at much lower NaTC concentrations, indicating a dramatic impact of the presence of salts on the NaTC aggregation. In both buffered solutions NaTC aggregation occurred at much lower NaTC concentrations (about 3mM in the two buffers).

Taurine-conjugated bile acids are strong sulfonic acids with pKa values <2. [251] NaTC pKa value is about 1.8 at 37 ºC. [261] Being an anionic surfactant, NaTC self-assembling behaviour can be affected by the medium pH, but considering its pKa value, no significant difference is expected between pH 5 and pH 6.5. Indeed both media are weakly acidic and have pH values well above the pKa of the surfactant. If the pH is sufficiently above the pKa of the bile salt, all the bile salt molecules are in their ionized form. [262] A pH close to the pKa implies that dissociated and undissociated, i.e. charged and uncharged, molecules are both involved in micelle formation, effect that has been reported to lower CMC. [94] Thus, as already described in the Introduction Chapter (section 1.4.2), a change in pH has a significant effect only when the ionization state of the bile salt molecules is changed. Considering the pH values of the media employed in this study, the ionization state of NaTC

was similar in the buffered media and consequently the pH did not have an impact on NaTC micellization.

Another important factor that can influence bile salt aggregation is the ionic strength of the medium. Ionic strength increase leads to reduction of the electrostatic repulsion between charged groups. Such effect is more significant for micellar than monomeric bile salt molecules. This is because that charges carried by the molecules are closer in micelles than in bulk solution. Therefore increasing the ionic strength favours aggregation and decreases the CMC. [85] The two buffers employed differed significantly for their ionic strength and osmolarity values, as described in Chapter 3 (Section 3.2.1, Table 3.1). Despite these differences (much higher osmolarity at pH 5, 670 mOsmol/l, than at pH 6.5, 270 mOsmol/l) the effects of the two buffers on the NaTC aggregation were very similar. Thus, this may suggest that the effects of the buffer ions on the surfactant anions were already saturated in the phosphate buffer (pH 6.5) with an osmolarity of 270 mOsmol/l, and the presence of higher salts concentration in the acetate buffer (pH 5) could not further impact on the aggregation.

The same samples have been analysed using DOSY NMR technique. The NaTC self-diffusion coefficients (*D*) obtained in D_2O, acetate and phosphate *d*-buffers were plotted as a function of NaTC concentration and the results are shown in Figure 4.5 and Table 4.3.

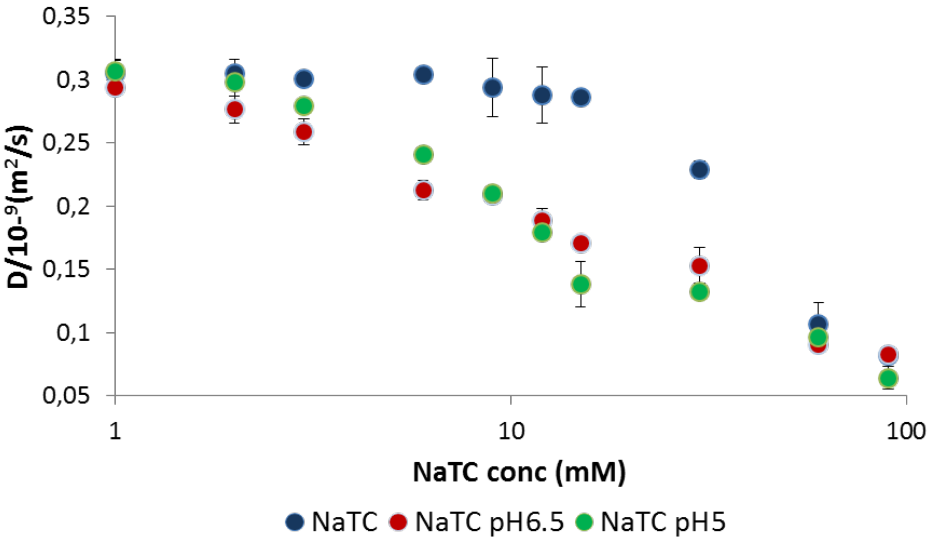

Figure 4.5: NaTC self-diffusion coefficient as a function of NaTC concentration, in D_2O, acetate (pH 5) and phosphate buffers (pH 6.5). (n=3)

Table 4.3: NaTC self-diffusion coefficients in D_2O, acetate (pH 5) and phosphate buffers (pH 6.5). (n=3)

NaTC concentration (mM)	$D/10^{-9}(m^2/s)$ D_2O	$D/10^{-9}(m^2/s)$ pH 5	$D/10^{-9}(m^2/s)$ pH 6.5
1	**0.295±0.011**	**0.293±0.008**	**0.299±0.010**
2	**0.294±0.011**	**0.286±0.011**	**0.285±0.021**
3	**0.295±0.005**	**0.268±0.005**	**0.266±0.019**
6	**0.286±0.002**	**0.235±0.003**	**0.219±0.015**
9	**0.270±0.023**	**0.213±0.006**	**0.198±0.020**
12	**0.268±0.022**	**0.190±0.006**	**0.178±0.022**
15	**0.181±0.005**	**0.161±0.018**	**0.165±0.010**
20	**0.154±0.007**	**0.132±0.005**	**0.147±0.022**
60	**0.097±0.017**	**0.093±0.006**	**0.102±0.021**
90	**0.082±0.018**	**0.075±0.009**	**0.085±0.006**

It can be seen that the *D* value of NaTC does not vary significantly in D_2O at NaTC concentration ranging between 1-12mM. This indicates that no aggregation between the NaTC monomers occurred in this concentration range, as the diffusion of NaTC molecules did not slow down (the slow-down of diffusion should be observed in the case of formation of aggregates). For the samples with NaTC concentration of 15 mM, the self-diffusion coefficient lowered from 0.268±0.022 to 0.181±0.005 ($10^{-9}(m^2/s)$), indicating the occurrence of NaTC aggregation (most likely to be micellization). The reduced self-diffusion coefficient value indicates the formation of bigger aggregates, which diffuse slower in solution. The CMC of NaTC measured by the DOSY experiments is 3 mM in both *d*-buffers, which agrees well with the ^1H NMR results.

In summary, the NMR results have provided useful information on the aggregation states of NaTC in blank FaSSIF and blank FeSSIF. In the case on blank FeSSIF, a large number of micelles are already formed, as the NaTC concentration is 15mM and consequently well above the CMC value indicated by NMR results at pH 5. The obtained data confirmed the presence of NaTC micelles mainly in blank FeSSIF medium. The NaTC concentration in blank FaSSIF is 3mM, which corresponds to the initiation concentration of the surfactant micellisation process. Therefore only few micelles can be present in this condition.

4.3.3.1 ^{1}H and DOSY NMR studies on NaTC-polymers interaction

^{1}H and DOSY NMR experiments were used to study the molecular interaction between NaTC and the two model polymers employed as polymeric carriers for the preparation of solid dispersions formulations in Chapter 3, HPMC and PVP. Polymer concentration of 0.5 mg/ml was used in order to work in a diluite regime, which is close to the polymer concetration in intestinal condition after the dissolution of a polymer based solid dispersion formulation.

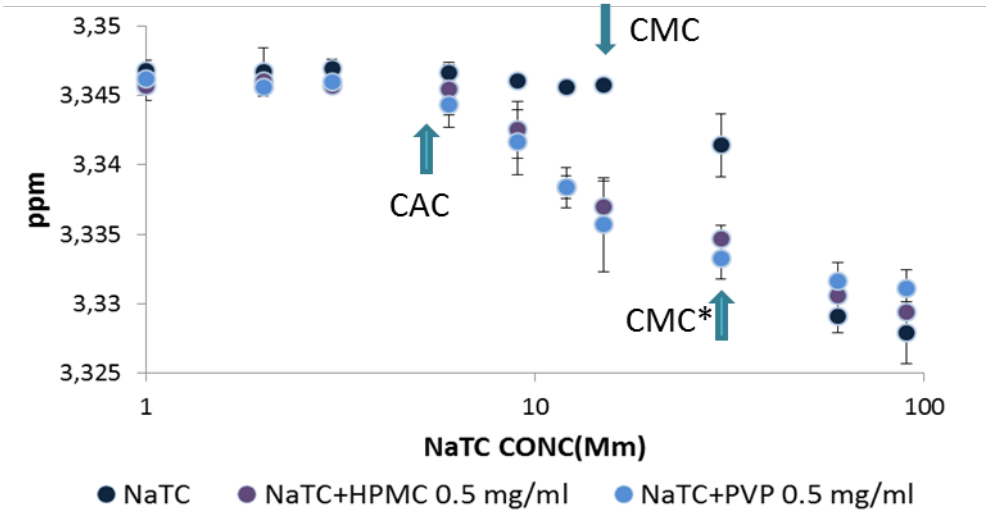

Figure 4.6: NaTC H12 chemical shift as a function of NaTC concentration in D_2O, HPMC 0.5 mg/ml and PVP 0.5 mg/ml solutions (n=3).

NaTC H12 ∂ were measured in D_2O at different NaTC concentrations in the presence of PVP and HPMC and plotted as a function of NaTC concentrations. Data shown in Figure 4.6 clearly indicate that the apparent CMC of NaTC was lowered in the presence of the polymers. This value is referred as critical aggregation concentration (CAC) in polymer-surfactant system. [132] This result indicates the presence of NaTC-polymer interaction. From the plot it can be seen that the CAC values of NaTC-HPMC and NaTC-PVP CAC values are very similar and both in the range of 3-6 mM. A plateau region between 12 and 15mM can be observed in Figure 4.6, indicating the continuous binding of NaTC to the polymers in this concentration range. A new shift of 12H ∂ occurred above 15mM. This second change in slope indicates that free NaTC micelles started to form and that no NaTC further binding occurred onto the polymers. This concentration therefore can be treated as the CMC* of NaTC.

As described by La Mesa, the solution phase in polymer-surfactant systems can be divided into three parts. Figure 4.7 shows a schematic representation of these three phases

for NaTC-polymer systems based on their ^{1}H NMR results. In phase I no significant interaction between NaTC and the polymer occurs, and only free NaTC molecules and polymeric chains/entanglements are present in solution. Once CAC is reached, the solution phase starts to change and NaTC-polymer interaction is dominant. Therefore in phase II mixed NaTC-polymer aggregates are formed. In phase 3 there is competition between NaTC-polymer interaction and micellization, and when saturation of the polymer binding sites by micellar aggregates is reached (CMC*), free surfactant micelles are formed.

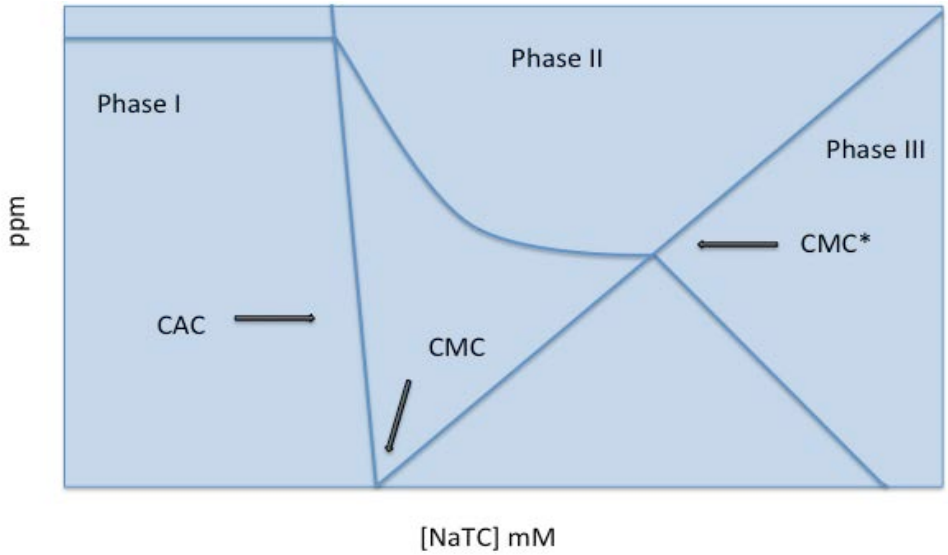

Figure 4.7: Schematic representation of the phase behaviour of NaTC-polymer solutions

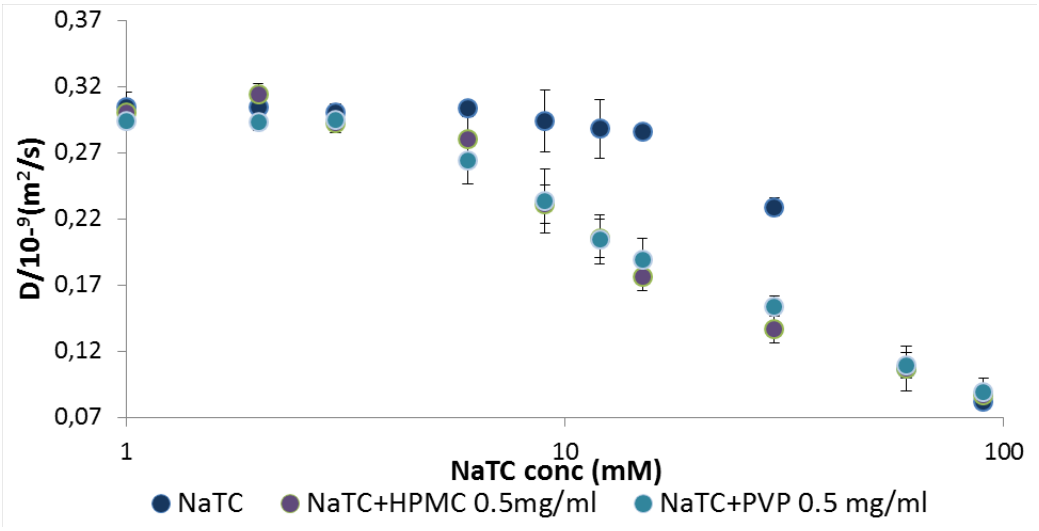

Figure 4.8: NaTC self-diffusion coefficients as a function of NaTC concentration in D_2O, HPMC 0.5 mg/ml and PVP 0.5 mg/ml solutions (n=3).

Table 4.4: NaTC self-diffusion coefficients in D_20, with and without the presence of polymer. (n=3)

NaTC concentration (mM)	$D/10^{-9}(m^2/s)$ D_2O	$D/10^{-9}(m^2/s)$ HPMC 0.5mg/ml/D_20	$D/10^{-9}(m^2/s)$ PVP 0.5mg/ml/D_20
1	**0.295±0.011**	**0.300±0.008**	**0.294±0.001**
2	**0.294±0.011**	**0.313±0.009**	**0.293±0.006**
3	**0.295±0.005**	**0.292±0.008**	**0.294±0.007**
6	**0.286±0.002**	**0.279±0.017**	**0.264±0.017**
9	**0.270±0.023**	**0.231±0.014**	**0.233±0.024**
12	**0.268±0.022**	**0.205±0.014**	**0.204±0.018**
15	**0.181±0.005**	**0.176±0.011**	**0.189±0.016**
20	**0.154±0.007**	**0.136±0.010**	**0.153±0.007**
60	**0.097±0.017**	**0.106±0.006**	**0.109±0.010**
90	**0.082±0.018**	**0.087±0.004**	**0.009±0.010**

NaTC interaction with HPMC and PVP in D_2O were also investigated by measuring the self-diffusion coefficients of the species using NMR. Obtained NaTC self-diffusion values are plotted in Figure 4.8 as a function of NaTC concentration. The data are summarised in Table 4.4. In the presence of polymers NaTC self-diffusion coefficient (*D*) values showed a significant decrease at a NaTC concentration of 6mM. This decrease of NaTC self-diffusion coefficient indicates the slowing down of surfactant molecules diffusion. Such effect cannot be attributed to the surfactant micellization, which, as proved by both ^{1}H and DOSY NMR data, occurs at 12mM. Therefore the decrease of NaTC self-diffusion coefficient at 6mM may be related to the bile salt aggregation with the polymers, which was shown to occur between 3 and 6mM for both HPMC and PVP by ^{1}H NMR data. Differently from ^{1}H NMR results, it is not possible to observe a second shift in the NaTC-polymer graph plots (Figure 4.8) of DOSY data. Hence it is not possible to assign a precise NaTC CMC* value. Nevertheless, considering the high NaTC concentration (90mM) reached during the experiments, the possibility of the formation of free NaTC micelles in solution cannot be excluded, despite the absence of a clear second shift in NaTC/HPMC and NaTC/PVP *D* plots. The absence of a clear shift indicating NaTC CMC* can be due to similar diffusional behaviour of NaTC micelles and NaTC-polymer aggregates, which makes not possible the identification the onset of NaTC micellization.

^{1}H NMR experiments on NaTC-PVP and NaTC-HPMC systems have been performed also in acetate and phosphate *d*-buffers in order to investigate the impact of pH

and ionic strength of the buffers on the NaTC-polymer aggregation. Obtained results are shown in Figure 4.9. As previously discussed in Section 4.3.1.2, the presence of salts had a critical impact on NaTC aggregation in both acetate and phosphate buffers. In Figure 4.9 it can be seen that the presence of salts had a dramatic impact on NaTC-polymer aggregation. The plot shows progressive aggregation behaviour. At pH 5 (Figure 4.9a) the plots of NaTC and of NaTC-PVP and NaTC-HPMC systems are very similar, showing a H12 NaTC shift at 3mM. At pH 6.5 (Figure 4.8b), such shift can be observed at slightly lower NaTC concentration, 2mM. For the NaTC-polymer-*d*-buffer systems this value is likely to represent CAC, as it is close to the CAC value obtained for the same system in D_2O (3-6mM).

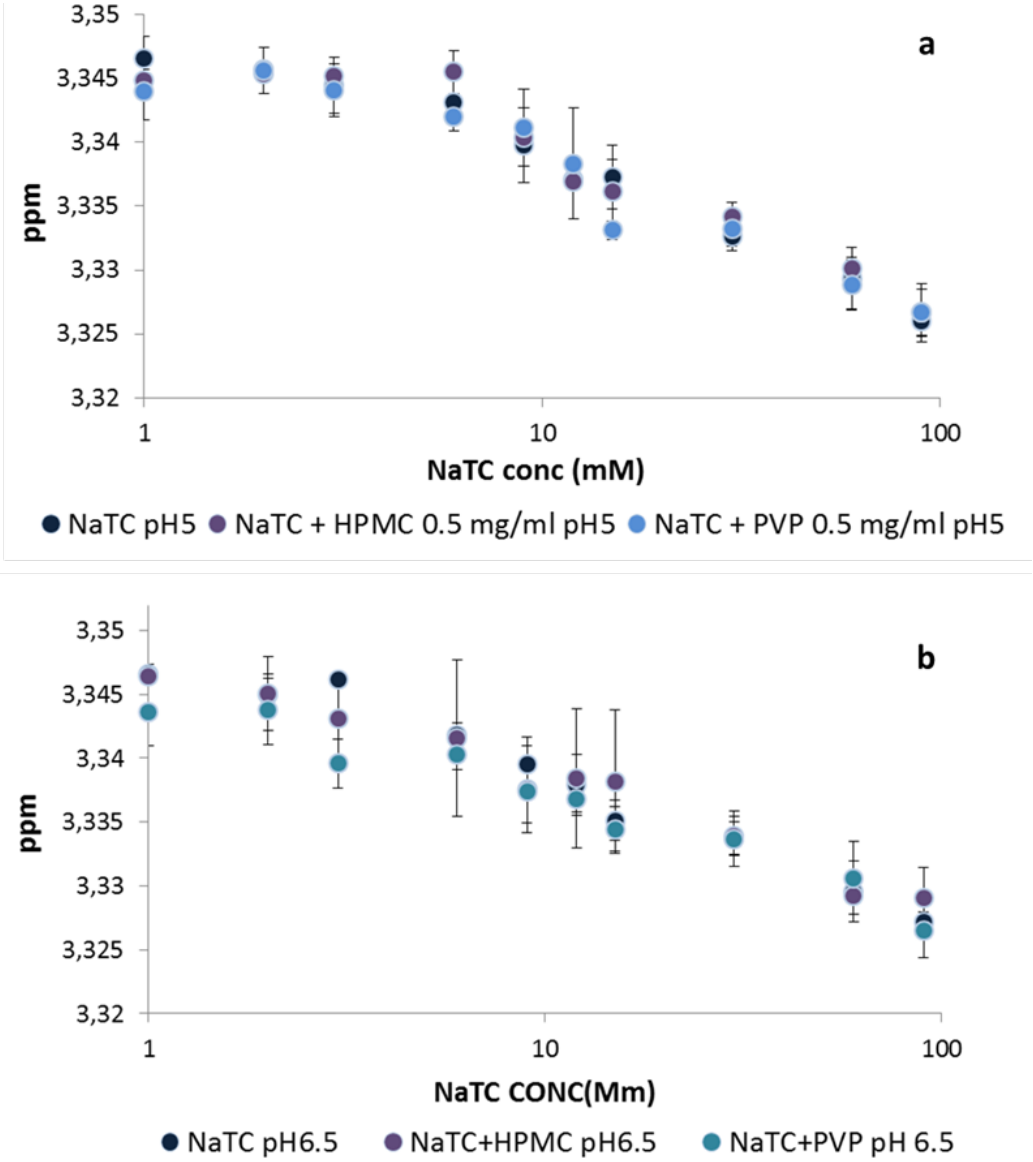

Figure 4.9: NaTC H12 chemical shift as a function of NaTC concentration in buffer pH 5, HPMC 0.5 mg/ml and PVP 0.5 mg/ml solutions (buffer pH 5; a) and in buffer pH 6.5, in HPMC 0.5 mg/ml and PVP 0.5 mg/ml solutions (buffer pH 6.5;b). (n=3)

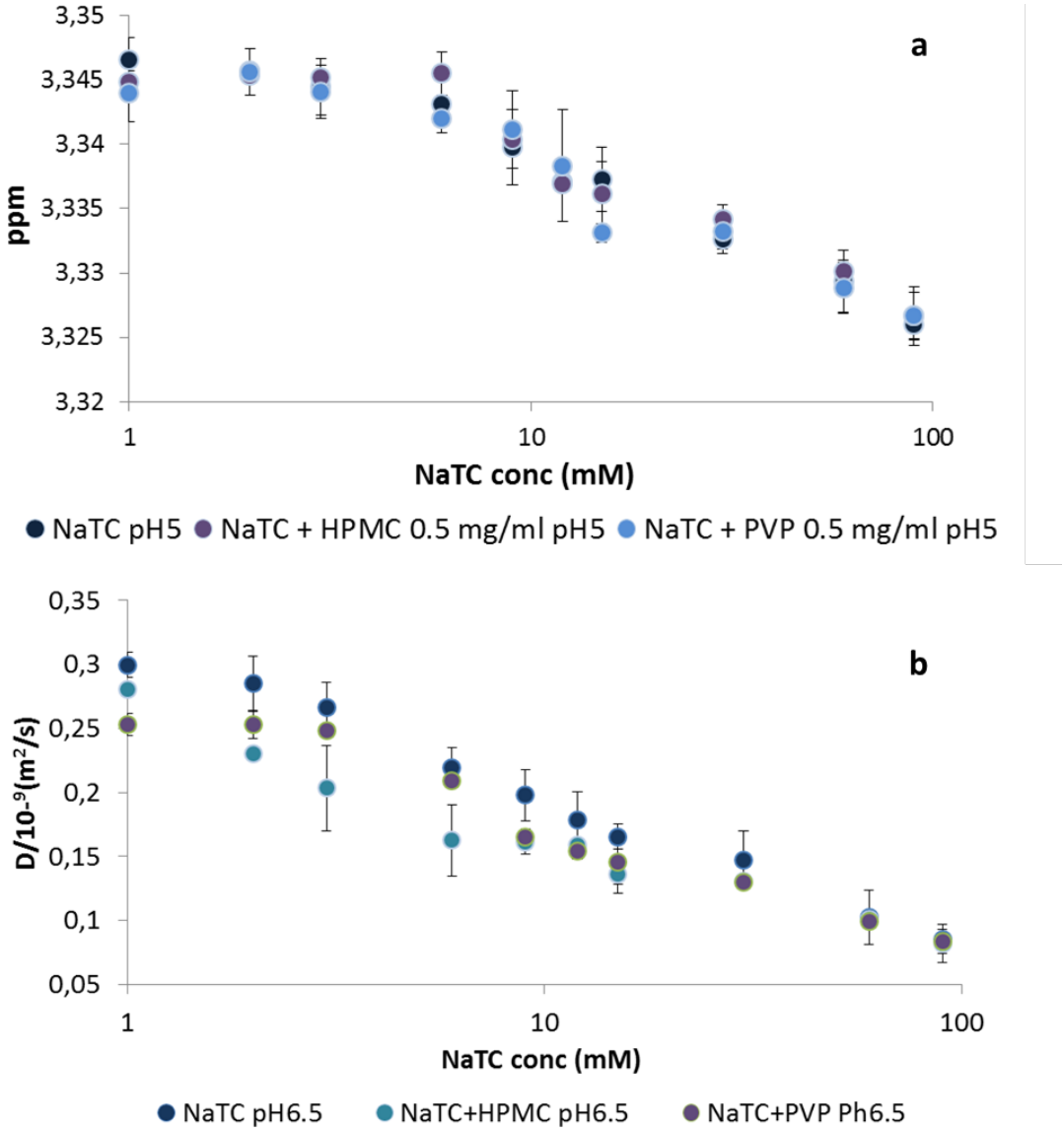

Figure 4.10: NaTC self-diffusion coefficients as a function of NaTC concentration in buffer pH 5, HPMC 0.5 mg/ml and PVP 0.5 mg/ml solutions (buffer pH 5; a) and in buffer pH 6.5, in HPMC 0.5 mg/ml and PVP 0.5 mg/ml solutions (buffer pH 6.5;b). (n=3)

NaTC-polymer-*d*-buffer systems have been characterised also by DOSY NMR experiments. It can be seen in Figure 4.10 that the *D* value of NaTC in the presence of HPMC at pH 5 is lower than the value obtained in the absence of the polymers. This may be due to the increased viscosity of the system as a consequence of the presence of HPMC. According to the Stokes-Einstein equation (Refer to Chapetr 2, section 2.3.10.1, Eq. 2.14), *D* value is dependent of the viscosity of the sample, and an increase of viscosity causes a decrease of molecular diffusion. *D* further decreased at NaTC concentration of 3mM, indicating 2mM as CAC. *D* values did not vary in the region 3-6 mM, while a second *D* decrease could be observed at NaTC concentration 20mM, indicating the onset of free micelles formation

between 15 and 20mM, range that can therefore be considered as CMC* value. For the system NaTC-PVP-*d*-buffer at pH 5, it is possible to observe that the *D* value at the lowest NaTC concentration is almost identical to the one obtained in the absence of polymer. Therefore, differently form HPMC, the presence of PVP did not lead to significant changes in the viscosity of the system. As for NaTC-HPMC-*d*-buffer system the NaTC CAC value is 2 mM. CMC* could not be assigned clearly, as from the CAC the addition of more surfactant led to a progressive *D* reduction and no clear shifts in the plot can be observed. Considering *D* values shown in Table 4.5, it is likely that NaTC free micelles started forming at NaTC concentration of 15mM, as the most dramatic *D* reduction is obtained at NaTC 20mM.

Table 4.5: NaTC self-diffusion coefficients in acetate *d*-buffer (pH 5) with and without the presence of polymer. (n=3)

NaTC concentration (mM)	$D/10^{-9}$(m^2/s) pH 5	$D/10^{-9}$(m^2/s) HPMC 0.5mg/ml/ pH5	$D/10^{-9}$(m^2/s) PVP 0.5mg/ml/pH 5
1	**0.293±0.008**	**0.238±0.002**	**0.287±0.002**
2	**0.286±0.011**	**0.245±0.003**	**0.280±0.003**
3	**0.268±0.005**	**0.215±0.001**	**0.226±0.008**
6	**0.235±0.003**	**0.202±0.001**	**0.232± 0.002**
9	**0.213±0.006**	**0.188±0.010**	**0.216±0.009**
12	**0.190±0.006**	**0.185±0.014**	**0.195±0.005**
15	**0.161±0.018**	**0.185±0.001**	**0.172±0.001**
20	**0.132±0.005**	**0.143±0.001**	**0.133±0.006**
60	**0.093±0.006**	**0.095±0.001**	**0.092±0.005**
90	**0.075±0.009**	**0.076±0.012**	**0.080±0.001**

For the system NaTC-HPMC-*d*-buffer system at pH 6.5 the association between NaTC and HPMC seemed to start at the lowest NaTC concentration tested (1mM). Indeed a first decrease of the *D* value was observed at the NaTC concentration 2mM. As for the same system at pH 5, a plateau region for the *D* values between 6 and 12 Mm (Table 4.5) can be observed. The *D* value of NaTC further decreased at 15 mM, suggesting that the formation of free micelles started at NaTC 12-15mM. Hence both CAC and CMC* of the NaTC-HPMC system resulted to be lower in the phosphate *d*-buffer at pH 6.5 than in the acetate *d*-buffer at pH 5. Such result is in contrast with the higher osmolarity of the acetate buffer, which, considering the much higher concentration of ions, was expected to have more dramatic impact on the NaTC/polymer aggregation. The higher impact of the phosphate buffer may be due to a different effect of the phosphate and acetate ions on the NaTC-

HPMC aggregation, and further investigation is required. NaTC-PVP-*d*-buffer at pH 6.5 system showed a very similar behaviour compared the same system at pH 5.

Table 4.6: NaTC self-diffusion coefficients in phosphate *d*-buffer (pH 6.5), with and without the presence of polymer. (n=3)

NaTC concentration (mM)	D/10^{-9}(m^2/s) pH 6.5	D/10^{-9}(m^2/s) HPMC 0.5mg/ml/ pH6.5	D/10^{-9}(m^2/s) PVP 0.5mg/ml/pH 6.5
1	**0.299±0.010**	**0.259±0.027**	**0.253±0.030**
2	**0.285±0.021**	**0.223±0.003**	**0.253±0.033**
3	**0.266±0.019**	**0.203±0.002**	**0.248±0.003**
6	**0.219±0.015**	**0.162±0.001**	**0.209±0.001**
9	**0.198±0.020**	**0.156±0.002**	**0.165±0.002**
12	**0.178±0.022**	**0.159±0.003**	**0.154±0.001**
15	**0.165±0.010**	**0.127±0.001**	**0.146±0.004**
20	**0.147±0.022**	**0.131±0.002**	**0.129±0.007**
60	**0.102±0.021**	**0.102±0.001**	**0.099±0.001**
90	**0.085±0.006**	**0.078±0.018**	**0.083±0.005**

A summary of CMC, CAC and CMC* values is shown in Table 4.7. ^{1}H and DOSY NMR data indicated the decrease of CAC and CMC* for both HPMC/NaTC and in *d*-buffer media, compared to values obtained in D_2O. It has been reported that the addition of electrolytes increases the binding ratio of surfactant to polymers. [263] Different studies have also shown that the association between polymers and surfactants starts at much lower surfactant concentration in the presence of salts, leading to a decrease of the CAC. [264,265] Xia et al also proved that the number of micelles bound to polymer increase when higher ionic strength is used. [266] The ions effect on NaTC-polymer association is related to the ions charge screening effect on the surfactant anions, but can also be attributed to the ions effect on the polymers behaviour. Both HPMC and PVP are non-ionic polymers, therefore the presence of salts is not expected to impact he polymers behaviour. Nevertheless, previous studies have demonstrated that ions can affect polymer behaviour in solution, exerting salting-in and salting out effects. The ions effect is mainly due to their water structuring capability. The formation of a more ordered water structure causes a reduction of the number of free water molecules available to interact with the polymer chains. [267] Therefore the reduction of CAC is likely to be a consequence of ions effect on both NaTC and polymeric carriers. This effect from the presence of ions seemed to favour polymer-NaTC association.

Table 4.7: CMC, CAC and CMC*(mM) value in the different media studied obtained by NMR studies

Medium	CMC	CAC	CMC*
D_2O	12	-	-
Acetate D-buffer	3	-	-
Phosphate D-buffer	3	-	-
HPMC/D_20	-	3-6	15
PVP/D_20	-	3-6	15
HPMC/Acetate D-buffer pH5	-	2	15
HPMC/Phosphate D-buffer pH6.5	-	1	12
PVP/Acetate D-buffer pH5	-	2	Not assignable
PVP/Phosphate D-buffer pH6.5	-	3	15

4.3.3.2 Predicted solution phase composition of blank FaSSIF and blank FeSSIF media containing model polymers

NMR results suggested the possible NaTC-HPMC and NaTC-PVP aggregations in *d*-FaSSIF and *d*-FeSSIF. Therefore obtained results can provide information about the nanostructure of the solutions of blank FaSSIF and FeSSIF during the dissolution of a solid dispersion formulation. ^{1}H and DOSY data showed that NaTC interacts with both PVP and HPMC even at very low concentrations. In particular for NaTC-HPMC system CAC was 1mM at pH 6.5 and 2mM and pH 5. As the NaTC concentration in blank FaSSIF is 3mM, NaTC-HPMC aggregation hence can occur during the dissolution of spray dried HPMC solid dispersions in blank FaSSIF. CMC* value for the same system was 15 mM in both acetate and phosphate *d*-buffers. Therefore no NaTC free micelles can form in blank FaSSIF. Instead in blank FeSSIF, due to the higher NaTC concentration (15mM), both CAC and CMC* are reached. This can lead to the formations of both NaTC-HPMC complexes and free NaTC micelles. The possible solution composition of blank FaSSIF and blank FeSSIF in the presence of HPMC are schematically illustrated in Figure 4.11.

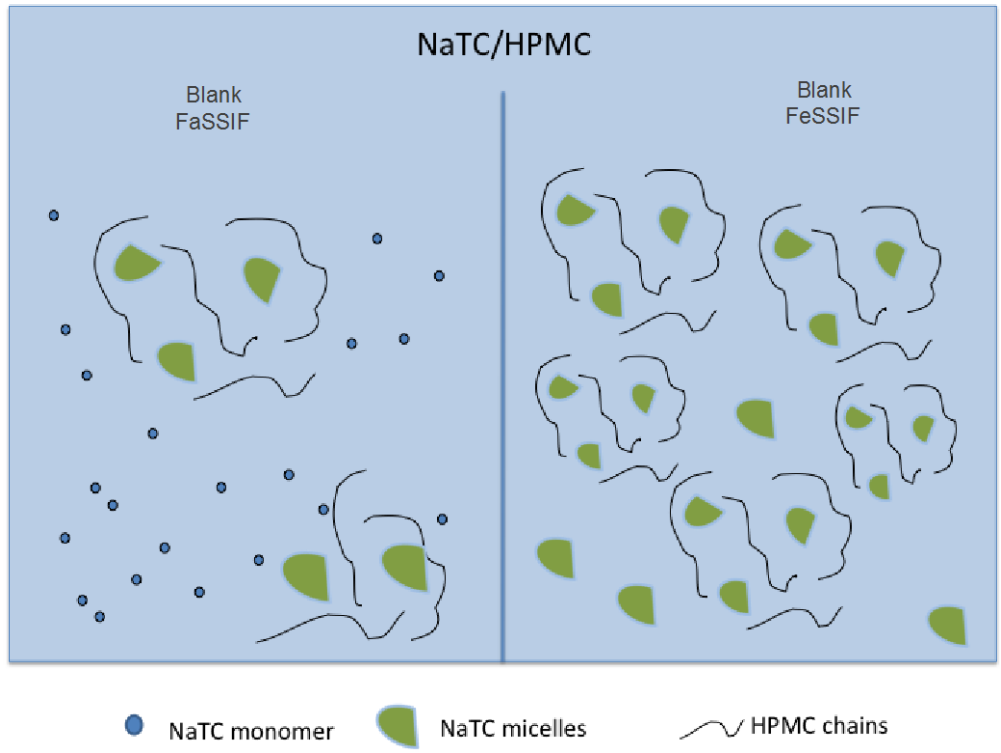

Figure 4.11: Schematic representation of HPMC/NaTC aggregation in blank FaSSIF and blank FeSSIF media.

PVP also interacts with NaTC in the blank FaSSIF medium, as NaTC concentration in blank FaSSIF medium close to the CAC value of NaTC-PVP system. However only few aggregates can be formed in solution as 3mM represents the onset point for NaTC-PVP aggregation. As for NaTC-HPMC system in blank FeSSIF, the NaTC concentration matches the CMC* value of NaTC-PVP system, which makes the saturation of PVP binding sites possible and leads to the presence of free NaTC micelles formation, as illustrated in Figure 4.12. The detailed physicochemical properties of the NaTC-HPMC and NaTC-PVP aggregates were investigated by light and neutron scattering techniques, and the obtained results are discussed in Chapter 5.

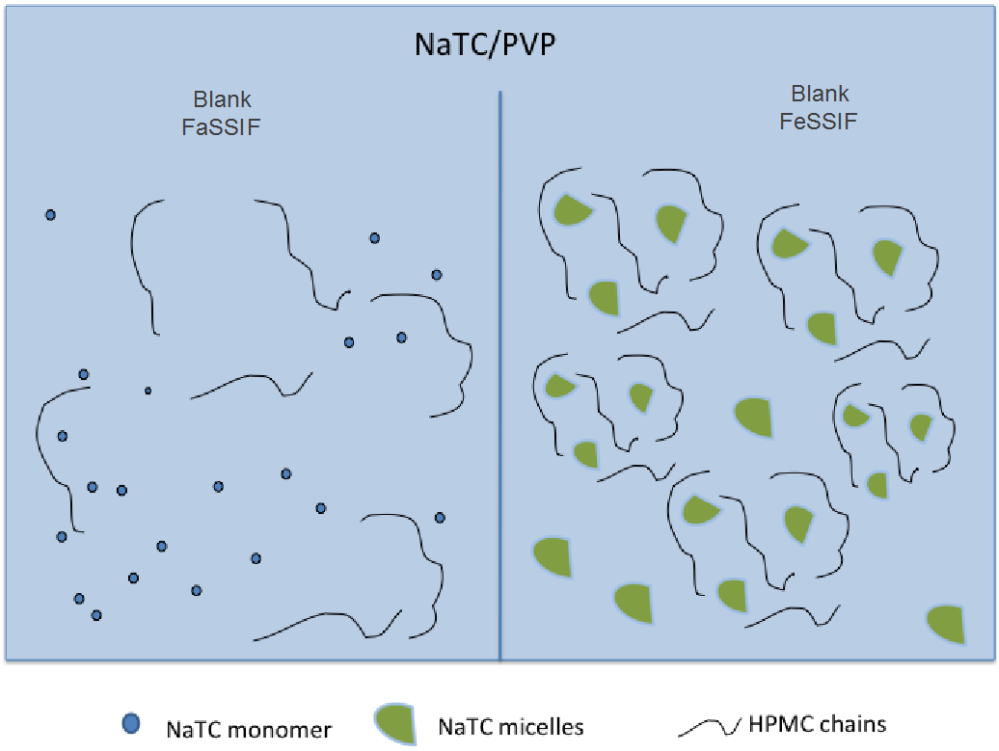

Figure 4.12: Schematic representation of NaTC/PVP aggregation in blank FaSSIF and blank FeSSIF media.

4.3.4. NMR investigation into the effect of polymer-bile salts aggregation on piroxicam solubilisation

^{1}H NMR was employed to study the possible impact of HPMC and PVP association with NaTC on piroxicam solubility in aqueous based solutions. As shown by steady state solubility studies described in Chapter 3 (Section 3.3.2), piroxicam was more soluble in FaSSIF than FeSSIF medium. The drug solubility obtained in the presence of PVP (≈0.3 mg/ml) was higher than the one obtained in the presence of HPMC (≈0.2 mg/ml). Figure 4.13 shows that piroxicam spectrum in D_2O is characterised by the presence of poorly resolved peaks and a low signal-to-noise ratio. This is a consequence of the poor water solubility of the drug, which limited piroxicam solubilisation in D_2O and consequently the NMR resonance of the sample. The signal-to-noise ratio of the piroxicam spectrum improved in blank FaSSIF, suggesting a higher solubilisation of the drug in the medium compared to D_2O. Further spectrum quality improvement was obtained in the presence of HPMC, but the most resolved spectrum was obtained in the presence of PVP. Although the ^{1}H NMR spectrum quality was still not ideal, the comparison provided clear indication of

piroxicam solubility increase in the presence of both the NaTC and polymer, which is in agreement with steady state solubility studies.

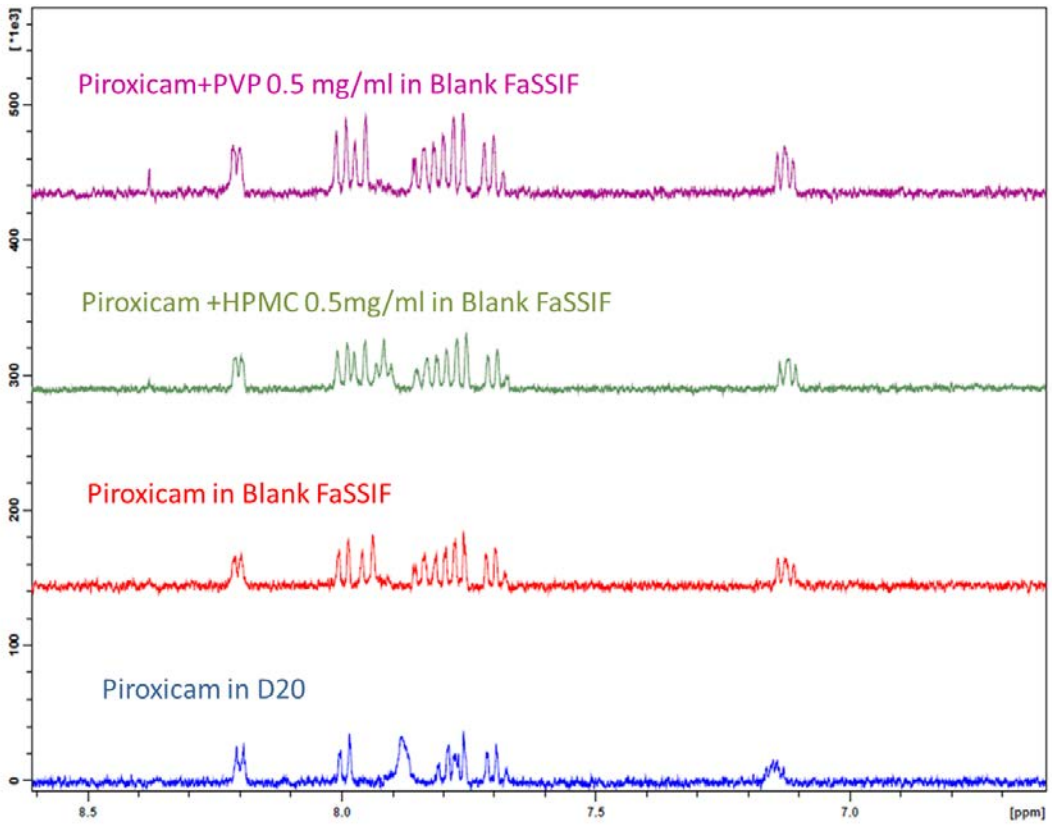

Figure 4.13: ^{1}H piroxicam NMR spectra in D_2O, blank FaSSIF, blank FaSSIF in the presence on HPMC and blank FaSSIF in the presence of HPMC.

Figure 4.14 shows piroxicam ^{1}H NMR results obtained in blank FeSSIF, with and without the presence of polymers. In this case the presence of NaTC and the polymers yielded a complete different effect on the drug spectrum. Indeed the number of peaks decreased in the presence of surfactant. Such effect is likely to be due to the drug solubilisation in NaTC micelles and/or NaTC/polymer aggregates, leading to the hindrance of the original drug peaks in the spectrum. [268]

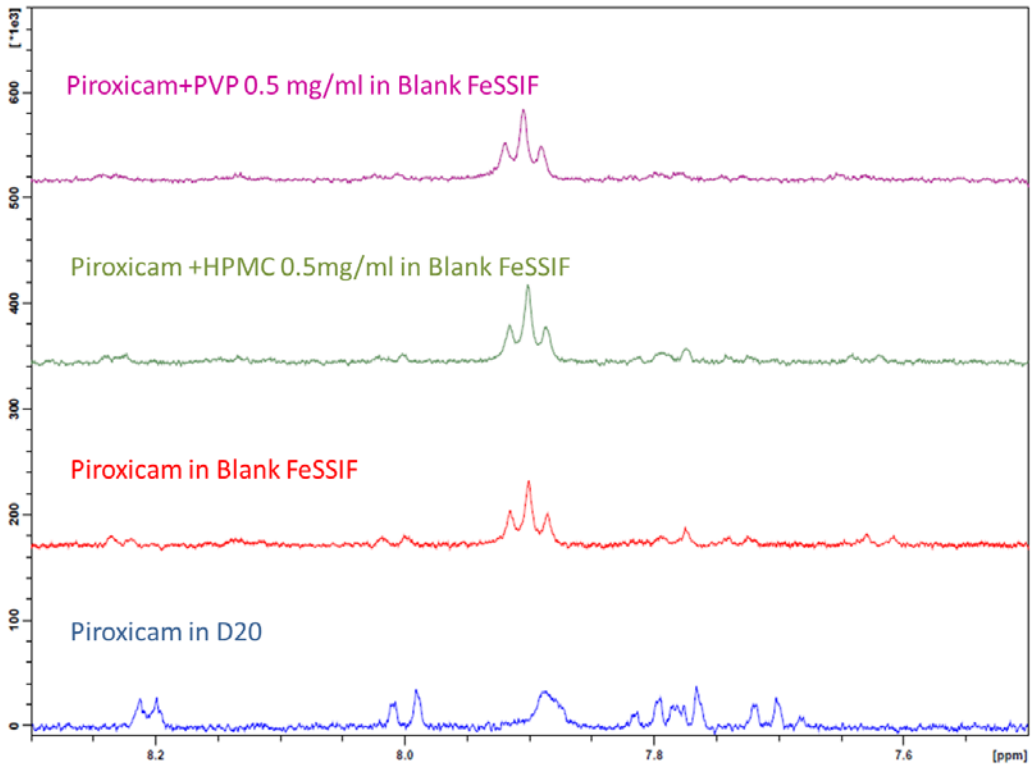

Figure 4.14: piroxicam ^{1}H NMR spectra in D_2O, blank FaSSIF, blank FaSSIF in the presence on HPMC and blank FaSSIF in the presence of HPMC.

The different effects of blank FaSSIF and blank FeSSIF on the piroxicam ^{1}H NMR spectrum suggest that drug solubilisation effect is governed by different mechanisms in the two media. In blank FaSSIF the higher solubilisation of piroxicam is mainly due to the pH of the media causing disassociation of the drug. As described in Chapter 3 piroxicam is pH sensitive and is more soluble in blank FaSSIF. Therefore the primary role in the drug NMR signal improvement might be played by the pH rather than by NaTC-polymer aggregates. Considering that NaTC concentration is slightly above the CAC values of NaTC-HPMC and NaTC/PVP systems, it is likely that only low number of aggregates present in solution. Due to the higher NaTC concentration in blank FeSSIF, many more NaTC-polymer complexes can be formed. Moreover free NaTC micelles might also be present, as NaTC concentration reaches both NaTC-HPMC and NaTC-PVP CMC* values. Therefore free NaTC micelles could potentially be involved in the drug solubilisation. It can be concluded that both blank FaSSIF and FeSSIF significantly improve the piroxicam ^{1}H NMR signal. Drug signal was further improved by the presence of PVP and HPMC, suggesting that the polymer and NaTC-polymer complexes may play an role in the drug solubilisation.

4.4 Surface tension measurements

4.4.1 Characterisation of NaTC aggregation

NaTC aggregation behaviour in water, acetate and phosphate buffers was investigated by the use of pendant drop technique. The average interfacial tension values measured continuously within 15 minutes equilibration using the pendant drop method are shown in Figure 4.15. It can be seen that the interfacial tension of NaTC in water was relatively high (45mN/m) even at the maximum surfactant concentration studied. This indicated a loose arrangement of NaTC at the air-water interface, rather than the formation of a compact layer, as described by previous work. [269] The concentration at which the interfacial tension starts to be constant corresponds to the saturation of the interface and is a good indication of CMC. This result on CMC is in good agreement with the values reported in literature. As shown by Figure 4.15 this value was about 12mM, as surface tension value did not change between 12 and 20mM, indicating the saturation of the air water interface with NaTC micelles. These interfacial tension results indicate a progressive aggregation of the surfactant, which is in agreement with data obtained by NMR experiments.

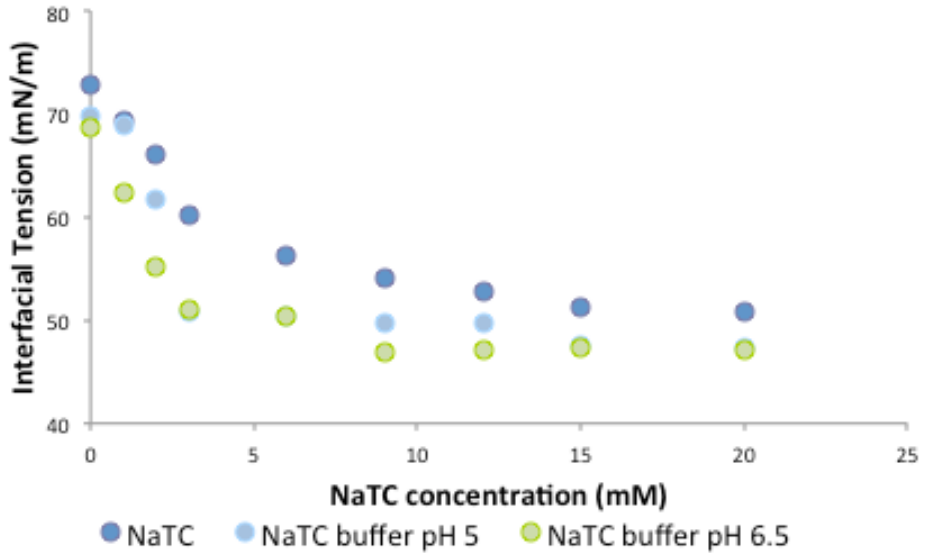

Figure 4.15:NaTC interfacial tension as a function of NaTC concentration in MilliQ water, acetate (pH 5) and phosphate buffers (pH 6.5). (n=2)

As already proved by NMR data (Section 4.3.1.3), the presence of salts can significantly impact the NaTC aggregation. CMC was lowered as a consequence of the decreased electrostatic repulsion between charged groups on the surfactant molecules, which favoured the micellisation. The presence of salts decreased NaTC interfacial tension, as seen

in Figure 4.15. In particular the saturation point was reached at NaTC concentration of 3mM in acetate buffer and at 9mM in phosphate buffer. In contrast to the NMR results, a significant difference can be seen between the two buffers. This may suggest that NaTC charges that can cause repulsion between NaTC molecules were not neutralized in phosphate buffer (270mOsmol/l), and that the higher salts concentration present in acetate buffer led to further CMC reduction.

4.4.2 Characterisation of NaTC-polymer aggregation

Pendant drop experiments were performed to investigate NaTC-polymer aggregation. Figure 4.16 shows the effects of PVP and HPMC on the surface tension of the aqueous solutions before NaTC addition. It can be seen that, as already described in literature, HPMC is surface active even in dilute regime. [270] This caused a reduction of the interfacial tension from 72.8mN/m to 63.11mN/m. In contrast to HPMC, the presence of PVP lead to much lower interfacial tension reduction, yielding a value of 68.9 mN/m and confirming the lower surface activity of PVP in dilute regime compared to HPMC. [271]

The addition of NaTC caused further surface tension reduction in both systems. In the case of NaTC-HPMC system, interfacial tension decreased to 50.78mN/m at NaTC concentration of 3mM. Further addition of NaTC did not cause further interfacial tension reduction. This suggested the possible formation of NaTC-HPMC aggregates and the saturation of the air/water interface with such aggregates. Therefore 3mM can be considered as the CAC of NaTC-HPMC solution. Interfacial tension further decreased to 47.09mN/m at NaTC concentration of 15mM, indicating the reach of CMC* and the formation of free NaTC micelles. Both CAC and CMC* value are in excellent agreement with results obtained in D_2O by NMR ^1H and DOSY measurements.

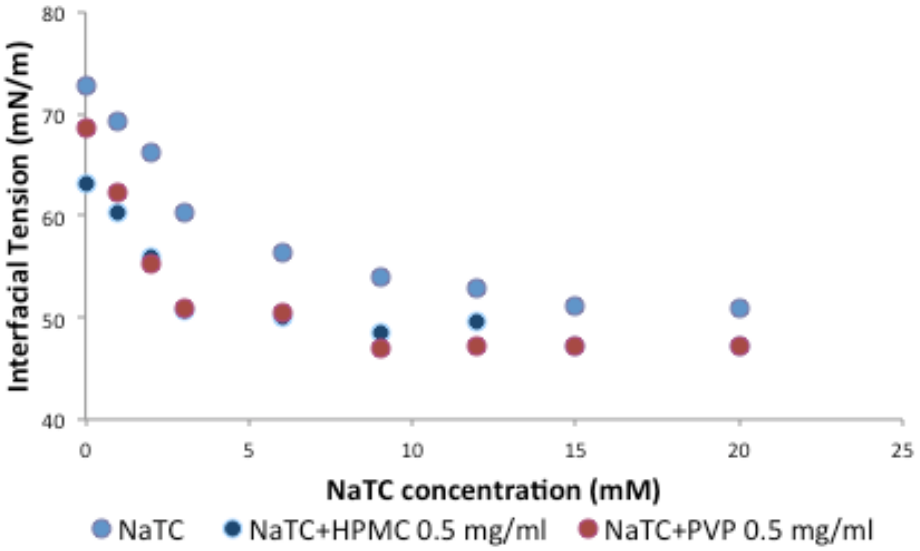

Figure 4.16:NaTC interfacial tension as a function of NaTC concentration in MilliQ water, HPMC 0.5 mg/ml and PVP 0.5 mg/ml solution (MilliQ water). (n=2)

In the case of NaTC-PVP system, two plateaux can be seen in Figure 4.16. The first one is between 3 and 6mM indicating the CAC being 3mM. The second plateau is between 9 and 20mM, suggesting the occurrence of free NaTC micelles formation. In this case NaTC aggregation started at NaTC concentration 9mM, therefore at lower concentration compared to NaTC/HPMC system. Such results suggest of HPMC binding sites are saturated at higher HPMC concentration than PVP ones, indicating higher binding of NaTC to HPMC than to PVP.

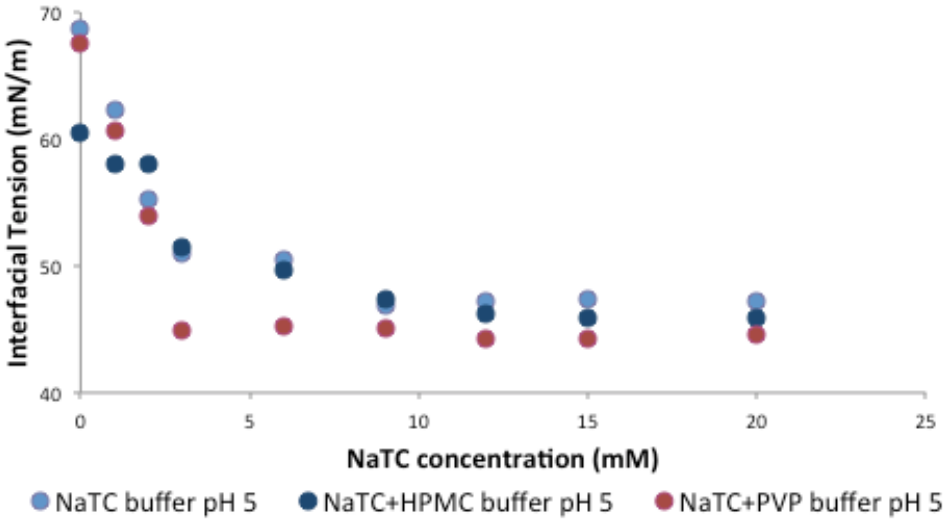

Figure 4.17:NaTC interfacial tension as a function of NaTC concentration in acetate buffer (pH 5), HPMC 0.5 mg/ml and PVP 0.5 mg/ml buffered solutions (pH 5). (n=2)

Figure 4.17 shows interfacial tension results obtained in acetate buffer with and without the presence of polymers. Results show the impact of salts on the NaTC-polymer aggregation. Indeed lower interfacial tension values were obtained in comparison to NaTC-polymer systems in water. For NaTC-HPMC systems the interfacial tension profile revealed a progressive aggregation with a small plateau between 1 and 2mM, suggesting that NaTC-HPMC aggregation occurred at the lowest NaTC aggregation (1mM). Interfacial tension value decreased in the NaTC concentration range from 3-12mM. The second plateau is between 12 and 20 mM. The start of the second plateau corresponds to NaTC CMC*. Therefore both CAC and CMC* decreased in the presence of salts in NaTC-HPMC system. In the case of NaTC-PVP systems interfacial tension progressively decreased with NaTC concentrations between 1 and 3mM, indicating 3mM as CAC. The interfacial tension reached a plateau between 3 and 20mM, thus it is not possible to establish whether free NaTC micelles were formed or not and CMC* was not assignable.

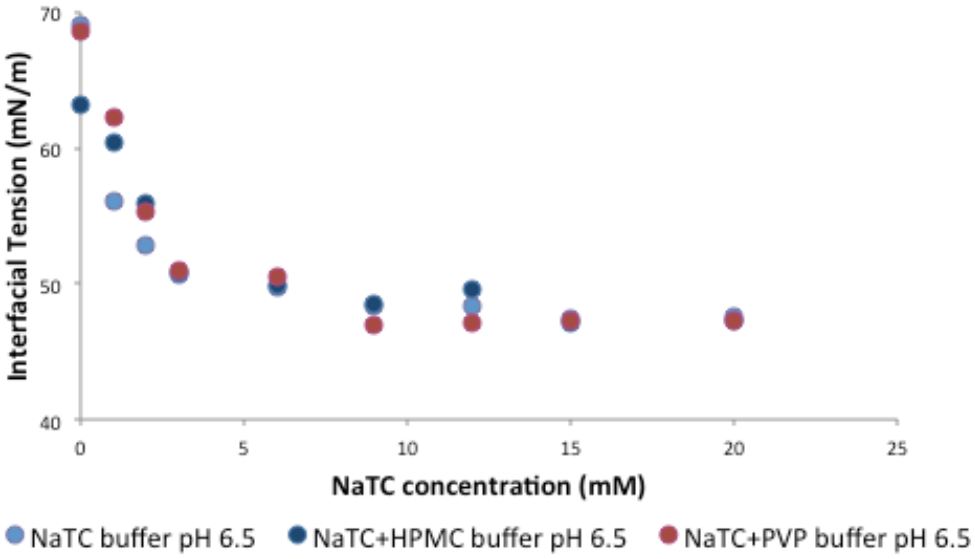

Figure 4.17:NaTC interfacial tension as a function of NaTC concentration in MilliQ water, HPMC 0.5 mg/ml and PVP 0.5 mg/ml solution (MilliQ water). (n=2)

Figure 4.17 shows the interfacial tension results obtained in phosphate buffers. It can be seen that the interfacial tension values for NaTC and NaTC-PVP and NaTC-HPMC in the phosphate buffers are very similar to the ones obtained at pH 5, confirming a similar impact of the two buffers on NaTC-polymer aggregation. For NaTC-HPMC systems, the CAC value is about 3mM as in acetate buffer and the CMC* value is 15mM. For NaTC-PVP systems, the CAC value is 3mM, confirming the result obtained at pH 5. In contrast to the results obtained in acetate buffer, a second interfacial tension decrease was observed at 9mM, indicating such value as possible CMC*. As summarised in Table 4.8, the interfacial tension

results confirmed the occurrence of NaTC-polymers aggregation, yielding CAC and CMC* values similar to the one obtained by NMR techniques.

Table 4.8: CMC, CAC and CMC* (mM) value in the different media studied obtained by interfacial tension studies

Medium	CMC	CAC	CMC*
H_20	12	-	-
Acetate buffer	3	-	-
Phosphate buffer	3	-	-
HPMC/H_20	-	3-6	15
PVP/H_20	-	3-6	15
HPMC/Acetate buffer pH5	-	2	15
HPMC/Phosphate buffer pH6.5	-	1	12
PVP/Acetate buffer pH5	-	2	Not assignable
PVP/Phosphate buffer pH6.5	-	3	15

4.5 Conclusions

In this Chapter NaTC-HPMC and NaTC-PVP aggregation was characterised by the use of NMR analysis and pendant drop technique. The occurrence of NaTC-HPMC and NaTC-PVP aggregation was indicated in aqueous medium. Both NMR and interfacial tension results confirmed the important impact of salts on the surfactant-polymer aggregation. Based on obtained results it is possible to conclude that the occurrence of NaTC-HPMC and NaTC-PVP interaction can be expected in blank FeSSIF, as for both system NaTC CAC is well below the bile salt concentration employed in blank FeSSIF. The presence of few free NaTC micelles is also possible. As CMC* is 15mM for both systems, both NaTC-polymer aggregates and NaTC micelles can be present in the blank FeSSIF media. In the case of FaSSIF only few NaTC-HPMC aggregates can be expected, as CAC value of the system corresponds to NaTC concentration in the medium (3mM). No free NaTC micelles can be expected, as NaTC concentration is well below CMC* of the system. In the case of NaTC-PVP systems, NMR and pendant drop experiments yielded different

CAC values, which are very close. Therefore the phase solution composition of NaTC-PVP system in blank FaSSIF is likely to be composed mainly by free NaTC molecules and free polymeric chains.

Size and shape of NaTC/polymer aggregates and NaTC micelles were further studied by different light and neutron scattering techniques and cryo-TEM microscopy. The possible encapsulation of the drug in the different species of aggregations was also studied and is discussed in Chapter 5.

Chapter 5. Characterisation of polymer-bile salts complexation in simulated intestinal fluids

5.1 Introduction

The dissolution mechanism of solid dispersion has widely been studied [69] and the possible factors affecting the drug release from solid dispersion formulations have been investigated and characterized. [221,272,273] Nevertheless, as discussed in previous Chapters, the possible impact of the interactions occurring between intestinal fluids components and polymeric carriers used in solid dispersions is still poorly understood and only few studies have focused on this topic. [246]

Due to the complexity of intestinal fluid composition, [18] the mechanistic study of solid dispersion dissolution in gastrointestinal condition is extremely challenging. In particular the study of the interaction between each key component of intestinal fluid and the polymeric carrier and the characterization of species yielded by such interaction are very difficult to perform. For this reason this study solely focused on the characterization of the interactions of NaTC, a model bile salt, with HPMC and PVP, two of the model polymeric carriers employed for the preparation of solid dispersions in this research project (Chapter 3).

As shown in Chapter 4 hydrophilic polymers can interact with NaTC, which is a primary component of intestinal fluids. Similar interactions have been reported in literature by studies in which other bile salts where employed. [274,275] These interactions can lead to the formation of polymer-surfactant aggregates.

The focus of this Chapter is to characterise the resulting polymer-bile salts aggregates, with particular focus on the aspects of their size, shape and ability to encapsulate drug molecules. Dynamic light and neutron scattering techniques were employed to investigate these properties of the aggregates in different simulated intestinal media, with and without the presence of drug. Cryo-TEM technique was used to image the aggregates in FaSSIF and FeSSIF media.

5.2 Experimental methods

5.2.1 Dynamic Light Scattering (DLS)

DLS experiments were performed on a Zetasizer Nano ZS, Malvern Instrument, (Malvern, Worcestershire, United Kingdom) fitted with a 633 nm red laser. Sample were prepared by dissolving accurately weighed materials in the medium and left in magnetic agitation for 1 hour at 37 °C. Samples were centrifuged at 2000g for 10 minutes, in order to remove dust particles from the scattering volume. Approximately 1 ml of sample was transferred in a disposable cuvette (pathlenght 1cm) and left to reach equilibration for 15 minutes. The autocorrelation functions were measured at a fixed angle of 173° (Back Scattering detection). Measurements were performed at 37 °C. Each measurement was composed of 5 runs of 1 minute and was repeated three times (n=3). All final hydrodynamic size distributions (intensity-weighted) of the studied aggregates were derived by fitting autocorrelation functions using the CONTIN algorithm.

5.2.2 Nanosight measurements

Nanosight experiments were carried out using a LM10 Nanosight (Nanosight Ltd-Malvern Instruments Ltd, Malvern Worcestershire, United Kingdom), fitted with a 638 nm laser. Nanosight technique was used to visualize and size polymer, bile salts and bile salts-polymer aggregates in solution. Experiments were performed at room temperature. The temperature of each run was measured and taken into consideration when the size calculation was performed by the software. Particle tracking analysis was performed using Nano-tracking Analysis (NTA) software. All samples were analysed in triplicate (n=3).

5.2.3 Neutron scattering measurements

5.2.3.1 Spin-Echo Small Angle Neutron Scattering (SESANS)

SESANS measurements were carried out using the ISIS Off-spec reflectometer (ISIS-Rutherford Appleton Facilities-Didcot, UK). Sample were prepared by dissolving accurately weighed materials in the medium and left in magnetic agitation for 1 hour at 37 °C. Tested media were prepared in D-buffer and all samples were measured using 1mm cells.

Off-spec at ISIS was one of the newest equipment installed in the ISIS which is able to study a broad range of surfaces and interfaces. This study was the first ever study performed using SESANS on such kind of sample (aqueous samples). As described in

literature the spin-echo length ζ in a SESANS experiment is described by

$$\zeta = \frac{c\lambda^2 BLcot\theta_0}{2\pi} \qquad Eq.5.4$$

where λ is the neutron wavelength, L is the length of the first precession region and B its magnetic induction, θ is the inclination angle. c is given by

$$c = \frac{\gamma m}{h}$$

with γ the gyromagnetic ratio and m the mass of neutrons respectively and h the Plank's constant.

5.2.3.2 Small Angle Neutron Scattering (SANS)

SANS measurements were carried out at the ISIS SANS2-D spectrometer (ISIS-Rutherford Appleton Facilities-Didcot, UK). Sample were prepared by dissolving accurately weighed materials in the medium and left in magnetic agitation for 1 hour at 37 °C. Sample were centrifuged at 2000g for ten minutes to remove dust particles and un-dissolved drug molecules from the samples. Tested media were prepared in D-buffer and all samples were measured using 2mm cells. The Q-range covered in these experiment was 0.005-0.5 A^{-1}. Experiments were performed at 37 °C. Each measurement was performed in duplicate (n=2).

Collected data were analysed using SansView software. The data were fitted using the Cylinder Elliptical Model, which gave the best fit to the experimental data. The 2-D scattering intensity for elliptical cylinders is given by

$$I(q) = \frac{Scale}{Vcyl} \int d\psi \int d\phi \int p(\theta,\phi,\psi) F^2(q,a,\psi) \sin\theta d\theta + bkg \qquad Eq.\ 5.1$$

where the angles θ and ϕ define the cylinder orientation, while ψ defines the orientation of the major axis of the ellipse with respect to the vector *Q*. *bkg* is the background, V_{Cyl} is the cylinder volume, and functions are given by

$$F(q,\alpha,\psi) = 2\frac{J_1(a)}{a} * \frac{\sin(b)}{b} \qquad Eq.5.2$$

$$a = q * \sin(\alpha)[r_{major}^2 sin^2(\psi) + r_{minor}^2 \cos(\psi)]^{1/2} \qquad Eq.5.3$$

$$b = q\frac{L}{2}\cos(\alpha) \qquad Eq.5.3$$

where *L* is the cylinder length.

5.2.4 Cryogenic-Transmission Electron Microscopy (Cryo-TEM)

Cryo-TEM measurements were performed to visualize NaTC/HPMC aggregates in blank FeSSIF and blank FeSSIF media. Samples were prepared by dissolving appropriately weighed solid dispersion in the studied medium and left in magnetic agitation for 1 hour at 37 °C. Samples were centrifuged at 2000g for 10 minutes and the supernatant solutions were analysed after 24 hours.

All cryo-TEM analysis was performed via a characterisation service provided by the Department of Physical Chemistry, Uppsala University, Sweden. Samples were prepared according to the reported routine procedure described briefly as follow.[203] A small droplet of the sample solution was placed under controlled conditions on a pre-treated Cu grid of about 20 μm thickness, which was covered by a perforated cellulose acetate butyrate film. Excess material was removed by a gentle wiping off with a filter paper. The specimen was vitrified by being rapidly transferred into liquid ethane. The sample examination was performed with a Zeiss 902 A electron microscope operating at 80 kV at 100K.

5.3 Results and discussion

5.3.1 Light scattering characterisation of simulated intestinal fluids

In order to investigate the aggregation behaviour of NaTC, DLS analysis was performed on blank FaSSIF and FeSSIF media. As reported in Chapter 4, the NaTC concentration in blank FaSSIF (3mM) is close to the CMC value of NaTC in phosphate buffer. Therefore only few micelles could be present in solution. Scattering intensity of the DLS result was too weak (data not shown) for blank FaSSIF, confirming the absence of micelles or the presence of a limited number of them. DLS analysis was also performed for blank FeSSIF. Similar to the results obtained for blank FaSSIF, autocorrelation function was not reproducible and reliable (data not shown). For this reason, a different type of light scattering technique, Nanosight, with more direct visualisation capability, was used instead of DLS. The advantage of Nanosight technique is being suitable for both monodispersed and polydispersed samples and can be used for more dilute samples characterisation compared to DLS. [276] Nanosight technique was employed to characterize these two samples.

Nanosight analysis showed the presence of only few aggregates in solution for blank FaSSIF and, consequently, accurate statistic of particle size could not be performed (data not shown). This result was in agreement with DLS data that showed an extremely weak scattering, suggesting the presence of very low number of micelles in solution.

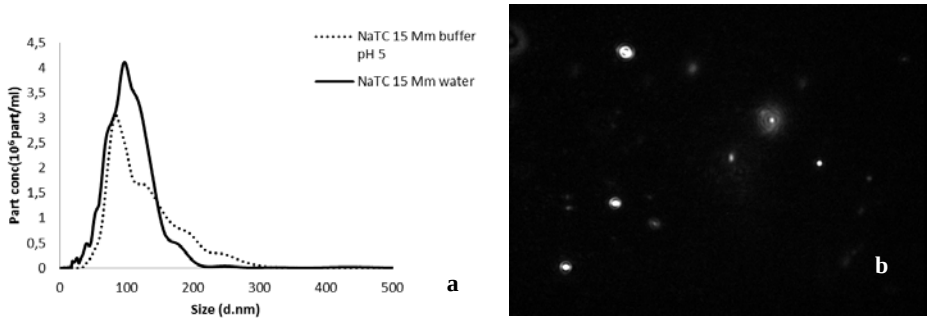

Figure 5.1: Nanosight size distribution of NaTC (15mM) micelles in MilliQ water and blank FeSSIF (a), and Nanosight NaTC micelles in blank FeSSIF image (b). (n=3)

Nanosight analysis was performed on blank FeSSIF and, in order to investigate the effect on salts on the NaTC aggregates features, a NaTC 15 mM in milliQ water was also analysed (Figure 5.1). It can be seen that large populations of micelles with mean diameters of 100 nm are present in both samples. The presence of salts shows an impact on NaTC aggregation, as it led to the formation of more polydispersed micelles. As already discussed in Chapter 4 an increase of the ionic strength can favour NaTC aggregation by decreasing the CMC of the surfactant. [85] Furthermore as described in the Chapter 1, bile salts can form secondary micelles via the hydroxyl groups hydrogen bonding interaction. Therefore the large size obtained for NaTC micelles is likely to be at least partially due to the occurrence of secondary micelles formation.

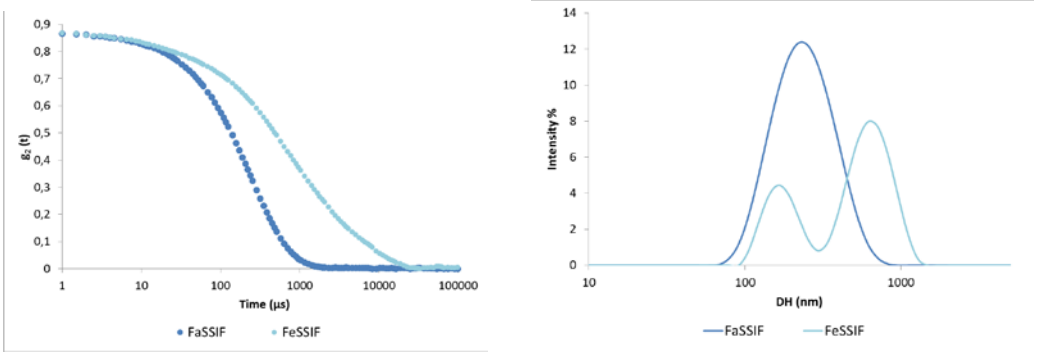

Figure 5.2: DLS intensity autocorrelation function and size distribution by intensity of FaSSIF and FeSSIF media (n=3).

DLS analysis was performed also on FaSSIF and FeSSIF (with lecithin), in order to investigate the impact of lecithin on the aggregation behaviour of the bile salts. Obtained results are shown in Figure 5.2. As shown by Figure 5.2 the two media have different autocorrelation functions, indicating the presence of different aggregates in the two samples solutions. FaSSIF yielded a mono-modal autocorrelation function, suggesting the presence of one population of aggregates with size of 258±13 d.nm. For FeSSIF a bimodal decay can be seen in Figure 5.2, indicating the presence of two populations of aggregates, labelled as fast (smaller) and slow (bigger) modes, having sizes of 133±14 and 552±39 d.nm respectively. The formation of two populations of aggregates may be attributed to the higher NaTC concentration in FeSSIF than FaSSIF medium, which might lead to the formation of mixed lecithin-NaTC aggregates having different sizes. As described in literature, bile salts-lecithin solution composition and aggregates features are strictly dependent on the lecithin-bile salts ratios. [277] The phase diagram of phospholipid-surfactant-water mixtures was reported by Andrieux et al., as shown in Figure 5.3. [278] At low surfactant concentration mainly lecithin vesicles are present in solution, while the increase of surfactant concentration leads to the formation of mixed micelles with smaller sizes.

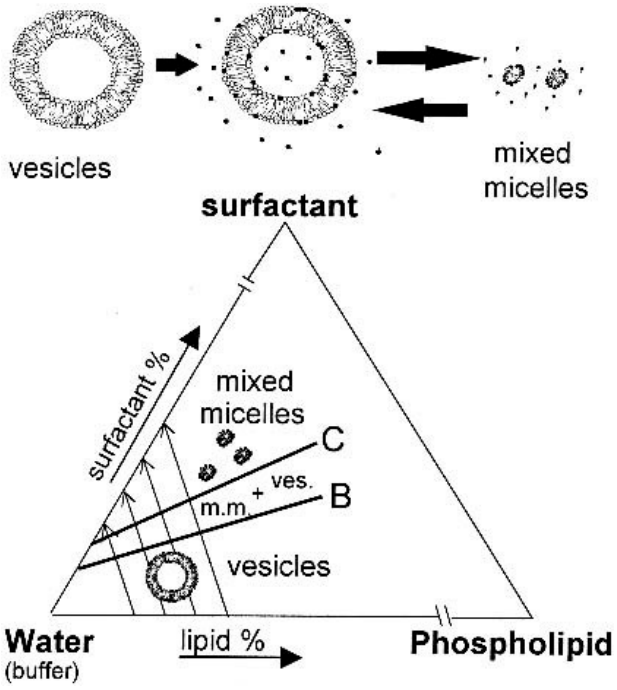

Figure 5.3: Ternary phase diagram of phospholipid/surfactant/water mixture and vesicle to micelles transition. [278]

Boni et al described FaSSIF and FeSSIF phase composition. [279] Reported data showed the presence of a mono-modal distribution of aggregates in FaSSIF and a bimodal distribution in FeSSIF. This is in good agreement with data obtained in this study. However, the sizes of the aggregates reported in literature are significantly smaller than the ones obtained in this study. Such difference might be related to different raw materials used and/or equipment employed for the media preparation.

5.3.2 Light scattering characterisation of HPMC-NaTC complexes

DLS was also employed to study the aggregation between HPMC and NaTC. As already mentioned in Chapter 4, HPMC is a surface-active polymer, therefore, in order to investigate the polymer aggregation on its own, spray dried HPMC dissolved in the buffers was firstly analysed. As shown by Figure 5.4, DLS results of spray dried HPMC in pH 6.5 phosphate buffer show the presence of two populations of polymeric aggregates. The bimodal distribution is in good agreement with literature data, which reported the formation of two populations of HPMC aggregates even in highly diluted regimes. [150]

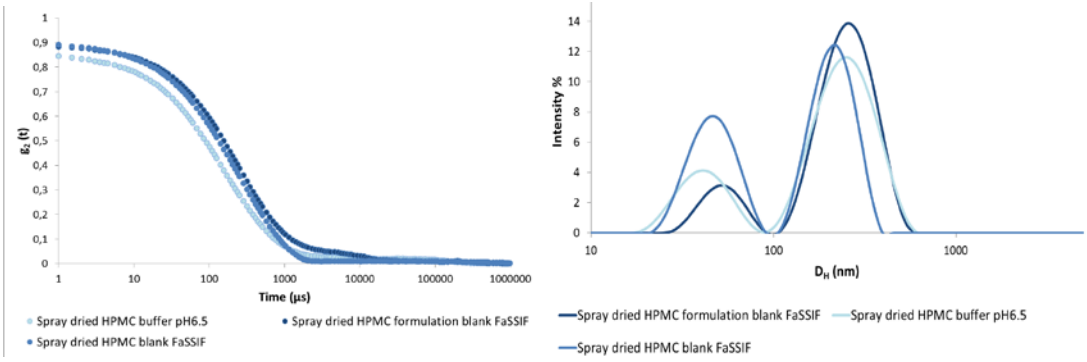

Figure 5.4: DLS intensity autocorrelation functions and size distribution by intensity of spray dried HPMC in buffer pH 6.5, spray dried HPMC in blank FaSSIF and spray dried HPMC:piroxicam 2:1 solid dispersion in blank FaSSIF (n=3).

The smaller population of HPMC aggregates is characterized by a size of 40±9 d.nm, while the bigger population is 231±45 in size. As shown by sizes distribution graph in Figure 5.4, DLS measurements performed in blank FaSSIF yielded the aggregates sizes very close to the ones obtained for HPMC in buffer. Two populations of aggregates with sizes of 48±5 and 238±20 d.nm were obtained for HPMC in blank FaSSIF sample (as summarised in Table 5.1). This data indicates that the presence of NaTC did not impact significantly on the

aggregation behaviour of HPMC. As reported in Chapter 4 NaTC concentration (3mM) of blank FaSSIF close to the CAC value of the system, which according to NMR and surface tension results was in the range of 3-6 mM. Therefore HPMC/NaTC aggregation is expected to be limited in blank FaSSIF media. The similar sizes obtained from the samples of HPMC in buffer pH 6.5 and in blank FaSSIF suggest that the low NaTC concentration may be the cause of the limited aggregation between HPMC and NaTC in blank FaSSIF.

As shown in Figure 5.4 the presence of piroxicam slightly changed the autocorrelation function of the DLS results. For the spray dried formulation dissolved in blank FaSSIF an increase in aggregate size was obtained in the bigger population of aggregates (333±59 d.nm), suggesting a possible role of the polymer aggregates in the drug solubilisation via drug encapsulation. The smaller population yielded a size of 44±5 d.nm.

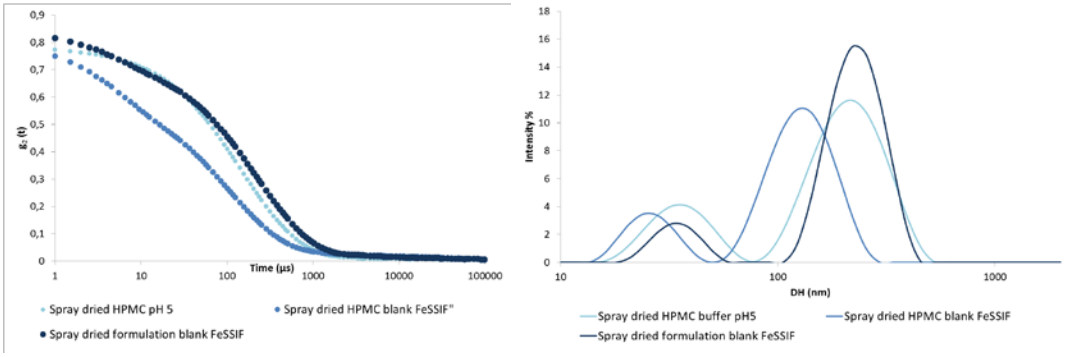

Figure 5.5: DLS normalised autocorrelation function and size distribution by intensity of spray dried HPMC in buffer, spray dried HPMC in blank FeSSIF and spray dried HPMC:piroxicam 2:1 solid dispersion in blank FeSSIF (n=3).

As seen in Figure 5.5, DLS results obtained for spray dried HPMC at pH 5 were similar to the one obtained at pH 6.5, indicating a bimodal distribution of aggregates. Nevertheless, the size of the slower (and therefore bigger in size) population is bigger in the media with pH 5 than in the media with pH 6.5. The sizes of the aggregate populations obtained for HPMC at pH 5 are 42±8 and 341±39 d.nm. The two buffers have different osmolarity (buffer pH 5 270 mOsmol/Kg, buffer pH 5 670 mOsmol/Kg) and, as mentioned in Chapter 4 (Section 4.3.1.3), salts can influence polymer aggregation via salting-in and salting-out effect. [267] Therefore the different size obtained for the bigger population of aggregates might be due to the different osmolarity of the phosphate and acetate buffer employed which can influence the hydration of the polymeric chains and the hydration sphere of polymeric aggregates.

In Blank FeSSIF the scattering curve of HPMC/blank FeSSIF sample shows different relaxation times compared to HPMC in buffer pH 5. In particular the second population of aggregates decreased in size to 221±26 d.nm, while the smaller population was constant in size yielding a diameter of 40.9±10 nm. As shown in Figure 5.5 in the presence of drug the smaller population of polymer aggregates did not change in size, while the bigger one increased in size to 423±70 d.nm. Both NMR and surface tension experiments (Chapter 4) indicated the occurrence of HPMC/NaTC aggregation in blank FeSSIF. DLS data showed the presence of a population of particles with consistently smaller size. This population is likely to be mainly composed of dissolved polymers and/or polymeric aggregates. The bigger population size change in the presence of NaTC, suggested the possible formation of NaTC/HPMC aggregates, which are likely to be structurally more retained and therefore smaller than the polymeric ones. The size increase of the HPMC/NaTC aggregates for the spray dried formulation sample is likely to be due to the drug encapsulation in the aggregates. This is in agreement with what shown by NMR spectrum of spray dried formulation sample (refer to Chapter 4, Section 4.3.4) that suggested a possible drug solubilisation via NaTC and/or NaTC/HPMC aggregates.

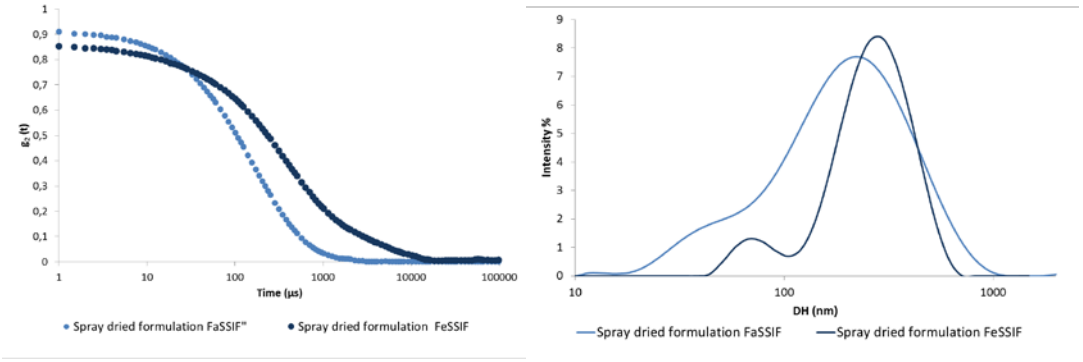

Figure 5.6: DLS normalised autocorrelation functions and size distributions by intensity of spray dried HPMC:piroxicam 2:1 solid dispersion in FaSSIF and FeSSIF (n=3).

In order to evaluate the impact of lecithin on HPMC-NaTC aggregation, DLS analysis was performed also on spray dried samples dissolved in FaSSIF and FeSSIF. Figure 5.6 shows DLS results obtained for the two samples. It can be seen that the size distributions changed completely for both samples compared to the ones obtained in blank FaSSIF and blank FeSSIF, indicating a significant influence of lecithin on the aggregation. A very broad peak was obtained for spray dried formulation in FaSSIF containing lecithin. As reported in Section 5.3.1 FaSSIF itself yielded a population of aggregates having a diameter of 258±13 d.nm. In the presence of the spray dried formulation much broader peak was obtained, with

an average size of 330±73 d.nm, suggesting the formation of possible new species in solution that lead to a much more polydisperse size distribution. This resulting solution possibly contained different populations of aggregates that could not be distinguished in the scattering pattern (due to possible overlaying). For spray dried HPMC:piroxicam formulation dissolved in FeSSIF two populations of aggregates were present, as shown by Figure 5.6. This is in agreement with the bimodality of FeSSIF medium aggregates distribution, but a significant increase in size was observed for both populations of the aggregates. The increase in size of aggregates in HPMC:piroxicam 2:1 in FeSSIF and FaSSIF compared to media without lecithin, suggests the possible formation of new species in solution. The size increase may also indicate the possible drug molecules encapsulation in the aggregates, which might cause their swelling and subsequently increase in size.

Literature data previously reported HPMC ability to associate with anionic surfactant. [280] Furthermore NMR and interfacial tension data provided consistent indications of formation of HPMC/NaTC aggregation (refer to Chapter 4). Therefore obtained DLS data suggest that HPMC and NaTC are likely to interact in the simulated intestinal fluids employed in this study, in particular in blank FeSSIF due to the higher NaTC concentration. Nevertheless, due to the complexity of the systems analysed and the possible presence of different species in solution, a detailed description of the scattering aggregates composition could not be accurately obtained by only relying on DLS data. Therefore further studies, described in the next part of this Chapter, were performed in order to better clarify the solution phase composition of the different samples and the aggregates features. The particle sizes of different HPMC samples measured by DLS are summarised in Table 5.1.

Table 5.1: Summary of PVP and PVP/NaTC aggregates in different dissolution media

Sample	SIZE (d.mn) population 1	SIZE (d.mn) population 2
Spray dried HPMC buffer pH 6.5	40±9	231±45
Spray dried HPMC blank FaSSIF	48±5	238±20
Spray dried formulation HPMC:Pir 2:1 blank FaSSIF	44±5	333±59
Spray dried formulation HPMC:Pir 2:1 FaSSIF	330±73	-
Spray dried HPMC buffer pH 5	42±8	341±39
Spray dried HPMC blank FeSSIF	40±9	221±26
Spray dried formulation HPMC:Pir 2:1 blank FeSSIF	52±10	423±70
Spray dried formulation HPMC:Pir 2:1 FeSSIF	58±9	448±30

5.3.3. DLS characterisation of PVP-NaTC complexes

As for HPMC based spray dried formulations, DLS was used to study the interaction between PVP and NaTC in the different dissolution media employed in this study. PVP on its own was firstly analysed in buffer, without the presence of NaTC, in order to investigate the possible aggregation behaviour of PVP alone.

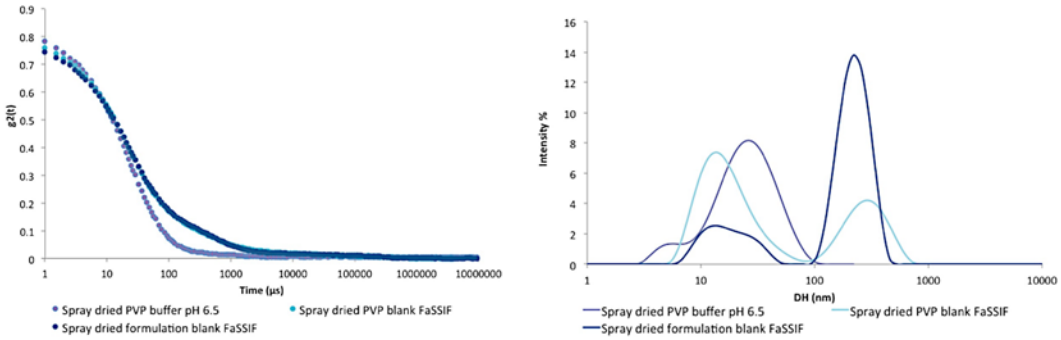

Figure 5.7: DLS normalised autocorrelation function and size distribution by intensity of spray dried PVP in buffer, spray dried PVP in blank FeSSIF and spray dried PVP:piroxicam 2:1 solid dispersion in blank FeSSIF (n=3).

As shown in Figure 5.7 PVP on its own (concentration 0.27 mg/ml) yielded an averaged size (intensity weighed) of 25±4 d.nm. The size distribution plot also shows the presence of a not well-defined small peak that indicates the presence of aggregates with smaller size. However since the peak is not defined, only one size was obtained by CONTIN analysis. In the presence of NaTC two populations of aggregates were indicated by DLS results. Two relaxation times can be clearly seen in the scattering curve (light blue curve shown in the scattering graph in Figure 5.7), corresponding to two populations having a diameter of 18±0.4 nm and 323± 41 nm, respectively. Therefore this indicates that the presence of NaTC has an impact on the PVP association, leading to the formation of a second population of aggregates, which, considering the low NaTC concentration is likely to be composed by a low number of PVP/NaTC aggregates. The CAC value of PVP/NaTC system in buffer pH 6.5 was measured to be approximately 3 mM (refer to Sections 4.3.1.3 and 4.4.2 of Chapter 4). Therefore in blank FaSSIF, NaTC concentration corresponds to the onset of the polymer and surfactant aggregation and only a small number of PVP/NaTC complexes can be present in solution. In the presence of piroxicam no size change was observed for the smaller population, which kept constant in size as 18±2 d.nm. The population of aggregates with bigger size slightly decreased in size in the presence of drug, as shown by size distribution of the spray dried PVP:piroxicam formulation in blank FaSSIF in Figure 5.7. As for HPMC:piroxicam spray dried formulation in blank FaSSIF, no indication of drug encapsulation in the aggregates was obtained. This suggests that piroxicam significant increase in solubility shown by steady state solubility studies (Section 3.3.2, Chapter 3) in blank FaSSIF, is likely to be due mainly to the solution pH, which favours piroxicam solubilisation. Piroxicam solubilisation might also be favoured by the surface tension reduction which eases the wetting of the drug particle surface and subsequently dissolution caused by the presence of polymer and surfactant, rather than to the

drug encapsulation in NaTC micelles and/or NaTC/polymer aggregates, which are likely to be present in a very low number.

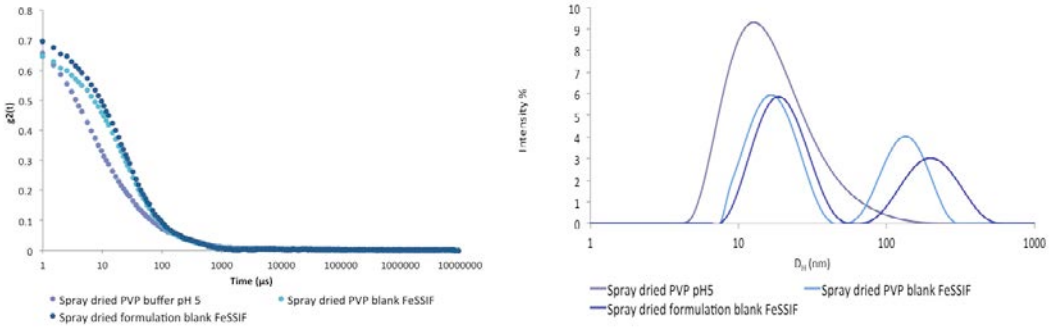

Figure 5.8: DLS normalised autocorrelation function and size distribution by intensity of spray dried PVP in buffer, spray dried PVP in blank FeSSIF and spray dried PVP:piroxicam 2:1 solid dispersion in blank FeSSIF (n=3).

DLS data for PVP in buffer pH 5 are very similar to the ones obtained for the polymer in buffer pH 6.5. The scattering curve in Figure 5.8 indicates the presence of only one relaxation time, related to aggregates having a size of 19±3 d.nm. In blank FeSSIF bimodal distribution was obtained. The smaller population was characterized by a size of 19±0.8 d.nm, which corresponds to the PVP aggregates in buffer pH 5. This result suggests that such population in blank FeSSIF is likely to be composed only of the PVP aggregates. The bigger population has a size of 188±34 d.nm, and may possibly be composed of PVP/NaTC aggregates, as PVP/NaTC aggregation was shown to occur in blank FeSSIF by both NMR and interfacial tension data (Sections 4.3.1.3 and 4.4.2, Chapter 4).

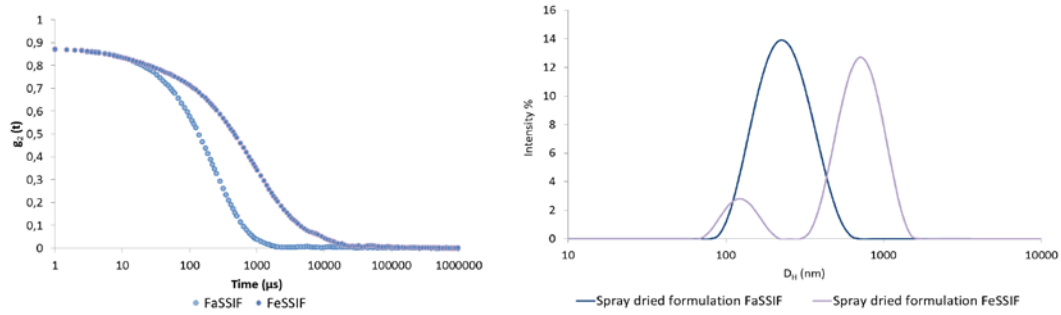

Figure 5.9: DLS normalised autocorrelation functions and size distributions by intensity of spray dried PVP:piroxicam 2:1 solid dispersion in FaSSIF and FeSSIF (n=3).

As for HPMC based solid dispersions, the impact of lecithin on PVP/NaTC association was also investigated. The results shown in Figure 5.9 confirmed the formation of a monodispersed population of aggregates having a size of 273±9 d.nm in FaSSIF. This size is close to the size obtained for FaSSIF medium (258 ±13 d.nm), indicating that no significant change in the solution phase composition occurred. Therefore, the solution is likely to be mainly composed of lecithin vesicles, and no aggregation with PVP took place. The slight increase in size might be an indication of piroxicam encapsulation by lecithin vesicles, which have already be shown to play a role in poorly water-soluble drugs solubilisation. [281] For PVP:piroxicam spray dried formulation dissolved in FeSSIF, a bimodal distribution was obtained, yielding aggregates of 177±15 and 656±48 d.nm in size (as summarised in Table 5.2), respectively. Obtained size for spray dried PVP:piroxicam in FeSSIF are bigger for both populations compared to the sizes obtained FeSSIF medium itself (133±14 and 552±39 d.nm). The swelling of the aggregates can possibly be attributed to both associations with PVP and drug encapsulation. Considering the complexity of the sample, from DLS data it is not possible to further clarify the solution composition. However the occurrence of aggregation indicated by NMR and interfacial tension data (Sections 4.3.1.3 and 4.4.2, Chapter 4) and the increased piroxicam solubility in blank FeSSIF in the presence of PVP suggest the possible formation of new species in solution and their possible involvement in the drug solubilisation. The particle size PVP and PVP/NaTC aggregates in the different dissolution media measured by DLS are summarized in Table 5.2.

Table 5.2: Summary of PVP and PVP/NaTC aggregates in different dissolution media

Sample	SIZE (d.mn) population 1	SIZE (d.mn) population 2
Spray dried PVP buffer pH 6.5	25±4	-
Spray dried PVP blank FaSSIF	18±0.4	323±41
Spray dried formulation PVP:Pir 2:1 blank FaSSIF	18±2	333±59
Spray dried formulation PVP:Pir 2:1 FaSSIF	-	273±9
Spray dried PVP buffer pH 5	19±3	-
Spray dried PVP blank FeSSIF	19±0.8	188±34
Spray dried formulation PVP:Pir 2:1 blank FeSSIF	20±6	216±18
Spray dried formulation PVP:Pir 2:1 FeSSIF	177±15	656±48

5.3.3. Impact of polymer weight ratio on polymer-bile salts aggregation

One of the factor that can possible impact polymer/surfactant aggregation is the polymer:surfactant ratio. In order to investigate the impact of polymer weight ratio in solution on the HPMC/NaTC complexation in blank FaSSIF and FeSSIF, DLS analysis was performed on HPMC:piroxicam spray dried solid dispersions having polymer:weight ratios of 4:1 and 9:1. The obtained results in blank FaSSIF are shown in Figure 5.10.

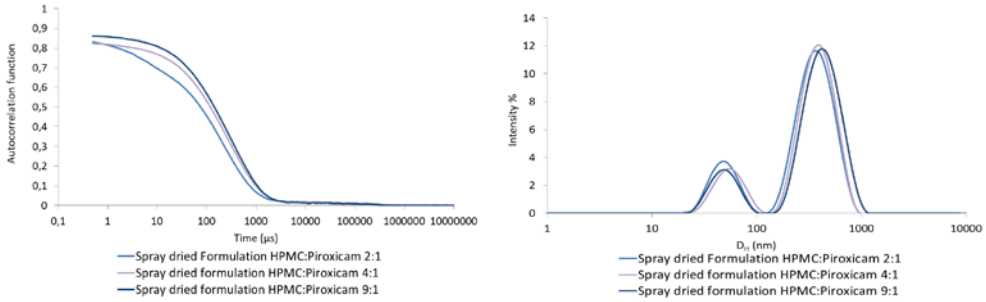

Figure 5.10: DLS normalised autocorrelation functions and size distributions by intensity of spray dried HPMC:piroxicam solid dispersion with different HPMC:piroxicam ratios in blank FaSSIF (n=3).

It can be seen that the presence of higher HPMC concentration led to the formation of slightly bigger aggregates, for both populations present in solution, but did not impact significantly on the scattering curves and sizes distributions of the aggregates. This result indicates that higher concentration of polymer did not lead to a significant change of the solution composition, but only caused an increase in size of the aggregates.

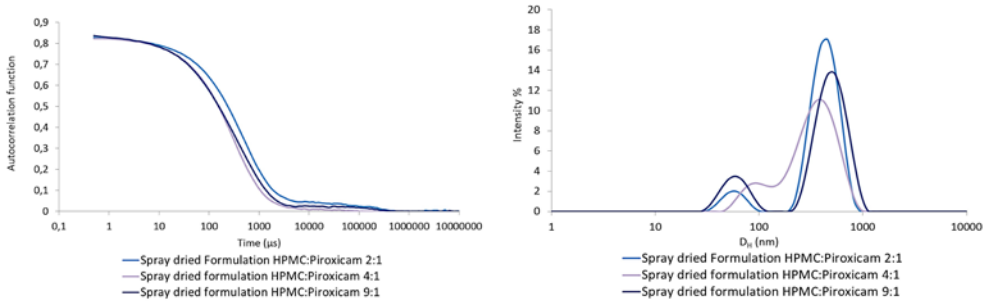

Figure 5.11: DLS normalised autocorrelation functions and size distributions by intensity of spray dried HPMC:piroxicam solid dispersion with different HPMC:piroxicam ratios in blank FeSSIF (n=3).

Figure 5.11 shows the comparison between DLS data obtained from spray dried HPMC:piroxicam solid dispersion 2:1, 4:1, and 9:1 in blank FeSSIF. Results clearly show a change in the size distribution from polymer:drug ratio 2:1 to 4:1. For the HPMC:piroxicam 4:1 sample, the two populations are closer in size as shown by the size distribution in Figure 5.11. Nevertheless the distribution of aggregates is still bimodal and the obtained sizes, 90±10 and 377±14 d.nm are close to the ones obtained for the sample with HPMC:piroxicam ratio of 2:1. Similarly to results obtained in blank FaSSIF, these data indicate minor influence of polymer weight ratio on HPMC and or HPMC/NaTC aggregates features.

The role of polymer weight ratio in solid dispersions has widely been studied and different studies reported that the presence of higher polymer weight ratios normally facilitates drug solubilisation. This study proved that the use of different polymer weight ratios might also influence the formation of colloidal species, such as polymer and/or polymer/surfactant aggregates in the intestinal fluids, which may play a role in poorly water-soluble drugs dissolution and solubilisation.

Table 5.3: Summary of HPMC/NaTC aggregates from HPMC:piroxicam spray dried formulations 2:1, 4:1 and 9:1 in blank FaSSIF and blank FeSSIF

Sample	SIZE (d.mn) population 1	SIZE (d.mn) population 2
Spray dried formulation HPMC:Pir 2:1 FaSSIF	44±5	333±59
Spray dried formulation HPMC:Pir 4:1 FaSSIF	46±9	333±59
Spray dried formulation HPMC:Pir 9:1 FaSSIF	53±3	414±58
Spray dried formulation HPMC:Pir 2:1 FeSSIF	58±9	448±30
Spray dried formulation HPMC:Pir 4:1 FeSSIF	90±10	377±14
Spray dried formulation HPMC:Pir 9:1 FeSSIF	60±0.6	503±21

5.3.4 Nanosight characterisation of polymer-NaTC complexes

To further characterize HPMC and PVP aggregation behaviour with NaTC in simulated intestinal fluids, Nanosight analysis was also performed. The rational of using Nanosight as an additional complimentary characterisation technique is due to the advantages of this techquie being able to direct visualise and study both mono-dispersed and poly-dispersed colloidal systems. Figure 5.12 a, b and c show the Nanosight images of spray HPMC in buffer 6.5, spray dried HPMC in blank FaSSIF and spray dried HPMC:piroxicam 2:1formulation .

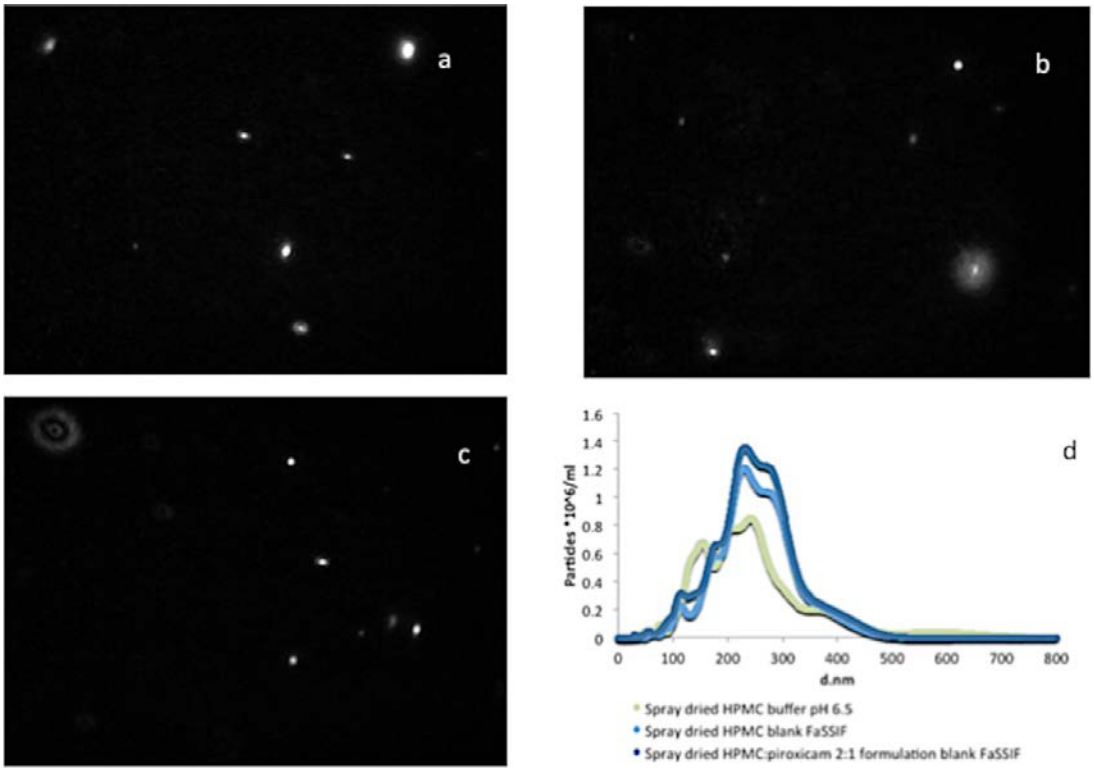

Figure 5.12: Nanosight images of spray dried HPMC in buffer pH 6.5 (a), spray dried HPMC in blank FaSSIF (b) and spray dried HPMC:piroxicam 2:1 in blank FaSSIF (c); Nanosight sizes distribution of samples a,b and c (d).

It can be seen that a limited number of aggregates was imaged for all the samples. This result is in agreement with DLS data that showed a weak scattering of HPMC samples in blank FaSSIF, which indicated the presence of a low number of aggregates. Spray dried HPMC in buffer pH 6.5 yielded a broad peak including sizes between 100 and 300 d.nm. Therefore Nanosight results confirmed the possible bimodal distribution for HPMC aggregates, as already shown by DLS analysis and as reported in literature. [150]Considering the broadness of the peak, the obtained average size by the Nanosight software analysis is not expected to be reliable, but serves as an indicative estimation of the samples aggregates sizes.

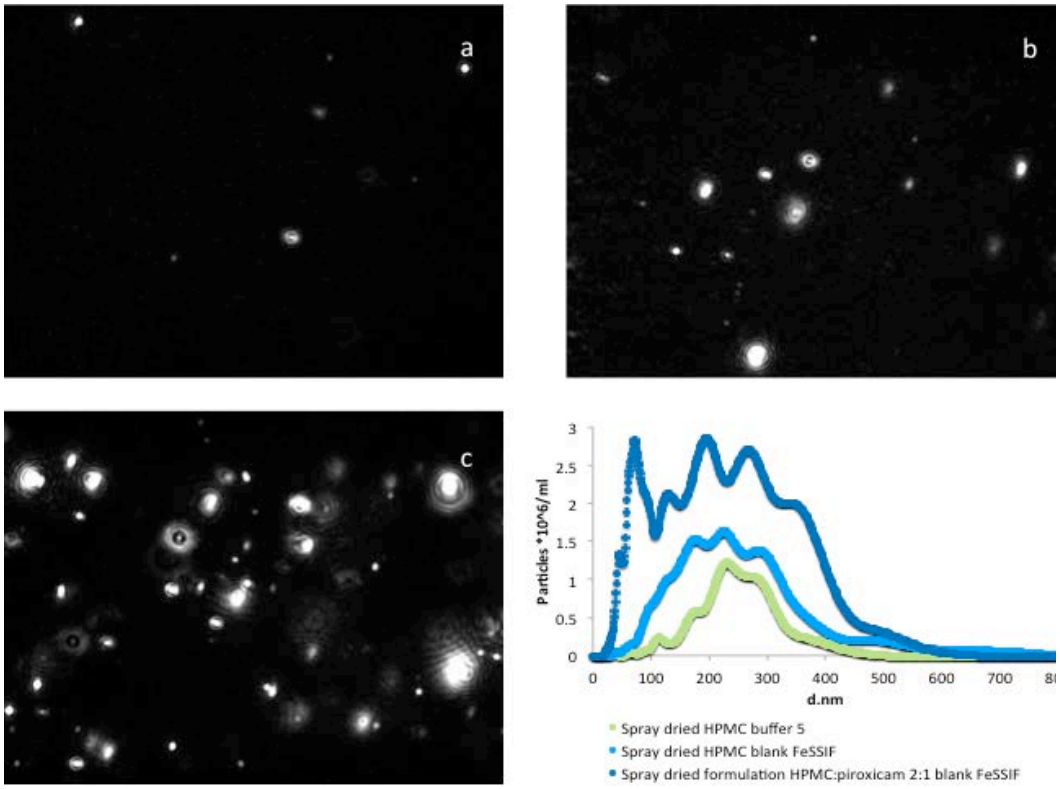

Figure 5.13: Nanosight images of spray dried HPMC in buffer pH 5 (a), spray dried HPMC in blank FeSSIF (b) and spray dried HPMC:piroxicam 2:1 in blank FeSSIF (c); Nanosight sizes distribution of samples a,b and c (d).

As shown in Figure 5.13 a limited number of aggregates was present also for HPMC in buffer pH 5, with a particle concentration slightly higher that 10^6 particle/ml. The size range (100-400 nm) is slightly bigger than the one obtained at pH 5, which is in agreement with the corresponding DLS results, suggesting again a possible impact of the ions species on the polymer chains aggregation and/or hydration. Differently from the results obtained for the HPMC sample in blank FaSSIF, in blank FeSSIF HPMC aggregates increase in concentration, as shown by Image b in Figure 5.13, and in size as shown by Figure 5.13 d. The increase in aggregates size and concentration can possibly prove the aggregation between HPMC and NaTC in blank FeSSIF, as already suggested by DLS results and indicated by NMR and interfacial tension data (refer to Chapter 4). The peak broadness is very high for the spray dried HPMC in blank FeSSIF, indicating a high polydispersity which suggests the presence of different aggregates species (and possibly aggregates with different particle sizes) in solution. As shown by Figure 5.13 c, in the presence of piroxicam a significant swelling in size of the aggregates was observed. Such result may be an indication of the drug encapsulation in HPMC, HPMC/NaTC aggregates and NaTC free micelles. The latest are possibly formed in solution considering that NaTC concentration reaches the system CMC*, as shown by NMR and interfacial tension data. From Figure 5.13 d it can be

seen that spray dried HPMC:piroxicam formulation in blank FeSSIF yielded a highly polydispersed population of aggregates, therefore it is not possible to obtain a defined size for this sample.

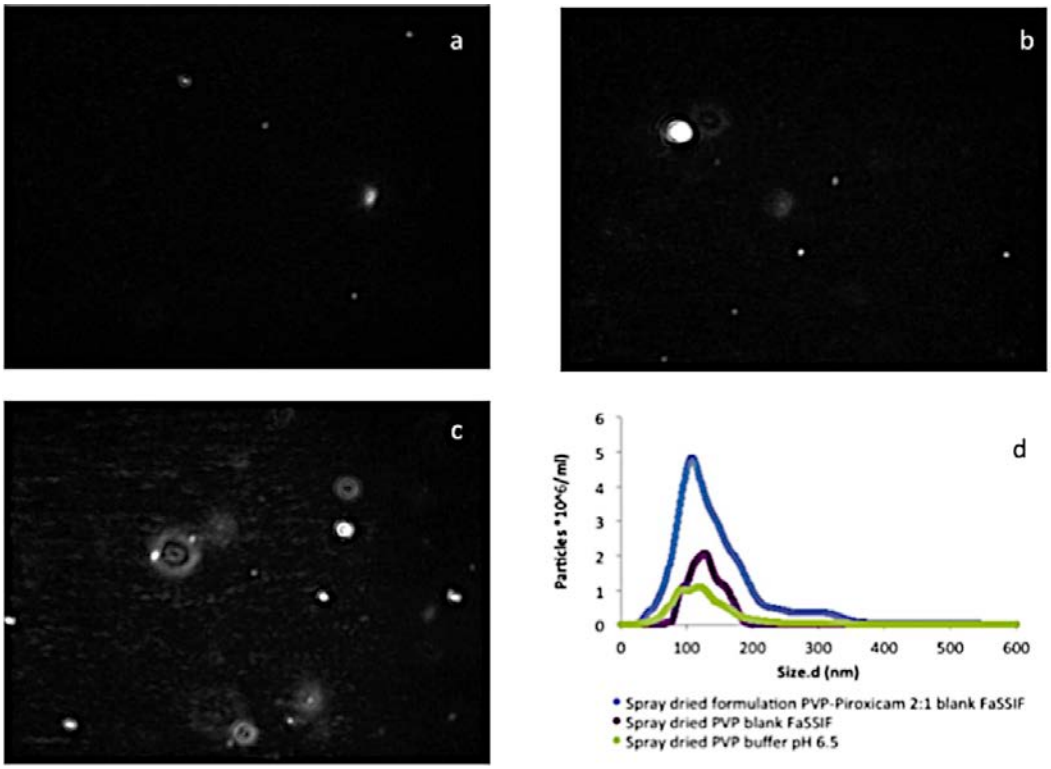

Figure 5.14: Nanosight images of spray dried PVP in buffer pH 6.5 (a), spray dried PVP in blank FaSSIF (b) and spray dried PVP:piroxicam 2:1 in blank FaSSIF (c); Nanosight sizes distribution of samples a,b and c (d).

Nanosight analysis was performed also for spray dried PVP and spray dried PVP:piroxicam 2:1 samples. As for spray dried HPMC, spray dried PVP only yielded an extremly low number of aggregates in buffer pH 6.5. The particles concentration of the sample was 10^6 particles /ml (Figure 5.14 d) and increased up to 2*10^6 particles /ml in blank FaSSIF. The sizes of the aggregates obtained by the Nanosight software are not reliable due to the low number of aggregates tracked. Nevertheless it can be seen in Figure 5.14 d that aggregates size distribution did not change significantly for spray dried PVP in blank FaSSIF, compared to the same sample in buffer. Therefore, as already seen for spray dried HPMC in blank FaSSIF, limited aggregation/association between PVP and NaTC occurred in blank FaSSIF. As previously discussed such effect is likely to be related to the low NaTC (3mM) concentration in the medium. As clearly shown by Figure 5.14 c, the number of scattering particles significantly increased for the spray dried PVP:piroxicam 2:1 formulation, compared to the spray dried PVP. The particle concentration of the sample rose

up to 5*10^6 particles/ml and a broadening of the size distribution peak can also be observed, indicating the possible drug encapsulation by aggregates present in solution.

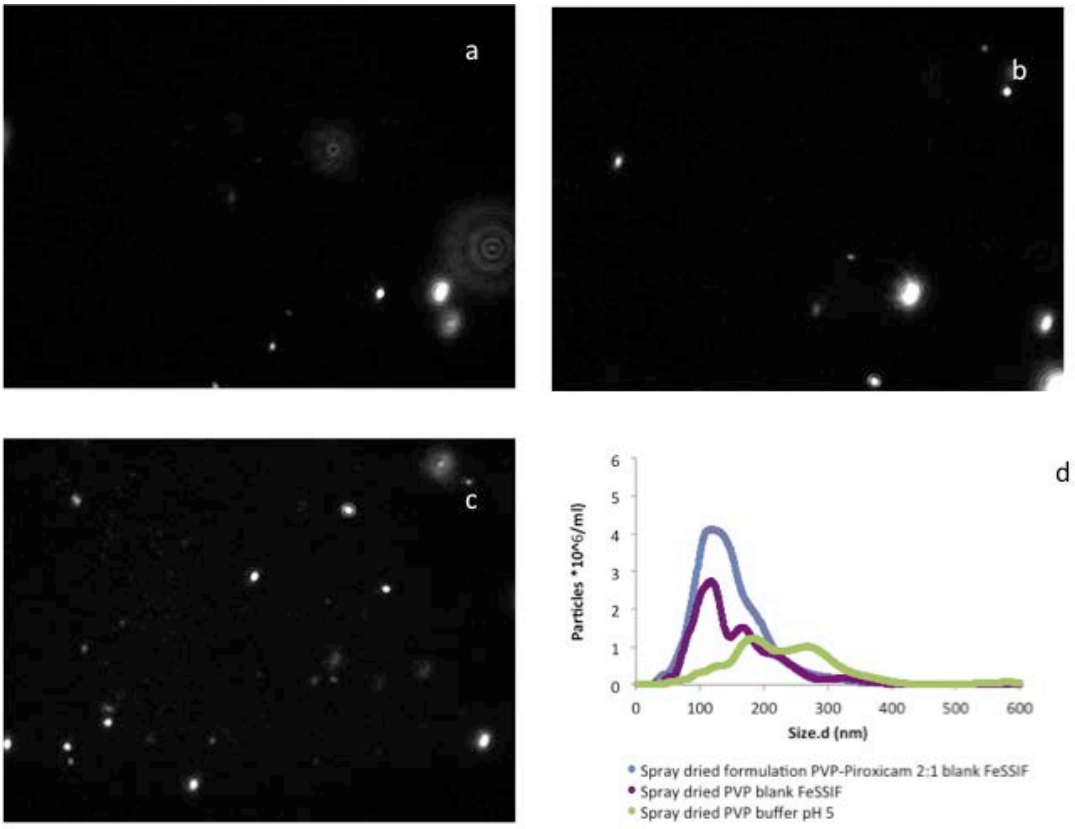

Figure 5.15: Nanosight images of spray dried PVP in buffer pH 5 (a), spray dried PVP in blank FeSSIF (b) and spray dried HPMC:piroxicam 2:1 in blank PVP (c); Nanosight sizes distribution of samples a,b and c (d).

An extremely low number of scattering aggregates can be seen also in Figure 5.15 a, indicating a very weak scattering by spray dried PVP in buffer pH 5, as seen in buffer pH 6.5 (Figure 5.14 a). The particle concentration of PVP in pH 5 buffer was still around 10^6 particles/ml, but a broader size distribution was observed, confirming the possible different polymer aggregations in the two buffers. In blank FeSSIF medium, the particle concentration increased up to 3*10^6 particles/ml, as a consequence of the higher NaTC concentration and the possible HPMC/NaTC aggregation. As shown in Figure 5.15 d, a bimodal distribution was obtained for spray dried PVP in blank FeSSIF, which is in good agreement with the corresponding DLS data. For the PVP sample in blank FaSSIF, the presence of drug resulted in the presence of larger aggregates and an increase in particle concentration. The particles concentration for the spray dried PVP:piroxicam formulation in blank FeSSIF was about 4*10^6 particles/ml and with an average size of about 150 d.nm.

Nanosight data for all the samples analysed showed broad sizes distribution, indicating the formation of polydispersed aggregates. The high polydispersity may be an indication of the

formation of different species, such as polymer aggregates, polymer/NaTC complexes and free NaTC micelles, particularly in the case of the samples in blank FeSSIF. However, a detailed description of the solution phase composition for the different sample could not be obtained from Nanosight and DLS data.

5.3.7 SESANS characterisation of solid dispersion in simulated intestinal fluids

Spin-echo small angle neutron scattering (SESANS) is a neutron scattering technique that can be used to study structures with sizes from 20 nm to 20 µm. [282] Considering polymer-NaTC aggregates sizes estimated by DLS and Nanosight analysis, SESANS is suitable for studying these aggregates and was employed to obtained structural information of HPMC-NaTC aggregates in different simulated intestinal fluids .

As described in Chapter 2, in SESANS experiments a neutron beam is polarised through its passage via two precession regions, which apply to the beam an identical but opposite magnetic induction. The scattering of the neutron takes place between the two precession regions. Therefore for non-scattered neutrons the precession angle in front of the sample is completely compensated in the precession region located behind the sample, resulting in an identical beam polarisation after experiment completion. The polarised neutrons are scattered after the first precession region, the compensation of the precession angle in the second procession region is not complete, resulting in a depolarisation of the beam. [282]

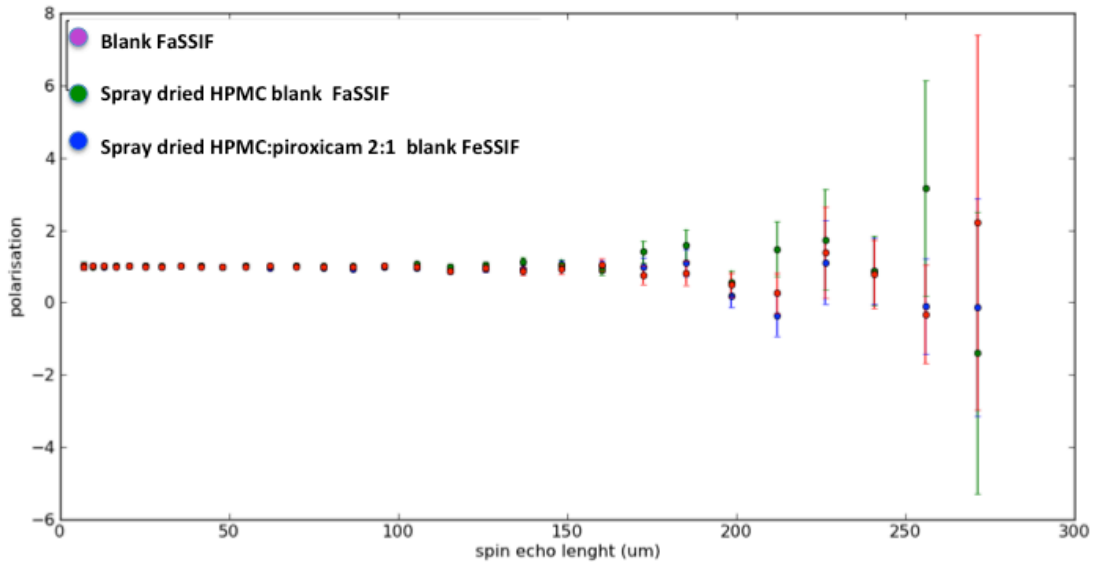

Figure 5.16: Spin echo signal of blank FaSSIF, spray dried HPMC in blank FaSSIF (0.27 mg/ml) and spray dried formulation HPMC:piroxicam 2:1 in blank FaSSIF.

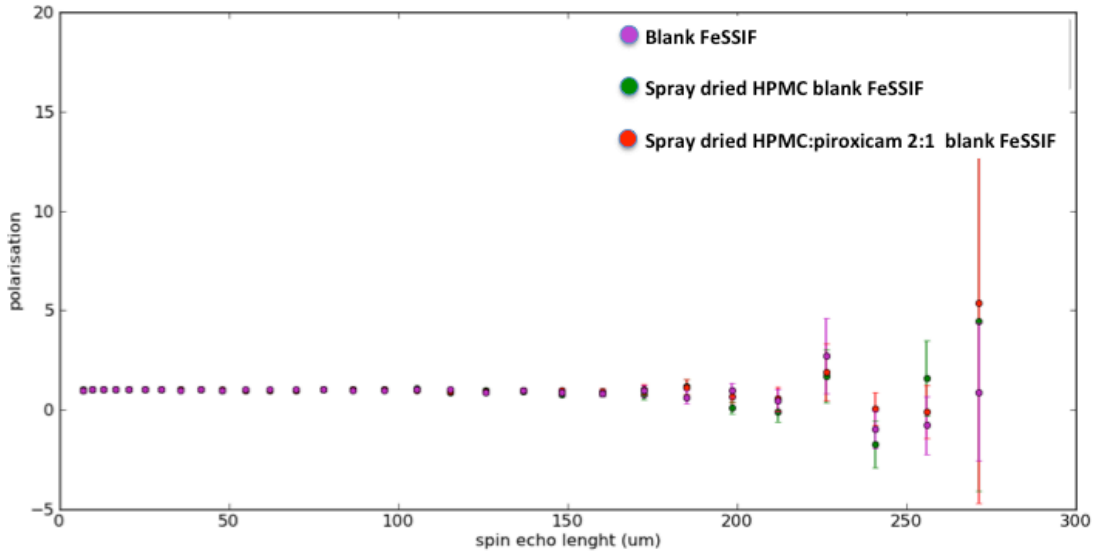

Figure 5.17: Spin echo signal of blank FeSSIF, spray dried HPMC in blank FeSSIF (0.27 mg/ml) and spray dried formulation HPMC:piroxicam 2:1 in blank FeSSIF.

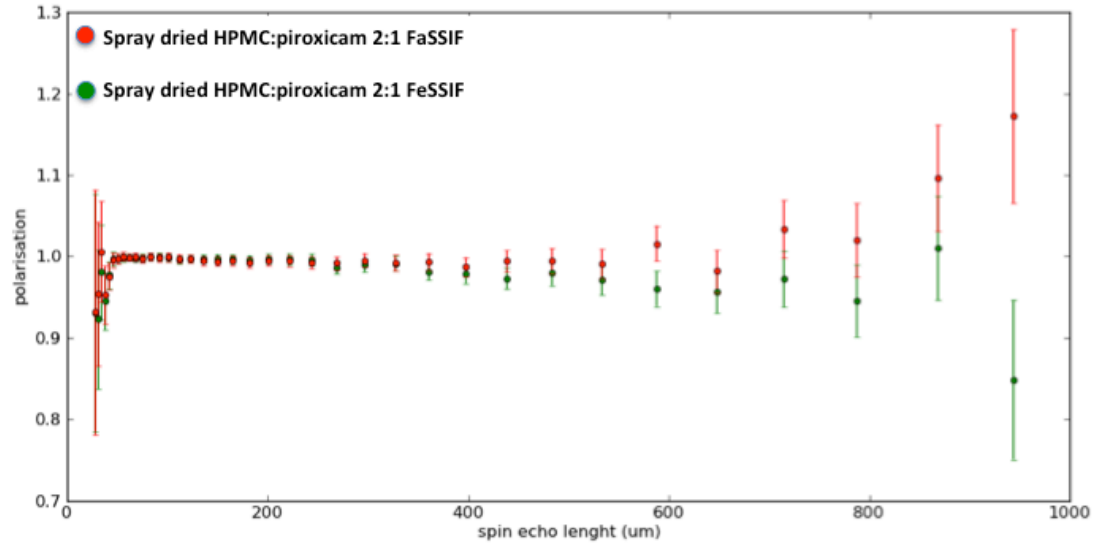

Figure 5.18: Spin echo length signal of spray dried formulation HPMC:piroxicam 2:1 in FaSSIF and FeSSIF as a function of normalised neutron beam polarisation.

As shown in Figures 5.16, 5.17, 5.18, no change on the neutron beam polarisation was obtained for all samples studied. Such results firstly suggest the absence of neutron scattering by the samples analysed. This may possibly be valid for the samples in blank FaSSIF, which were known to have a very low number of particles present by Nanosight experiments and a weak scattering by DLS analysis. For the samples in blank FeSSIF, FaSSIF and FeSSIF the absence of neutron scattering is more difficult to explain as both Nanosight and DLS data showed the occurrence of strong light scattering by these samples. The lack of the neutron beam depolarisation may also be due to the high polydispersity of

the samples and to the possible more open-shape of the aggregates. It is well known that the formation of structure/shape of polymeric and micellar aggregates is a highly dynamic process, which can yield a weaker scattering in neutron experiments when studied in dilute regimes. It should also bear in mind that the ISIS off-Spec spectrometer was a brand new equipment and its optimisation was still on-going when our experiments were performed. In particular our experiment were the first set of experiments in aqueous solvents performed at the ISIS Off-spec facilities. Therefore further SESANS studies on similar samples might clarify the possible application of this brand new equipment for polymer/surfactant mixtures characterisation.

In order to further confirm the results, the experiments were repeated using increased acquisition time and increased polymer concentration (data not shown). However no change on the results was obtained in both cases. To further investigate the samples, SANS experiments were performed.

5.3.8 SANS characterisation of solid dispersion in simulated intestinal fluids

SANS has been extensively employed for the study of polymer/surfactant aggregation.[141,283,284] In this study, SANS was firstly performed on spray dried formulations PVP:piroxicam 2:1 and HPMC:piroxicam 2:1 in blank FaSSIF (Figure 5.19 and 5.20). Blank FaSSIF medium was also analysed, but no scattering was obtained (data not shown), suggesting the absence of NaTC micelles in such medium. This result is in agreement with both DLS and Nanosight data that did not shown any light scattering in blank FaSSIF (Sections 5.3.3 and 5.3.4). It can be seen in Figures 5.19 and 5.20 that the neutron scattering is still weak (low scattering intensity) in the presence of the spray-dried formulation.

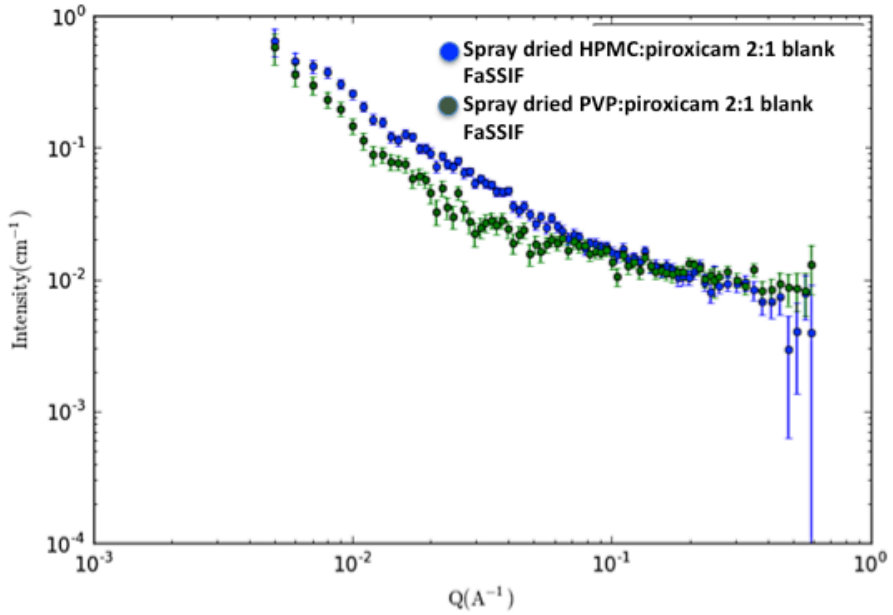

Figure 5.19: Neutron Scattering intensity (cm^{-1}) for spray dried HPMC:piroxicam 2:1 and for spray dried PVP:piroxicam 2:1 in blank FaSSIF, as a function of scattering vector Q (A^{-1}).

Due the low scattering obtained in blank FaSSIF, the fitting of the scattering curve was not successful. Therefore structural information could not be obtained for these samples. Slightly stronger scattering was obtained for the samples measured in FaSSIF. The presence of lecithin changed the scattering pattern completely as shown in Figure 5.20.

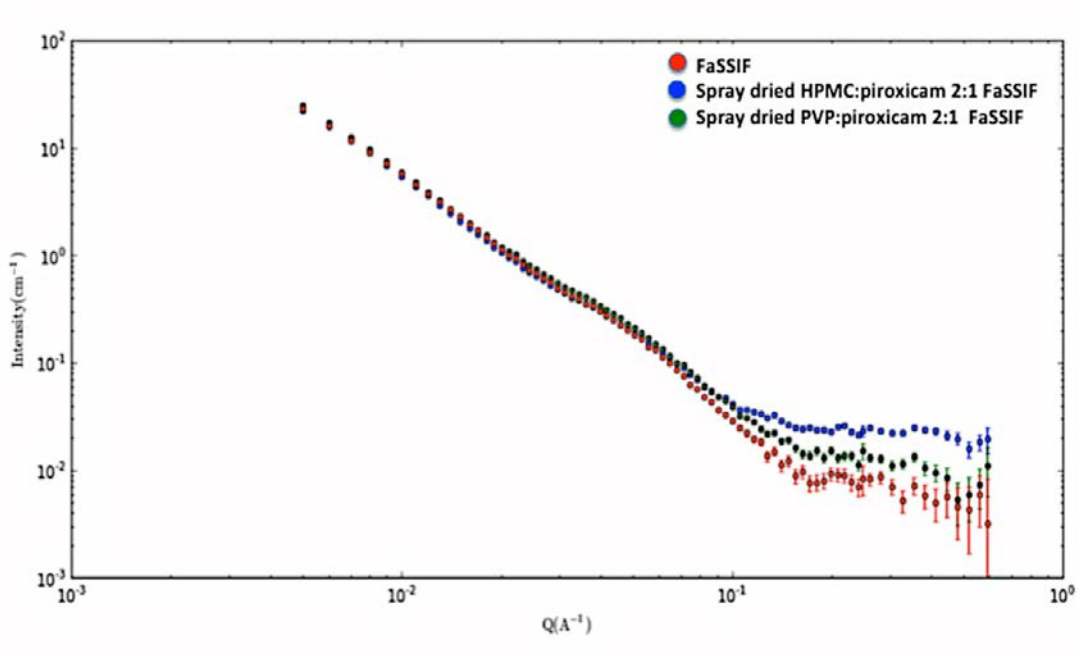

Figure 5.20: Neutron Scattering intensity (cm^{-1}) for FaSSIF, spray dried HPMC:piroxicam 2:1 and for spray dried PVP:piroxicam 2:1 in FaSSIF, as a function of scattering vector Q (A^{-1}).

In the presence of lecithin scattering intensity significantly increased. It can also be seen that in the low Q range scattering curve is very similar for FaSSIF and spray dried HPMC:piroxicam 2:1 and PVP:piroxicam 2:1. This indicates that the scattering pattern is dominated by the lecithin/NaTC aggregates and that the presence of the polymeric carrier did not significantly impact on the scattering pattern in the low Q range. In the high Q range the scattering pattern indicates the presence of larger aggregates for the samples containing spray dried HPMC:piroxicam 2:1 and PVP:piroxicam 2:1. This suggests the formation of new and/or larger structures that may result from the aggregation of the polymeric carriers and the aggregates present in FaSSIF.

Bile salts/lecithin complexes have widely been characterized using SANS. Different fitting model have been applied to analyse the scattering data and obtain structural information about the aggregates. Some of the proposed models in literature were cylinders and vesicles, [285] flexible ellipsoid cylinders [215] and wormlike micelles. [214,286]

In this study the scattering curves of FaSSIF medium, spray dried HPMC:piroxicam 2:1 in FaSSIF and PVP:piroxicam 2:1 in FaSSIF were fitted using a elliptical cylinder model. The fitting results are shown in Figure 5.21 and obtained size parameters are summarised in Table 5.4.

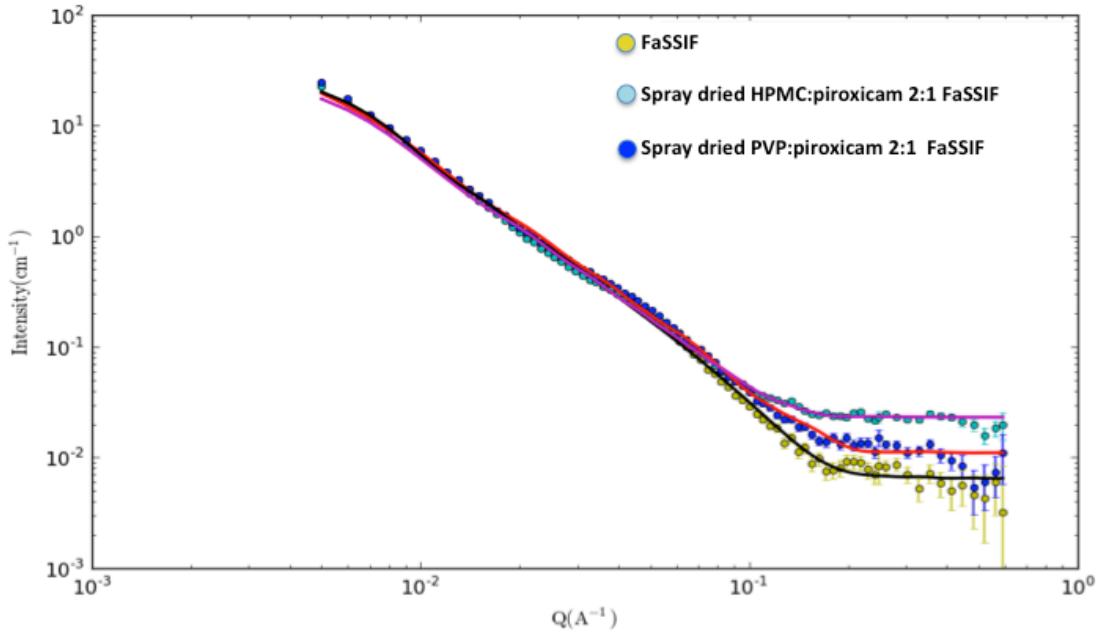

Figure 5.21: Neutron Scattering intensity (cm^{-1}) for FaSSIF, spray dried HPMC:piroxicam 2:1 and for spray dried PVP:piroxicam 2:1 in FaSSIF, as a function of scattering vector Q (A^{-1}), fitted using an elliptical cylindrical model.

Table 5.4: Size parameters obtained for FaSSIF, spray dried HPMC:piroxicam 2:1 and spray dried PVP:piroxicam 2:1 in FaSSIF by neutron scattering curves fitting (Elliptical Cylindrical model).

Fitting Parameters	FaSSIF	Spray dried HPMC:piroxicam 2:1 FaSSIF	Spray dried PVP:piroxicam 2:1 FaSSIF
Length [Å]	401.35±4.26	492.36±6.3929	458.39±5.19
R minor [Å]	16.78±0.26	16.964±0.24866	13.864±0.24
R ratio	23,91±1.87	27.092±1.1689	75.928±2.05

As shown in Table 5.4, the obtained results indicate the presence of elliptical cylinder having similar sizes in the three samples studied. Slight swelling of the aggregates was obtained in the presence of the spray dried formulation, with lengths of 458.39±5.19 Å and 492.36±6.39 Å for spray dried PVP:piroxicam 2:1 formulation and spray dried HPMC:piroxicam formulation, respectively, compared to FaSSIF on its own that yielded a length of 401.35±4.26 Å. The minor radius value was similar for all the three samples, indicating that the presence of the polymeric carrier mainly impacted on the length of the cylinders. The SANS measured cylinder length values are close to the hydrodynamic diameter values obtained by DLS analysis for the smaller population of aggregates (Section 5.2.3). From Figure 5.21 it can be seen that the last part of the scattering curve is not well fitted. This may be due to the presence of bigger and/or polydispersed aggregates which make the fitting more challenging. The similar scattering pattern obtained with and without the presence of the spray dried formulations, suggest that the scattering pattern is mainly attributed by the NaTC/lecithin aggregates and that the presence of spray dried formulation mainly led to a slight swelling of such aggregates. Considering that the NaTC/lecithin interaction is mainly driven by hydrophobic forces, [287] interaction is likely to be stronger between NaTC and lecithin than NaTC and lecithin with the hydrophilic polymeric carriers. Nevertheless the formation of polymer/NaTC and polymer/lecithin complexes cannot be excluded, but no evidence is provided by the SANS data in this study.

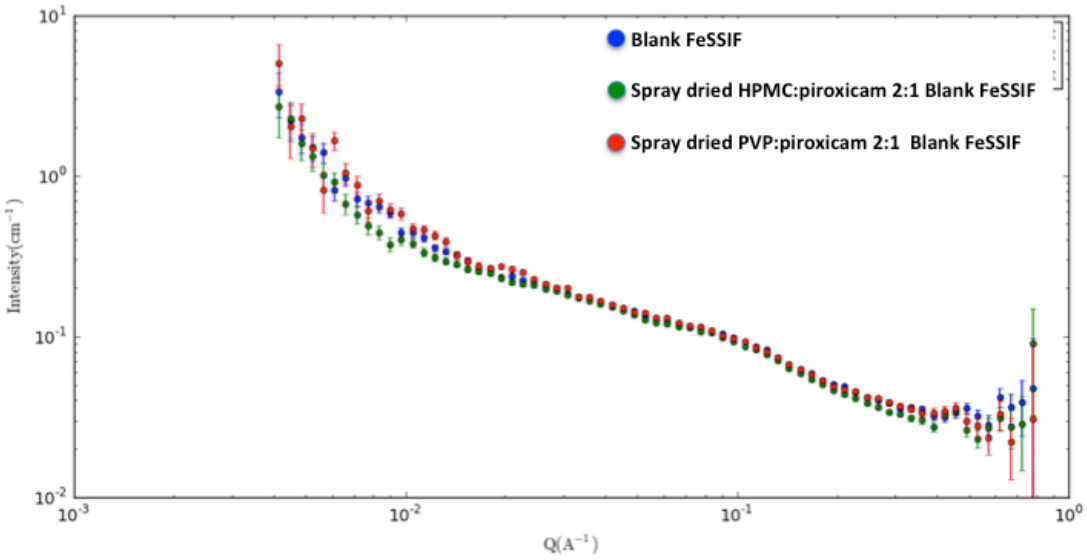

Figure 5.22: Neutron Scattering intensity (cm^{-1}) for FaSSIF, spray dried HPMC:piroxicam 2:1 and for spray dried PVP:piroxicam 2:1 in FaSSIF, as a function of scattering vector Q (A^{-1}).

SANS experiments were also performed in blank FeSSIF and the results are shown in Figure 5.22. It can be seen that, in agreement with light scattering data, higher scattering intensity was obtained compared to samples in blank FaSSIF, as a consequence of the higher NaTC concentration (15 mM). The fitting of the curves was unsuccessful and this is likely to be due to the high polydispersity of the samples, which was clearly shown by the Nanosight data, in particular for HPMC based solid dispersion in blank FeSSIF.

SANS was also used to study FeSSIF and spray dried HPMC:2:1 and spray dried PVP:piroxicam 2:1 in FeSSIF. As shown in Figure 5.23, the scattering pattern changed completely compared to samples in blank FeSSIF (Figure 5.22), indicating a remarkable impact of the presence of lecithin on the aggregation behaviour in solution. In terms of scattering curve fitting, similar to the samples in blank FeSSIF, the fitting was unsuccessful due to the high polydispersity of the aggregates as indicated by DLS and Nanosight results.

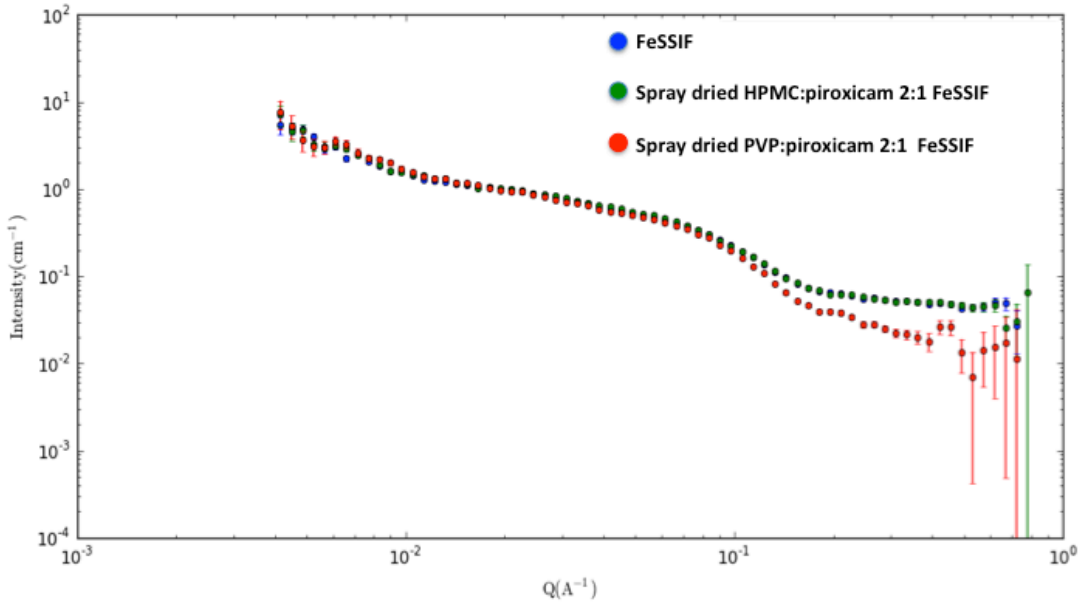

Figure 5.23: Neutron Scattering intensity (cm^{-1}) for FeSSIF, spray dried HPMC:piroxicam 2:1 and for spray dried PVP:piroxicam 2:1 in FeSSIF, as a function of scattering vector Q (A^{-1}).

The SANS data clearly indicate that the absence of signal in SESANS measurements is not to be related to the absence of the polarised neutron beam scattering by the samples studied. The only samples showed extremely weak scattering are the samples in blank FaSSIF, while the other samples analysed by SANS showed the occurrence of neutron scattering. Therefore the absence of signal in SESANS experiments was likely caused by the samples polydispersity. Accurate measurement using SANS is extremely challanging in the case of polydispersed samples. Therefore neutron scattering experiments are possibly unsuitable for the systems analysed in this study. Therefore more direct visualisation method, such as cryo-TEM was used to further study these complex colloidal systems.

5.3.9 Cryo-TEM characterisation of polymer-bile salts aggregates

To further investigate HPMC/NaTC and NaTC/lecithin aggregates shape and size cryo-TEM was performed on spray dried HPMC:piroxicam 2:1 in blank FeSSIF, FeSSIF and spray dried HPMC:piroxicam 2:1 in FeSSIF. Due the low number of aggregates present in blank FaSSIF and FaSSIF, the contrast analyses using cryo-TEM was likely to be unsuccessful, thus the samples in such media were not analysed.

Figure 5.24 and 5.25 show cryo-TEM images of spray dried solid dispersion HPMC:piroxicam 2:1 in blank FeSSIF. The image in Figure 5.24 shows the presence of globular aggregates having a size of about 50 d.nm. Aggregates imaged are consistent with the size obtained for the smaller population of the bimodal distribution yielded by DLS

analysis on the same sample. Considering the CAC and CMC* values obtained by NMR and interfacial tension measurements for such system, the presence of free NaTC micelles should be limited, as NaTC concentration in blank FeSSIF correspond to its CMC* value. Therefore the globular aggregates imaged by cryo-TEM technique are likely to be the NaTC/HPMC aggregates. In Figure 5.25 the arrow indicates the presence of elongated structures of about 200 d.nm with low contrast. The nature of such elongated structure is not clear and may be associated with HPMC aggregates. Cryo-TEM images confirm the presence of two different aggregates in solution, which explained the bimodal distribution shown by DLS measurements and the broad size distribution peak obtained with Nanosight measurements. It should be bear in mind that the analysis was performed after 48-72 hours from sample preparation (due to the delivery time required from UK to Sweden and possibly with temperature fluctuation during this period). Therefore sample aging may affect the solution composition and subsequently the cryo-TEM aggregates imaging.

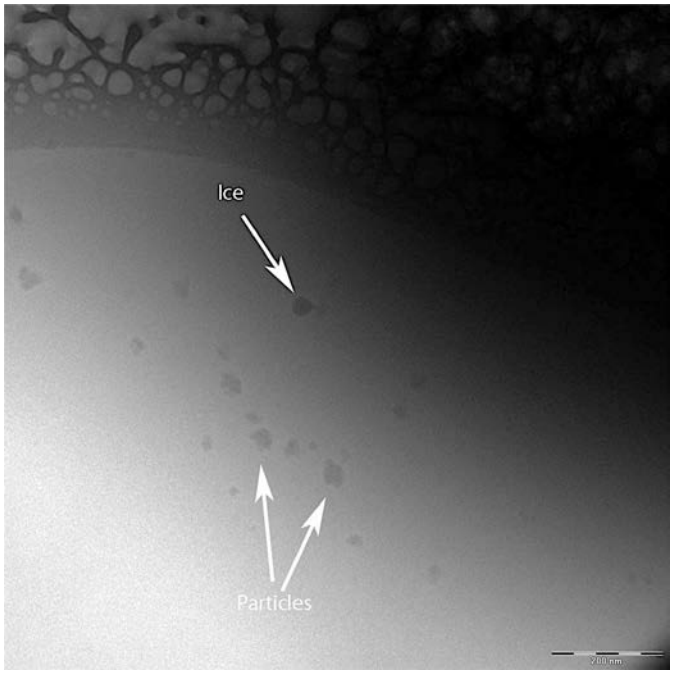

Figure 5.24: Cryo-TEM images of spray dried formulation HPMC:Piroxicam 2:1 in Blank FeSSIF. Presence of globular aggregates of about 50 nm in size (a). Bar=200nm

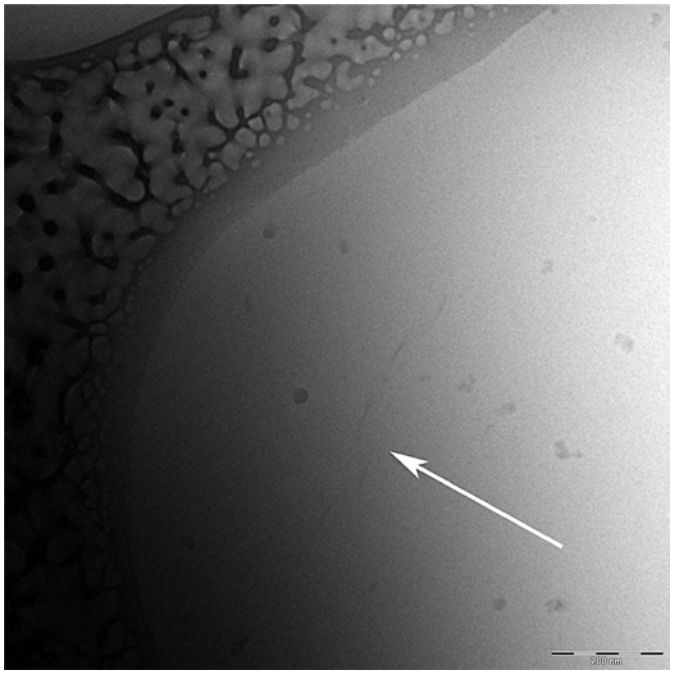

Figure 5.25: Cryo-TEM images of spray dried formulation HPMC:Piroxicam 2:1 in Blank FeSSIF. The arrow indicates the presence of elongated structures (b). Bar=200nm

Cryo-TEM analysis was also performed on FeSSIF and the obtained image is shown in Figure 5.26. The image shows the presence of globular small micelles with a size of about 5 nm. This result is not in agreement with DLS analysis that showed the presence of two populations of aggregates of 133±14 and 552±39 d.nm. As previously mentioned cryo-TEM analysis could not be performed on fresh samples, but was instead carried out on samples aged for 48-72 hours. Literature data reported possible size and shape changes of NaTC/Lecithin aggregates over time. [285] Therefore the inconsistency between cryo-TEM and DLS results might be caused by the samples aging.

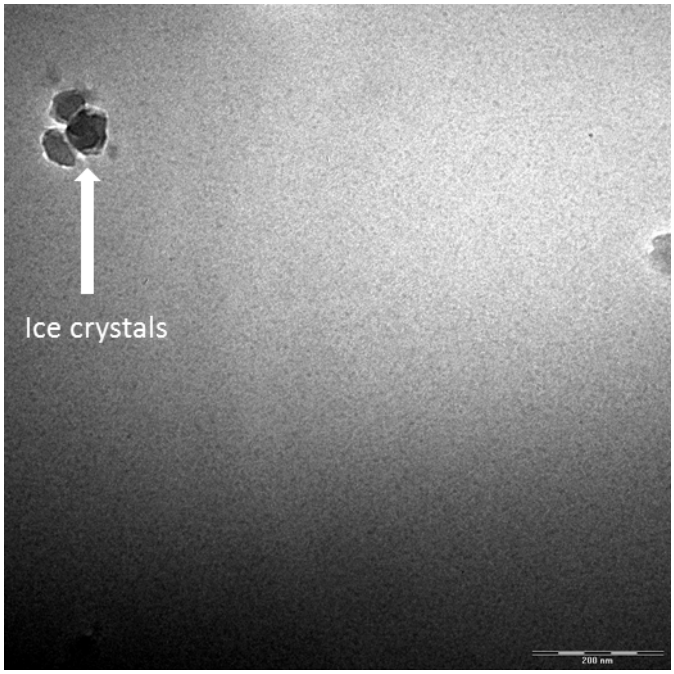

Figure 5.26: Cryo-TEM images FeSSIF. The image shows the presence of globular aggregates of about 5 nm in size (a). Bar=200nm

Spray dried HPMC:piroxicam 2:1 solid dispersion in FeSSIF was also analysed and the cryo-TEM image is reported in Figure 5.27. It can be seen that the aggregates are very similar to the ones imaged for FeSSIF alone, confirming that there are mainly NaTC/lecithin aggregates present. For these samples Cryo-TEM results are in disagreement with DLS, which showed the presence of much bigger aggregates with a bimodal distribution. As for FeSSIF it is likely that the sample aging affected the aggregates features.

Lecithin-bile salts aggregation has been extensively described in literature. [277,288] Mazer et al proposed a "mixed disk" model for the structure of bile salt-lecithin mixed micelles, while a rod-like morphology of the aggregates based on SANS data was described by Hjelm et al. More recently bile salt-lecithin micelles were found to be flexible rods, having different sizes between 5 to 300 nm depending on the micelles composition. [215] Kloefer et al also reported cryo-TEM analysis for instant FaSSIF and FeSSIF (obtained from redissolution of freeze dried FaSSIF and FeSSIF media), but the different preparation procedure and the different aging of the aggregates do not allow a direction comparison of our results with the existing literature. Further cryo-TEM studies on fresh samples are needed to help accurately image the aggregate studied in this study.

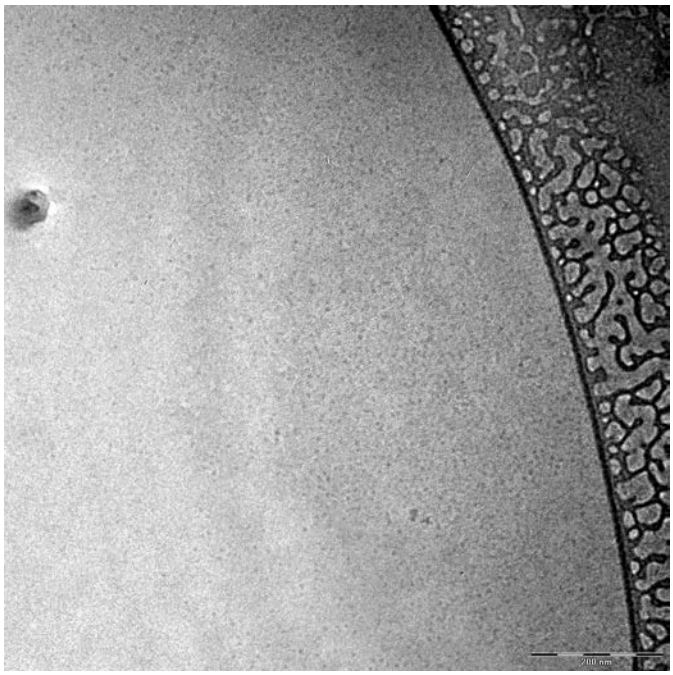

Figure 5.27: Cryo-TEM images of spray dried formulation HPMC:Piroxicam 2:1 in Blank FeSSIF. Presence of globular aggregates of about 50 nm in size (a). Presence of elongated structures (b). Bar=200m

5.4 Discussion on studied solution phase composition

Data obtained in this Chapter provided more detailed indicative information on the solution phase composition of the different samples analysed. Based on the DLS, Nanosight, and neutron scattering results, a model about the possible aggregation between the polymeric carriers employed and NaTC in blank FaSSIF is shown in Figure 5.28.

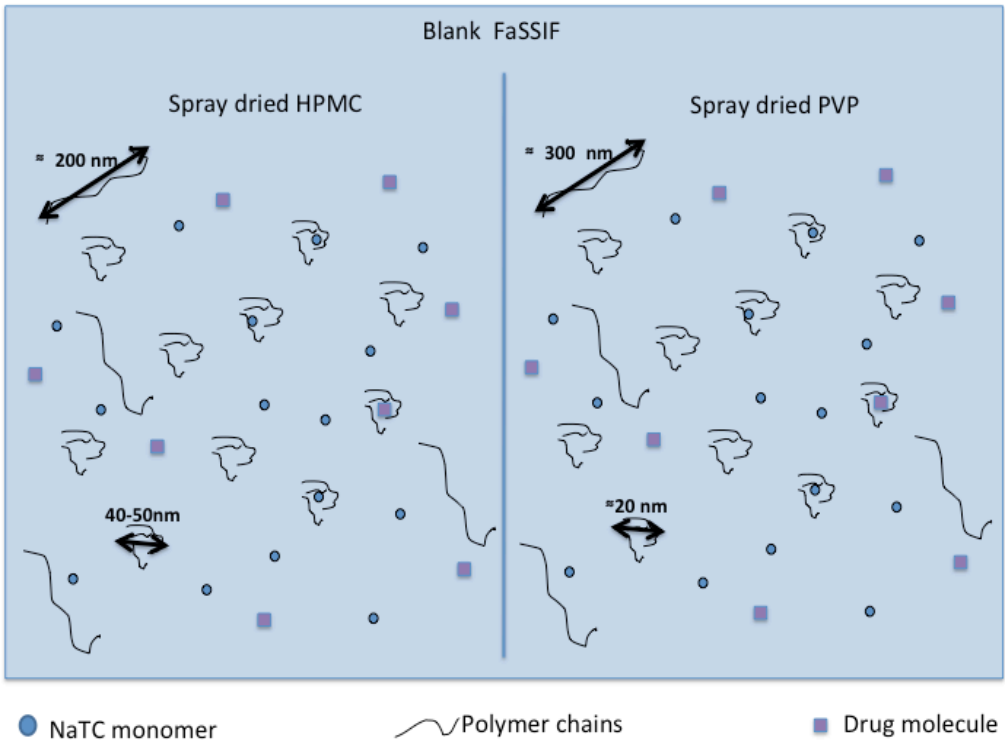

Figure 5.28: Schematic representation of solution phase composition and NaTC/polymeric carrier features in spray dried solid dispersions dissolved in blank FaSSIF.

DLS analysis for spray dried HPMC:piroxicam 2:1 solid dispersion in blank FaSSIF yielded a bimodal distribution of sizes. As described in this Chapter, in blank FaSSIF no free NaTC micelles are formed and NaTC/HPMC aggregation is limited by the low NaTC concentration. Therefore, the two populations indicated by DLS, may be composed by polymer aggregates. NaTC monomers and drug molecules do not scatter, therefore the light scattering signal can only be attributed to the polymer aggregates and possibly free chains. Drug solubilisation is likely to be facilitated by the reduced surface tension caused by the HPMC presence, by the increase of the drug molecules wettability and possibly via their encapsulation in the polymeric aggregates.

A bimodal distribution was also obtained for the sample of spray dried PVP:piroxicam 2:1 solid dispersion in blank FaSSIF, with smaller sizes for the first population, in agreement with the smaller size obtained in buffer for spray dried PVP in buffer pH5.

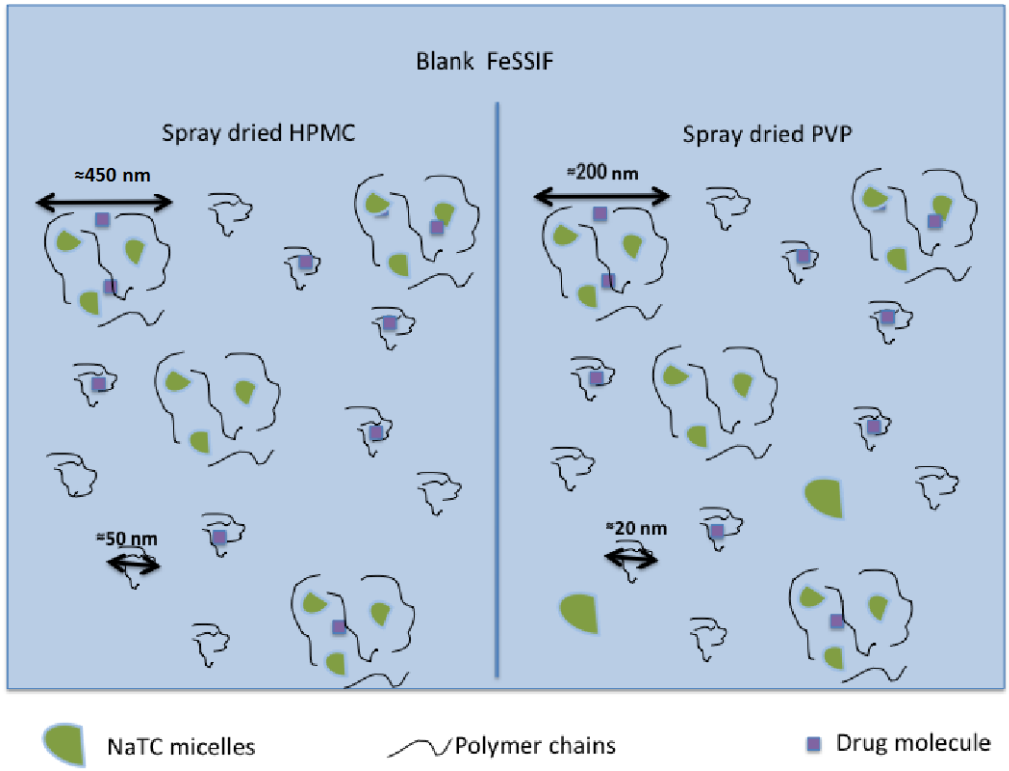

Figure 5.29: Schematic representation of solution phase composition and NaTC/polymeric carrier features in spray dried solid dispersions dissolved in blank FeSSIF.

In blank FeSSIF the possible presence of polymeric carrier/NaTC aggregation yielded different sizes distribution compared to blank FaSSIF. SANS, SESANS and Nanosight data indicated high polydispersity for spray dried formulations in blank FeSSIF, suggesting the formation of different species in solution. Based on DLS and Nanosight data the solution phase composition was speculated and illustrated in Figure 5.29. As indicated by NMR and interfacial tension measurements in Chapter 4, NaTC/HPMC aggregation occurred in blank FeSSIF. DLS results indicated the formation of two populations of aggregates having sizes of 58±9 and 448±30 d.nm. The smaller population of aggregates is likely to be composed of HPMC aggregates, as the size of the population is very close to the one obtained for spray HPMC in buffer pH5. The bigger population of aggregates is likely composed by HPMC/NaTC aggregates. Solubility studies described in Chapter 3 (Section 3.3.2) showed piroxicam apparent solubility increase in blank FeSSIF. The increased solubility may be partially contributed to the drug encapsulation in the aggregates of NaTC/HPMC, as well as in HPMC aggregates. For PVP based spray dried formulation in blank FeSSIF, a bimodal distribution was also obtained. Therefore, also in this case the smaller population may be mainly composed of PVP aggregates, while the bigger one may be a result of the complexation between NaTC micelles and PVP. For PVP/NaTC system the

CMC* value could not be clearly assigned, therefore the formation of free NaTC micelles cannot be excluded and as possible solution composition is illustrated in Figure 5.29, also free NaTC micelles may be present in solution. Three different aggregates, PVP and PVP/NaTC aggregates and free NaTC micelles, may be involved in the drug solubilisation for the spray dried PVP:piroxicam solid dispersion.

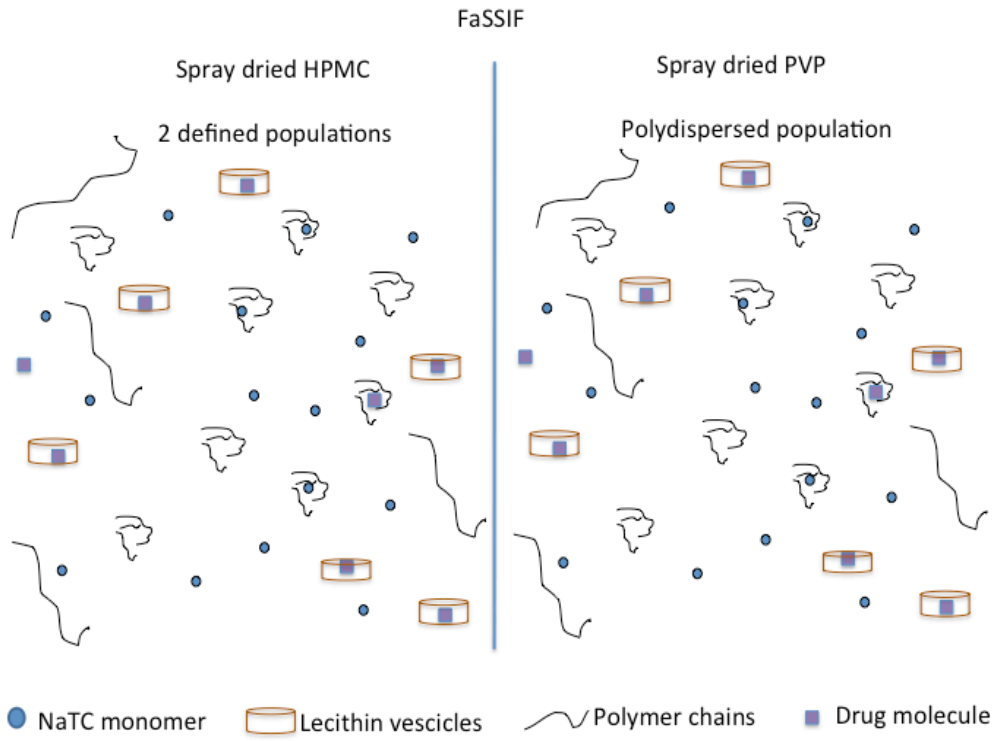

Figure 5.30: Schematic representation of solution phase composition and NaTC/polymeric carrier features in spray dried solid dispersions dissolved in FaSSIF.

The samples in FaSSIF yielded completely different scattering pattern compared to the samples in blank FaSSIF, for both light and neutron experiments. This indicated the impact of lecithin on the aggregation in solution and the possible formation of new species. SANS data analysis indicated that the scattering pattern is mainly attributed to the scattering of lecithin vesicles. As previously discussed in this Chapter (Section 5.3.1) at low NaTC concentration, the bile salt is mainly in its monomeric form, but its concentration is not high enough to lead to lecithin vesicles dissolution by surfactants, bile salts in particular, which leads to the formation of mixed micelles. [278] Therefore, as represented in Figure 5.30, elliptic cylindrical lecithin vesicles are possibly present in solution, for both spray dried PVP and HPMC based formulation in FaSSIF. The high solubility of piroxicam in FaSSIF highlighted by apparent solubility studies (refer to Chapter 3, Section 3.3.2) may be

attributed to piroxicam solubilisation via lecithin vesicles. Considering DLS results obtained for spray dried formulation in the presence of polymer, polymeric aggregates and free polymeric chains that may contribute to the overall scattering, as illustrated in Figure 5.30. HPMC and PVP aggregates could also contribute to the drug solubilisation, as well as the reduction in the overall system surface tension.

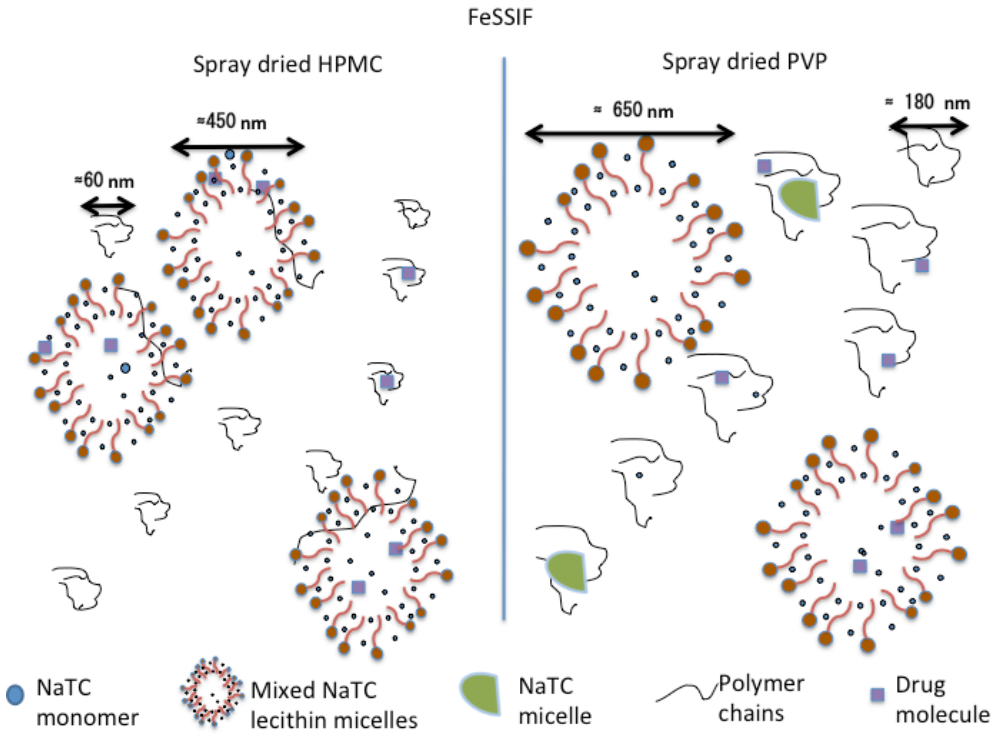

Figure 5.31: Schematic representation of solution phase composition and NaTC/polymeric carrier features in spray dried solid dispersions dissolved in FaSSIF.

In FeSSIF medium, high polydispersity was indicated by SANS analysis for which the data fitting was not possible. Also DLS data indicated the presence of large aggregates for both spray dried formulations. A bimodal size distribution was obtained for both HPMC and PVP based spray dried formulation in FeSSIF. The solution phase composition can be speculated as the smaller population being mainly composed by polymeric aggregates. This was suggested by DLS results performed on spray dried HPMC:piroxicam samples having different drug:polymer ratios (Section. 5.3.3). The increase in polymer weight ratio led to the increase in size of the smaller population of aggregates. Such result indicated that the smaller population of aggregates was mainly composed of polymeric complexes. The high NaTC concentration in FeSSIF could lead to the lecithin vesicles dissolution, resulting in the formation of NaTC/lecithin mixed micelles. The possible structure of such mixed colloidal

system is speculated in Figure 5.31, being the co-existence of lecithin, NaTC monomers, and possibly polymeric chains. Drug solubilisation may be attributed to both polymeric aggregates and NaTC/lecithin mixed micelles.

5.5 Conclusions

In this Chapter NaTC/HPMC and NaTC/PVP complexes were characterised by the use of light scattering techniques including DLS and Nanosight, neutron scattering techniques including SANS and SESANS, and cryo-TEM. All data obtained indicated the occurrence of polymeric carriers/NaTC interaction in blank FeSSIF, while very limited aggregation was find to occur in blank FaSSIF. Therefore different drug solubilisation mechanism was speculated for spray dried formulations dissolved in the two media. Polymeric aggregates in blank FaSSIF are likely to play a major role in the drug solubilisation, while a possible involvement of NaTC/polymer aggregates may occur in blank FeSSIF. PVP and HPMC formulations yielded similar results, being with bigger aggregates formed in the case of spray dried HPMC based solid dispersions.

Lecithin vesicles were found to dominate the light and neutron scattering patterns in FaSSIF, suggesting the possible role of such vesicles in the drug solubilisation. In FeSSIF polymeric aggregates and mixed NaTC/lecithin aggregates were possibly formed, despite cryo-TEM result, which indicated the presence of very small micelles. Analysis conducted by neutron and light scattering techniques on such complex systems is proven to be very challenging. It can be concluded that the solution composition of spray dried solid dispersion in simulated intestinal media is extremely complex, due to the presence of many components and the possible occurrence of interaction between them. Nevertheless consistency between NMR and Interfacial tension data was obtained. The possible role of the different aggregates in piroxicam solubilisation was further investigated by cellular absorption studies and the results are described in Chapter 6.

Chapter 6. Assessment of the potential effects of polymer/NaTC complexes on poorly water-soluble drugs absorption in the intestinal tract

6.1 Introduction

Effective drug dissolution is essential for proper drug absorption and realising the pharmacological effect after oral administration. [289] In this study the uses of solid dispersion formulations were proven to lead to an increase of drug solubilisation of three model poorly water-soluble drugs, in particular in the simulating intestinal fluids (Chapter 3). The study of the possible interactions between the polymeric carriers employed and the components in the simulated intestinal fluids (Chapters 4 and 5) suggested the possible formation of polymeric carrier/NaTC and polymeric carries/NaTC/lecithin aggregates that may play a role in the model drug solubilisation. In theory, the increase in solubility obtained for the model drug piroxicam (a BSC class II drug) should potentially lead to an increase in its intestinal absorption compared to crystalline form of the model drug. In order to further gain insights into the effect of these aggregates on the *in-vitro* absorption of the drugs, cellular drug absorption and transport assessment were performed using Caco-2 cells as the model cell line.

Caco-2 cells culture model has been widely used in drug discovery and development studies. [290] The Caco-2 cell monolayers have been used as an *in vitro* cell model to identify drug absorption problems and possibly predict drugs absorption *in-vivo* after oral administration in the early stage drug development. [291,292] In literature, Caco-2 cells model has been recognised as a good predictive tool to investigate oral absorption for drugs passively transported via the transcellular route, such as piroxicam. In these studies, the use of bio-relevant media in Caco-2 transport and absorption studies has been remarked as an important factor to obtain reliable prediction of drugs absorption in the intestinal tract. [293,294].

Bile salts are known to have a cytotoxic detergent effect that can cause cell membrane damage. Therefore, in this study in order to find the suitable condition to perform Caco-2 cell experiments using blank FaSSIF, blank FeSSIF, FaSSIF and FeSSIF, cytotoxicity studies were performed in the first instance. Absorption and transport studies were also carried out using Caco-2 cells monolayer to investigate the impact of solid dispersion formulation and the bio-relevant media on the drug absorption by the Caco-2 cell monolayer.

6.2 Materials

75 cm^2 flasks, cells scrapers, 6 and 96-well plates were purchased from Greiner bio-one. All the reagents employed were purchased from Sigma-Aldrich unless differently stated.

6.3 Experimental methods

6.3.1 Cell Culture

Growth and maintenance of cultured cells were carried out in an Envair Class II model safety cabinet with laminar flow hood using aseptic technique to ensure sterility of cells and growth media. All glassware were sterilised by double high pressure and temperature autoclave. All consumables were packaged pre-sterilised or sterilised by autoclave prior to use. All water was of Milli-Q grade and was double distilled using a Millipore filtration unit (Millipore, Massachusetts, USA) and was sterilised using an autoclave. All media and solutions were pre-warmed at 37 ºC in a water bath.

6.3.2 Clonal Caco-2/TC7 Cells

Caco-2/TC7 cells were obtained from Dr M. Rousset (U178 INSERM, Villejuif, France), and were cultured between passages 49 and 59. Cells were grown in 75 cm^2 flasks and maintained in Dulbecco Modified Eagle's Medium (DMEM) with 1 % non-essential amino acids, 1 % L-glutamine, 100 IU/ML penicillin and 100 µg/ml streptomycin, and supplemented with 20 % (v/v) heat inactivated foetal calf serum. Cells were maintained in a Napco 4530 water-jacketed CO_2 incubator at 37 ºC with 5 % CO_2 and 95 % air. Cell seeding was assessed by light microscope and was undertaken at 80 % confluency (approximately a week after seeding). All media and solutions were pre-warmed to 37 ºC in a water bath. The cells were washed three times with phosphate buffered saline solution (PBS). A solution containing 0.05 % trypsin and 0.2 % ethylenediaminetetraacetate (EDTA) was added to the cells (2 ml per dish or flask) and excess removed before the flask was incubated at 37 ºC until the cells became detached from the flask. The remaining trypsin was neutralised by dilution using 10ml of DMEM. Flasks were seeded at 2-4 × 104 cells per cm^2. All media was changed every other day. Cells were re-seeded once 80% of confluency was reached

6.3.3 Solution samples preparation for cells studies

Samples for cytotoxicity, absorption and transport studies were prepared employing sterile glassware. All the sample solutions were prepared in safety cabinet with laminar flow hood using aseptic technique, to reduce the risk of samples contamination. Accurately weighed piroxicam and spray dried HPMC:piroxicam 4:1 solid dispersion were dissolved in the different media and incubated at 37 ºC for 1 hour. Spray dried samples were freshly prepared after thorough spray dryer cleaning. Instrument cleaning was performed by spray drying a mixture of ethanol and water and drying the instrument at 130 ºC prior to spray-drying formulation samples.

6.3.4 Cytotoxicity studies

Cells were cultured in 96-well tissue culture plates at culture conditions described in Section 6.3.2 in 200 µl per well. Once 80 % confluency was reached (approximately 3 weeks), cells were washed twice using pre-warmed sterile PBS. Subsequently 200 µl of test solution samples were added and the cells were placed in the incubator (Napco 4530 water jacketed CO_2 incubator at 37 ºC with 5 % CO_2 and 95 % air**)** for two hours. Cytotoxicity test was run after two hours as the duration of the later absorption and transport experiments was both two hours.

6.3.4.1 Lactate dehydrogenase (LDH) cytotoxicity test

LDH test is a routinely used cytotoxicity test based on the colorimetric determination of LDH released from lysed cells. In this study apical release of LDH enzyme was determined using a colorimetric kit following a previously reported method. [295]

After two hours of incubation, 100 µl of apical medium was transferred into a clean plate. 50 µl of substrate reagent were added to the samples and a 30-minute of reaction period was allowed at room temperature and the plates were protected from light. After 30 minutes 50 µl of stopping solution were added. Absorbance was measured at 492 nm. (Hitachi spectrophotometer, Hitachi High Technologies America, Schaumburg, USA) LDH content was calculated as % of the total LDH content measured by inducing total cell lysing with 0.1% Triton X-100.

6.3.4.2 Cyto-Tox Glo™ test

Another cell viability assay employed in this study was the Cyto-Tox Glo™ test. This assay uses a luminogenic peptide, the (alanyl-alanyl-phenylalanyl-aminoluciferin)

AAF-Glo™ substrate, to measure the activity of protease released by the dead cells. The AAF-Glo™ substrate cannot cross the membrane of living cells. The assay exploits thermostable luciferase (Ultra-Glo™ Recombinant Luciferase), which uses AAF-Glo™ substrate to generate a luminescent signal. By the use of the Lysis Reagent provided in the assay kit, the luminescent signal associated with the total number of cells in each well can also be obtained. This allows the viability calculation by subtracting the luminescent signal obtained for lysed cell from total luminescence of the samples.

100 µl of apical media were transferred into a clean opaque well. 50 µl of the assay reagents were added to each well. The samples were incubated for 30 minutes at room temperature. After 30 minutes luminescence was measured using a FLUOstar OPTIMA microplate reader (BMG LABTECH GMBH, Ortenberg, Germany). Meanwhile 100 µl of lysing buffer were added to the original plate and left in oscillation for 10-15 minutes. 100 µl of apical media were then withdrawn from the original plate containing the lysing buffer and transferred to the opaque plate containing apical media added with assay reagents. Luminescence was measured again after 15 minutes of oscillation.

6.3.5 Drug uptake studies

Cells were grown in 6-well plates until 21 days post confluency. Before performing uptake study confluent cells were washed twice using sterile PBS and aspirated as described in Section 6.3.1. After washing, the cells were treated with 2 ml of the solution sample and placed in the incubator for 2 hours. For each sample 5 replicates were studied. 1 ml of apical media was withdrawn from each well. Cells were then washed twice using sterile PBS and scraped after addition of 400 µl of sterile water. Apical media and scraped cells were collected in sterile eppendorf and frozen after addition of 25 µl of ethanol and 25µl acetic acid for each eppendorf (sample frozen ≈ 1 ml). Samples were later analysed using HPLC analysis. Data analysis was performed by dividing piroxicam (µg) detected in the cells lysate by the total amount (µg) of drug detected (lysed cells+apical media content). Absorbed piroxicam was expressed as % of total drug load.

6.3.6 Transport studies

Caco-2/TC7 cells were seeded at 2-4 x 104 cells per cm^2 on Transwell polycarbonate filters (Greiner bio-one, Stonehouse, UK) with growth surface of 4.5 cm^2 (6 well format). Monolayer integrity was assessed using transepithelial electrical resistance

(TEER), and those wells showing values higher than 180 ohms per cm^2 were aspirated of media from both apical and basolateral compartments and washed three times with phosphate buffered saline (PBS). Phenol red free DMEM was added to the lateral side (1 ml). 1 ml of test sample solution was added to the apical side. Control and treatment cells were incubated at 37 ºC, for 2 hours. After 2 hours 400 µl of apical and lateral media were withdrawn and the sample was frozen at -20 ºC after addition of methanol and acetic acid (10% of final volume for both). The samples were later analysed by HPLC analysis.

6.3.6.1. Evaluation of monolayer integrity: Transepithelial electrical resistance measurements (TEER)

TEER of 6-well Transwells monolayers was routinely measured before changing cell culture media. A Millicell-ERS volt ohmmeter (Millipore corporation, Massachusetts) was used to take the measurements as per the supplied instructions. TEER was expressed as $\Omega \cdot cm^2$ (or mohms·cm^2) and was calculated by subtracting the reading of the resistance of the supporting filter and multiplying obtained result by the surface area of the monolayer (4.5 cm^2). TEER measurements were performed before each transport experiment to ensure adequate monolayer integrity. The monolayers with TEER readings below the minimum level were discarded (below 180 ohms per cm^2).

6.3.7 HPLC analysis of cells absorption and transport samples

Samples collected from absorption and transport studies were firstly defrosted and sonicated for 10 minutes using a sonication bath. Samples were subsequently vortexed and centrifuged at 15000 rpm for 15 minutes. Supernatant was used for HPLC analysis. In this study, HPLC analysis was carried out in reverse phase with a Perkin Elmer (Whaltam, Massachussets, USA) high performance liquid chromatography having a Serier 200 isocratic pump, equipped with a Series 600 link interface and a Series 200 UV-VIS detector. TC-NAV (Perkin Elmer, Whaltam, Massachussets, USA) software was used to collect, integrate and analyse the chromatographic data. UV detection was carried out at 314 nm. A C18 150 x 4.6mm column Supelco Li-Chrospher, RP18 Sum was used. For the analysis, the mobile phase consisted of HPLC grade acetonitrile (MeCN)-phosphate buffer (40:60 v/v) adjusted to pH 3 with phosphoric acid, at an injection volume of 10 µL and a flow rate of 1 mL min-1. The retention time of piroxicam was approximately 5.2 minutes with this system. Linearity between absorbance and concentration was tested using external standards at various concentrations and the response was linear with a correlation coefficient r2 = 0.99595 (data shown in appendix), over the whole range of used concentrations. A standard stock solution

of piroxicam (0.7 mg/ml) in the mobile phase and a series of diluitions with concentration between 0.28 to 0.0007 mg/ml were prepared. Each sample was prepared in triplicate and analysed three times.

6.4 Results and discussion

6.4.1 Cell viability

Cytotoxicity studies were performed in order to identify the non-cytotoxic condition for the later absorption and transport studies, with particular regards to the suitable concentrations of agents, such as bile salts, should be used in the bio-relevant media. Previous studies reported FaSSIF to be compatible with Caco-2 cells, while FeSSIF was cytotoxic. [294] For this reason the cytotoxicities of the solutions containing piroxicam, HPMC, buffers pH 5 and pH 6.5, lecithin and NaTC with different concentrations were evaluated.

Table 6.1: LDH assay cytotoxicity results expressed as % of lysed cells (n=6)

Sample	Averaged cytotoxicity (%)	Standard deviation (%)
Buffer pH 6.5	3.88	2.29
Buffer pH 5	21.42	19.35
NaTC 15mM in DMEM	51.77	9.38
NaTC 3mM in DMEM	40.10	12.62
Spray dried HPMC (0.5 mg/ml) in DMEM	-0.11	2.03

As summarised in Table 6.1, the buffer pH 6.5 is slightly cytotoxic, as 3.88±2.29% cell died in two hours. The buffer pH 5 was even more cytotoxic and 21.42±19.25% of cells death was achieved in two hours. The higher cytotoxicity of acetate buffer is likely to be caused by its lower pH and higher osmolality (670mOsmol/kg) in comparison to phosphate buffer at pH 6.5 (270mOsmol/kg). Strong cytotoxicity was obtained for all NaTC solutions in DMEM, even at the lower concentration employed (3mM), confirming the cytotoxicity of bile salts possibly via membrane damage as described in literature. [296] HPMC was compatible with Caco-2 cells as no cytotoxic effect was observed. This is in agreement with literature data. [297]

In order to obtain a time profile of the progression of NaTC cytotoxicity and evaluate the possibility of using NaTC solution for shorter experiments, LDH cytotoxicity

test was repeated for the lower NaTC concentration (3mM) and cells viability was measured at regular time intervals. The results are shown in Table 6.2.

Table 6.2: LDH assay cytotoxicity results expressed as % of lysed cells (n=6)

Sample	Average cytotoxicity (%)	Standard deviation (%)
NaTC 3mM 15 minutes	25.30	2.76
NaTC 3mM 30 minutes	32.07	2.32
NaTC 3mM 60 minutes	32.23	9.05
NaTC 3mM 120 minutes	53.36	11.73

As shown by the results summarised in Table 6.2, 25.30±2.76% Caco-2 cells were already dead after 15 minutes exposure to NaTC 3mM in DMEM. Cytotoxicity reached the 32.23±9.05 % in one hour and the 53.36±11.73% in two hours, indicating that the suitable NaTC concentration of Caco-2 cell experiments with NaTC concentration should be below 3mM.

Table 6.3: LDH assay cytotoxicity results expressed as % of lysed cells (n=6)

Sample	Average cytotoxicity (%)	Standard deviation (%)
NaTC 0.3mM in DMEM	0.07	2.76
NaTC 0.6mM in DMEM	2.27	3.97
Lecithin 0.75mM in DMEM	0.28	2.16
FaSSIF	50.33	15.91
Spray dried HPMC:Piroxicam 4:1 in blank FaSSIF	37.17	7.79
Spray dried HPMC:Piroxicam 4:1 in FaSSIF	30.28	6.33

Results reported in Table 6.3 show that at very low concentration NaTC was not significantly cytotoxic. Lecithin was also shown to be compatible with Caco-2 cells as no significant cytotoxicity was observed for the solutions with lecithin concentration of 0.75mM which is the same concentration used in FaSSIF. On the contrary, FaSSIF itself was very cytotoxic, as 50% of Caco-2 cells death was observed after 2 hours of exposure to the media. Considering that lecithin was not toxic, such result can be attributed to NaTC (3mM) cell membrane damage. The high cytotoxicity obtained for FaSSIF is in disagreement with literature data, that reported compatibility of FaSSIF use in with Caco-2 cells experiments. [293,294] Moreover Patel et al suggested that bile salts cytotoxicity could be reduced by the

presence of lecithin, as phospholipids have been shown to protect cellular membrane from bile-salts damage. [298,299] However, in this study no decrease in NaTC cytotoxicity was observed in the presence of lecithin. Interestingly, the decrease of NaTC cytotoxic was observed in the presence of spray dried formulation. As shown in Tables 6.2 and 6.3, obtained cytotoxicity for spray dried HPMC:piroxicam 4:1 solid dispersion in blank FaSSIF was 37.17±7.79%, which is significantly lower than the cytotoxicity value obtained for NaTC 3mM in DMEM. Such decrease may be a consequence of the NaTC/HPMC interaction, which has previously been suggested to occur by NMR, interfacial tension (refer Chapter 4) and light scattering (Chapter 5) data in this study. The aggregation of NaTC with HPMC would decrease the amount of free NaTC which can interact with membrane lipids and cause the cellular membrane damage.

Table 6.4: CYTO-TOX GLO™ assay cytotoxicity results expressed as % of lysed cells (n=6)

Sample	Averaged cytotoxicity (%)	Standard deviation (%)
Piroxicam 0.4mg/ml in DMEM (Ethanol 2%)	3.69	0.95
NaTC 1mM in DMEM	11.61	7.05
NaTC 1.5mM in DMEM	21.41	3.86
NaTC 2mM in DMEM	36.17	6.98
Spray dried HPMC:Piroxicam 4:1 in DMEM	1.74	0.81
Spray dried HPMC:Piroxicam 4:1 in NaTC 1.5 mM DMEM	10.78	7.24

Further cytotoxicity studies were performed using Cyto-Tox Glo™ assay, with and without the presence of bovine serum, and the results are summarised in Tables 6.4 and 6.5. The cytotoxicity of piroxicam was reported in Table 6.4. At the used concentrations, the model drug showed very low cytotoxic effect on Caco-2 cells. For piroxicam solutions with increasing concentration of NaTC, significant cytotoxic effects on the cells monolayer were observed with 11.61±7.05, 21.41±3.86 and 36.17±6.98 % of cells death after two hours of treatment for the solutions containing NaTC 1, 1.5 and 2mM, respectively. The solution of spray dried HPMC:piroxicam 2:1 in DMEM was not cytotoxic. Interestingly, as already shown by LDH assay, the spray dried solid dispersion dissolved in NaTC 1.5mM (in DMEM) yielded a lower cytotoxicity value of 10.78±7.24 %. Therefore the cytotoxic effect of NaTC decreased of about 50 % in the presence of spray dried polymer, compared to the NaTC

1.5mM in DMEM without polymer. This result suggests again the possible occurrence of NaTC/HPMC interaction in the tested solution, which may play a protective role of cellular membrane from NaTC damage. It should be bear in mind that NMR and interfacial tension data indicated the occurrence of NaTC/HPMC aggregation for the samples with NaTC concentration above 3mM. But NMR and interfacial tension data were performed in acetate and phosphate buffers. DMEM used in the cell studies may affect the NaTC/HPMC aggregation and possibly change the CAC of the system. Therefore it is possible that CAC value was lowered in DMEM and consequently NaTC/HPMC interaction could take place at a lower NaTC concentration, such as 1.5mM. An investigation into the HPMC/NaTC aggregation in DMEM may help clarify this hypothesis.

Table 6.5: CYTO-TOX GLO™ assay cytotoxicity results expressed as % of lysed cells (n=6). Assay was perfomed in DMEM added with foetal serum.

Sample	Averaged cytotoxicity (%)	Standard deviation (%)
NaTC1.5mM in DMEM+serum	13.46	4.77
NaTC1.5mM in DMEM+serum	17.84	8.70
Spray dried HPMC:Piroxicam 4:1 in NaTC 1.5 mM DMEM+serum	12.36	1.76
Spray dried HPMC:Piroxicam 4:1 in NaTC 3 mM DMEM+serum	16.52	4.49
Spray dried HPMC:Piroxicam 4:1 in FaSSIF in DMEM+serum	10.66	1.84

Table 6.5 shows cytotoxicity results obtained for samples in DMEM added with foetal serum. The presence of serum showed significant impact on the cytotoxicity results. For all tested samples, the cytotoxicity was lowered compared to the results obtained in DMEM without serum. Such result suggests that the cell death may at least partially be due to the absence of proper conditions for cell maintenance during cytotoxicity experiments. Another possible indication is the possible interaction between NaTC and serum components. However the presence of such complex mixture of proteins would have made HPLC analysis less reliable, in particular for the UV detection. Therefore despite the lower cytotoxicity shown by the cell viability experiments in the presence of serum, drug uptake and transport studies were performed without the addition serum.

For transport and absorption studies the threshold of cytotoxicity was set as 25%. Therefore samples that yielded cytotoxicity values higher than 25% were not employed in Caco-2 cell monolayer experiments. In order to simplify media nomenclature NaTC 1.5mM

solutions at pH 5 and 6.5 were labelled as blank FeSSIF-2 and blank FaSSIF-2, respectively, while the same media in the presence of lecithin 0.75mM were labelled FeSSIF-2 and FaSSIF-2. These modified non-cytotoxic biorelevant media (with low NaTC concentration than FaSSIF and FeSSIF) were used in drug uptake and transport studies.

6.4.2 Piroxicam uptake studies

Piroxicam uptake studies using Caco-2 as model cell line were performed in order to evaluate the impact of polymers and the components in the biorelevant media used in this study on the passively drug absorption. [300] Firstly piroxicam uptake by Caco-2 in the media containing DMEM, acetate and phosphate buffers was assessed. The influence of NaTC on piroxicam absorption was investigated by studying the uptake of the drug solubilised in acetate and phosphate buffered NaTC 1.5mM solution. This concentration was chosen based on the cytotoxicity results. This NaTC concentration led to about 20% cell death, whereas higher concentration of NaTC led to much high cytotoxic effect on Caco-2 cells monolayers. The impact of spray drying formulation on the drug uptake was also investigated by performing absorption studies of spray dried HPMC:piroxicam 4:1 solid dispersions. Solid dispersions were solubilised in the acetate and phosphate buffers employed in steady state solubility and dissolution studies and in NaTC buffered solution with and without the presence of lecithin. The obtained results of above samples are shown in Figure 6.1.

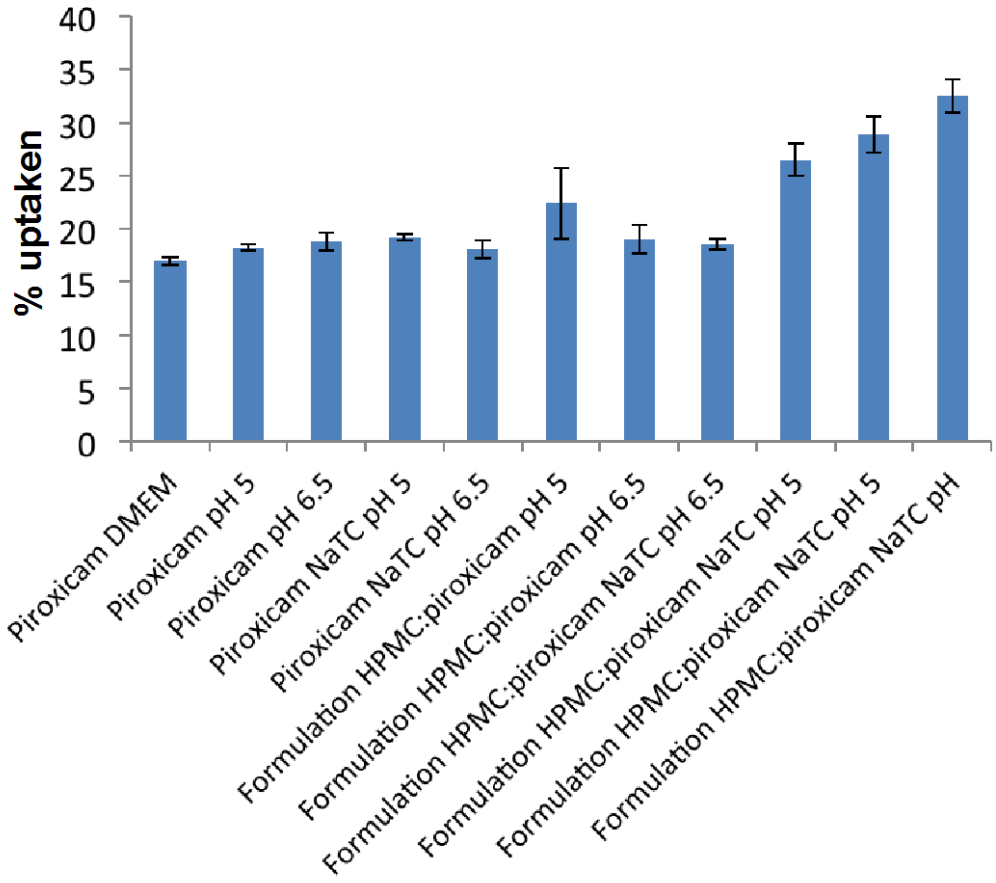

Figure 6.1: Caco-2 cellular uptake studies results for piroxicam in different media. (n=5)

It can be seen that 16.95±0.36 % of piroxicam in DMEM was absorbed by Caco-2 cells at the end of 2 hours testing period. No significant change in the drug absorption % was obtained for piroxicam in acetate (pH 5) and phosphate (pH 6.5) buffers, which yielded 18.17±0.31% and 18.74±0.84%, respectively. This result indicates that, despite the higher solubility of piroxicam in phosphate buffer shown by steady state solubility studies (Section 3.3.2.1, Chapter 3), *in vitro* cellular drug absorption was not affected by the pH of the media. The presence of NaTC 1.5mM did not lead to significant absorption increase, indicating low cell damage and little role NaTC played in enhancing drug absorption by Caco-2 cells. 19.22±0.35% and 18.06±0.85% of drug were absorbed from the buffer pH 5 piroxicam solution containing NaTC 1.5 mM and the buffer pH 6.5 piroxicam solution containing NaTC 1.5 mM, respectively. It is possible that NaTC solubilisation effect is not exerted at the concentration of 1.5 mM. Piroxicam absorption values obtained for spray dried formulation was 19.05±1.32% in buffer pH 6.5 and 22.38±3.31% in buffer pH 5. The solid dispersion formulation only showed slight impact on drug absorption and mainly for the samples in buffer pH5, despite the higher piroxicam solubility in phosphate buffer at pH 6.5.

Similar value of piroxicam absorption was obtained from spray dried HPMC:piroxicam 4:1 solid dispersion in blank FaSSIF-2, from which 18.49±0.5% of piroxicam was absorbed by Caco-2 cells monolayer. Higher drug absorption (26.44±1.52%) was obtained for the spray dried formulation in blank FeSSIF-2. The presence of lecithin in the solution showed a significant impact on piroxicam absorption. Piroxicam absorption reached 28.87±1.72% and 32.47±1.54%, when spray dried HPMC:piroxicam formulation was dissolved in FeSSIF-2 and FaSSIF-2, respectively. This is in good agreement with steady state solubility results that showed the highest piroxicam solubilisation in FaSSIF, confirming the potential contribution of enhanced solubility on drug absorption.

Uptake data are only partially in agreement with steady state solubility studies, suggesting that drug solubilisation is only one of the factors ruling drug absorption in the intestinal cells. The absorption values obtained from the spray dried formulation in buffer suggest that the formation of solid dispersion did not significantly facilitate the drug absorption. Solid-state analysis of spray dried formulation performed in Chapter 3 highlighted that the physical state of piroxicam in HPMC based spray dried solid dispersion was mainly amorphous. In literature, it is commonly agreed that the amorphous state of drugs usually favours drug solubilisation and consequent absorption. [33] Despite the higher piroxicam dissolution rate obtained in blank FaSSIF and blank FeSSIF (refer to Chapter 3, section 3.3.9), the results of this study indicate that the physical state of piroxicam is not the main determinant for its intestinal absorption. Moreover, the use of modified biorelevant media did not cause a significant increase in the drug uptake by Caco-2 cells. Enhanced drug absorption was instead obtained when the spray dried HPMC:piroxicam 4:1 formulation was dissolved in modified biorelevant media FaSSIF-2 and FeSSIF-2. Such results confirm the importance of using simulated intestinal fluids media in Caco-2 cells models experiments, as already stated in literature. [293,301]

The results of the absorption studies support the hypothesis that the occurrence of polymeric carrier/bile salts aggregation may play a role in the absorption of poorly water-soluble drugs in the GIT. The highest absorption of piroxicam was obtained when both polymeric carrier and simulated intestinal media were used in the tests. Lecithin resulted to be as well a key component of biorelevant media for improved piroxicam absorption, as well as for its solubilisation as shown in Chapter 3 (Section 3.3.2.1).

6.4.3 Piroxicam transport studies

The attempts of quantitatively studying piroxicam transport across Caco-2 cell monolayer were unsuccessful. Almost no signal could be measured by HPLC analysis, indicating a limited transport of the drug across the Caco-2 cells monolayer. Further studies are needed in order to confirm the results and further investigate piroxicam transport across the intestinal membrane applying Caco-2 cells model.

6.5 Conclusions

The results reported in this chapter confirmed piroxicam, polymeric carrier and lecithin are non-cytotoxic for Caco-2 cells, while high cytotoxicity was associated with the presence of bile salts. Different NaTC concentrations were tested to identify a possible concentration compatible with Caco-2 cells and 1.5 mM gave acceptable cytotoxicity value (≈ 20 %). Therefore biorelevant media were modified with reduced NaTC concentration for Caco-2 cells drug uptake and transport studies. Significant reduction of bile salts cytotoxic effect was obtained in the presence of HPMC. We speculate that this may be a consequence of HPMC/NaTC interaction, which reduces the interaction between NaTC and the cell membrane lipid and subsequently decreases the NaTC cytotoxicity.

Absorption studies showed higher piroxicam absorption from spray dried HPMC:piroxicam 4:1 formulation in FeSSIF-2 and FaSSIF-2. Obtained data proved the importance of biorelevant media employment in Caco-2 cells studies and also supported the indication of a possible interaction occurrence between polymeric carrier and biorelevant media components which may facilitate drug uptake.

Chapter 7. Conclusions

Solid dispersion technology represents one of the most researched formulation approaches for the delivery of poorly water-soluble drugs. [23,24,38,302] It can be argued that a general consensus has been reached about the ability of solid dispersion to increase the dissolution rate of drugs and potentially favour an improvement of their bioavailability. [303–305] In order to overcome possible limitations related to the use of solid dispersions, many efforts have been made in the last decades to improve the physical stability of solid dispersions and their *in vitro* dissolution performance. [306–308] The importance of *in vitro* dissolution tests has been extensively emphasised and its potential as bioavailability predictive tool has arose from many studies. [20,67,208,289] Despite the high number of publications in the field of solid dispersions, the mechanism of how solid dispersion formulation can enhance the bioavailability of poorly soluble drugs, particularly in in human intestinal fluid, is still not fully understood. This study focused on the characterisation of the physico-chemical behaviour the polymeric carriers of solid dispersion formulations in simulated intestinal media, in order to provide new insights into the role of these polymers in the drug solubilisation and absorption processes. Particular remark was given to the possible role of bile salts/polymer aggregates in the solubilisation and subsequent absorption of poorly water-soluble drugs in the intestinal tract.

7.1 Effects of drug physical state and dissolution media composition on the *in vitro* performance of solid dispersions

In Chapter 3 solid-state characterisation revealed conversion of the model drug from crystalline to amorphous state in the spray dried solid dispersions, with partial crystallinity of the model drugs in the solid dispersions having high drug content (33%). The steady state solubility studies of the model drugs performed in different biorelevant media revealed dramatic effects of the simulated fluids compositions on the apparent solubilities of the drugs. The importance of mimicking the physiological conditions by the use biorelevant fluids in solubility and dissolution studies has previously been highlighted in literature. [15,19,20] The results obtained in this study indicated remarkable impact of NaTC and lecithin on increasing the model drugs solubilisation, in both crystalline and amorphous forms. Highest apparent solubility values of the model drugs were obtained in FaSSIF and FeSSIF in the presence of the polymeric carriers. Such result suggested that both simulated fluids

components and polymeric carriers were possibly contributing to the drug solubilisation observed. This raised the question whether the effects were originating by the presences of the single components (bile salts, lecithin and polymeric carriers) or by an interaction between them.

Dissolution studies performed in media with and without the addition of NaTC demonstrated the primary effect of this model bile salt in drug solubilisation, particularly for piroxicam and fenofibrate. The type of polymer and the physical state of the model drugs also showed clear impacts on the dissolution behaviour of the solid dispersions. For HPMC based solid dispersions, fastest dissolution profile was obtained after spray drying, indicating the impact of the drug physical state conversion from crystalline to amorphous on the drug dissolution rate for such system. Differently, fastest dissolution rate was obtained from PVP:drug physical mixtures compared to the spray dried solid dispersions. The reason behind this observation is still not well understood. However, similar results have been reported previously. [309] The concomitant presence of polymeric carrier and surfactant in the dissolution media yielded the fastest dissolution profiles, the involvement of different chemical entities in the drug solubilisation process.

Chapter 3 provided strong evidences indicating the potential interactions between hydrophilic polymers and dissolution media compositions. This led to the proposal of the involvements of such interactions in drug solubilisation and dissolution processes. Therefore major focus of the next stage of study was directed to the investigation of polymeric carriers-bile salts interaction.

7.2 Polymer-bile salts interactions in simulated intestinal fluids

Chapter 4 and 5 described the investigation of NaTC-polymer interactions and the characterisation of the resulting polymer/bile salts aggregates. In particular NMR and interfacial tension studies reported in Chapter 4 focused on the characterisation of the possible polymer-NaTC interactions. The occurrence of NaTC-HPMC and NaTC-PVP aggregation was indicated in aqueous medium. Both NMR and interfacial tension results confirmed the important impact of salts on the surfactant-polymer aggregation, with a decrease in the CAC value for both systems, indicating possible facilitation of the occurrence of polymer-bile salts interactions by the presence of salts in the media. Obtained results indicated the occurrence of NaTC-HPMC and NaTC-PVP interactions in blank FeSSIF, suggesting during the dissolution of a PVP or HPMC based solid dispersion in blank FeSSIF, the formation of polymer-NaTC aggregates may occur. According to NMR

and interfacial tension data the presence of few free NaTC micelles is also possible. As CMC* (surfactant concentration value at which the formation of free micelles occurs in polymer/surfactant systems) resulted to be 15mM for both HPMC:NaTC and PVP:NaTC systems, both NaTC-polymer aggregates and NaTC micelles can be present in the blank FeSSIF media. Therefore different aggregates species may be involved in the solubilisation of the model drug.

For NMR and interfacial tensions studies performed in blank FaSSIF, the obtained results indicated the possible formation of only few NaTC-HPMC aggregates at low NaTC concentration, as CAC value of the system corresponded to NaTC concentration in the medium (3mM). No free NaTC micelles can be formed in blank FaSSIF, as NaTC concentration is well below CMC* of the system. Therefore the phase compositions of the solution of NaTC-PVP system in blank FaSSIF are likely to be mainly free NaTC molecules and free dissolved polymer. Considering the solution phase composition indicated by NMR and interfacial tension data, the increase in apparent solubility and dissolution rate of the model drugs obatained in blank FaSSIF, is likely to be mainly due to system surface tension reduction caused by NaTC monomer and to drug solubilisation through polymer aggregates. Therefore it is reasonable to predict that only a minor role was played by polymer/NaTC interaction in blank FaSSIF on drug solubilisation.

As described in Chapter 5, with high NaTC concentration in blank FeSSIF, significant numbers of aggregates were detected, while very limited aggregation was find to occur in blank FaSSIF. Therefore size and shape of NaTC/polymer aggregates and NaTC micelles were further studied by different light and neutron scattering techniques and cryo-TEM. Only minor role in the drug solubilisation can potentially be played by polymeric aggregates in blank FaSSIF, while a possible role of NaTC/polymer aggregates can be played in blank FeSSIF.DLS and Nanosight characterisations of PVP and HPMC based solid dispersion formulations solutions yielded similar results, with bigger aggregates formed in dissolved spray dried HPMC based solid dispersions in all the media employed.

Lecithin vesicles were clearly detected by light and neutron scattering methods in FaSSIF. The significant drug solubilisation increase obtained for piroxicam showed by steady state solubility studies (reported in Chapter 3) might be related to lecithin vesicles possible role in the drug solubilisation. In FeSSIF polymer aggregates and mixed NaTC/lecithin aggregates were possibly formed. As for FaSSIF, in FeSSIF much higher apparent solubility values were obtained for model drugs, compared to simple buffered media. Therefore the influence of employed medium phase solution composition on the model drugs solubilisation was again highlighted. Nevertheless composition of the dissolved

solution of spray dried solid dispersion in simulated intestinal media is extremely complex, due to the presence of many components and the possible occurrence of interaction between them. The complete clarification of each type of aggregate's possible role in the drug solubilisation therefore could not be made, but the combination of dissolution, steady state solubility studies and colloidal characterisation of solid dispersion formulation in biorelevant media employed in this study strongly suggested a possible key role of solid dispersion carrier/ media components on the drug solubilisation. Based on literature data, the nature of interaction between the polymeric carriers employed and NaTC is likely to be hydrophobic. [110] The nature of interaction was not the key point of this study, as it was mainly focused on the polymeric carriers/bile salts interaction and its possible drug solubilisation impact. Further studies might be useful to provide insights about the interaction driving forces.

7.3 Possible effects of polymer-bile salts aggregation on drug uptake

As discussed in Chapter 6, to investigate the effects of polymer-NaTC complexation on the drug absorption in the intestinal tract, Caco-2 cells were used to conduct the drug uptake studies. In order to understand the possible impact of biorelevant media components on the drug absorption by Caco-2 cells monolayer, media with increasing complexity were used. Model crystalline drug absorption resulted to be not influenced by the medium pH, and only slightly impacted by the presence of NaTC (which was 1.5mM in concentration to meet cell compatibility) and by the drug physical state. Indeed absorption studies performed on spray dried solid dispersion did not show significant drug uptake increase indicating minor role of drug amorphisation on drug absorption by Caco-2 cells. Moreover significant increase in the model drug absorption from spray dried HPMC:piroxicam 4:1 formulation was obtained for studies performed using FeSSIF-2 and FaSSIF-2 (modified media with NaTC concentration 1.5mM and lecithin concentration 0.75mM). Obtained data confirmed the importance of biorelevant media used in Caco-2 cells, which has increasingly been highlighted in literature.[294,299,301,310,311] Furthermore performed Caco-2 cells uptake studies supported the indication of a possible interaction occurrence between polymeric carrier and bio-relevant media components and the possible role of such interactions in enhancing the drug uptake of poorly water soluble drug in the intestinal tract. The proposed possible working mechanism of how spray dried solid dispersion formulations containing piroxicam can increase the dissolution rate, the solubility in simulated intestinal fluids and drug uptake via Caco-2 cells model is schematically illustrated in Figure 7.1

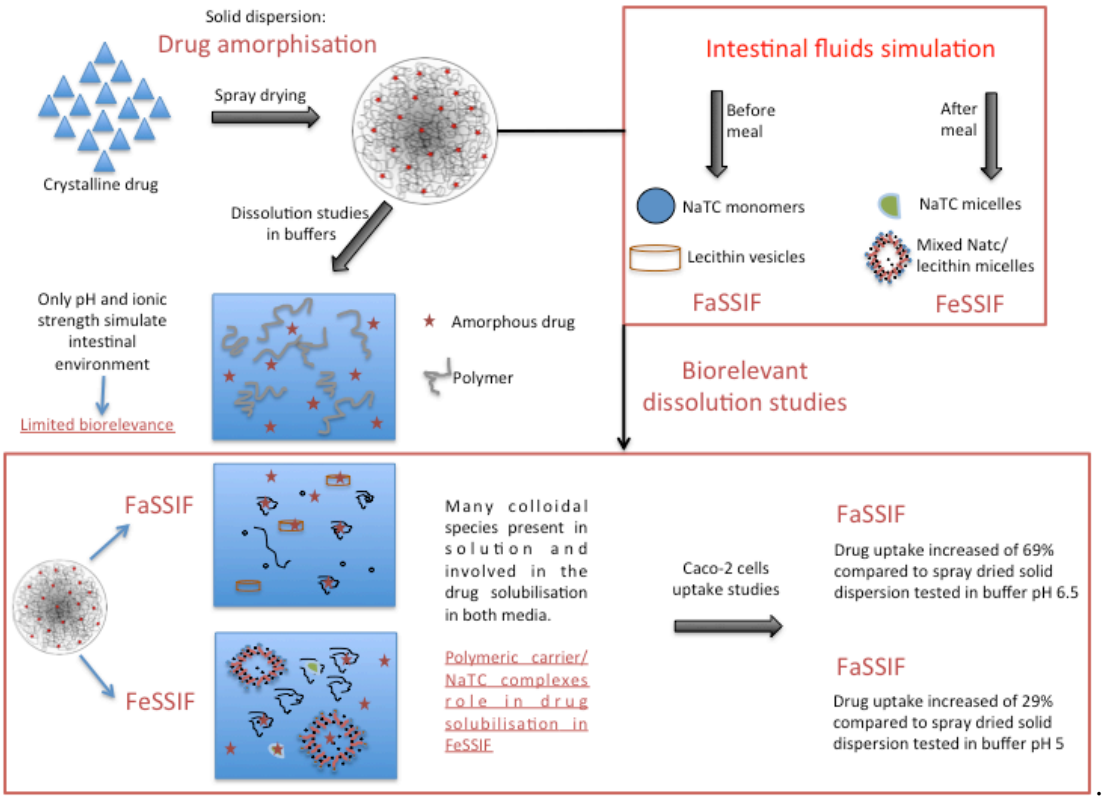

Figure 7.1: Schematic representation of the impact of polymer-NaTC complexation on the dissolution, solubilisation and intestinal uptake of model drug, piroxicam, delivered via spray dried solid dispersions.

7.4 Final remarks and future perspectives

This study highlighted the importance of molecular level investigation of the excipient-media interaction on understanding the dissolution and drug release behaviour of solid dispersion in bio-relevant conditions. The main aim of the project was to investigate whether interactions occurring between polymers used in solid dispersion preparation and intestinal fluids components may influence drug solubilisation and absorption in the intestine. Wide indication of polymer-bile salts interactions occurrence has been provided by different experiments and Caco-2 cells studies clearly showed a significant dependence of the drug uptake from the dissolution medium composition and drug formulation. Therefore it is possible to conclude that, in order to develop successful formulations of poorly water-soluble drugs, proper prediction of the formulation behaviour in the intestine represents a key factor to have effective *in vitro* prediction of drug solubilisation and absorption and possibly achieve good *in vitro/in vivo* correlation. A proper prediction of molecular

behaviour of polymer in simulating media can potentially provide a useful guide for the study of new solid dispersions formulations. Fuller understanding of the behaviour of polymeric carriers in bio-relevant condition can be used to highlight limitations and advantages of each carrier in terms of drug solubilisation enhancement in a bio-relevant environment.

This study provided new insights into the interactions of polymer and biorelevant surfactant post-dissolution of polymer based solid dispersions and the possible role of such interactions on the drug solubilisation and uptake. In order to confirm the findings of this study, the following further studies are required:

1. The further investigation of physical and chemical properties of polymer on the interactions with bile salts, by the use of more pharmaceutical polymers employed in the preparation of solid dispersions.

2. The study of polymeric carrier/bile salts interaction occurring in more updated simulating intestinal fluids, such as FaSSIF-2 and FeSSIF-2. These media are both prepared starting from maleate buffered solution, therefore their use might provide further information about the interaction occurrence between polymer and bile salts excluding the possible buffer species difference impact that might be present for FaSSIF and FeSSIF.

3. The study of the polymeric carrier interaction with bile salts, other intestinal fluids components and possible combination of more components in other conditions, such as gastric fluids, more complex biorelavent media and human intestinal fluids.

4. The study of polymeric carrier/GIT fluids components interaction impact, occurring in more complex media, on the drug transport across the intestinal media through Caco-2 cells.

Reference

1. Lipinski, C. A. Drug-like properties and the causes of poor solubility and poor permeability. *J. Pharmacol. Toxicol. Methods* **44,** 235–49 (2000).
2. Lipinski, C. A., Lombardo, F., Dominy, B. W. & Feeney, P. J. Experimental and computational approaches to estimate solubility and permeability in drug discovery and development settings. *Adv. Drug Deliv. Rev.* **46,** 3–26 (2001).
3. Pouton, C. W. Formulation of poorly water-soluble drugs for oral administration: physicochemical and physiological issues and the lipid formulation classification system. *Eur. J. Pharm. Sci.* **29,** 278–87 (2006).
4. Amidon, G. L., Lennernäs, H., Shah, V. P. & Crison, J. R. A theoretical basis for a biopharmaceutic drug classification: the correlation of in vitro drug product dissolution and in vivo bioavailability. *Pharm. Res.* **12,** 413–20 (1995).
5. Plakkot, S., de Matas, M., York, P., Saunders, M. & Sulaiman, B. Comminution of ibuprofen to produce nano-particles for rapid dissolution. *Int. J. Pharm.* **415,** 307–14 (2011).
6. Gwak, H.-S., Choi, J.-S. & Choi, H.-K. Enhanced bioavailability of piroxicam via salt formation with ethanolamines. *Int. J. Pharm.* **297,** 156–61 (2005).
7. Bunjes, H. Lipid nanoparticles for the delivery of poorly water-soluble drugs. *J. Pharm. Pharmacol.* **62,** 1637–45 (2010).
8. Basarab, G. S., Hill, P. J., Rastagar, A. & Webborn, P. J. H. Design of Helicobacter pylori glutamate racemase inhibitors as selective antibacterial agents: a novel pro-drug approach to increase exposure. *Bioorg. Med. Chem. Lett.* **18,** 4716–22 (2008).
9. Agüeros, M., Zabaleta, V., Espuelas, S., Campanero, M. A. & Irache, J. M. Increased oral bioavailability of paclitaxel by its encapsulation through complex formation with cyclodextrins in poly(anhydride) nanoparticles. *J. Control. Release* **145,** 2–8 (2010).
10. Abdalla, A., Klein, S. & Mäder, K. A new self-emulsifying drug delivery system (SEDDS) for poorly soluble drugs: characterization, dissolution, in vitro digestion and incorporation into solid pellets. *Eur. J. Pharm. Sci.* **35,** 457–64 (2008).
11. Leuner, C. Improving drug solubility for oral delivery using solid dispersions. *Eur. J. Pharm. Biopharm.* **50,** 47–60 (2000).
12. Van den Mooter, G., Weuts, I., De Ridder, T. & Blaton, N. Evaluation of Inutec SP1 as a new carrier in the formulation of solid dispersions for poorly soluble drugs. *Int. J. Pharm.* **316,** 1–6 (2006).
13. Yüksel, N. *et al.* Enhanced bioavailability of piroxicam using Gelucire 44/14 and Labrasol: in vitro and in vivo evaluation. *Eur. J. Pharm. Biopharm.* **56,** 453–459 (2003).
14. Sheen, P.-C., Khetarpal, V. K., Cariola, C. M. & Rowlings, C. E. Formulation studies of a poorly water-soluble drug in solid dispersions to improve bioavailability. *Int. J. Pharm.* **118,** 221–227 (1995).
15. Vertzoni, M. *et al.* Dissolution media simulating the intralumenal composition of the small intestine: physiological issues and practical aspects. *J. Pharm. Pharmacol.* **56,** 453–62 (2004).
16. Vertzoni, M., Dressman, J., Butler, J., Hempenstall, J. & Reppas, C. Simulation of fasting gastric conditions and its importance for the in vivo dissolution of lipophilic compounds. *Eur. J. Pharm. Biopharm.* **60,** 413–7 (2005).
17. Levis, K. A., Lane, M. E. & Corrigan, O. I. Effect of buffer media composition on the solubility and effective permeability coefficient of ibuprofen. *Int. J. Pharm.* **253,** 49–59 (2003).
18. McConnell, E. L., Fadda, H. M. & Basit, A. W. Gut instincts: explorations in intestinal physiology and drug delivery. *Int. J. Pharm.* **364,** 213–26 (2008).

19. Söderlind, E. *et al.* Simulating fasted human intestinal fluids: understanding the roles of lecithin and bile acids. *Mol. Pharm.* **7,** 1498–507 (2010).
20. Reppas, C. & Vertzoni, M. Biorelevant in-vitro performance testing of orally administered dosage forms. *J. Pharm. Pharmacol.* **64,** 919–30 (2012).
21. Kavanagh, N. & Corrigan, O. I. Swelling and erosion properties of hydroxypropylmethylcellulose (Hypromellose) matrices--influence of agitation rate and dissolution medium composition. *Int. J. Pharm.* **279,** 141–52 (2004).
22. Chiou, W. L. & Riegelman, S. Pharmaceutical applications of solid dispersion systems. *J. Pharm. Sci.* **60,** 1281–1302 (1971).
23. Serajuddin, A. T. Solid dispersion of poorly water-soluble drugs: early promises, subsequent problems, and recent breakthroughs. *J. Pharm. Sci.* **88,** 1058–66 (1999).
24. Vasconcelos, T., Sarmento, B. & Costa, P. Solid dispersions as strategy to improve oral bioavailability of poor water soluble drugs. *Drug Discov. Today* **12,** 1068–75 (2007).
25. Bevernage, J. *et al.* Excipient-mediated supersaturation stabilization in human intestinal fluids. *Mol. Pharm.* **8,** 564–70 (2011).
26. Bates, S. *et al.* Analysis of amorphous and nanocrystalline solids from their X-ray diffraction patterns. *Pharm. Res.* **23,** 2333–49 (2006).
27. Vippagunta, S. R., Wang, Z., Hornung, S. & Krill, S. L. Factors affecting the formation of eutectic solid dispersions and their dissolution behavior. *J. Pharm. Sci.* **96,** 294–304 (2007).
28. Sekiguchi, K. & Obi, N. Studies on Absorption of Eutectic Mixture. I. A Comparison of the Behavior of Eutectic Mixture of Sulfathiazole and that of Ordinary Sulfathiazole in Man. *Chem. Pharm. Bull. (Tokyo).* **9,** 866–872 (1961).
29. Goldberg, A. H., Gibaldi, M. & Kanig, J. L. Increasing dissolution rates and gastrointestinal absorption of drugsvia solid solutions and eutectic mixtures I. Theoretical considerations and discussion of the literature. *J. Pharm. Sci.* **54,** 1145–1148 (1965).
30. Park, Y.-J. *et al.* Development of novel itraconazole-loaded solid dispersion without crystalline change with improved bioavailability. *Arch. Pharm. Res.* **33,** 1217–25 (2010).
31. Yan, Y.-D. *et al.* Novel valsartan-loaded solid dispersion with enhanced bioavailability and no crystalline changes. *Int. J. Pharm.* **422,** 202–10 (2012).
32. Wunderlich, B. A classification of molecules, phases, and transitions as recognized by thermal analysis. *Thermochim. Acta* **340-341,** 37–52 (1999).
33. Hancock, B. C. & Zografi, G. Characteristics and significance of the amorphous state in pharmaceutical systems. *J. Pharm. Sci.* **86,** 1–12 (1997).
34. Alonzo, D. E., Zhang, G. G. Z., Zhou, D., Gao, Y. & Taylor, L. S. Understanding the behavior of amorphous pharmaceutical systems during dissolution. *Pharm. Res.* **27,** 608–18 (2010).
35. Ambike, A. A., Mahadik, K. R. & Paradkar, A. Spray-dried amorphous solid dispersions of simvastatin, a low tg drug: in vitro and in vivo evaluations. *Pharm Res* **22,** 990–998 (2005).
36. Six, K., Verreck, G., Peeters, J., Brewster, M. & Van Den Mooter, G. Increased physical stability and improved dissolution properties of itraconazole, a class II drug, by solid dispersions that combine fast- and slow-dissolving polymers. *J. Pharm. Sci.* **93,** 124–31 (2004).
37. Yamashita, K. *et al.* Establishment of new preparation method for solid dispersion formulation of tacrolimus. *Int. J. Pharm.* **267,** 79–91 (2003).
38. Williams, H. D. *et al.* Strategies to address low drug solubility in discovery and development. *Pharmacol. Rev.* **65,** 315–499 (2013).
39. Bhardwaj, S. P. *et al.* Correlation between molecular mobility and physical stability of amorphous itraconazole. *Mol. Pharm.* **10,** 694–700 (2013).

40. Baird, J. A., Van Eerdenbrugh, B. & Taylor, L. S. A classification system to assess the crystallization tendency of organic molecules from undercooled melts. *J. Pharm. Sci.* **99,** 3787–806 (2010).
41. Ahlneck, C. & Zografi, G. The molecular basis of moisture effects on the physical and chemical stability of drugs in the solid state. *Int. J. Pharm.* **62,** 87–95 (1990).
42. Konno, H., Handa, T., Alonzo, D. E. & Taylor, L. S. Effect of polymer type on the dissolution profile of amorphous solid dispersions containing felodipine. *Eur. J. Pharm. Biopharm.* **70,** 493–9 (2008).
43. Huang, Y. & Dai, W.-G. Fundamental aspects of solid dispersion technology for poorly soluble drugs. *Acta Pharm. Sin. B* **4,** 18–25 (2014).
44. Zhu, Q., Taylor, L. S. & Harris, M. T. Evaluation of the microstructure of semicrystalline solid dispersions. *Mol. Pharm.* **7,** 1291–300 (2010).
45. Cal, K. & Sollohub, K. Spray Drying Technique. I: Hardware and Process Parameters. *J Pharm Sci* **99,** 575–586 (2010).
46. Paudel, A., Worku, Z. A., Meeus, J., Guns, S. & Van den Mooter, G. Manufacturing of solid dispersions of poorly water soluble drugs by spray drying: formulation and process considerations. *Int. J. Pharm.* **453,** 253–84 (2013).
47. Sollohub, K. & Cal, K. Spray Drying Technique: II. Current Applications in Pharmaceutical Technology. *J Pharm Sci* **99,** 587–597 (2010).
48. Weuts, I. *et al.* Physicochemical properties of the amorphous drug, cast films, and spray dried powders to predict formulation probability of success for solid dispersions: etravirine. *J. Pharm. Sci.* **100,** 260–74 (2011).
49. Janssens, S. *et al.* Influence of preparation methods on solid state supersaturation of amorphous solid dispersions: a case study with itraconazole and eudragit e100. *Pharm. Res.* **27,** 775–85 (2010).
50. Ng, Y. C., Yang, Z., McAuley, W. J. & Qi, S. Stabilisation of amorphous drugs under high humidity using pharmaceutical thin films. *Eur. J. Pharm. Biopharm.* **84,** 555–65 (2013).
51. Qi, S., Moffat, J. G. & Yang, Z. Early stage phase separation in pharmaceutical solid dispersion thin films under high humidity: improved spatial understanding using probe-based thermal and spectroscopic nanocharacterization methods. *Mol. Pharm.* **10,** 918–30 (2013).
52. Usui, F. *et al.* Dissolution improvement of RS-8359 by the solid dispersion prepared by the solvent method. *Int. J. Pharm.* **170,** 247–256 (1998).
53. Sertsou, G., Butler, J., Hempenstall, J. & Rades, T. Solvent change co-precipitation with hydroxypropyl methylcellulose phthalate to improve dissolution characteristics of a poorly water-soluble drug. *J. Pharm. Pharmacol.* **54,** 1041–7 (2002).
54. Sertsou, G., Butler, J., Scott, A., Hempenstall, J. & Rades, T. Factors affecting incorporation of drug into solid solution with HPMCP during solvent change co-precipitation. *Int. J. Pharm.* **245,** 99–108 (2002).
55. Pearce, E. M. Introduction to polymer science and technology: An SPE text-book, Herman S. Kaufman and Joseph J. Falcetta, Eds., Wiley-Interscience, New York, 1977, 613 pp., $27.50. *J. Polym. Sci. Polym. Lett. Ed.* **16,** 55–55 (1978).
56. Crowley, M. M. *et al.* Pharmaceutical applications of hot-melt extrusion: part I. *Drug Dev. Ind. Pharm.* **33,** 909–26 (2007).
57. Repka, M. A. *et al.* Pharmaceutical Applications of Hot-Melt Extrusion: Part II. (2008). at <http://informahealthcare.com/doi/abs/10.1080/03639040701525627>
58. Radl, S., Tritthart, T. & Khinast, J. G. A novel design for hot-melt extrusion pelletizers. *Chem. Eng. Sci.* **65,** 1976–1988 (2010).
59. Willart, J. F. & Descamps, M. Solid state amorphization of pharmaceuticals. *Mol. Pharm.* **5,** 905–20 (2008).
60. Parrott, E. L. Milling of pharmaceutical solids. *J. Pharm. Sci.* **63,** 813–29 (1974).

61. Singh, S. K. *et al.* Investigation of preparation parameters of nanosuspension by top-down media milling to improve the dissolution of poorly water-soluble glyburide. *Eur. J. Pharm. Biopharm.* **78,** 441–6 (2011).
62. Otte, A., Zhang, Y., Carvajal, M. T. & Pinal, R. Milling induces disorder in crystalline griseofulvin and order in its amorphous counterpart. *CrystEngComm* **14,** 2560 (2012).
63. Pirttimäki, J., Laine, E., Ketolainen, J. & Paronen, P. Effects of grinding and compression on crystal structure of anhydrous caffeine. *Int. J. Pharm.* **95,** 93–99 (1993).
64. Newman, A. *Pharmaceutical Amorphous Solid Dispersions*. (Wiley, 2015). at <http://eu.wiley.com/WileyCDA/WileyTitle/productCd-1118455207.html>
65. Van den Mooter, G. *et al.* Physical stabilisation of amorphous ketoconazole in solid dispersions with polyvinylpyrrolidone K25. *Eur. J. Pharm. Sci.* **12,** 261–269 (2001).
66. Weuts, I. *et al.* Study of the physicochemical properties and stability of solid dispersions of loperamide and PEG6000 prepared by spray drying. *Eur. J. Pharm. Biopharm.* **59,** 119–126 (2005).
67. Dressman, J. B., Amidon, G. L., Reppas, C. & Shah, V. P. Dissolution Testing as a Prognostic Tool for Oral Drug Absorption: Immediate Release Dosage Forms. *Pharm. Res.* **15,** 11–22 (1998).
68. Noyes, A. A. & Whitney, W. R. THE RATE OF SOLUTION OF SOLID SUBSTANCES IN THEIR OWN SOLUTIONS. *J. Am. Chem. Soc.* **19,** 930–934 (1897).
69. Craig, D. Q. . The mechanisms of drug release from solid dispersions in water-soluble polymers. *Int. J. Pharm.* **231,** 131–144 (2002).
70. Kleberg, K., Jacobsen, J. & Müllertz, A. Characterising the behaviour of poorly water soluble drugs in the intestine: application of biorelevant media for solubility, dissolution and transport studies. *J. Pharm. Pharmacol.* **62,** 1656–68 (2010).
71. Klein, S. The use of biorelevant dissolution media to forecast the in vivo performance of a drug. *AAPS J.* **12,** 397–406 (2010).
72. Nicolaides, E., Galia, E., Efthymiopoulos, C., Dressman, J. B. & Reppas, C. Forecasting the In Vivo Performance of Four Low Solubility Drugs from Their In Vitro Dissolution Data. *Pharm. Res.* **16,** 1876–1882 (1999).
73. Nicolaides, E., Symillides, M., Dressman, J. B. & Reppas, C. Biorelevant Dissolution Testing to Predict the Plasma Profile of Lipophilic Drugs After Oral Administration. *Pharm. Res.* **18,** 380–388 (2001).
74. Kostewicz, E. S., Brauns, U., Becker, R. & Dressman, J. B. Forecasting the Oral Absorption Behavior of Poorly Soluble Weak Bases Using Solubility and Dissolution Studies in Biorelevant Media. *Pharm. Res.* **19,** 345–349 (2002).
75. Mithani, S. D., Bakatselou, V., TenHoor, C. N. & Dressman, J. B. Estimation of the Increase in Solubility of Drugs as a Function of Bile Salt Concentration. *Pharm. Res.* **13,** 163–167 (1996).
76. Jantratid, E., Janssen, N., Reppas, C. & Dressman, J. B. Dissolution media simulating conditions in the proximal human gastrointestinal tract: an update. *Pharm. Res.* **25,** 1663–76 (2008).
77. Fadda, H. & Basit, A. Dissolution of pH responsive formulations in media resembling intestinal fluids: Bicarbonate versus phosphate buffers. *J. Drug Deliv. Sci. Technol.* (2005). at <http://discovery.ucl.ac.uk/1367954/>
78. Varum, F. J. O. *et al.* Accelerating the dissolution of enteric coatings in the upper small intestine: evolution of a novel pH 5.6 bicarbonate buffer system to assess drug release. *Int. J. Pharm.* **468,** 172–7 (2014).
79. Badley, B. W. Bile salts. *Can. Med. Assoc. J.* **102,** 159–64 (1970).
80. Maldonado-Valderrama, J., Wilde, P., Macierzanka, A. & Mackie, A. The role of bile salts in digestion. *Adv. Colloid Interface Sci.* **165,** 36–46 (2011).

81. MUKHOPADHYAY, S. & MAITRA, U. Chemistry and biology of bile acids. *Curr. Sci.* **87,** 1666–1683 (2004).
82. Stamp, D. & Jenkins, G. *Bile Acids*. (Royal Society of Chemistry, 2008). doi:10.1039/9781847558336
83. Dawson, P. A., Lan, T. & Rao, A. Bile acid transporters. *J. Lipid Res.* **50,** 2340–57 (2009).
84. Garidel, P., Hildebrand, A., Neubert, R. & Blume, A. Thermodynamic Characterization of Bile Salt Aggregation as a Function of Temperature and Ionic Strength Using Isothermal Titration Calorimetry. *Langmuir* **16,** 5267–5275 (2000).
85. Madenci, D. & Egelhaaf, S. U. Self-assembly in aqueous bile salt solutions. *Curr. Opin. Colloid Interface Sci.* **15,** 109–115 (2010).
86. Amenitsch, H., Edlund, H., Khan, A., Marques, E. F. & La Mesa, C. Bile salts form lyotropic liquid crystals. *Colloids Surfaces A Physicochem. Eng. Asp.* **213,** 79–92 (2003).
87. DONALD M. SMALL. *Molecular Association in Biological and Related Systems*. **84,** (AMERICAN CHEMICAL SOCIETY, 1968).
88. Funasaki, N. *et al.* Micelle formation of bile salts and zwitterionic derivative as studied by two-dimensional NMR spectroscopy. *Chem Phys Lipids* **142,** 43–57 (2006).
89. Pártay, L. B., Jedlovszky, P. & Sega, M. Molecular aggregates in aqueous solutions of bile acid salts. Molecular dynamics simulation study. *J. Phys. Chem. B* **111,** 9886–96 (2007).
90. Warren, D. B., Chalmers, D. K., Hutchison, K., Dang, W. & Pouton, C. W. Molecular dynamics simulations of spontaneous bile salt aggregation. *Colloids Surfaces A Physicochem. Eng. Asp.* **280,** 182–193 (2006).
91. Kawamura, H. *et al.* Spin-label studies of bile salt micelles. *J. Phys. Chem.* **93,** 3321–3326 (1989).
92. Mazer, N. A., Carey, M. C., Kwasnick, R. F. & Benedek, G. B. Quasielastic light scattering studies of aqueous biliary lipid systems. Size, shape, and thermodynamics of bile salt micelles. *Biochemistry* **18,** 3064–3075 (1979).
93. Janich, M., Lange, J., Graener, H. & Neubert, R. Extended Light Scattering Investigations on Dihydroxy Bile Salt Micelles in Low-Salt Aqueous Solutions. *J. Phys. Chem. B* **102,** 5957–5962 (1998).
94. Hofmann, A. F. & Small, D. M. Detergent properties of bile salts: correlation with physiological function. *Annu. Rev. Med.* **18,** 333–76 (1967).
95. Charman, W. N., Porter, C. J., Mithani, S. & Dressman, J. B. Physiochemical and physiological mechanisms for the effects of food on drug absorption: the role of lipids and pH. *J. Pharm. Sci.* **86,** 269–82 (1997).
96. Bakatselou, V., Oppenheim, R. C. & Dressman, J. B. Solubilization and Wetting Effects of Bile Salts on the Dissolution of Steroids. *Pharm. Res.* **8,** 1461–1469 (1991).
97. Bell, C. G., Breward, C. J. W., Howell, P. D., Penfold, J. & Thomas, R. K. Macroscopic modeling of the surface tension of polymer-surfactant systems. *Langmuir* **23,** 6042–52 (2007).
98. Goddard, E. D. Polymer/Surfactant Interaction: Interfacial Aspects. *J. Colloid Interface Sci.* **256,** 228–235 (2002).
99. Goddard, E. D. & Hannan, R. B. Polymer/surfactant interactions. *J. Am. Oil Chem. Soc.* **54,** 561–566 (1977).
100. Hansson, P. & Lindman, B. Surfactant-polymer interactions. *Curr. Opin. Colloid Interface Sci.* **1,** 604–613 (1996).
101. Goddard, E. D. Polymer—surfactant interaction Part I. uncharged water-soluble polymers and charged surfactants. *Colloids and Surfaces* **19,** 255–300 (1986).

102. Piculell, L., Guillemet, F., Thuresson, K., Shubin, V. & Ericsson, O. Binding of surfactants to hydrophobically modified polymers. *Adv. Colloid Interface Sci.* **63,** 1–21 (1996).
103. Carlsson, A., Karlstroem, G. & Lindman, B. Characterization of the interaction between a nonionic polymer and a cationic surfactant by the Fourier transform NMR self-diffusion technique. *J. Phys. Chem.* **93,** 3673–3677 (1989).
104. Brackman, J. C. & Engberts, J. B. F. N. Influence of polymers on the micellization of cetyltrimethylammonium salts. *Langmuir* **7,** 2097–2102 (1991).
105. Brackman, J. C. & Engberts, J. B. F. N. Polymer-micelle interactions: physical organic aspects. *Chem. Soc. Rev.* **22,** 85 (1993).
106. Bain, C. D. *et al.* Complexes of surfactants with oppositely charged polymers at surfaces and in bulk. *Adv. Colloid Interface Sci.* **155,** 32–49 (2010).
107. Bárány, S. Interaction between water soluble polymers and surfactants. *Macromol. Symp.* **166,** 71–92 (2001).
108. Ruckenstein, E., Huber, G. & Hoffmann, H. Surfactant aggregation in the presence of polymers. *Langmuir* **3,** 382–387 (1987).
109. Tharwat F. Tadros, T. F. T. *Applied surfactants: principles and applications.* (Wiley, 2005).
110. Holmberg, K., Jönsson, B., Kronberg, B. & Lindman, B. Surfactants and polymers in aqueous solution. *J. Synth. Lu-brication* **20,** 367–370 (2004).
111. Abe, M. *Mixed surfactant systems*. (CRC Press, 2010).
112. Purcell, I. P., Lu, J. R., Thomas, R. K., Howe, A. M. & Penfold, J. Adsorption of Sodium Dodecyl Sulfate at the Surface of Aqueous Solutions of Poly(vinylpyrrolidone) Studied by Neutron Reflection. *Langmuir* **14,** 1637–1645 (1998).
113. Taylor, D. J. F., Thomas, R. K. & Penfold, J. Polymer/surfactant interactions at the air/water interface. *Adv. Colloid Interface Sci.* **132,** 69–110 (2007).
114. Holmberg, K., Jonsson, B. Kronberg, B., Lindman, B. *Surfactants and Polymers in Aqueous Solutions*. (Wiley, 2003).
115. Myers, D. *Surfactant Science and Technology*. **2005,** (2005).
116. Tadros, T. F. Physical chemistry of surfactant solutions. *Appl. Surfactants Princ. Appl.* 19–51 (2005).
117. Tam, K. C. & Wyn-Jones, E. Insights on polymer surfactant complex structures during the binding of surfactants to polymers as measured by equilibrium and structural techniques. *Chem. Soc. Rev.* **35,** 693–709 (2006).
118. Beheshti, N., Zhu, K., Kjøniksen, A.-L. & Nyström, B. Interaction behaviors in aqueous solutions of negatively and positively charged hydrophobically modified hydroxyethylcellulose in the presence of an anionic surfactant. *Colloids Surfaces A Physicochem. Eng. Asp.* **328,** 79–89 (2008).
119. La Mesa, C. Binding of surfactants onto polymers: a kinetic model. *Colloids Surfaces A Physicochem. Eng. Asp.* **160,** 37–46 (1999).
120. Thuresson, K., Lindman, B. & Nyström, B. Effect of Hydrophobic Modification of a Nonionic Cellulose Derivative on the Interaction with Surfactants. Rheology. *J. Phys. Chem. B* **101,** 6450–6459 (1997).
121. Anthony, O. & Zana, R. Interactions between Water-Soluble Polymers and Surfactants: Effect of the Polymer Hydrophobicity. 1. Hydrophilic Polyelectrolytes. *Langmuir* **12,** 1967–1975 (1996).
122. Anthony, O. & Zana, R. Interactions between Water-Soluble Polymers and Surfactants: Effect of the Polymer Hydrophobicity. 2. Amphiphilic Polyelectrolytes (Polysoaps). *Langmuir* **12,** 3590–3597 (1996).
123. Mészaros, R., Varga, I. & Gilanyi, T. Effect of polymer molecular weight on the polymer/surfactant interaction. *J. Phys. Chem. B* **109,** 13538–44 (2005).

124. Brackman, J. C. & Engberts, J. B. F. N. Effect of surfactant charge on polymer-micelle interactions: n-dodecyldimethylamine oxide. *Langmuir* **8,** 424–428 (1992).
125. Yan, P. & Xiao, J.-X. Polymer–surfactant interaction: differences between alkyl sulfate and alkyl sulfonate. *Colloids Surfaces A Physicochem. Eng. Asp.* **244,** 39–44 (2004).
126. Taylor, D. J. F., Thomas, R. K., Hines, J. D., Humphreys, K. & Penfold, J. The Adsorption of Oppositely Charged Polyelectrolyte/Surfactant Mixtures at the Air/Water Interface: Neutron Reflection from Dodecyl Trimethylammonium Bromide/Sodium Poly(styrene sulfonate) and Sodium Dodecyl Sulfate/Poly(vinyl pyridinium chloride). *Langmuir* **18,** 9783–9791 (2002).
127. Wallin, T. & Linse, P. Monte Carlo simulations of polyelectrolytes at charged micelles. 1. Effects of chain flexibility. *Langmuir* **12,** 305–314 (1996).
128. Thongngam, M. & McClements, D. J. Influence of pH, ionic strength, and temperature on self-association and interactions of sodium dodecyl sulfate in the absence and presence of chitosan. *Langmuir* **21,** 79–86 (2005).
129. Bell, C. G., Breward, C. J. W., Howell, P. D., Penfold, J. & Thomas, R. K. A theoretical analysis of the surface tension profiles of strongly interacting polymer-surfactant systems. *J. Colloid Interface Sci.* **350,** 486–93 (2010).
130. Macdonald, P. M., Staring, D. & Yue, Y. Polyelectrolyte binding to ionic surfactant micelles observed using deuterium NMR. *Langmuir* **9,** 381–384 (1993).
131. Monduzzi, M. NMR of Liquid Crystals and Micellar Solutions. *Nucl. Magn. Reson.* **32,** (2003).
132. Hammarström, A. & Sundelöf, L.-O. NMR study of polymer surfactant interaction in the system HPMC/SDS/water. *Colloid Polym. Sci.* **271,** 1129–1133 (1993).
133. Proietti, N., Amato, M. E., Masci, G. & Segre, A. L. Polyelectrolyte/Surfactant Interaction: An NMR Characterization. *Macromolecules* **35,** 4365–4372 (2002).
134. Veggeland, K. & Nilsson, S. Polymer-Surfactant Interactions Studied by Phase Behavior, GPC, and NMR. *Langmuir* **11,** 1885–1892 (1995).
135. Fundin, J. & Brown, W. Polymer/Surfactant Interactions. Sodium Poly(styrene sulfonate) and CTAB Complex Formation. Light Scattering Measurements in Dilute Aqueous Solution. *Macromolecules* **27,** 5024–5031 (1994).
136. Brown, W., Fundin, J. & Miguel, M. da G. Poly(ethylene oxide)-sodium dodecyl sulfate interactions studied using static and dynamic light scattering. *Macromolecules* **25,** 7192–7198 (1992).
137. Lee, L.-T. Polymer–surfactant interactions: neutron scattering and reflectivity. *Curr. Opin. Colloid Interface Sci.* **4,** 205–213 (1999).
138. Mears, S. J., Deng, Y., Cosgrove, T. & Pelton, R. Structure of Sodium Dodecyl Sulfate Bound to a Poly(NIPAM) Microgel Particle. *Langmuir* **13,** 1901–1906 (1997).
139. Cabane, B., Lindell, K., Engström, S. & Lindman, B. Microphase Separation in Polymer + Surfactant Systems †. *Macromolecules* **29,** 3188–3197 (1996).
140. Lindell, K. & Cabane, B. Structures of Physical Gels in the EHEC−SDS−Water System †. *Langmuir* **14,** 6361–6370 (1998).
141. Cabane, B. & Duplessix, R. Organization of surfactant micelles adsorbed on a polymer molecule in water : a neutron scattering study. *J. Phys.* **43,** 1529–1542 (1982).
142. Cabane, B. & Duplessix, R. Neutron scattering study of water-soluble polymers adsorbed on surfactant micelles. *Colloids and Surfaces* **13,** 19–33 (1985).
143. Kuntsche, J., Horst, J. C. & Bunjes, H. Cryogenic transmission electron microscopy (cryo-TEM) for studying the morphology of colloidal drug delivery systems. *Int. J. Pharm.* **417,** 120–37 (2011).

144. Goldraich, M., Schwartz, J. R., Burns, J. L. & Talmon, Y. Microstructures formed in a mixed system of a cationic polymer and an anionic surfactant. *Colloids Surfaces A Physicochem. Eng. Asp.* **125,** 231–244 (1997).
145. Zheng, Y. & Davis, H. T. Mixed Micelles of Nonionic Surfactants and Uncharged Block Copolymers in Aqueous Solutions: Microstructure Seen by Cryo-TEM. *Langmuir* **16,** 6453–6459 (2000).
146. Müllertz, A., Fatouros, D. G., Smith, J. R., Vertzoni, M. & Reppas, C. Insights into intermediate phases of human intestinal fluids visualized by atomic force microscopy and cryo-transmission electron microscopy ex vivo. *Mol. Pharm.* **9,** 237–47 (2012).
147. Sethia, S. & Squillante, E. Solid dispersion of carbamazepine in PVP K30 by conventional solvent evaporation and supercritical methods. *Int. J. Pharm.* **272,** 1–10 (2004).
148. Lee, J. H. *et al.* Enhanced dissolution rate of celecoxib using PVP and/or HPMC-based solid dispersions prepared by spray drying method. *J. Pharm. Investig.* **43,** 205–213 (2013).
149. KIM, E. *et al.* Preparation of a solid dispersion of felodipine using a solvent wetting method. *Eur. J. Pharm. Biopharm.* **64,** 200–205 (2006).
150. Nilsson, S. Interactions between Water-Soluble Cellulose Derivatives and Surfactants. 1. The HPMC/SDS/Water System. *Macromolecules* **28,** 7837–7844 (1995).
151. Froehner, S. J., Belarmino, A. & Zanette, D. The role of the counterion in poly(ethylene oxide)-dodecyl sulfate interactions. *Colloids Surfaces A Physicochem. Eng. Asp.* **137,** 131–139 (1998).
152. Oliveira, C. P. *et al.* The effect of water-soluble polymers, PEG and PVP, on the solubilisation of griseofulvin in aqueous micellar solutions of Pluronic F127. *Int. J. Pharm.* **421,** 252–257 (2011).
153. Yu, L. Amorphous pharmaceutical solids: preparation, characterization and stabilization. *Adv Drug Deliv Rev* **48,** 27–42 (2001).
154. Lombardino, J. G., Wiseman, E. H. & Chiaini, J. Potent antiinflammatory N-heterocyclic 3-carboxamides of 4-hydroxy-2-methyl-2H-1,2-benzothiazine 1,1-dioxide. *J. Med. Chem.* **16,** 493–496 (1973).
155. Law, D. *et al.* Properties of rapidly dissolving eutectic mixtures of poly(ethylene glycol) and fenofibrate: the eutectic microstructure. *J. Pharm. Sci.* **92,** 505–15 (2003).
156. Dutta, P. & Dey, J. Drug solubilization by amino acid based polymeric nanoparticles: Characterization and biocompatibility studies. *Int. J. Pharm.* **421,** 353–363 (2011).
157. Sotomayor, R. G., Holguín, A. R., Cristancho, D. M., Delgado, D. R. & Martínez, F. Extended Hildebrand Solubility Approach applied to piroxicam in ethanol+water mixtures. *J. Mol. Liq.* **180,** 34–38 (2013).
158. Sköld, C. *et al.* Presentation of a structurally diverse and commercially available drug data set for correlation and benchmarking studies. *J. Med. Chem.* **49,** 6660–71 (2006).
159. Hollósy, F. *et al.* Estimation of volume of distribution in humans from high throughput HPLC-based measurements of human serum albumin binding and immobilized artificial membrane partitioning. *J. Med. Chem.* **49,** 6958–71 (2006).
160. Guichard, J. P., Blouquin, P. & Qing, Y. A New Formulation of Fenofibrate: Suprabioavailable Tablets. (2008). at <http://informahealthcare.com/doi/abs/10.1185/0300799009117017>
161. Rinaki, E., Valsami, G. & Macheras, P. Quantitative Biopharmaceutics Classification System: The Central Role of Dose/Solubility Ratio. *Pharm. Res.* **20,** 1917–1925 (2003).
162. Dodds, J. *et al.* Structure and properties of ibuprofen–hydroxypropyl methylcellulose nanocomposite gel. *Powder Technol.* **190,** 221–224 (2009).

163. Ford, J. L. Thermal analysis of hydroxypropylmethylcellulose and methylcellulose: powders, gels and matrix tablets. *Int. J. Pharm.* **179,** 209–228 (1999).
164. Siepmann, J. Modeling of drug release from delivery systems based on hydroxypropyl methylcellulose (HPMC). *Adv. Drug Deliv. Rev.* **48,** 139–157 (2001).
165. Ma, D. *et al.* Development of a HPMC-based controlled release formulation with hot melt extrusion (HME). *Drug Dev. Ind. Pharm.* **39,** 1070–83 (2013).
166. Bühler, V. *Kollidon® Polyvinylpyrrolidone excipients for the pharmaceutical industry*. (2008).
167. Kvamme, B. B., Husey, G. & Forrisdahal, O. K. Molecular dynamics simulations of PVP kinetic inhibitor in liquid water and hydrate/liquid water systems. *Mol. Phys.* **90,** 979–992 (1997).
168. Tantishaiyakul, V., Kaewnopparat, N. & Ingkatawornwong, S. Properties of solid dispersions of piroxicam in polyvinylpyrrolidone K-30. *Int. J. Pharm.* **143,** 59–66 (1996).
169. Dong, Z. & Choi, D. S. Hydroxypropyl methylcellulose acetate succinate: potential drug-excipient incompatibility. *AAPS PharmSciTech* **9,** 991–7 (2008).
170. Tanno, F., Nishiyama, Y., Kokubo, H. & Obara, S. Evaluation of Hypromellose Acetate Succinate (HPMCAS) as a Carrier in Solid Dispersions. (2004). at <http://informahealthcare.com/doi/abs/10.1081/DDC-120027506>
171. Konno, H. & Taylor, L. S. Influence of different polymers on the crystallization tendency of molecularly dispersed amorphous felodipine. *J. Pharm. Sci.* **95,** 2692–705 (2006).
172. Shin-Etsu AQOA. at <http://www.elementoorganika.ru/files/aqoat.pdf>
173. Murugesan, R. & Orsat, V. Spray Drying for the Production of Nutraceutical Ingredients-A Review. *Food Bioprocess Technol.* **5,** 3–14 (2012).
174. Peighambardoust, S. H., Tafti, A. G. & Hesari, J. Application of spray drying for preservation of lactic acid starter cultures: a review. *Trends Food Sci. Technol.* **22,** 215–224 (2011).
175. Vega-Mercado, H., Marcela Góngora-Nieto, M. & Barbosa-Cánovas, G. V. Advances in dehydration of foods. *J. Food Eng.* **49,** 271–289 (2001).
176. Amelinckx Dirk; van Landuyt, J.; van Tendeloo, Gustaaf, S. . van D. *Electron Microscopy: Principles and Fundamentals*. (Wiley, 2008).
177. Vernon-Parry, K. D. Scanning Electron Microscopy: an introduction. *III-Vs Rev.* **13,** 5 (2000).
178. Paradkar, A., Ambike, A. A., Jadhav, B. K. & Mahadik, K. R. Characterization of curcumin-PVP solid dispersion obtained by spray drying. *Int. J. Pharm.* **271,** 281–286 (2004).
179. Harris, K. D. M., Tremayne, M. & Kariuki, B. M. Contemporary advances in the use of powder X-ray diffraction for structure determination. *Angew. Chemie-International Ed.* **40,** 1626–1651 (2001).
180. Bandyopadhyay, R., Selbo, J., Amidon, G. E. & Hawley, M. Application of powder X-ray diffraction in studying the compaction Behavior of bulk pharmaceutical powders. *J Pharm Sci* **94,** 2520–2530 (2005).
181. Bates, S. *et al.* Analysis of amorphous and nanocrystalline solids from their X-ray diffraction patterns. *Pharm. Res.* **23,** 2333–2349 (2006).
182. D.Q.M. Craig, M. R. & M.Reading, D. Q. M. C. and. *Thermal Analysis of Pharmaceuticals*. (CRC Press Taylor &Francis Group, 2007).
183. Baird, J. A. & Taylor, L. S. Evaluation of amorphous solid dispersion properties using thermal analysis techniques. *Adv. Drug Deliv. Rev.* **64,** 396–421 (2012).
184. Coats, A. W. & Redfern, J. P. Thermogravimetric Analysis. *Analyst* **88,** 906–& (1963).
185. Smith, B. C. *Fundamentals of Fourier Transformed Infrared Spectroscopy*. (CRC Press, 2011).

186. Vippagunta, S. R., Maul, K. A., Tallavajhala, S. & Grant, D. J. W. Solid-state characterization of nifedipine solid dispersions. *Int. J. Pharm.* **236,** 111–123 (2002).
187. Forster, A., Hempenstall, J. & Rades, T. Characterization of glass solutions of poorly water-soluble drugs produced by melt extrusion with hydrophilic amorphous polymers. *J. Pharm. Pharmacol.* **53,** 303–315 (2001).
188. Hornak, J. P. The basic of NMR. (1997).
189. Price, W. S. Pulsed-Field Gradient Nuclear Magnetic Resonance as a Tool for Studying Translational Diffusion:Part 1. basic Theory. *Concepts Magn. Reson.* **9,** 299–336 (1997).
190. *Surface and Colloid Science*. (Springer US, 1979). doi:10.1007/978-1-4615-7969-4
191. Woodward, P. oger. Contact Angle Measurements Using the Drop Shape Method. *http://www.firsttenangstroms.com* at <http://www.firsttenangstroms.com>
192. Chang, C.-H. & Franses, E. I. Adsorption dynamics of surfactants at the air/water interface: a critical review of mathematical models, data, and mechanisms. *Colloids Surfaces A Physicochem. Eng. Asp.* **100,** 1–45 (1995).
193. Berne J.B., P. R. *Dynamic Light Scattering: With Applications to Chemistry, Biology, and Physics*. (Courier Dover Publications, 2000).
194. Pecora, R. *Dynamic Light Scattering: Applications of Photon Correlation Spectroscopy*. (Springer, 1985).
195. Bombelli, F. B., Berti, D., Almgren, M., Karlsson, G. & Baglioni, P. Light scattering and cryo-transmission electron microscopy investigation of the self-assembling behavior of Di-C12P-nucleosides in solution. *J. Phys. Chem. B* **110,** 17627–37 (2006).
196. Carr B., W. M. Nanoparticle Tracking Analysis. (2013).
197. Sivia, D. S. *Elementary Scattering Theory*. (Oxford UNIVERSITY PRESS, 2011).
198. *Neutron Imaging and Applications*. (Springer US, 2009). doi:10.1007/978-0-387-78693-3
199. Grillo, I. in *Soft Matter Charact. SE - 13* (Borsali, R. & Pecora, R.) 723–782 (Springer Netherlands, 2008). doi:10.1007/978-1-4020-4465-6_13
200. Rogers, S. E. in *ISIS Neutron Train. Course Man.*
201. Ay, M. *et al.* Real-space neutron scattering methods. *Nucl. Instruments Methods Phys. Res. Sect. A Accel. Spectrometers, Detect. Assoc. Equip.* **586,** 9–14 (2008).
202. Almgren, M., Edwards, K. & Karlsson, G. Cryo transmission electron microscopy of liposomes and related structures. *Colloids Surfaces A Physicochem. Eng. Asp.* **174,** 3–21 (2000).
203. Vinson, P. ., Bellare, J. ., Davis, H. ., Miller, W. . & Scriven, L. . Direct imaging of surfactant micelles, vesicles, discs, and ripple phase structures by cryo-transmission electron microscopy. *J. Colloid Interface Sci.* **142,** 74–91 (1991).
204. Grass, G. M. Simulation models to predict oral drug absorption from in vitro data. *Adv. Drug Deliv. Rev.* **23,** 199–219 (1997).
205. Volpe, D. A. Application of method suitability for drug permeability classification. *AAPS J.* **12,** 670–8 (2010).
206. Hilde Bohets, B. S. P. *et al.* Strategies for Absorption Screening in Drug Discovery and Development. *Curr. Top. Med. Chem.* **1,** 367–383 (2001).
207. Snyder, L. R., Kirkland, J. J. & Dolan, J. W. *Introduction to Modern Liquid Chromatography (Google eBook)*. (John Wiley & Sons, 2011). at <http://books.google.com/books?id=taurNJu0u2AC&pgis=1>
208. Kogermann, K. *et al.* Dissolution testing of amorphous solid dispersions. *Int. J. Pharm.* **444,** 40–6 (2013).
209. Choi, Y. K. *et al.* Enhanced solubility and oral bioavailability of itraconazole by combining membrane emulsification and spray drying technique. *Int. J. Pharm.* **434,** 264–71 (2012).

210. Siepmann, J. *et al.* Manufacturing of solid dispersions of poorly water soluble drugs by spray drying: Formulation and process considerations. *Int. J. Pharm.* **453,** 253–284 (2013).
211. Marques, M. Dissolution media simulating fasted and fed states.
212. Karataş, A., Yüksel, N. & Baykara, T. Improved solubility and dissolution rate of piroxicam using gelucire 44/14 and labrasol. *Farmaco* **60,** 777–82 (2005).
213. Shankland, W. The equilibrium and structure of lecithin-cholate mixed micelles. *Chem. Phys. Lipids* **4,** 109–130 (1970).
214. Pedersen, J. S., Egelhaaf, S. U. & Schurtenberger, P. Formation of Polymerlike Mixed Micelles and Vesicles in Lecithin-Bile Salt Solutions: A Small-Angle Neutron-Scattering Study. *J. Phys. Chem.* **99,** 1299–1305 (1995).
215. Madenci, D., Salonen, A., Schurtenberger, P., Pedersen, J. S. & Egelhaaf, S. U. Simple model for the growth behaviour of mixed lecithin-bile salt micelles. *Phys. Chem. Chem. Phys.* **13,** 3171–8 (2011).
216. Luner, P. E., Babu, S. R. & Radebaugh, G. W. The effects of bile salts and lipids on the physicochemical behavior of gemfibrozil. *Pharm. Res.* **11,** (1994).
217. Luner, P. E. & Vander Kamp, D. Wetting behavior of bile salt-lipid dispersions and dissolution media patterned after intestinal fluids. *J. Pharm. Sci.* **90,** 348–59 (2001).
218. Shozo, M., Noriyuki, M. & Hitoshi, S. Improvement of absolute bioavailability of normally poorly absorbed drugs: inducement of the intestinal absorption of streptomycin and gentamycin by lipid-bile salt mixed micelles in rat and rabbit. *Int. J. Pharm.* **2,** 101–111 (1979).
219. Nilsson, S., Sundelöf, L.-O. & Porsch, B. On the characterization principles of some technically important water soluble non-ionic cellulose derivatives. *Carbohydr. Polym.* **28,** 265–275 (1995).
220. Mitchell, S. A., Reynolds, T. D. & Dasbach, T. P. A compaction process to enhance dissolution of poorly water-soluble drugs using hydroxypropyl methylcellulose. *Int. J. Pharm.* **250,** 3–11 (2003).
221. Jamzad, S. & Fassihi, R. Role of surfactant and pH on dissolution properties of fenofibrate and glipizide--a technical note. *AAPS PharmSciTech* **7,** E33 (2006).
222. Balakrishnan, A., Rege, B. D., Amidon, G. L. & Polli, J. E. Surfactant-mediated dissolution: contributions of solubility enhancement and relatively low micelle diffusivity. *J. Pharm. Sci.* **93,** 2064–75 (2004).
223. Velikov, V., Borick, S. & Angell, C. A. The glass transition of water, based on hyperquenching experiments. *Science* **294,** 2335–8 (2001).
224. Duddu, S. P. & Sokoloski, T. D. Dielectric analysis in the characterization of amorphous pharmaceutical solids. 1. Molecular mobility in poly(vinylpyrrolidone)–water systems in the glassy state. *J. Pharm. Sci.* **84,** 773–776 (1995).
225. Crowley, K. J. & Zografi, G. Water vapor absorption into amorphous hydrophobic drug/poly(vinylpyrrolidone) dispersions. *J. Pharm. Sci.* **91,** 2150–65 (2002).
226. Rumondor, A. C. F. & Taylor, L. S. Effect of polymer hygroscopicity on the phase behavior of amorphous solid dispersions in the presence of moisture. *Mol. Pharm.* **7,** 477–90 (2010).
227. Wu, K., Li, J., Wang, W. & Winstead, D. A. Formation and characterization of solid dispersions of piroxicam and polyvinylpyrrolidone using spray drying and precipitation with compressed antisolvent. *J. Pharm. Sci.* **98,** 2422–31 (2009).
228. Bandyopadhyay, R., Selbo, J., Amidon, G. E. & Hawley, M. Application of powder X-ray diffraction in studying the compaction behavior of bulk pharmaceutical powders. *J. Pharm. Sci.* **94,** 2520–30 (2005).
229. Vrečer, F., Vrbinc, M. & Meden, A. Characterization of piroxicam crystal modifications. *Int. J. Pharm.* **256,** 3–15 (2003).

230. Weuts, I. *et al.* Phase behaviour analysis of solid dispersions of loperamide and two structurally related compounds with the polymers PVP-K30 and PVP-VA64. *Eur. J. Pharm. Sci.* **22,** 375–85 (2004).
231. Karavas, E., Ktistis, G., Xenakis, A. & Georgarakis, E. Effect of hydrogen bonding interactions on the release mechanism of felodipine from nanodispersions with polyvinylpyrrolidone. *Eur. J. Pharm. Biopharm.* **63,** 103–14 (2006).
232. Mihalić, M. *et al.* Piroxicam. *Anal. Profiles Drug Subst.* **15,** 509–531 (1986).
233. Janik, M., Malarski, Z., Mroziński, J., Wajcht, J. & Zborucki, Z. Influence of solvent effect on polymorphism of 4-hydroxy-2-methyl-N-2-pyridyl-2H-1,2-benzothiazine-3-carboxamide-1, 1-dioxide (piroxicam). *J. Crystallogr. Spectrosc. Res.* **21,** 519–522 (1991).
234. Reck, G. *et al.* X-ray studies on piroxicam modifications. *Pharmazie* **43,** 477–81 (1988).
235. Sethia, S. & Squillante, E. Solid dispersion of carbamazepine in PVP K30 by conventional solvent evaporation and supercritical methods. *Int. J. Pharm.* **272,** 1–10 (2004).
236. Zhang, M. *et al.* Formulation and delivery of improved amorphous fenofibrate solid dispersions prepared by thin film freezing. *Eur. J. Pharm. Biopharm.* **82,** 534–44 (2012).
237. Huang, Q.-P. *et al.* Preparation of ultrafine fenofibrate powder by solidification process from emulsion. *Int. J. Pharm.* **368,** 160–4 (2009).
238. Nair, R., Nyamweya, N., Gönen, S., Martínez-Miranda, L. J. & Hoag, S. W. Influence of various drugs on the glass transition temperature of poly(vinylpyrrolidone): a thermodynamic and spectroscopic investigation. *Int. J. Pharm.* **225,** 83–96 (2001).
239. Nair, R., Nyamweya, N., Gönen, S., Martínez-Miranda, L. J. & Hoag, S. W. Influence of various drugs on the glass transition temperature of poly(vinylpyrrolidone): a thermodynamic and spectroscopic investigation. *Int. J. Pharm.* **225,** 83–96 (2001).
240. Marsac, P. J., Shamblin, S. L. & Taylor, L. S. Theoretical and practical approaches for prediction of drug-polymer miscibility and solubility. *Pharm. Res.* **23,** 2417–26 (2006).
241. Doherty, C. & York, P. Mechanisms of dissolution of frusemide/PVP solid dispersions. *Int. J. Pharm.* **34,** 197–205 (1987).
242. Mosharraf, M. & Nyström, C. The effect of particle size and shape on the surface specific dissolution rate of microsized practically insoluble drugs. *Int. J. Pharm.* **122,** 35–47 (1995).
243. Vogt, M., Kunath, K. & Dressman, J. B. Dissolution enhancement of fenofibrate by micronization, cogrinding and spray-drying: comparison with commercial preparations. *Eur. J. Pharm. Biopharm.* **68,** 283–8 (2008).
244. Ahuja, N., Katare, O. P. & Singh, B. Studies on dissolution enhancement and mathematical modeling of drug release of a poorly water-soluble drug using water-soluble carriers. *Eur. J. Pharm. Biopharm.* **65,** 26–38 (2007).
245. Lue, B.-M. *et al.* Using biorelevant dissolution to obtain IVIVC of solid dosage forms containing a poorly-soluble model compound. *Eur. J. Pharm. Biopharm.* **69,** 648–57 (2008).
246. Qi, S. *et al.* Insights into the role of polymer-surfactant complexes in drug solubilisation/stabilisation during drug release from solid dispersions. *Pharm. Res.* **30,** 290–302 (2013).
247. Stevens, R., Ribeiro, A., Lack, L. & Killenberg, P. Proton magnetic resonance studies of the aggregation of taurine- conjugated bile salts. *J. Lipid Res.* **33,** 21–29 (1992).

248. Barnes, S. & Geckle, J. High resolution nuclear magnetic resonance spectroscopy of bile salts: individual proton assignments for sodium cholate in aqueous solution at 400 MHz. *J. Lipid Res.* **23,** 161–170 (1982).
249. Reich, H. J. 8.1 Relaxation in NMR Spectroscopy. (2011). at <http://www.chem.wisc.edu/areas/reich/nmr/08-tech-01-relax.htm>
250. Holz, M., Heil, S. R. & Sacco, A. Temperature-dependent self-diffusion coefficients of water and six selected molecular liquids for calibration in accurate 1H NMR PFG measurements. *Phys. Chem. Chem. Phys.* **2,** 4740–4742 (2000).
251. Hofmann, A. F. & Mysels, K. J. Bile acid solubility and precipitation in vitro and in vivo: the role of conjugation, pH, and Ca2+ ions. *J. Lipid Res.* **33,** 617–26 (1992).
252. Chang, Y. & Cardinal, J. R. Light-scattering studies on bile acid salts I: Pattern of self-association of sodium cholate, sodium glycocholate, and sodium taurocholate in aqueous electrolyte solutions. *J. Pharm. Sci.* **67,** 174–181 (1978).
253. Li, G. & McGown, L. B. Model for Bile Salt Micellization and Solubilization from Studies of a 'Polydisperse' Array of Fluorescent Probes and Molecular Modeling. *J. Phys. Chem.* **98,** 13711–13719 (1994).
254. Ryu, K., Lowery, J. M., Evans, D. F. & Cussler, E. L. Studies of model bile solutions using surfactant ion electrodes. *J. Phys. Chem.* **87,** 5015–5019 (1983).
255. Ammon, H. V. & Walter, L. G. Determination of bile acid monomers in micellar solutions. *Anal. Chem.* **54,** 2079–2082 (1982).
256. Meyerhoffer, S. M. & McGown, L. B. Critical micelle concentration behavior of sodium taurocholate in water. *Langmuir* **6,** 187–191 (1990).
257. Kratohvil, J. P., Hsu, W. P., Jacobs, M. A., Aminabhavi, T. M. & Mukunoki, Y. Concentration-dependent aggregation patterns of conjugated bile salts in aqueous sodium chloride solutions. *Colloid Polym. Sci.* **261,** 781–785 (1983).
258. Carey, M. C. & Small, D. M. Micellar properties of dihydroxy and trihydroxy bile salts: Effects of counterion and temperature. *J. Colloid Interface Sci.* **31,** 382–396 (1969).
259. Funasaki, N. *et al.* Two-Dimensional NMR Study on the Structures of Micelles of Sodium Taurocholate. *J. Phys. Chem. B* **108,** 438–443 (2004).
260. Matsuoka, K., Maeda, M. & Moroi, Y. Micelle formation of sodium glyco- and taurocholates and sodium glyco- and taurodeoxycholates and solubilization of cholesterol into their micelles. *Colloids Surfaces B Biointerfaces* **32,** 87–95 (2003).
261. Chung, R. S. K., Johnson, G. M. & Denbesten, L. Effect of sodium taurocholate and ethanol on hydrogen ion absorption in rabbit esophagus. *Am. J. Dig. Dis.* **22,** 582–588 (1977).
262. Reis, S. *et al.* Noninvasive methods to determine the critical micelle concentration of some bile acid salts. *Anal. Biochem.* **334,** 117–26 (2004).
263. Minatti, E. & Zanette, D. Salt effects on the interaction of poly(ethylene oxide) and sodium dodecyl sulfate measured by conductivity. *Colloids Surfaces A Physicochem. Eng. Asp.* **113,** 237–246 (1996).
264. Holmberg, C. & Evertsson, H. Salt influence in the polymer-surfactant interaction in solution. A fluorescence probe investigation of the EHEC/SDS/ water system. *Colloid Polym. Sci.* **275,** 830–840 (1997).
265. Dubin, P. L., Gruber, J. H., Xia, J. & Zhang, H. The effect of cations on the interaction between dodecylsulfate micelles and poly(ethyleneoxide). *J. Colloid Interface Sci.* **148,** 35–41 (1992).
266. Xia, J., Dubin, P. L. & Kim, Y. Complex formation between poly(oxyethylene) and sodium dodecyl sulfate micelles: Light scattering, electrophoresis, and dialysis equilibrium studies. *J. Phys. Chem.* **96,** 6805–6811 (1992).
267. Joshi, S. C. Sol-Gel Behavior of Hydroxypropyl Methylcellulose (HPMC) in Ionic Media Including Drug Release. *Materials (Basel).* **4,** 1861–1905 (2011).

268. Farías, T., de Ménorval, L. C., Zajac, J. & Rivera, A. Solubilization of drugs by cationic surfactants micelles: Conductivity and 1H NMR experiments. *Colloids Surfaces A Physicochem. Eng. Asp.* **345,** 51–57 (2009).
269. Maldonado-Valderrama, J., Muros-Cobos, J. L., Holgado-Terriza, J. A. & Cabrerizo-Vílchez, M. A. BILE SALTS AT THE AIR-WATER INTERFACE: ADSORPTION AND DESORPTION. *Colloids Surfaces B Biointerfaces* (2014). doi:10.1016/j.colsurfb.2014.05.014
270. Camino, N. A., Pérez, O. E., Sanchez, C. C., Rodriguez Patino, J. M. & Pilosof, A. M. R. Hydroxypropylmethylcellulose surface activity at equilibrium and adsorption dynamics at the air–water and oil–water interfaces. *Food Hydrocoll.* **23,** 2359–2368 (2009).
271. Noskov, B. A., Akentiev, A. V. & Miller, R. Dynamic Surface Properties of Poly(vinylpyrrolidone) Solutions. *J. Colloid Interface Sci.* **255,** 417–424 (2002).
272. Yang, L. & Fassihi, R. Examination of drug solubility, polymer types, hydrodynamics and loading dose on drug release behavior from a triple-layer asymmetric configuration delivery system. *Int. J. Pharm.* **155,** 219–229 (1997).
273. Varum, F. J. O., Hatton, G. B. & Basit, A. W. Food, physiology and drug delivery. *Int. J. Pharm.* **457,** 446–60 (2013).
274. Christoff, M., Silveira, N. da & Samios, D. Fluorescence and light scattering studies on the aggregation of sodium cholate in the presence of low molecular weight poly (ethylene oxide). *Langmuir* (2001). at <http://pubs.acs.org/doi/pdf/10.1021/la001060l>
275. De Martins, R. M., Becker, C. M., Samios, D. & Bica, C. I. D. Interaction of (Hydroxypropylmethyl)cellulose with Anionic Surfactants. *Macromol. Symp.* **245-246,** 287–296 (2006).
276. Filipe, V., Hawe, A. & Jiskoot, W. Critical evaluation of Nanoparticle Tracking Analysis (NTA) by NanoSight for the measurement of nanoparticles and protein aggregates. *Pharm. Res.* **27,** 796–810 (2010).
277. Mazer, N. A., Benedek, G. B. & Carey, M. C. Quasielastic light-scattering studies of aqueous biliary lipid systems. Mixed micelle formation in bile salt-lecithin solutions. *Biochemistry* **19,** 601–615 (1980).
278. Andrieux, K. *et al.* Insertion and Partition of Sodium Taurocholate into Egg Phosphatidylcholine Vesicles. *Pharm. Res.* **21,** 1505–1516 (2004).
279. Boni, J. & Brickl, R. Instant FaSSIF and FeSSIF-biorelevance meets practicality. *Dissolution …* (2009). at <http://www.dissolutiontech.com/DTresour/200908Articles/DT200908_A05.pdf>
280. Persson, B. On the characterization principles of some technically important water-soluble nonionic cellulose derivatives. Part II: Surface tension and interaction with a surfactant. *Carbohydr. Polym.* **29,** 119–127 (1996).
281. Porter, C. J. H., Pouton, C. W., Cuine, J. F. & Charman, W. N. Enhancing intestinal drug solubilisation using lipid-based delivery systems. *Adv. Drug Deliv. Rev.* **60,** 673–91 (2008).
282. Plomp, J., de Haan, V. O., Dalgliesh, R. M., Langridge, S. & van Well, A. A. Neutron spin-echo labelling at OffSpec, an ISIS second target station project. *Thin Solid Films* **515,** 5732–5735 (2007).
283. Claesson, P. M. *et al.* Mixtures of Cationic Polyelectrolyte and Anionic Surfactant Studied with Small-Angle Neutron Scattering. *J. Phys. Chem. B* **104,** 11689–11694 (2000).
284. and, J.-F. B., Hervé, P., Aguerre-Chariol, O. & Oberdisse, J. Colloidal Complexes Obtained from Charged Block Copolymers and Surfactants: A Comparison between Small-Angle Neutron Scattering, Cryo-TEM, and Simulations†. (2003). at <http://pubs.acs.org/doi/abs/10.1021/jp027740+>

285. Egelhaaf, S. U. & Schurtenberger, P. Shape Transformations in the Lecithin-Bile Salt System: From Cylinders to Vesicles. *J. Phys. Chem.* **98,** 8560–8573 (1994).
286. Arleth, L. *et al.* Growth Behavior of Mixed Wormlike Micelles: a Small-Angle Scattering Study of the Lecithin−Bile Salt System. *Langmuir* **19,** 4096–4104 (2003).
287. Njauw, C.-W., Cheng, C.-Y., Ivanov, V. A., Khokhlov, A. R. & Tung, S.-H. Molecular interactions between lecithin and bile salts/acids in oils and their effects on reverse micellization. *Langmuir* **29,** 3879–88 (2013).
288. Hjelm, R. P., Thiyagarajan, P. & Alkan-Onyuksel, H. Organization of phosphatidylcholine and bile salt in rodlike mixed micelles. *J. Phys. Chem.* **96,** 8653–8661 (1992).
289. Amidon, G. L., Lennernäs, H., Shah, V. P. & Crison, J. R. A Theoretical Basis for a Biopharmaceutic Drug Classification: The Correlation of in Vitro Drug Product Dissolution and in Vivo Bioavailability. *Pharm. Res.* **12,** 413–420 (1995).
290. Artursson, P., Palm, K. & Luthman, K. Caco-2 monolayers in experimental and theoretical predictions of drug transport1PII of original article: S0169-409X(96)00415-2. The article was originally published in Advanced Drug Delivery Reviews 22 (1996) 67–84.1. *Adv. Drug Deliv. Rev.* **46,** 27–43 (2001).
291. Artursson, P. & Karlsson, J. Correlation between oral drug absorption in humans and apparent drug permeability coefficients in human intestinal epithelial (Caco-2) cells. *Biochem. Biophys. Res. Commun.* **175,** 880–885 (1991).
292. P, A. Cell cultures as models for drug absorption across the intestinal mucosa. *Crit. Rev. Ther. Drug Carrier Syst.* **8,** 305–330 (1991).
293. Ingels, F., Beck, B., Oth, M. & Augustijns, P. Effect of simulated intestinal fluid on drug permeability estimation across Caco-2 monolayers. *Int. J. Pharm.* **274,** 221–32 (2004).
294. Ingels, F. *et al.* Simulated intestinal fluid as transport medium in the Caco-2 cell culture model. *Int. J. Pharm.* **232,** 183–192 (2002).
295. Korzeniewski, C. & Callewaert, D. M. An enzyme-release assay for natural cytotoxicity. *J. Immunol. Methods* **64,** 313–320 (1983).
296. MARTIN, G. P., EL-HARIRI, L. M. & MARRIOTT, C. Bile Salt- and Lysophosphatidylcholine-induced Membrane Damage in Human Erythrocytes. *J. Pharm. Pharmacol.* **44,** 646–650 (1992).
297. Rege, B. D., Yu, L. X., Hussain, A. S. & Polli, J. E. Effect of common excipients on Caco-2 transport of low-permeability drugs. *J. Pharm. Sci.* **90,** 1776–86 (2001).
298. MARTIN, G. P. & MARRIOTT, C. Membrane damage by bile salts: the protective function of phospholipids. *J. Pharm. Pharmacol.* **33,** 754–759 (1981).
299. Patel, N., Forbes, B., Eskola, S. & Murray, J. Use of Simulated Intestinal Fluids with Caco-2 Cells and Rat Ileum. (2008). at <http://informahealthcare.com/doi/abs/10.1080/03639040500465991>
300. Walter, E., Janich, S., Roessler, B. J., Hilfinger, J. M. & Amidon, G. L. HT29-MTX/Caco-2 cocultures as an in vitro model for the intestinal epithelium: in vitro-in vivo correlation with permeability data from rats and humans. *J. Pharm. Sci.* **85,** 1070–6 (1996).
301. Fossati, L. *et al.* Use of simulated intestinal fluid for Caco-2 permeability assay of lipophilic drugs. *Int. J. Pharm.* **360,** 148–55 (2008).
302. Habib, M. J. *Pharmaceutical solid dispersion technology*. (CRC Press, 2000).
303. Pan, R.-N., Chen, J.-H. & Chen, R. R.-L. Enhancement of Dissolution and Bioavailability of Piroxicam in Solid Dispersion Systems. *Drug Dev. Ind. Pharm.* **26,** 989–994 (2000).
304. El-Badry, M., Fetih, G. & Fathy, M. Improvement of solubility and dissolution rate of indomethacin by solid dispersions in Gelucire 50/13 and PEG4000. *Saudi Pharm. J. SPJ Off. Publ. Saudi Pharm. Soc.* **17,** 217–25 (2009).

305. Okonogi, S., Oguchi, T., Yonemochi, E., Puttipipatkhachorn, S. & Yamamoto, K. Improved dissolution of ofloxacin via solid dispersion. *Int. J. Pharm.* **156,** 175–180 (1997).
306. Qian, F., Huang, J. & Hussain, M. A. Drug-polymer solubility and miscibility: Stability consideration and practical challenges in amorphous solid dispersion development. *J. Pharm. Sci.* **99,** 2941–7 (2010).
307. Janssens, S. & Van den Mooter, G. Review: physical chemistry of solid dispersions. *J. Pharm. Pharmacol.* **61,** 1571–1586 (2009).
308. Weuts, I. *et al.* Study of the physicochemical properties and stability of solid dispersions of loperamide and PEG6000 prepared by spray drying. *Eur. J. Pharm. Biopharm.* **59,** 119–26 (2005).
309. Yee, C. S. The Development of PVP-based Solid Dispersions using Hot Melt Extrusion for the Preparation of Immediate Release Formulations. (2013).
310. Kataoka, M., Masaoka, Y., Sakuma, S. & Yamashita, S. Effect of food intake on the oral absorption of poorly water-soluble drugs: in vitro assessment of drug dissolution and permeation assay system. *J. Pharm. Sci.* **95,** 2051–61 (2006).
311. Lind, M. L., Jacobsen, J., Holm, R. & Müllertz, A. Development of simulated intestinal fluids containing nutrients as transport media in the Caco-2 cell culture model: assessment of cell viability, monolayer integrity and transport of a poorly aqueous soluble drug and a substrate of efflux mechanisms. *Eur. J. Pharm. Sci.* **32,** 261–70 (2007).

Appendix

Calibration curves

In this appendix UV calibration curves of the model drugs employed in this project are reported (Figure i-ix). HPLC piroxicam calibration is also shown (Figure x).

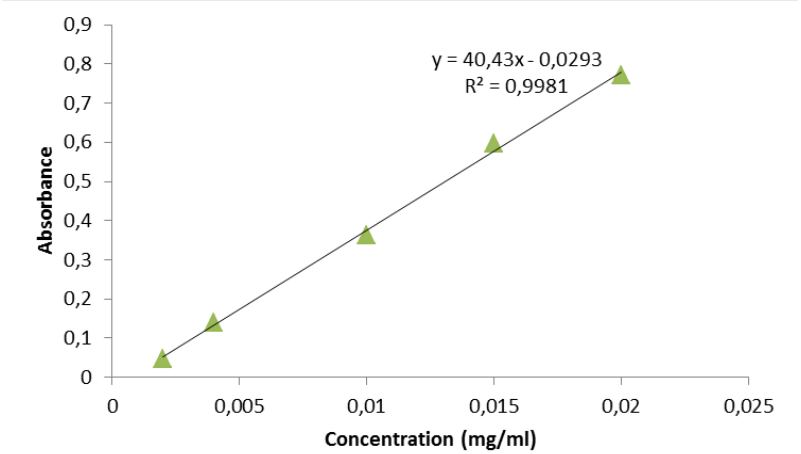

Figure i: UV piroxicam calibration curve buffer pH 6.5

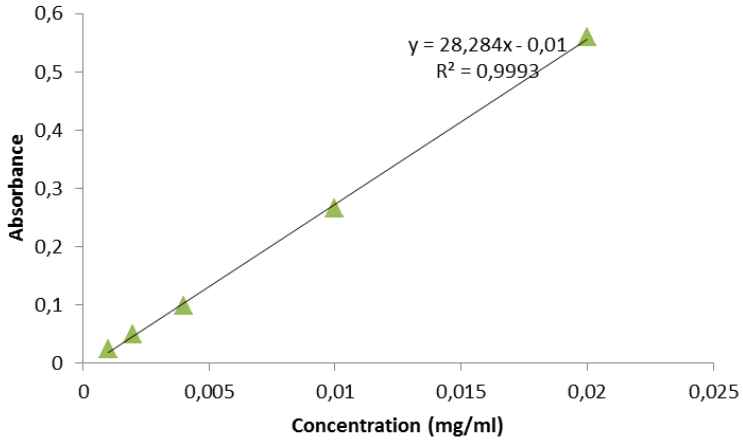

Figure ii: UV piroxicam calibration curve buffer pH 5

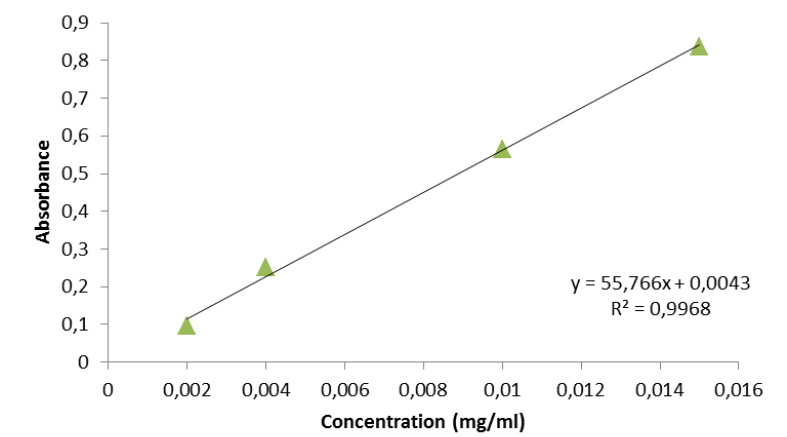

Figure iii: UV piroxicam calibration curve ethanol

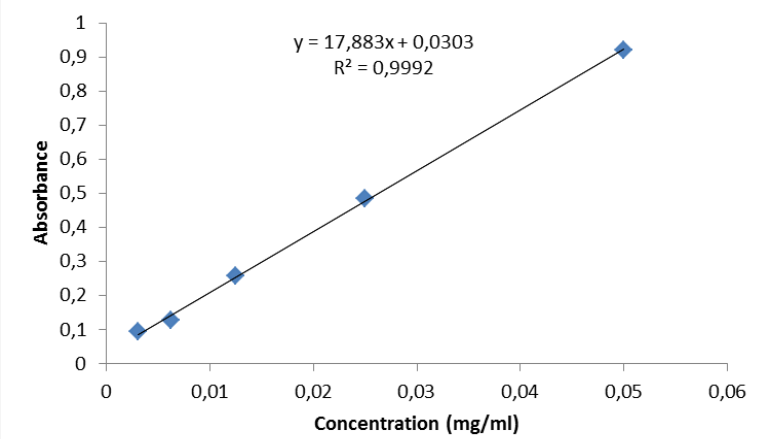

Figure iv: UV griseofulvin calibration curve buffer pH 5

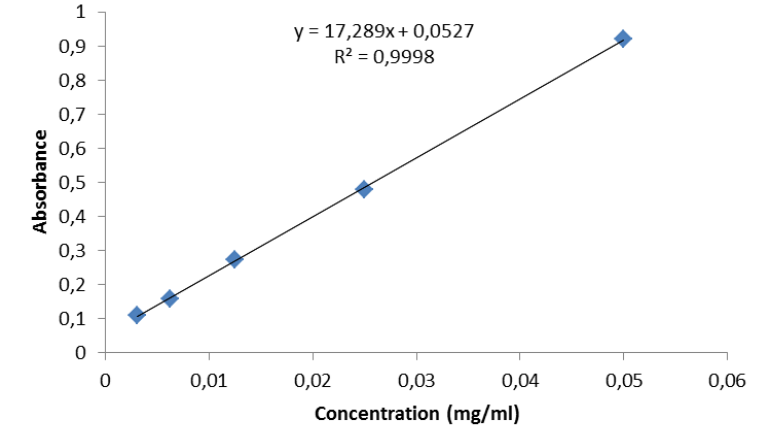

Figure v: UV griseofulvin calibration curve buffer pH 6.5

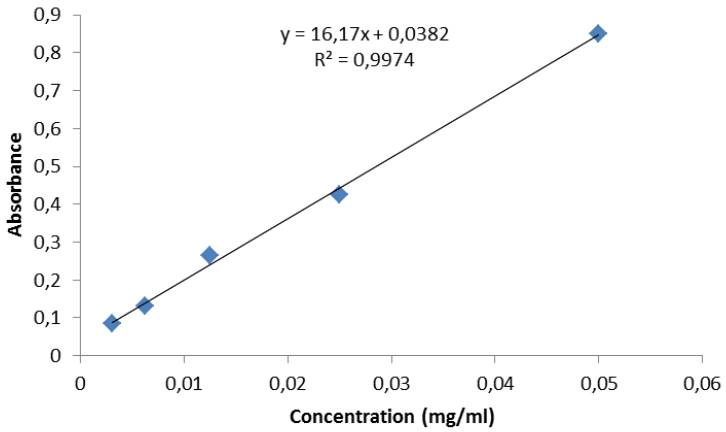

Figure vi: UV griseofulvin calibration curve ethanol

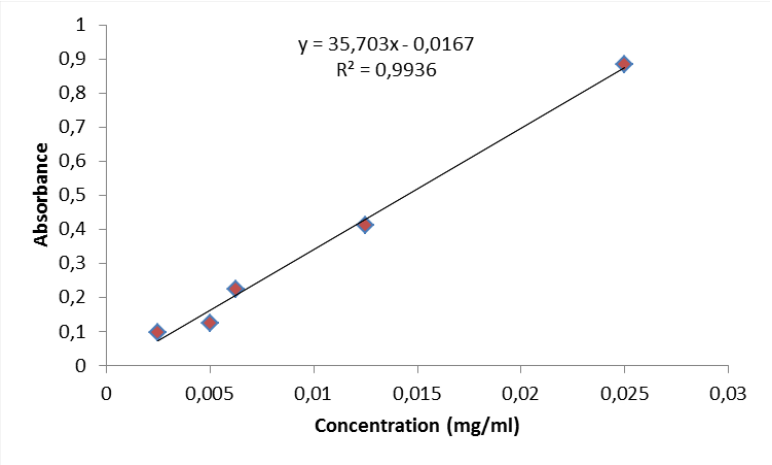

Figure vii: UV fenofibrate calibration curve buffer pH 5

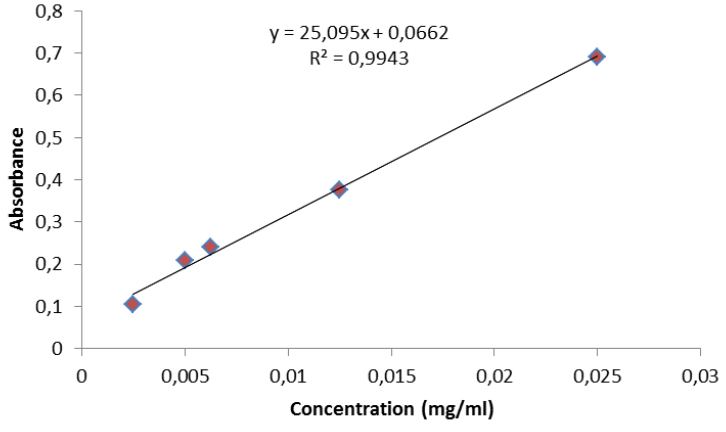

Figure viii: UV fenofibrate calibration curve buffer pH 6.5

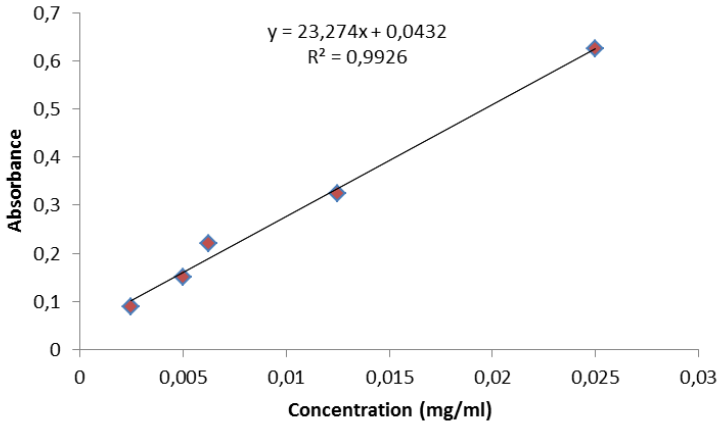

Figure ix: UV fenofibrate calibration curve ethanol

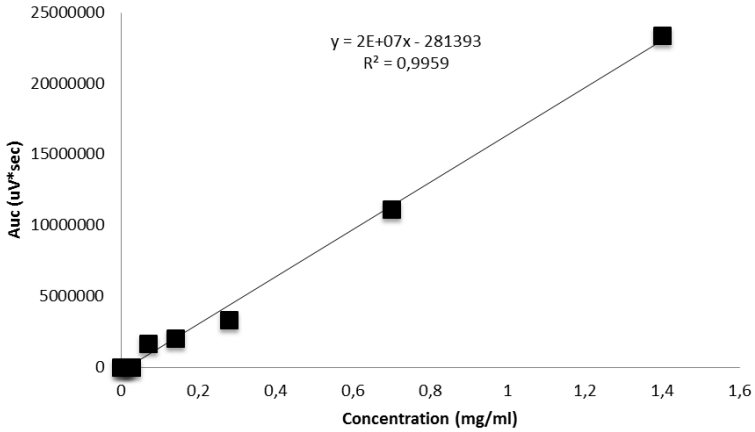

Figure x: HPLC-UV piroxicam calibration curve mobile phase (CH_3CN/phosphate buffer)

Publication

Insights into the Role of Polymer-Surfactant Complexes in Drug Solubilisation/Stabilisation During Drug Release from Solid Dispersions, *Qi, S., S. Roser, K.J. Edler, C. Pigliacelli, M. Rogerson, F. Van Dycke, S. Stokbroekx,* Pharmaceutical Research, **2013**, 30(1) 290-302

Abstract

Purpose

To evaluate the role of polymer-surfactant interactions in drug solubilisation/stabilisation during the dissolution of spray-dried solid dispersions and their potential impact on *in vivo* drug solubilisation and absorption.

Methods

Dissolution/precipitation tests were performed on spray-dried HPMC-Etravirine solid dispersions to demonstrate the impact of different surfactants on the *in vitro* performance of the solid dispersions. Interactions between HPMC and bio-relevant and model anionic surfactants (bile salts and SDS respectively) were further characterised using surface tension measurements, fluorescence spectroscopy, DLS and SANS.

Results

Fast and complete dissolution was observed in media containing anionic surfactants with no drug recrystallisation within 4 h. The CMCs of bile salts and SDS were dramatically reduced to lower CACs in the presence of HPMC and Etravirine. The maximum increases of the apparent solubility of Etravirine were with the presence of HPMC and SDS/bile salts. The SANS and DLS results indicated the formation of HPMC-SDS/bile salts complexes which encapsulated/solubilised the drug.

Conclusions

This study has demonstrated the impact HPMC-anionic surfactant interactions have during the dissolution of non-ionic hydrophilic polymer based solid dispersions and has highlighted the potential relevance of this to a fuller understanding of drug solubilisation/stabilisation *in vivo*.